ONE- AND TWO-DIMENSIONAL HIGH-RESOLUTION SOLID-STATE NMR INVESTIGATION OF ZEOLITE STRUCTURES

By

YI FENG
M.Sc., Nanjing University, P. R. China, 1982

A THESIS SUBMITTED IN PARTIAL FULFILLMENT OF
THE REQUIREMENTS FOR THE DEGREE OF
DOCTOR OF PHILOSOPHY

in

THE FACULTY OF GRADUATE STUDIES
(Department of Chemistry)

We accept this thesis as conforming
to the required standard

THE UNIVERSITY OF BRITISH COLUMBIA

July 1991

© Yi Feng, 1991

90

In presenting this thesis in partial fulfilment of the requirements for an advanced degree at the University of British Columbia, I agree that the Library shall make it freely available for reference and study. I further agree that permission for extensive copying of this thesis for scholarly purposes may be granted by the head of my department or by his or her representatives. It is understood that copying or publication of this thesis for financial gain shall not be allowed without my written permission.

Department of Chemistry

The University of British Columbia
Vancouver, Canada

Date Sep. 4, 1991

ABSTRACT

The work reported in this thesis describes for the first time the application of two-dimensional ^{29}Si high-resolution solid state NMR experiments to the investigation of the three-dimensional Si-O-Si bonding connectivities in zeolites. 2D COSY type, INADEQUATE type and spin-diffusion experiments are discussed and evaluated, the INADEQUATE experiments being particularly successful in this work. By preparing highly crystalline, highly siliceous samples of zeolites and careful optimization of all experimental parameters, it is possible to directly observe ^{29}Si-O-^{29}Si J couplings in these experiments.

The three-dimensional lattice connectivities obtained from this work for ^{29}Si enriched zeolite ZSM-39 and natural abundance ZSM-12 and ZSM-22 are in excellent agreement with the lattice structures determined by XRD techniques. In the case of a ^{29}Si enriched sample of zeolite DD3R, the ^{29}Si 2D NMR results indicate that the structure is of lower symmetry than has been postulated from diffraction studies.

Zeolite ZSM-5, which has the most complex three-dimensional framework of all the known zeolites, was extensively studied in its room temperature phase by 2D NMR spectroscopy. In addition, the effects of temperature and the presence of sorbed *p*-xylene and *p*-dichlorobenzene on the phase behavior of ZSM-5 were also investigated.

The ^{29}Si 2D NMR data on ZSM-11 at high temperature are in good agreement with the known structure, $I\bar{4}m2$. Low temperature 2D experiments on

ZSM-11 gave the assignment of space group symmetry $I\bar{4}$ to the structure which was previous unknown.

Finally, ^{29}Si 2D NMR results on ZSM-23 reveal that there are 12 independent T-sites in the structure which is not consistent with the space groups proposed in the literature which have 7 crystallographically inequivalent T-sites.

TABLE OF CONTENTS

LIST OF TABLES

LIST OF FIGURES

SYMBOLS AND ABBREVIATIONS

a, b, c	unit cell edges vectors parallel to the x, y, and z axes, respectively
Å	Angstrom unit; 1 Å = 10^{-10} m
B_0	strength of static magnetic field
B_1	strength of the radio-frequency field during a pulse
COSY	chemical shift correlation spectroscopy
CP	cross polarization
DANTE	delays alternating with nutation for tailored excitation
DQF COSY	double quantum filtered COSY
ESD	estimated standard deviation
FD	fixed delay
FID	free induction decay
F_1, F_2	frequency dimensions corresponding to t_1 and t_2
h	(i) hour
	(ii) Plank constant
H	Hamiltonian operator, subscripts indicate the nature of the operator
HPD	high power decoupling
Hz	hertz
INADEQUATE	incredible natural abundance double quantum transfer experiment
^nJ	nuclear spin-spin coupling constant through n bonds (in Hz)
MAS	magic angle spinning

ms	milli-second
M_0	equilibrium macroscopic magnetization of a spin sysytem in the presence of B_0
Mx, My, Mz	components of macroscopic magnetization
NMR	nuclear magnetic resonance
POF	product operator formalism
ppm	parts per million
Q_8M_8	cubic octamer silicic acid trimethylsilyl ester
rf	radio frequency
s	second
TMS	tetramethylsilane
T_X	T-site X in the structures of zeolites
T_1	longitudinal relaxation time
T_2	transverse relaxation time
T_2^*	decay constant describing inhomogeneity and transverse relaxation
t_1	length of the evolution period
t_2	running time during the detection period
XRD	X- ray diffraction
XRF	X- ray fluorescence
1D, 2D	one-dimensional, two-dimensional
α	T– O– T angle
γ_X	magnetogyric ratio of uncleus X
δ	chemical shift, usually in ppm
$\Delta\nu_{1/2}$	full width of a resonance line at half-height
ν_X	Larmor precession frequency of uncleus X (in Hz)

ACKNOWLEDGEMENTS

I would like to sincerely thank Dr. C. A. Fyfe for his guidance and encouragement during the course of the research programme and throughout the preparation of this thesis.

I am indebted to numerous friends and colleagues for their collaboration, advice, encouragement and discussions on several aspects of this work. In particular, I wish to thank Dr. H. Grondey, Dr. H. Gies, Dr. G. T. Kokotailo, Dr. N. Burlinson, Dr. B. Fahie and Dr. L. Randall.

I also wish to thank Dr. Cox, Brookhaven National Laboratory USA, for kindly providing the computing program for Rietveld refinement of crystal structures using powder XRD data.

I am thankful for permission to use the VAX computer system in the Electrical Engineering Department, and wish to thank Mr. R. Rose for his assistance in this regard.

I gratefully acknowledge the University of British Columbia for financial support in the form of graduate fellowship.

Finally, I wish to sincerely thank my husband, Changshi, and my son, Lei, for their patience and understanding over the past four years.

CHAPTER ONE

INTRODUCTION

A. ZEOLITES AND THE METHODS FOR THE INVESTIGATION OF THEIR STRUCTURES

I. ZEOLITE STRUCTURES

The name "zeolite" was coined by Cronstedt[1] in 1756 from the Greek words for 'to boil' and 'stone' to describe the behavior of the newly discovered mineral stilbite, which loses water rapidly on heating and thus seems to boil. Zeolites have been extensively studied during the last 30 years, leading to the synthesis of novel structures and to a great number of applications (as ion-exchangers, molecular sieves , catalysts and so on).

Zeolites are framework aluminosilicates composed of corner- and edge-sharing SiO_4^{4-} and AlO_4^{5-} tetrahedra and containing regular systems of intracrystalline cavities and channels of molecular dimensions (Fig. 1)[2-6].

The general oxide formula of a zeolite is given by Equation [1]:

$$M_{x/n}(AlO_2)_x(SiO_2)_y \bullet mH_2O \qquad [1]$$

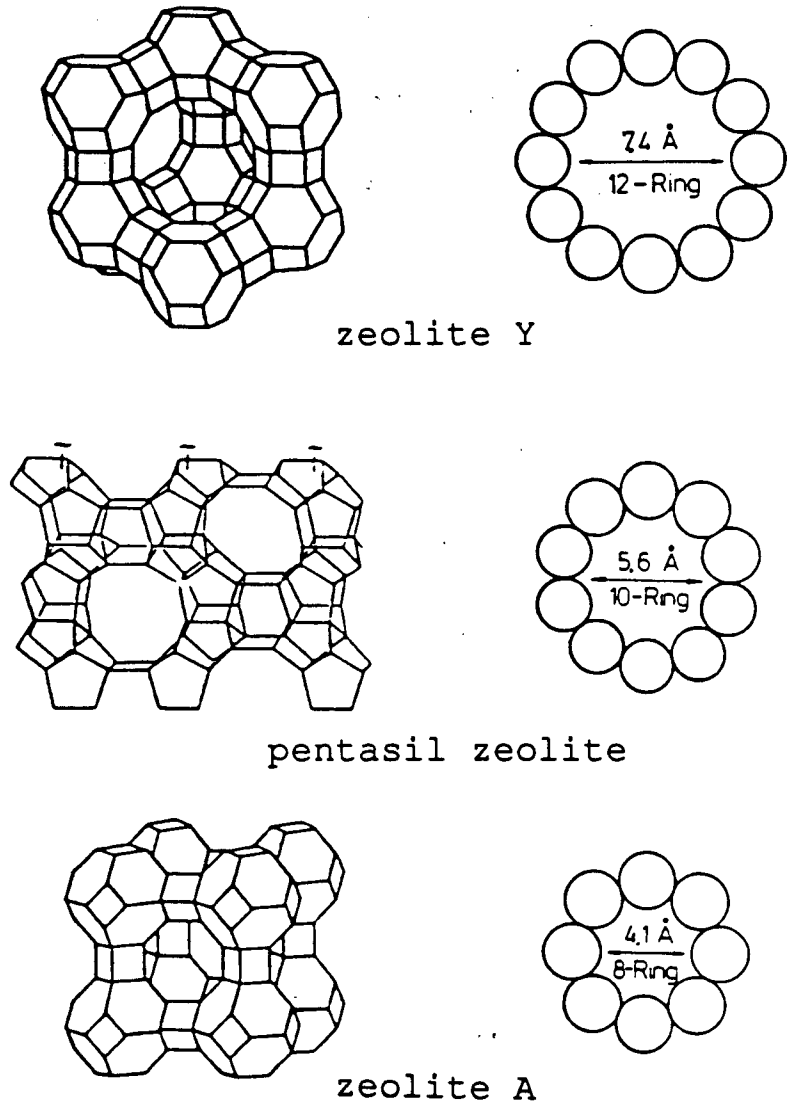

Figure 1 The framework structures of selected zeolites together with the apertures of their respective channels. (ref. 10)

where M represents exchangeable cations of valence n, which neutralize the net negative charge of the zeolite framework arising from the AlO_4^{5-} tetrahedra, and mH_2O represents the water molecules of hydration. The silicon to aluminum ratio, y/x, is invariably found to be equal to or greater than one and can approach infinity for completely 'aluminum free' frameworks.

As stated earlier, a zeolite framework consists of tetrahedral T-atoms (Si or Al atoms tetrahedrally coordinated to four oxygens) linked through common oxygen atoms to form a three-dimensional structure. Zeolite frameworks can also be thought to consist of finite or infinite (i.e. chain- or layer-like) component units. The recurring finite units are called secondary building units (SBU). One simple way to classify zeolite structures is based on the SBU's, which describes all known zeolite frameworks as arrangements linking the 16 possible SBU's. The commonly occurring SBU's are shown in Figure 2. In the SBU, a tetrahedral atom (Si,Al) is present at each corner or termination, but the oxygen atoms are not shown. These bridging oxygen atoms are located approximately half-way between the tetrahedral atoms but not usually on the line joining them. Table 1 lists some known zeolite structures classified by (a) their SBU content, (b) structure type (IUPAC nomenclature),[5] (c) their common names.

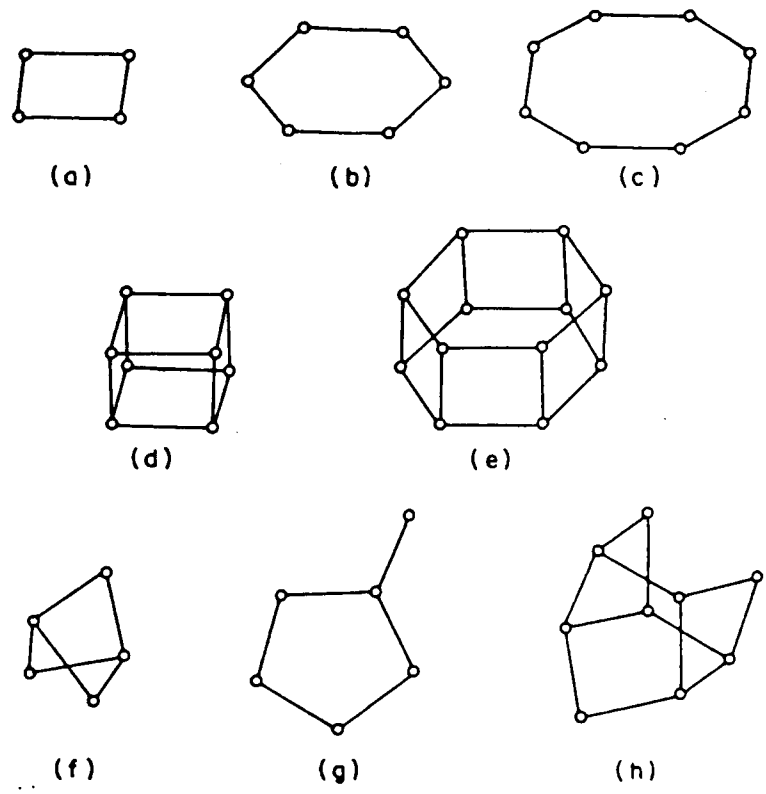

Figure 2 Secondary building units commonly occurring in zeolite frameworks. (a) single four ring (S4R), (b) single six ring (S6R), (c) single eight ring (S8R), (d) double four ring (D4R), (e) double six ring (D6R), (f) complex 4-1, (g) complex 5-1 and (h) complex 4-4-1. (ref.7)

Table 1 Classification of Some Zeolites (Ref. 8)

Secondary Building Unites	Structure type (IUPAC nomenclature)	Name
S4R	ANA	Analcime
	GIS	Gismondine
	PHI	Phillipsite
S6R	ERI	Erionite
	LTL	Zeolite L
	OFF	Offretite
	MAZ	Zeolite omega
S8R	Occurs in many structures but with other SBU'S. (i.e. chabazite, zeolite A)	
D4R	LTA	Zeolite A
D6R	CHA	Chabazite
	FAU	Faujasite
	FAU	Zeolite X
	GME	Gmelinite
	KFI	Zeolite ZK-5
4-1	NAT	Natrolite
	NAT	Scolecite
	THO	Thomsonite
5-1	MOR	Mordenite
	DAC	Dachiardite
	MF1	Zeolite ZSM-5
	MEL	Zeolite ZSM-11
4-4-1	HEU	Heulandite
	STI	Stilbite

II. APPLICATIONS OF ZEOLITES

To be interested in zeolites as ion-exchangers, molecular sieves and catalysts is to be become involved in many aspects of science and technology, such as petrochemistry and oil processing, organic synthesis of intermediates and fine chemicals, and nuclear waste treatment[2-4, 9, 10]. Many of these applications depend on the arrangement and internal dimensions of the intracrystalline channel structures. The accessibility of the intracrystalline pores is governed by the size of the apertures in the following way. The apertures are of such a size as to be able to selectively take up some molecules into their porous structure, whilst rejecting others on the basis of their larger effective molecular dimensions. The free dimensions of some n-ring apertures are given in Table 2 by assuming 2.8 Å as the diameter of the oxygens lining the inner surfaces.

Table 2 Free Dimensions of Some Planar n-Ring Apertures Found in Zeolites (Ref. 4)

Zeolite	Ring Size (n T-atoms)	Free Dimensions of Aperture (Å)
Sodalite	6	2.1
Zeolite A	8	4.1
Erionite		5.2 / 3.6
Offretite		5.2 / 3.6
Ferrierite	10	5.5 / 4.3
ZSM-5		5.6 / 5.4
Mordenite	12	7.0 / 6.7
Faujasite		7.4
Zeolite Y		7.4

The ion exchange property of zeolites which allows the replacement of cations held in their framework by ions present in an external solution has been intensively studied for two main reasons. One is their industrial importance in acting as ion exchangers. The other is the interest in modification of the catalytic or molecular sieving actions of the parent zeolite. Some of the uses of zeolites as ion exchangers are :

- Components in commercial detergent compositions for exchanging Ca^{2+} for Na^{+} to soften water.
- Treatment of liquid nuclear effluents.
- Waste-water treatment.

The applications of zeolites as molecular sieves depend on the dimensions of their framework apertures as discussed above. It is well known that Linde Molecular Sieve 4A (zeolite NaA, having the pore dimensions of approximately 4 Å) is used as a gas or solvent drying agent in almost every chemical laboratory in the world. Other important industrial applications are:

- Gas separation. e.g. n-paraffins are accepted by Molecular Sieve 5A (CaA) while i-paraffins are excluded by virtue of their larger effective kinetic diameters.
- Gas purification. For example, 13X zeolite (Na faujasite) is used to remove sulphur- and nitrogen- containing molecules from gaseous environments.

The characteristic properties of zeolites as catalysts are acidity, shape-selectivity and thermal stability, making them unique among catalytically active

materials and sharing many of the characteristics of enzymes [4]. The catalytic activity of zeolites is based upon the production of acidic Brönsted sites arising from the creation of 'hydroxyls' within the zeolite pore structure. These 'hydroxyls' are usually formed by ammonium cation exchange followed by a calcination step which involves heating in air at ~ 500° as in Equations [2] and [3], where 'Z' represents the zeolite structure.

$$NaZ(s) + NH_4^+ (aq.) \leftrightarrow NH_4Z(s) + Na^+(aq.) \qquad [2]$$

$$NH_4Z(s) \xrightarrow[500°c]{\text{calcine}} NH_3(g)\uparrow + HZ(s) \qquad [3]$$

The 'protonated' form contains protons associated with negatively charged framework oxygens linked into alumina tetrahedra, i.e. acidic Brönsted sites are created:

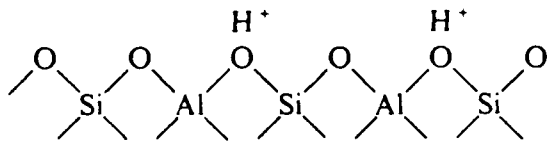

At 550°C protons can be lost in the form of water with the consequent formation of Lewis sites shown in Equation [4].

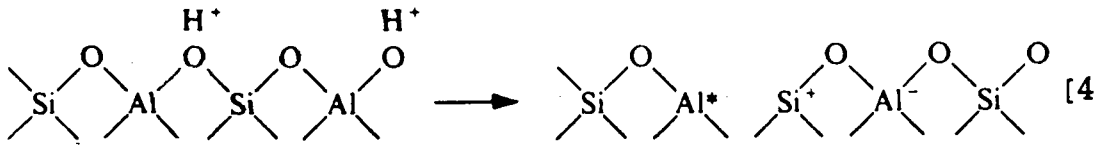

[4]

Brönsted site **Lewis site**

The acid strength and number of the acid centers (both Brönsted and Lewis acid centers) can be adjusted in a controlled manner during synthesis and/or by subsequent treatments. The shape selectivity means that only molecules smaller than the aperture of the zeolite can react with the zeolite catalyst. In addition, only those molecules whose transition state geometry is smaller than the cavity and/or pore diameter can be formed and released. The thermal stability of the zeolites permits them to be used above 150° C, and they are therefore very useful for reactions in which the thermodynamic equilibrium requires high temperatures. Some major commercial processes making use of zeolite catalysts are listed in Table 3.

Table 3 Some Commercial Processes using Zeolite Catalysts (Ref. 8)

Process	Catalyst	Advantage
Catalytic cracking	REY (REX,REHY,HY, REMgY)*	Selectivity and high conversion rates
Hydrocracking	X, Y, Mordenite loaded with Co,Mo, W,Ni, also HY, Ca MgY and H-ZSM-5	High conversion rates
Selectoforming	Ni clinoptilolite/ erionite,Ni erionite	Increase in octane number
Hydroisomerization	Pt mordenite	Converts low octane and hexane feeds to higher octane yields
Dewaxing	Pt mordenite	remove long-chain paraffins
Benzene alkylation	ZSM-5	Ethylbenzene and styrene production with low by-product yield
Xylene isomerization	ZSM-5	Increase in p-xylene yield with low by-product yield
Methanol to gasoline conversion	ZSM-5	High gasoline yield with high octane rating
NOx reduction	H-mordenite	Effluent clean-up in nitric acid and nuclear reprocessing plants

* REY stands for zeolite Y materials with rare earth metal cations

III. METHODS FOR THE CHARACTERIZATION OF ZEOLITE LATTICE STRUCTURES

In principle it should be possible to solve all zeolite structures by the use of modern single-crystal X-ray diffraction techniques and indeed a number of naturally occurring species have been studied in this way. In the case of synthetic materials, however, very few of them are available as large enough single crystals for conventional XRD measurements. These materials are highly crystalline, but with dimensions of the individual crystals of the order of a few microns or less. Even in the case where good quality crystals are available, distinguishing structural Al from Si is difficult because of the similarity in the scattering factors of these two elements and the fact that they are usually disordered over the available T- sites. When single-crystal X-ray crystallographic methods are inapplicable, other techniques have usually to be employed. These mainly involve the following four distinct approaches.

a) Developments in Powder Diffraction Methods[11,12]

Conventional powder X-ray diffraction has been the primary tool for the determination of the structures of zeolite materials. Recently, improvements in X-ray fluxes using synchrotron sources and developments in data analysis techniques based on Rietveld methods[13,14] have had a considerable impact in the area of zeolite structure determination[15]. X-rays from these sources are very intense, polarized and sharply focused, and give therefore a great improvement in the resolution of a powder diffraction experiment and dramatically increase the amount of structural information, while the Rietveld method predicts likely XRD patterns from simulated structures and presents

data outputs of the closeness of fit between experimental and computed patterns. Furthermore, the 'brightness' of the synchrotron source, in principle, also enables conventional single-crystal diffraction measurements of very small crystals. Although little has been published in this latter area, preliminary results[15] are described as promising.

b) High-Resolution Solid-State Nuclear Magnetic Resonance Spectroscopy[17]

In the study of zeolite structures, high-resolution solid-state NMR spectroscopy has emerged as an important complementary technique to X-ray diffraction measurements. The former probes short range ordering and structure, while the latter is sensitive to long range ordering and periodicities.

As is well known, the usefulness of NMR in chemistry in general rests on the fact that the chemical shifts of the nuclear magnetic resonance signals depend in a sensitive manner on the local chemical environments of the nuclei, while their intensities relate directly to the numbers of nuclei in the different environments. The contributions of ^{29}Si and ^{27}Al solid-state NMR in the study of the framework of zeolites can be summarized as follows.

- Determining the composition of low Si/Al ratio aluminosilicate framework in terms of the local silicon environments, i.e. Si[4Al], Si[3Al,Si], Si[2Al,2Si] Si[Al,3Si] and Si[4Si].
- Resolving crystallographically nonequivalent tetrahedral sites.
- Monitoring the effect of adsorbed organic species on the zeolite structure.

- Distinguishing tetrahedral from octahedral Al and framework from non-framework Al.

c) Electron Microscopy[18]

The technique of Scanning Electron Microscopy (SEM) is widely used in the characterization of the crystal morphologies of zeolites. It is useful in synthesis and quality control for the detection of new phases and mixed zeolite phases. High-Resolution Electron Microscopy (HREM) can yield structural information in 'real space' at the subnanometer level. Under suitable circumstances, even the pore openings can be clearly observed, giving the most direct structural information. It is the most appropriate way of examining defects and mixed phases in zeolite systems[19].

d) Computer-Modeling Techniques[20]

During the last decade, computer-modeling techniques have developed and are now considered by some to constitute a viable procedure for investigating the properties of perfect and defective materials. This process entails predicting the minimum energy configuration of a crystal structure. studies of zeolite structures using this techniques have been of two types

- Zeolite structures and relative stabilities[21].
- Structure and energetics of sorbed species[22,23].

The limiting factor in this area at present is the reliability of the available potential energy functions needed for the calculations.

B. HIGH-RESOLUTION SOLID STATE NMR [24-26]

I. NUCLEAR SPIN INTERACTIONS IN THE SOLID STATE

The nuclear spin interactions are generally anisotropic (orientation dependent). The main interactions which can occur for a nucleus are:

- The Zeeman interaction with the magnetic field;
- Direct dipole-dipole interactions with other nuclei;
- Magnetic shielding by the surrounding electrons giving rise to chemical shift effects;
- Spin-spin or J couplings to other nuclei;
- Quadrupolar interactions which will be present for nuclei with spin > 1/2 only.

In the liquid state these interactions apart from the Zeeman interaction are averaged by fast molecular motion, whereas they have a strong effect on solid state NMR spectra, because molecules are much less mobile in the solid state than in the liquid state.

In general, the Hamiltonian which describes the total nuclear spin interaction can be written as the sum of the Hamiltonians representing the individual interactions, as in Equation [5]:

$$H = H_Z + H_D + H_{CS} + H_J + H_Q \qquad [5]$$

Table 4 shows the approximate magnitudes of the various interactions for ^{13}C nuclei both in solution and solid state. In liquids, these terms are either averaged to isotropic values or vanish, while in solid state these Hamiltonians

must be represented as being proportional to the product of the appropriate vectors and a second rank tensor which characterizes the three-dimensional nature of the interactions.

Table 4 ^{13}C Nuclear Spin Interactions in a 4.7 Tesla Field (Ref. 33)

Interaction	Hamiltonian	Magnitude in solid	Magnitude in solution
Zeeman	H_Z	50 MHz	50 MHz
Dipolar	H_D	~15 kHz	0 Hz
Chemical Shift	H_{CS}	up to 10 kHz	σ_{iso}
Scalar Coupling (^{13}C-^{1}H)	H_J	~200 Hz	~200 Hz
Dipolar coupling of Quadrupolar nuclei	H_Q	up to 1 MHz	0 Hz

For solid state NMR spectroscopy, the three most important anisotropic interactions which dominate the NMR spectra are :

a) Direct Dipole-Dipole Interaction

The dipolar interaction H_D arises from the direct dipole-dipole interaction through space between two nuclei. In the heteronuclear case, i.e. one with spin i and the other with spin j, the dipolar interaction for two isolated spins may be written as in Equation [6]

$$H_{D\,(i\text{-}j)} = \frac{\gamma_i \gamma_j \hbar^2}{r_{ij}^3} \mathbf{I} \cdot \hat{D}_{ij} \cdot \mathbf{J}, \qquad [6]$$

where r_{ij} is the internuclear distance; $\hat{D}_{ij}$ is the dipolar coupling tensor; γ_i, γ_j are the gyromagnetic ratios of the two nuclei respectively and **I**, **J** are the spin operators of the two nuclei respectively. For a single crystal with only one orientation for r_{ij}, there are two lines in the spectrum of each nucleus with the resonance frequencies given by Equation [7][17].

$$\nu = \nu_0 \pm \frac{3\ \gamma_i\gamma_j\ \hbar\ \mu_0}{2\pi\ 4\ r_{ij}^3\ 4\pi}\ (1 - 3\cos^2\theta_{ij}), \qquad [7]$$

where θ_{ij} is the angle between the internuclear vector and the magnetic field, μ_0 is the magnetic permeability constant, and ν_0 the resonance frequency in the absence of dipolar interactions for the appropriate case. Typical values for homonuclear dipolar interaction of protons are of the order of 40 kHz, while ^1H - ^{13}C heteronuclear dipolar interactions are of the order of 15 kHz[28]. In a polycrystalline sample, where there are random orientations, the spectrum shows a dipolar powder pattern, as shown in Figure 3. The dotted curve gives the powder pattern for an isolated pair of nuclei, which is called a 'Pake doublet'[27]. The full curve shows the effect of neighboring nuclei on the isolated system.

Important features of the interaction are: (1) dipolar interactions have a dependence on the magnitudes of the magnetic moments and hence they will be more important for spin 1/2 nuclei with large magnetic moments; (2) There is a very strong inverse dependence ($1/r^3$) on the internuclear distance; thus only the nearest atomic neighbors will experience a strong effect; and (3) dipolar interactions are independent of the applied magnetic field strength.

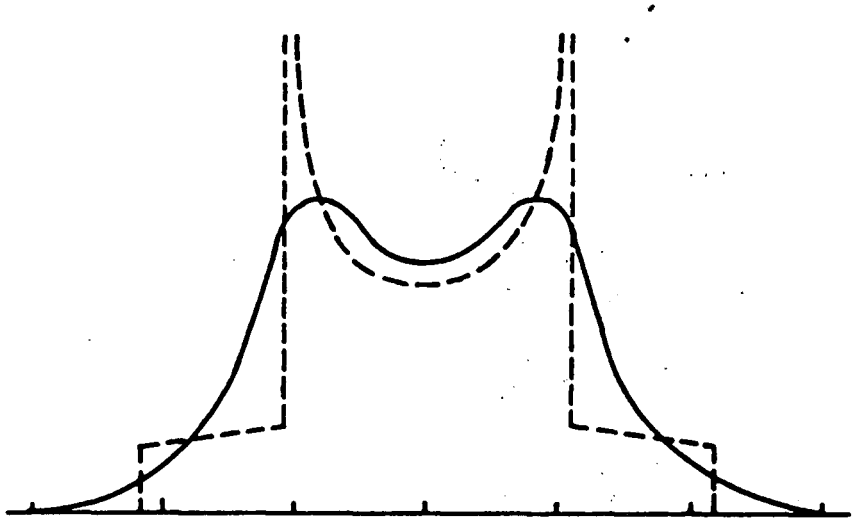

Figure 3 A powder pattern arising from dipolar coupling effects for a two-spin system. The dotted curve represents the spectrum for an isolated pair of nuclei and the full trace shows the effect of neighboring nuclei on the isolated system.(ref. 26)

b) Chemical Shift Interaction

Since the chemical shift interaction involves the surrounding electrons, it is very sensitive to the geometry and to the identities of the other atoms surrounding the nucleus being examined and is usually the most chemically diagnostic measurable in NMR studies. This interaction can be represented by Equation [8]:

$$H_{CS} = \gamma \hbar \mathbf{I} \cdot \hat{\sigma} \cdot \mathbf{B}_0 \ , \qquad [8]$$

where $\hat{\sigma}$ is the chemical shielding tensor. It is clear that the interaction is linear with the applied field $\mathbf{B}_0$ and will be more important at higher magnetic field strengths. In a single crystal, an isolated nucleus will give rise to a sharp signal whose frequency is dependent upon the orientation of the crystal with respect to the applied magnetic field. However, the spectrum of a single nucleus in a polycrystalline material will be a broad line whose exact shape depends on the principal elements of the shielding tensor. Figure 4 illustrates this orientation dependence of the chemical shift interaction.

c) Quadrupolar Interaction

The nuclear electric quadrupolar moment eQ interacts with the non-spherical field gradient around the nucleus. It is field independent and is described for a single spin $I > 1/2$ by Equation [9]

$$H_Q = \mathbf{I} \cdot \hat{Q} \cdot \mathbf{I} \ , \qquad [9]$$

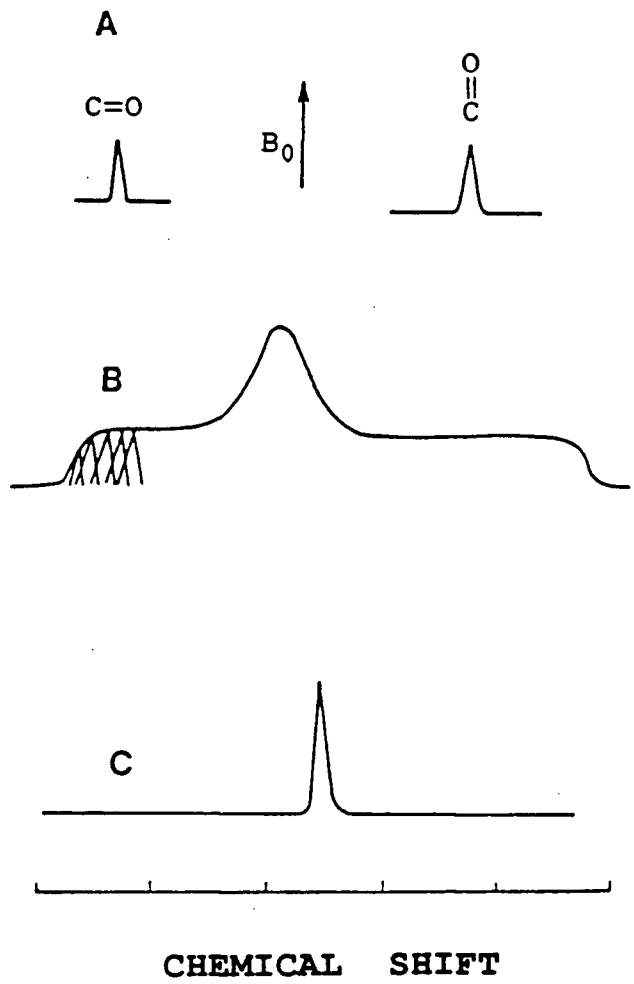

Figure 4 A schematic representation the chemical shift anisotropy: (A) A single crystal with two different orientations of the carbonyl function with respect to the magnetic field vector produces two different ^{13}C resonances. (B) A polycrystalline sample results in the superposition of peaks resulting from all possible orientations. (C) A solution shows only the isotropic average as a result of rapid molecular motion. (ref. 26)

where $\hat{Q}$ is the quadrupolar coupling tensor characterizing the three-dimensional nature of the interaction. The magnitude of the interaction is such that it usually dominates the spectra of most nuclei which have quadrupole moments.

The critical difference between solution and solid state NMR is that the rapid and random molecular motions in the liquid state produce an isotropic average of the interactions equal to 1/3 of the sum of the trace of the diagonalized matrix of their corresponding second rank tensors. Since the tensors describing the dipolar coupling and the quadrupolar interactions are traceless, their isotropic values are exactly zero. In the case of the chemical shift interaction, the traces are non-zero, resulting in discrete isotropic values for the shifts. In the solid state, however, the fundamental spin interactions lead to broad and featureless lines in the NMR spectra with linewidths of the order of a kHz or more as indicated in Table 4.

II. EXPERIMENTAL TECHNIQUES USED TO OBTAIN HIGH-RESOLUTION NMR SPECTRA OF SOLIDS

a) High Power Decoupling of Protons

For most dilute spin systems, in which the magnetically active nuclei of interest are present in low concentrations, the major line broadening interaction for the dilute spins is the heteronuclear dipolar coupling with the abundant spin system (usually protons). The local field, B_{loc}, at a nucleus i in the dilute spin system is altered by a nucleus j in the abundant spin system, as described by Equation [10]

$$B_{loc} = B_0 \pm \mu_j r_{ij}^{-3} (3 \cos^2\theta_{ij} - 1) \qquad [10]$$

where B_0 is the external magnetic field, μ_j is the magnetic moment of a nucleus j, r_{ij} is the internuclear distance, θ_{ij} is the angle between the internuclear axis and the static field, and the plus and minus signs arise because the spins which modulate the local field may be orientated with or against the applied field.

It is possible to eliminate this interaction by irradiating the abundant spin system with a strong rf field at its Larmor frequency. The effect of this decoupling irradiation is to induce rapid transitions in the abundant nuclei which cause their contribution to the effective local field to become zero on the NMR time scale. Since the interaction may be of the order of tens of kHz in the solid state, the decoupling power level has to be much higher ($\approx$ 1kW) than the relatively low decoupling power of ~5 W or less commonly used in solution NMR.

b) Magic Angle Spinning

Magic angle spinning (MAS) was first used by Andrew, and independently by Lowe, in 1959 [29,30]. MAS subjects the solid to a motion which produces to a first approximation, the same net averaging effect as a rapid isotropic molecular tumbling in solution. The basis of these experiments is the observation that most of the spin interactions have a spatial dependence of the form of $(3 \cos^2\theta - 1)$ where θ is the angle between some vector r and the magnetic field B_0. In the case of dipolar interaction, the vector r is the internuclear vector r_{ij}, and in the chemical shift interaction the vector r represents the principal axes

of the shielding tensor. If a sample is made to rotate about an axis R which is inclined to B_0 at an angle α and to the vector **r** by an angle of β (Figure 5). The average of $(3\cos^2\theta - 1)$ about the conical path indicated for the vector **r** is given in Equation [11]:[28]

$$(3\cos^2\theta - 1)_{avg.} = (1/2)(3\cos^2\beta - 1)(3\cos^2\alpha - 1) \qquad [11]$$

where the extremes of the angle θ are $\alpha+\beta$ and $\alpha-\beta$. Fortunately the angle α is under the control of the experimentalist. When $\alpha = 54.7°$, then $\cos\alpha = 1/\sqrt{3}$ and $3\cos^2\alpha - 1 = 0$, so that $(3\cos^2\theta - 1) = 0$ for all orientations (i.e. all values of θ). Therefore, the magic angle spinning technique reduces or eliminates both homonuclear and heteronuclear dipolar interactions, quadrupolar interactions to first order and yields the isotropic values for chemical shifts.

A critical feature of magic angle spinning is that the rate of rotation required to average the anisotropic interactions properly has to be greater than the static bandwidth expressed in Hz. Such speeds cannot always be achieved in practice. In this case, spinning sidebands will be present, located on each side of the isotropic chemical shift position and separated by distances equal to the spinning frequency, and broadening due to residual dipolar interactions may also be observed.

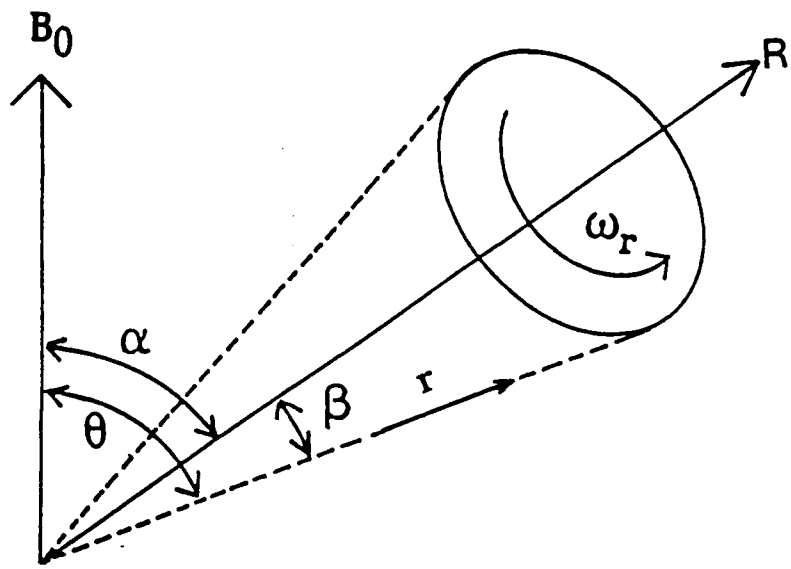

Figure 5 Schematic representation of the geometric arrangement for mechanical sample spinning: The solid sample is rotated with an angular velocity of ω_r about R which is inclined to the magnetic field by the angle α. A typical vector r is inclined at the angle β to the rotation axis. Its inclination to B_0 varies periodically with time. (ref. 28)

C) Cross Polarization (CP)

The line-narrowing techniques of dipolar decoupling and magic-angle spinning provide the resolution necessary to obtain chemical and structural information on individual dilute spins in solids. However, by their nature, dilute spin systems are of low sensitivity and some may also have extremely long relaxation times. Thus, direct one-pulse NMR experiments on dilute spin systems can be inefficient. Both disadvantages can be remedied with the help of the cross-polarization technique, first introduced by Pines, Gibby and Waugh[31,32], by which spin polarization and thus net magnetization is transferred from the abundant spins to the dilute spins in the system via the dipolar interaction, providing both signal enhancement and much shorter recycle delays. The magnetization transfer is accomplished by using the pulse sequence illustrated in Figure 6A. In this example, protons are taken as the abundant spins and ^{13}C the dilute spins. The first step is to apply an on-resonance 90° pulse to the protons, which rotates the proton magnetization along the Y' axis in the rotating frame. Then the ^{1}H magnetization is spin-locked by an on-resonance B_{1H} along Y'. At this point, a rf field, B_{1C}, is applied to the ^{13}C nuclei, with the amplitude of the B_{1C} adjusted so that the Hartmann-Hahn matching condition[34], equation [12], is fulfilled during the contact time period.

$$\gamma_H B_{1H} = \gamma_C B_{1C} \qquad [12]$$

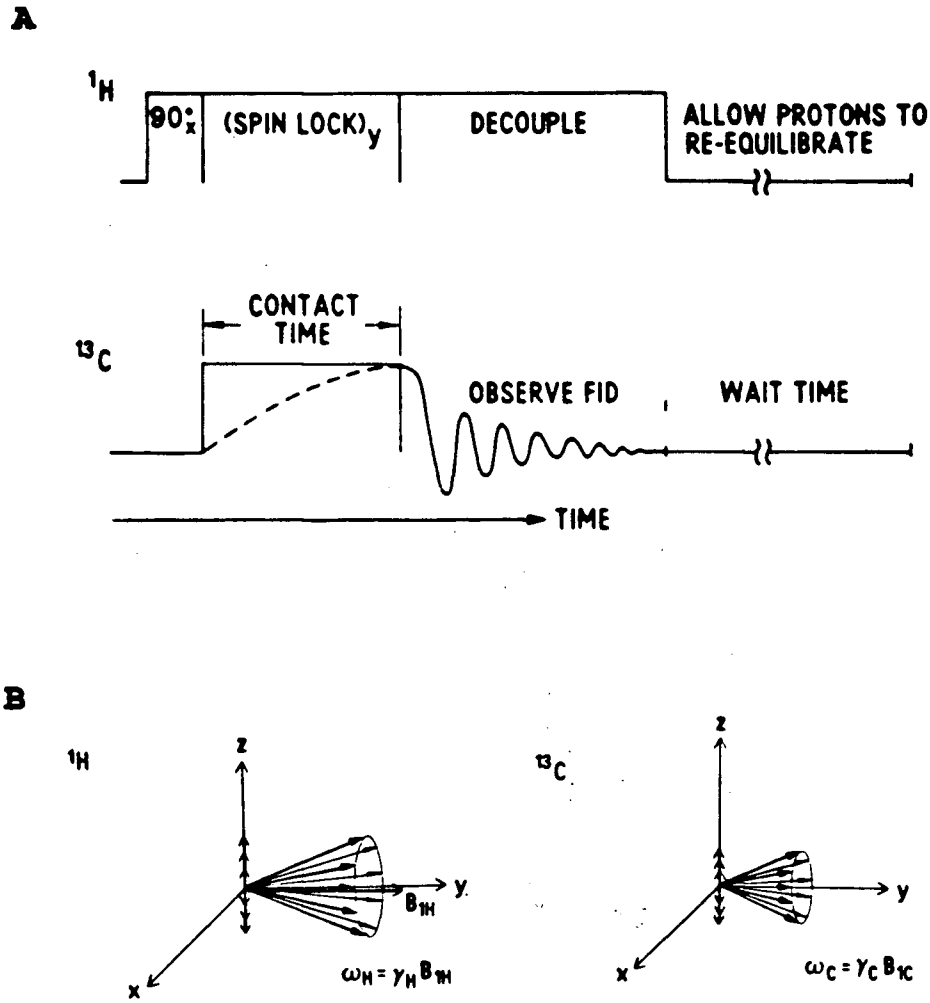

Figure 6 (A) Pulse sequence used for cross polarization to a dilute nucleus (in this case ^{13}C) from the abundant spin system(in this case ^1H).
(B) Schematic representation of ^1H and ^{13}C precessing around the spin locking fields B_{1H} and B_{1C} respectively when the Hartmann- Hahn match is achieved. (ref. 36)

This 'matching' condition means that, in their respective rotating frames, the protons and the ^{13}C nuclei both precess at equal rates in the spin locking fields and the energy required for spin flips between α and β states is identical for both spins, allowing a rapid transfer of magnetization (Figure 6B). Therefore, this 'spin-contact' results in the growth of ^{13}C-nucleus magnetization, since the protons are much more abundant. At the end of the contact time, the B_{1C} field is switched off and the free induction decay (FID) of the ^{13}C signal is recorded, while the B_{1H} field is maintained during this period for proton decoupling. The entire sequence is repeated many times until a suitable signal to noise ratio is achieved.

The use of the cross-polarization technique increases the sensitivity of the dilute nuclei in two ways. Firstly, there is a maximum enhancement of the X nuclear magnetization equal to the ratio of the magnetogyric ratios of the abundant and rare spins, γ_H/γ_X ($\gamma_{1H}/\gamma_{13C} \approx 4$). Secondly, since the X nucleus signal is generated from the proton magnetization, the rate at which the experiment may be repeated is determined only by the spin-lattice relaxation rate of the ^1H nuclei rather than the generally much longer X nuclei relaxation time. Thus, the recycle time can be much shorter than for a simple 90° pulse experiment on the X nuclei, resulting in a much better signal-to-noise ratio in a given time period.

Schaefer and Stejskal[35] were the first to combine MAS, CP and high-power decoupling techniques to obtain high-resolution solid- state spectra. To illustrate the effects of these different techniques, ^{13}C NMR experiments under a variety of conditions on bisphenol-A (4, 4'- dihydroxydiphenyl- 2, 2'-dimethylpropane) are presented in Figure 7. Figure 7a shows the spectrum of a

static sample obtained with a simple 90° pulse experiment. It is broad (ca. 15 kHz at the baseline), but shows some structure because of the large difference in chemical shift between aromatic and aliphatic carbons. In 7b proton decoupling and cross polarization are applied but without sample spinning. The aliphatic carbons show a discernible axially symmetric anisotropy patten, but the aromatic carbons give rise to a very broad, low intensity resonance. Figure 7c shows the spectrum obtained with magic angle spinning but without decoupling or cross polarization. The chemical shift anisotropy has been removed completely, but the dipolar broadening only partially. Figure 7d presents the high-resolution spectrum obtained by simultaneously using all three techniques. The small peaks labeled 'sb' are due to spinning sidebands.

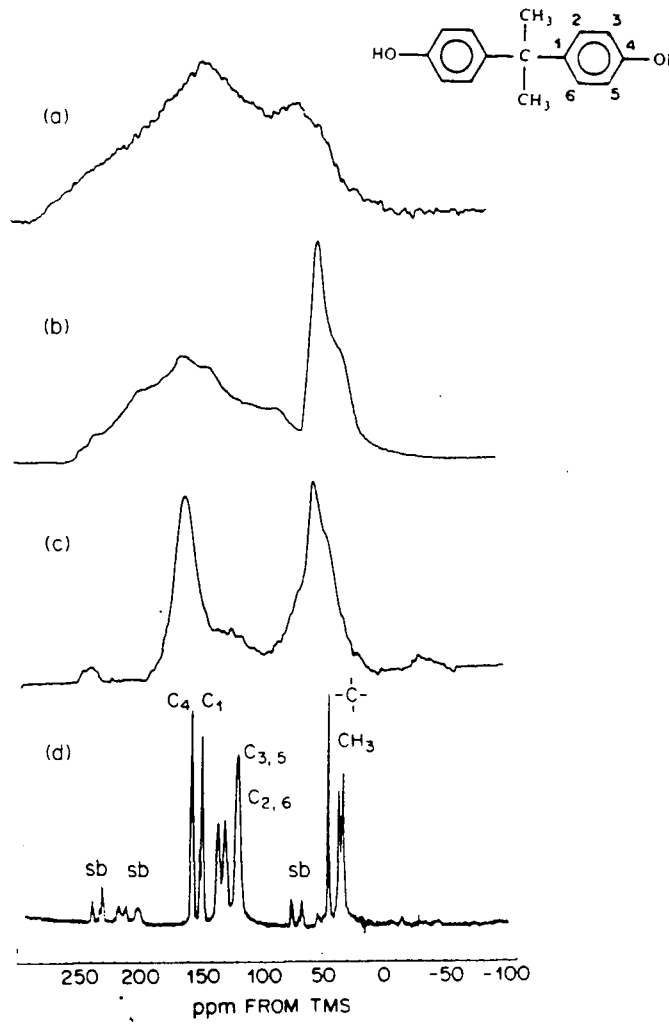

Figure 7 The 50.3 MHz ^{13}C solid state NMR spectra of bisphenol A. (a) Nonspinning and with no proton decoupling and cross polarization, (b) nonspinning but with proton dipolar decoupling and cross polarization, (c) with magic angle spinning but without decoupling and cross polarization, (d) with magic angle spinning, dipolar decoupling, and cross polarization. (ref.36)

C. HIGH RESOLUTION ^{29}SI SOLID STATE NMR STUDIES OF ZEOLITE STRUCTURES

I. INTRODUCTION

The importance of zeolites as catalysts, molecular sieves and ion-exchangers has been discussed in Section A. The properties of a particular zeolite are mainly dependent on the topology of its framework and the size of its free channels. Therefore, detailed structural information is critical in order to understand the sorptive and catalytic properties of zeolites[2-4]. Nuclear magnetic resonance spectroscopy is well suited as a technique to investigate the structure of zeolites as they are composed of elements which have NMR active isotopes such as ^{29}Si, ^{27}Al and ^{17}O. The use of various line-narrowing techniques, as discussed in Section B make high-resolution solid state NMR an important complementary technique to diffraction studies for the investigation of the structures of zeolites. Since there are no framework hydrogen atoms in pure zeolites, high power proton decoupling is not needed and the CP cannot be used. The experiment is thus reduced to a simple 90° pulse sequence with MAS and may be easily performed using a conventional high resolution spectrometer[26]. In the case of zeolites with sorbed molecules or templates, CP and high power decoupling can sometimes be used to discriminate between phases with mobile and immobile components. For zeolites with immobile sorbates, ^{29}Si CP MAS NMR experiments can be very efficient [37].

II. STRUCTURAL INFORMATION AVAILABLE FROM ^{29}SI AND ^{27}AL NMR STUDIES

a) Determination of the Composition of the Low Si/Al Aluminosilicate Frameworks

The first application of high resolution ^{29}Si NMR spectroscopy to the investigation of zeolites was made by Lippmaa and Engelhardt,[38] and they showed[39] that up to five peaks should be observed for ^{29}Si spectra of zeolites, corresponding to the five possible Si environments: $Si(OAl)_4$; $Si(OAl)_3(OSi)$; $Si(OAl)_2(OSi)_2$; $Si(OAl)(OSi)_3$ and $Si(OSi)_4$, based on ^{29}Si MAS NMR studies of minerals of known structure. The characteristic ranges of these isotropic chemical shifts could be defined as shown in Figure 8. A particularly important application is that the Si/Al ratio of the lattice can be calculated directly from the ^{29}Si spectra. When (1) a ^{29}Si spectrum is correctly interpreted in terms of Si(nAl) units, (2) assuming Loewenstein's Rule [41], which postulates that no Al-O-Al linkages are present, and (3) there is no appreciable shift dispersion due to crystallographically inequivalent sites, it is possible to calculate the Si/Al ratio of the sample from the ^{29}Si spectrum alone . In the absence of Al-O-Al linkages, the environment of every Al atom is Al(4Si). Each Si-O-Al linkage in a Si(nAl) unit therefore incorporates 1/4 Al atom, and the whole unit n/4 Al atoms. The Si/Al ratio in the aluminosilicate framework is given by Equation [13]

$$\frac{Si}{Al} = \frac{\sum_{n=0}^{4} I_{Si(nAl)}}{\sum_{n=0}^{4} 0.25 n I_{Si(nAl)}} \qquad [13]$$

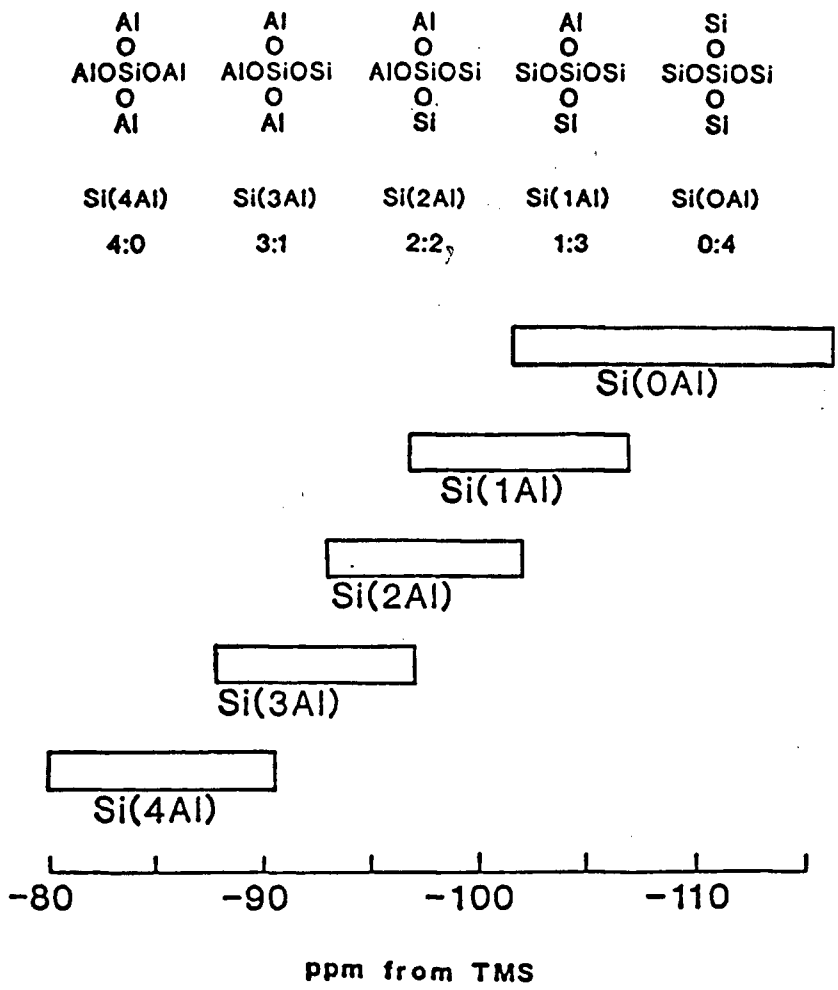

Figure 8 ^{29}Si chemical shift ranges of the five possible local silicon environments in aluminosilicates. (ref. 42)

where $I_{Si(nAl)}$ is the intensity of the NMR signal attributable to Si(nAl) units. Equation [13] is valid for all zeolites provided the assumptions made in its derivation are justified. Figure 9 shows ^{29}Si NMR spectrum of a series of faujasite zeolites with identical structures but different Si/Al ratios determined by the X-ray fluorescence (XRF) technique. The numbers above the resonances indicate the numbers of Al atoms connected to the silicon atom of the resonance. The spectra have been simulated by a computer program using Lorentzian peak shapes and are shown to the right of the spectra. The silicon to aluminum ratios calculated using Equation [13] are also shown in the figure and are in good agreement with those measured by XRF. As the Si/Al ratio increases, there is a corresponding increase in the relative intensities of the high-field peaks. A particular advantage of this method of calculating the Si/Al ratio compared with chemical or XRF analysis is that it only detects framework Al atoms, whereas the others will include both framework Al and also Al occluded in the cavities and channels and even outside the particles.

b) Coordination Number of Al

^{27}Al MAS NMR is capable of quantitatively distinguishing between tetrahedrally and octahedrally coordinated aluminum whose resonances are clearly separated with chemical shift ranges of about +50 to +80 ppm for AlO_4 and about -10 to +20 ppm for AlO_6 with respect to $Al(H_2O)_6^{3+}$. The ^{27}Al NMR spectrum of zeolite Y after dealumination is presented in Figure 10. The resonance at 60 ppm corresponds to the tetrahedrally coordinated Al of the framework. The other signal at about 0 ppm belongs to octahedral Al species extracted from the lattice by dealumination processes. Thus, ^{27}Al MAS NMR spectra can be used to monitor dealumination and also realumination processes.

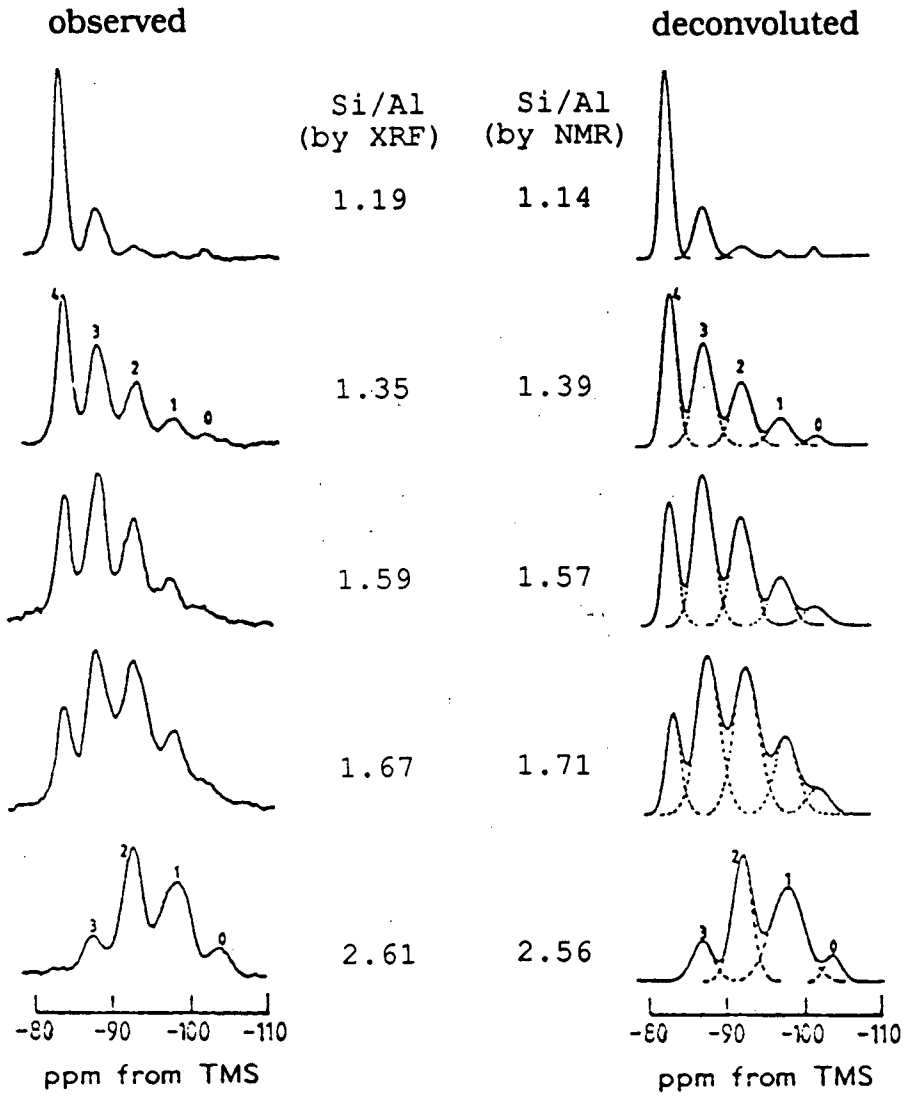

Figure 9 Observed and deconvoluted ^{29}Si MAS NMR spectra of a series of faujasite zeolites with various Si/Al ratios obtained from both XRF and XRD techniques. (ref. 40)

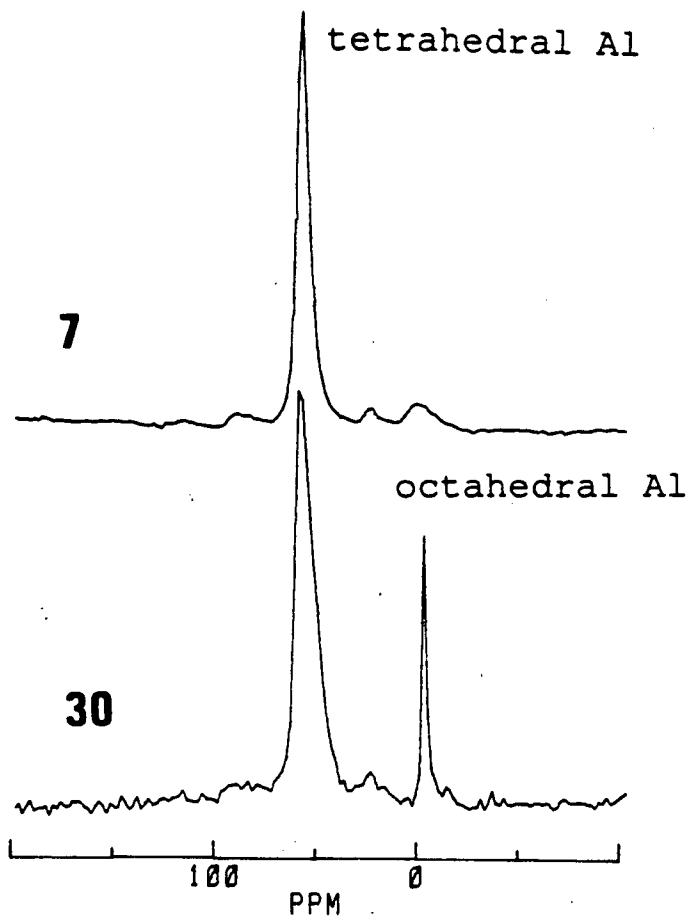

Figure 10 ^{27}Al MAS NMR spectra of Zeolite Y samples with the Si/Al ratios indicated. (ref. 43)

c) Highly siliceous zeolites

In the ^{29}Si MAS NMR spectra of highly siliceous zeolites, where the Al content is so low that it does not affect the ^{29}Si spectrum, sharp resonances are observed whose numbers and relative intensities reflect the numbers and relative populations of the crystallographically inequivalent sites in the unit cell and whose frequencies reflect the local geometries of the T-sites. A great deal of information can be obtained from high resolution ^{29}Si MAS NMR spectra of highly siliceous zeolites[44], which relate directly to the results of X-ray diffraction experiments.

These experiments may be used to:

i) Solve lattice structure problems in terms of determining the correct space groups by combining the NMR data with XRD information. Until recently, conventional powder X-ray diffraction has been the primary tool for the determination of the structures of zeolites. However, small changes in lattice symmetry related to subgroup-supergroup relationships are often difficult to observe using powder XRD techniques because of the adverse affects of small crystallite size on X-ray peak widths, which can correspond to large atom positional errors in a refined crystal structure. In contrast, ^{29}Si solid state NMR is very sensitive to local environments and can act as a very sensitive probe of the unit cell contents at the atomic level. Thus, high resolution ^{29}Si MAS NMR is an ideal technique to examine the correctness of the lattice structures proposed by XRD studies[45]. For example, the ^{29}Si MAS NMR spectrum of zeolite ZSM-12 (see Chapter Four) shows seven narrow resonances of exactly equal intensity indicating seven inequivalent T-sites in the asymmetric unit. This is in

agreement with the structure proposed by La Pierre et al [46]. However, synchrotron X-ray data collected recently indicate a doubling of the c- cell dimension parameter from 12.16Å to 24.33Å, the others being unaffected. The systematic extinctions led to two possible space groups, Cc and C2/c, which have respectively 14 and 7 symmetrically inequivalent T-sites of equal occupancies. The ^{29}Si MAS NMR spectrum of the same sample that was used for the XRD experiment shows seven resonances of equal intensity, unambiguously leading to the space group symmetry C2/c. The structure refinement based on this space group was successfully carried to an R factor of ~5.4% with all lengths and angles within reasonable limits [47].

ii) Study the effect of sorbates and elevated temperatures on the structures of zeolites[48-49]. The effect of temperature and the presence of sorbed organic species can induce phase transformations in some zeolites, e.g. ZSM-5 and ZSM-11, which result in changes in pore geometries , distributions of T-atoms and catalytic properties.

iii) Act as a 'fingerprint' to identify zeolites. This is based on the fact that ^{29}Si NMR spectra of a zeolite from different sources are usually similar and characteristic. Thus, it has been demonstrated by Fyfe and co-workers[50] that the series of zeolites KZ-2, ZSM-22, θ-1 and NU-10, which are prepared under different hydrothermal conditions from different reaction mixtures and using quite different templates, all have the same structure (Figure 11).

iv) Yield information on the nature of the interactions between the host zeolite framework and sorbed organic molecules. The ^{29}Si MAS NMR spectra of ZSM-5 loaded with *p*-xylene, *p*-chlorotoluene and *p*-dichlorobenzene are almost

identical (Figure 12), which indicates that, at least for hydrocarbons in this system, the molecule-lattice interactions are mainly based on size and shape alone [51].

The amount of information which can be obtained from these spectra depends ultimately on the resolution of the spectra. In turn, the resolution depends on the degree of crystallinity and perfection of local ordering of the completely siliceous sample examined and care in setting up and running the NMR experiments, as will be discussed in Chapter Two.

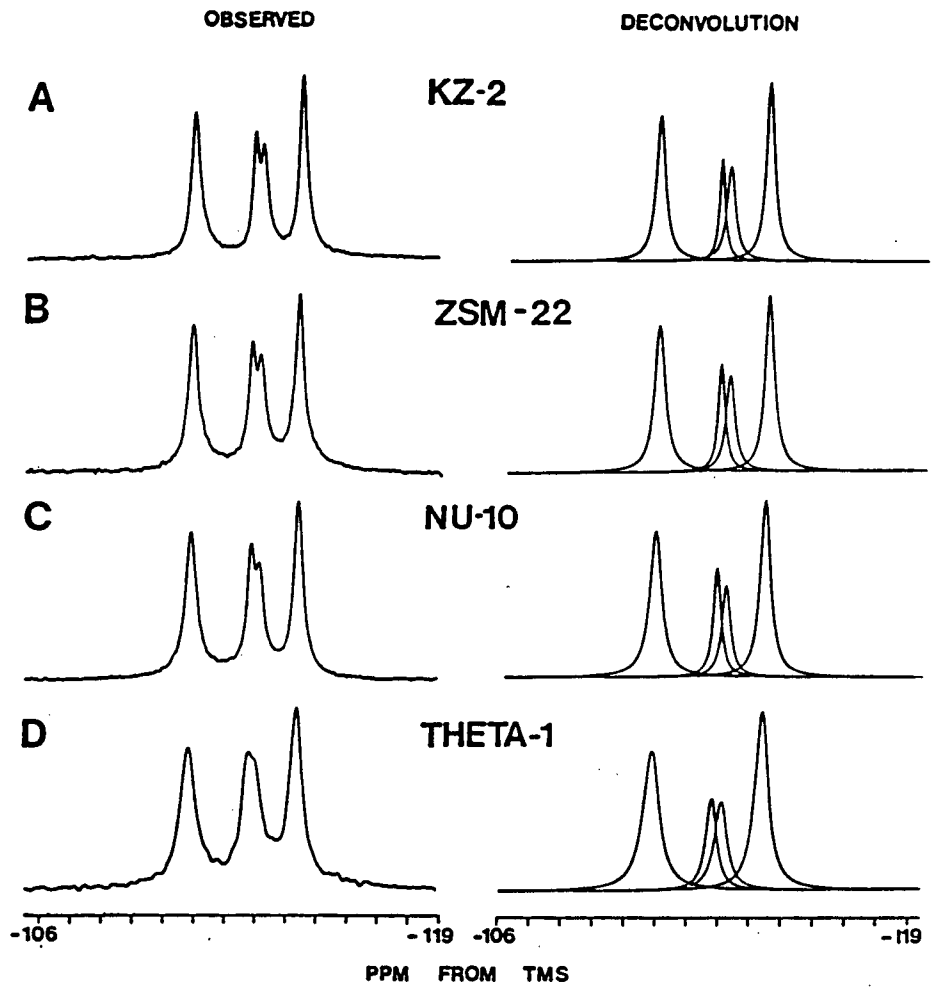

Figure 11 Observed and deconvoluted ^{29}Si MAS NMR spectra of: (A) KZ-2; (B) Zeolite ZSM-22; (C) NU-10; (D) Theta-1. (ref. 50)

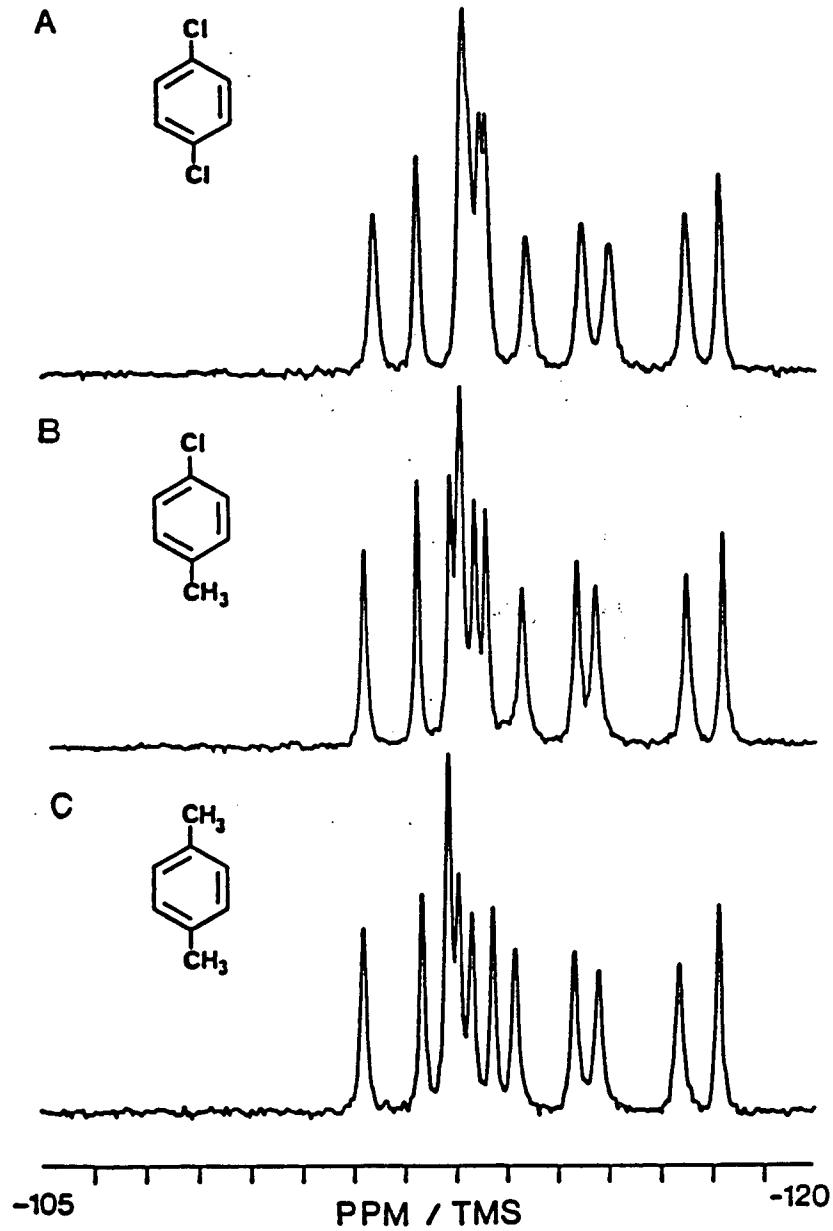

Figure 12 ^{29}Si MAS NMR spectra of Zeolite ZSM-5 loaded with (A) *p*-dichlorobenzene; (B) *p*-chlorotoluene; and (C) *p*-xylene. (Ref. 51)

CHAPTER TWO

TWO-DIMENSIONAL SOLID STATE NUCLEAR MAGNETIC RESONANCE SPECTROSCOPY

A. TWO-DIMENSIONAL (2D) NMR SPECTROSCOPY[52-56]

I. BASIC CONCEPTS

Two-dimensional NMR was first proposed conceptually in 1971 by Jeener [57], and there has been a very rapid growth in recent years in high-resolution NMR applications of these techniques in solution since Ernst and co-workers discussed and illustrated various possibilities for their application [58-60]. The common feature of one-dimensional NMR experiments is the timing sequence, "preparation - evolution - detection", as shown in Figure 13A. During the preparation period, the spins are first allowed to come to equilibrium, and then are perturbed by one or more rf pulses at the end of this period to initiate the NMR experiment. During the evolution time, t_1, the x, y, and z components of the spins evolve under all the forces acting on the nuclei. A signal (FID) is then detected as a function of time, S(t). The process of Fourier transformation converts this time-dependent function into a frequency-dependent one, S(F). In the most common one-dimensional NMR experiment, the evolution time t_1 is zero and acquisition immediately follows the single pulse preparation. However, there are a number of other experiments where a finite evolution

period is inserted. The inversion-recovery experiment for measuring spin-lattice relaxation time T_1 can be used as an example to demonstrate the function of the evolution period. The pulse sequence and vector diagrams for the magnetization of a nucleus are shown in Figure 13B. The z magnetization M_0 (Fig 13B, a) is inverted by a 180° pulse (b). This magnetization then begins to grow back through zero toward its equilibrium value due to the Zeeman interaction, as shown at (c). To sample this regrowth of the z magnetization, the magnetization vector is turned by a 90° pulse to the y′ axis (d) at the end of the evolution time t_1 and detected. Figure 14 displays a series of ^{29}Si MAS spectra of zeolite ZSM-12 obtained using this pulse sequence. For each experiment, the evolution time t_1 is indicated in the figure.

With 2D NMR spectroscopy, the evolution time, t_1, is also a variable. The timing sequence is shown in Figure 15A. The mixing period can consist of pulses and delays with fixed lengths or may be absent. The other three periods have the same meanings as in the 1D experiment. The evolution time in 2D experiments is linearly incremented by a constant amount in a series of experiments keeping all other parameters constant. Thus the received signal becomes dependent on the time period t_1 as well as on t_2, and the data can be arranged in a two dimensional matrix, $S(t_1, t_2)$. This data matrix is composed of n rows and k columns, where k is the number of data points collected during the acquisition time and n is the number of experiments performed with different values of t_1. Then, all rows or FID's are Fourier transformed, yielding a $S(t_1, F_2)$ data matrix, which is transposed to $S(F_2, t_1)$ matrix. Each row of $S(F_2, t_1)$ data matrix gives the time evolution for the corresponding point in F_2 or t_2, referred to as an 'interferogram'. The second set of Fourier transformations leads to a $S(F_2, F_1)$

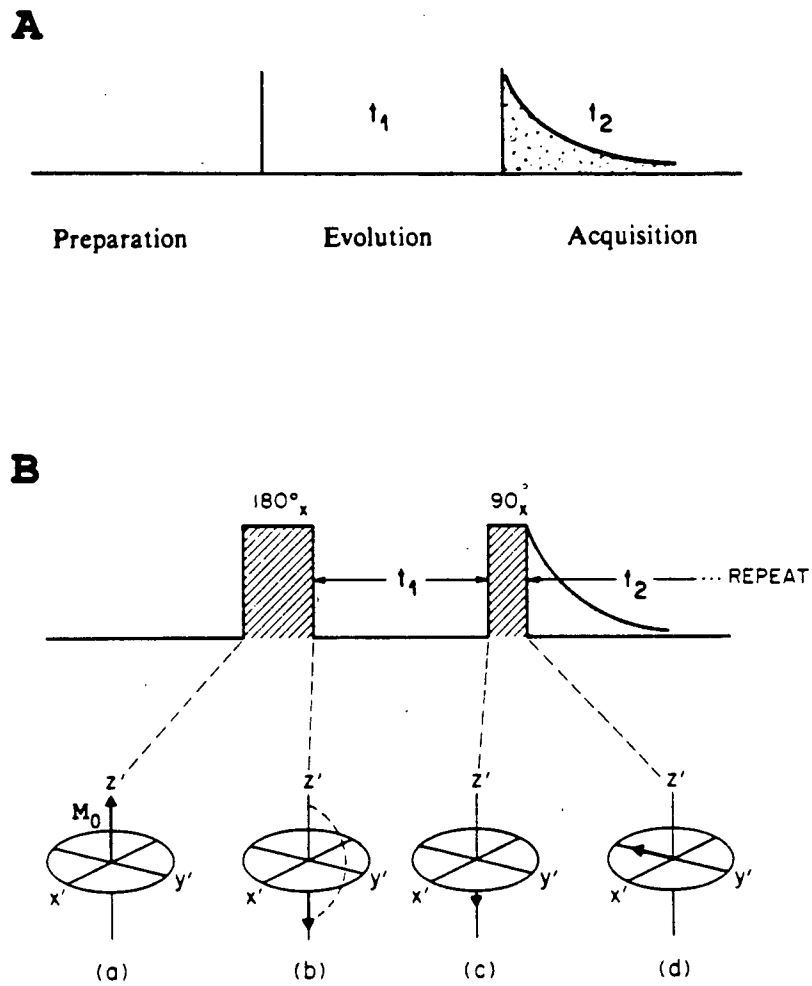

Figure 13 (A) Time sequence of one dimensional NMR experiment. (ref. 53)
(B) The inversion-recovery pulse sequence for measurement of T_1 and vector representation. (ref. 61)

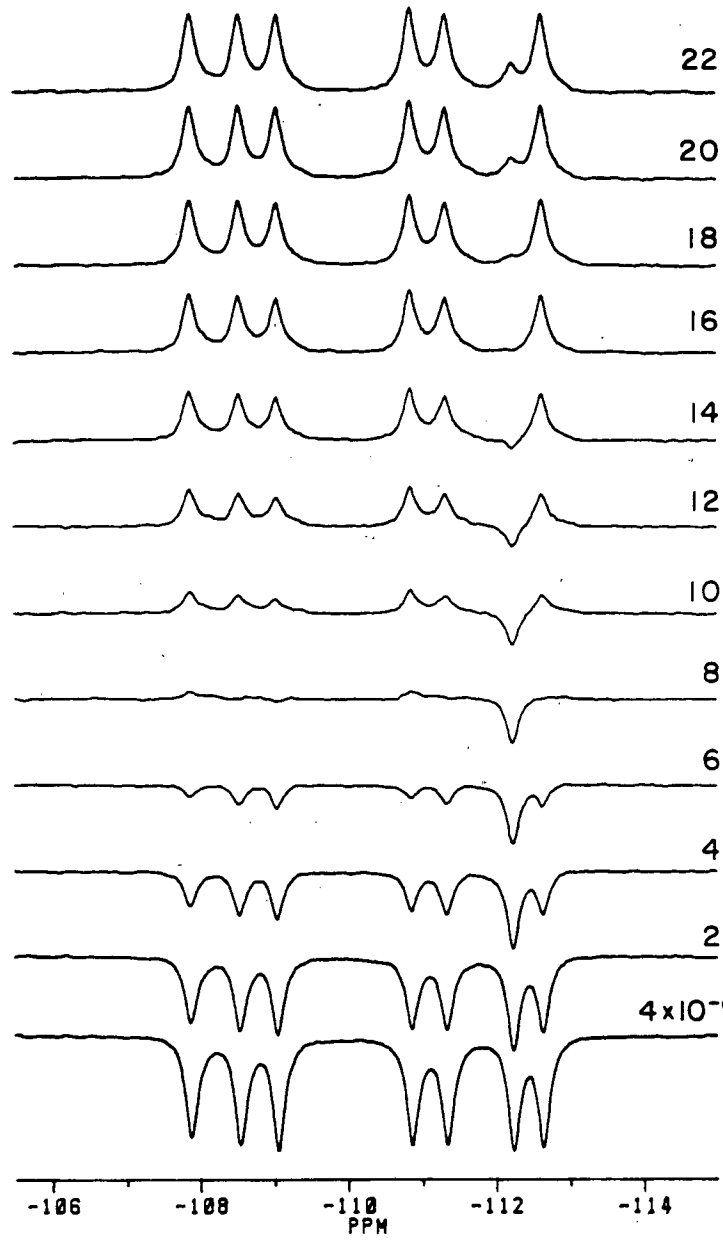

Figure 14 Vertical stacked plot of ^{29}Si MAS NMR spectra of zeolite ZSM-12 from an inversion-recovery experiment for the measurement of T_1. Spectra were obtained at 79.5 MHz with 28 scans for each experiment, using a 120 second recycle delay. The corresponding values of t_1 in seconds are indicated.

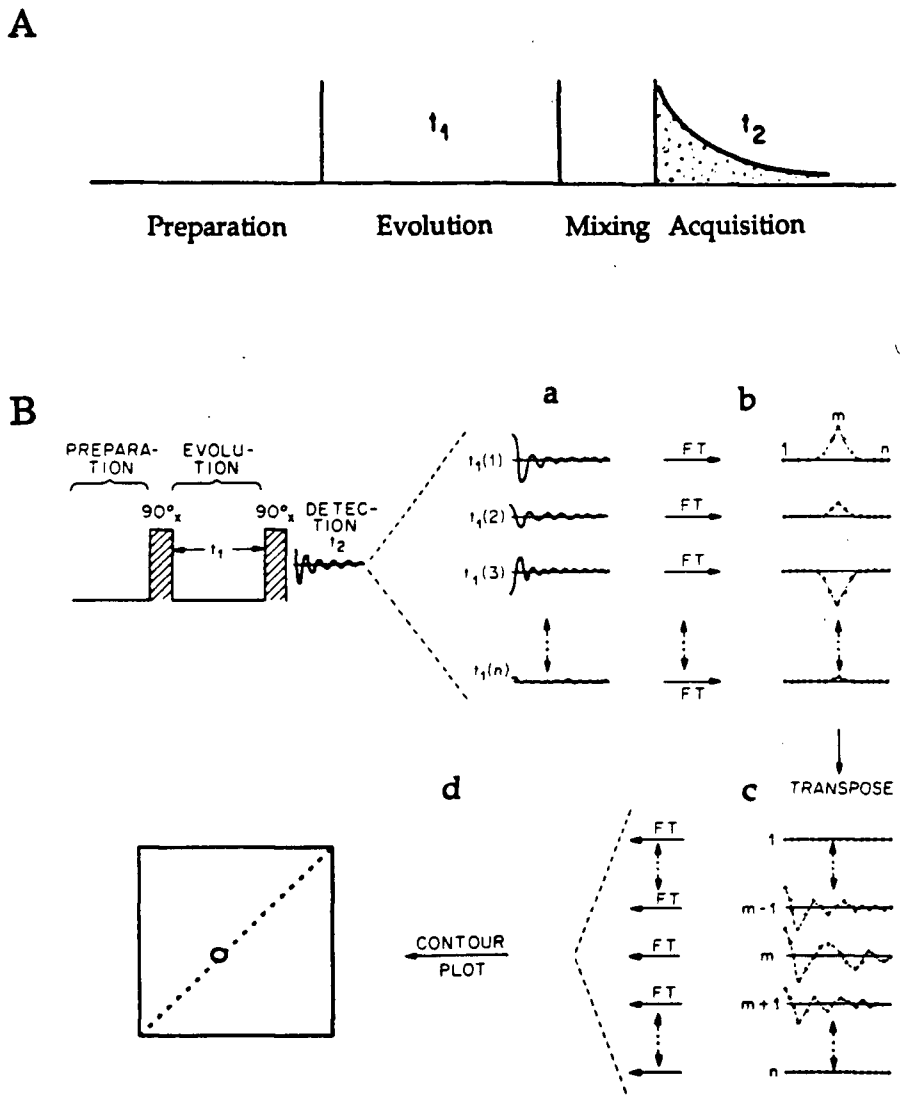

Figure 15 (A) Timing sequence of two dimensional NMR experiment. (ref. 53)
(B) Schematic representation of the steps involved in obtaining a 2D NMR spectrum. a) A number of FIDs are recorded with incremented values of the evolution time t_1. b) Each of the FIDs is subjected to Fourier transformation and a $S(t_1, F_2)$ data matrix is obtained. c) The data $S(t_1, F_2)$ is transposed to give a data set of $S(F_2, t_1)$. d) A second series of Fourier transformation is carried out and the final data is represented as contour plot. (ref. 36)

data set and is followed by a transposition, to obtain the final data matrix $S(F_1, F_2)$. The formation of a 2D spectrum is schematically represented in Figure 15B using the COSY (COrrelation SpectroscopY) experiment as an example. This pulse sequence will be discussed in Section IV. In a COSY experiment, both frequency domains contain the information on chemical shift. The number of rows and columns are usually made to be equal by adequate zero filling, forming a square data matrix. For a single resonance as the case in Figure 15B, the plot shows only one signal on the diagonal. In weakly-coupled spin systems, the 2D COSY experiment plots will show both diagonal and cross peaks, which display the J-coupled network of the spin system (see Section IV).

2D NMR spectroscopy is usually possible if a systematic variation in the evolution period results in a periodic change of phase and/or amplitude of the spin system at the end of the evolution time. Each peak in the chemical shift spectra formed in the first Fourier transformation may have one or more component modulation frequencies or none at all. Then the second transformation process can determine the frequencies of the modulations, resulting in a 2D spectrum displaying intensity as the third dimension. The spreading of the NMR spectrum in a second orthogonal direction gives increased spectral resolution and provides additional information.

II. DATA REPRESENTATION

a) White-Washed Stacked Plots

A white-washed stacked plot of a COSY experiment on Zeolite ZSM-39 is shown in Figure 16A. In this form, each successive spectral trace is plotted by keeping track of the vertical deflection of each point in previous traces. This

kind of plot gives a good impression of the three-dimensional nature of the data, and particularly the relative peak intensities, but it is not readily interpreted when some peaks are obscured by others.

b) Contour Plots

Contour lines are drawn through points of equal intensity and define the shape of resonances. Intensity information is indirectly portrayed in the numbers of contour levels. Figure 16B shows a contour plot from the same data set as Figure 16A. Obviously, the relationships in the frequency information are displayed more clearly. Thus, contour plots are often the preferred method of 2D NMR presentation.

c) Projections

Projections are one-dimensional 'spectra' created by recording the highest intensity level of each data point along a given axis and provide a useful means of portraying the information of a contour plot. The corresponding projections on the two frequency axes are shown flanking the contour plot in Figure 16B.

d) Cross Sections

In practice, the peaks with the crucial information lie on a limited number of cross sections in the 2D spectrum. The cross sections required are parallel to one of the main frequency axes, and it is often very useful to plot these different traces as separate one- dimensional "spectra". Figure 16C shows three spectra which correspond to the cross sections indicated in Figure 16B.

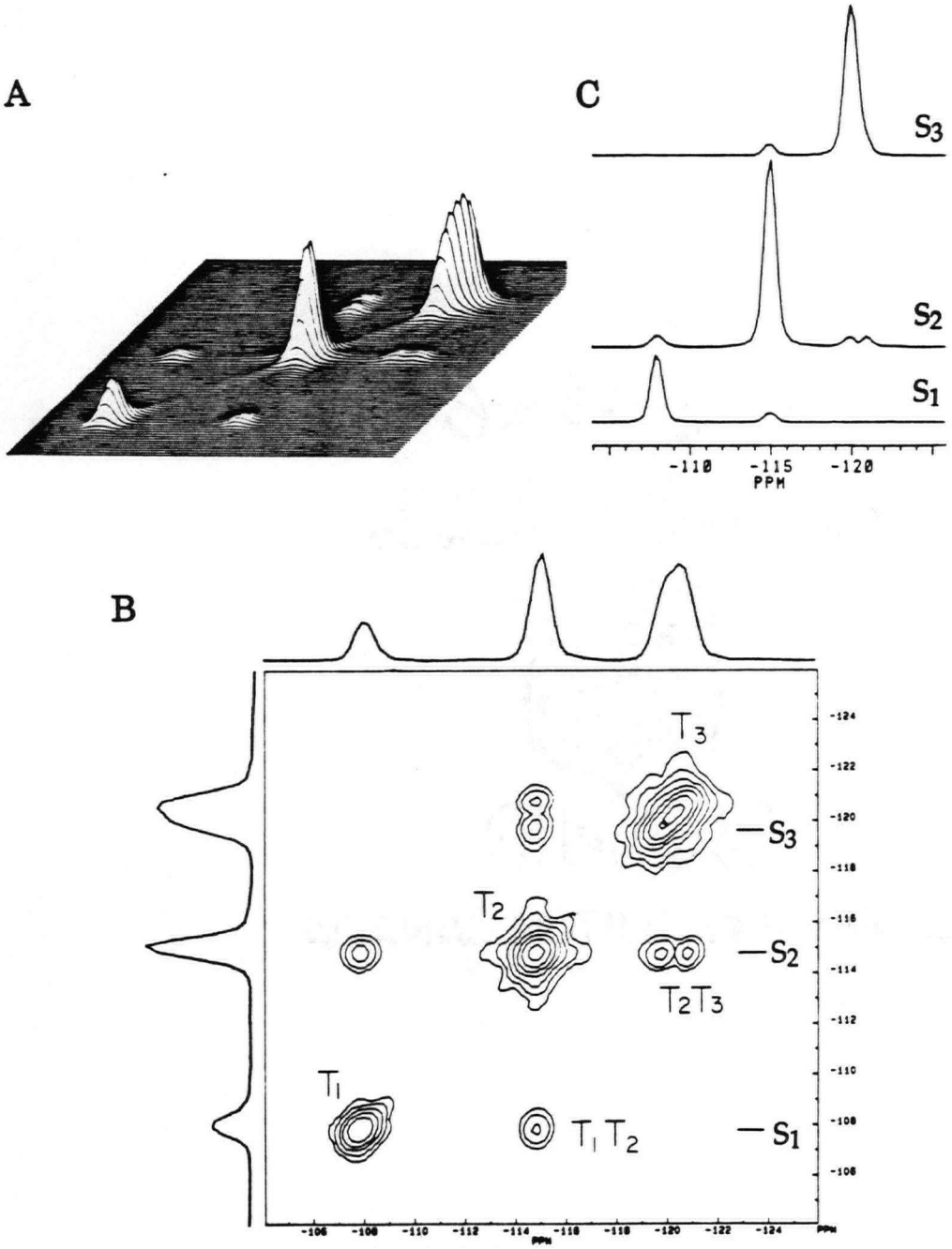

Figure 16 The representation of a 2D COSY experiment on zeolite ZSM-39 (see Chapter Three).
(A) A white-washed stacked plot.
(B) A contour plot with the projections in both dimensions.
(C) Three cross sections in the positions indicated in the contour plot.

III. CLASSIFICATION OF 2D SOLUTION NMR EXPERIMENTS

Two main categories of 2D NMR experiments which can be distinguished by their objectives have emerged from solution NMR studies:

a) Chemical Shift Correlation NMR Spectroscopy

This class of experiments uses interactions between groups of nuclei to establish correlations between them. Both frequency axes represent the chemical shift. The most common interactions used are:

- scalar coupling
- chemical exchange
- dipolar coupling (cross relaxation)
- multiple quantum coherence: 2D NMR experiments facilitate the detection and enlarge the applicability of multiple quantum transitions, which in general are not detected in simple 1D NMR experiments.

b) J-Resolved NMR Spectroscopy

In two-dimensional J-resolved spectra, the two parameters, coupling constant J and chemical shift δ, are separated along the two frequency axes. Therefore, multiplets which overlap in the conventional 1D spectrum are resolved in the 2D J-spectrum allowing chemical shifts and coupling constants to be measured readily and independently.

In all of these different experiments, the resultant spectrum is a map of interactions among spins. The position of a signal on the two dimensional map shows both the chemical shift of that signal, and an additional piece of information which depends on the nature of the interaction shown in F_1. Table 5 shows some examples of these two classes of experiments.

Table 5 Classification of Some 2D NMR Experiments (Ref. 53)

2D NMR Experiment		Interaction	Name	Variable	
				F_1	F_2
Shift Correlation	Homonuclear	J-Coupling	COSY	δ(X)*	δ(X)
		Chemical exchange	NOESY	δ(X)	δ(X)
		Dipolar coupling	NOESY	δ(X)	δ(X)
		Double quantum	INADEQUATE	δ(X)	DQF**
	Heteronuclear	J-Coupling	HETCOR	δ(^{1}H)	δ(Y)
		Dipolar Coupling		δ(^{1}H)	δ(Y)
J-resolved	Homonuclear	J-Coupling		J(^{1}H,^{1}H)	δ(^{1}H)
	Heteronuclear	J-Coupling		J(Y,^{1}H)	δ(Y)

* Nucleus X can be ^{1}H or any other nucleus Y.
** DQF stands for double quantum frequency.

IV. HOMONUCLEAR CHEMICAL SHIFT CORRELATION SPECTROSCOPY

a) Introduction

The main goal of the present work is to exploit the application of homonuclear chemical shift correlation experiments to determine the connectivities of T-atoms in zeolites in order to investigate the structures of their frameworks. For understanding the information derived from these experiments and performing the experiments efficiently, a brief description of the pulse sequences will be presented in this section.

There are three approaches commonly used to explain 1D and 2D NMR pulse experiments:

i) Classical or semiclassical vector models (see Figure 13B)[53]. This approach is satisfactory to describe many experiments, including spin-echoes and T_1 measurements. It is simple and provides a pictorial explanation, but has severe limitations for describing more sophisticated techniques, for example, COSY-type and multiple quantum coherence experiments.

ii) Density matrix formalism [62,63]. This quantum mechanical approach deals with the whole state of the spin system rather than the observable magnetization in the case of vector models. It provides a complete understanding of the pulse sequences, yet tends to be tedious for more than two coupled spins.

iii) Product operator formalism (POF) [64,65]. This method follows a middle course, which is founded on density operator theory but retains the intuitive concepts of the vector models. This approach will be adopted to analyze some homonuclear correlation experiments.

In density matrix theory, the state of a spin system is expressed by the density operator $\sigma(t)$. If relaxation is disregarded, the time evolution of the density operator is described by the Liouville-von Neumann equation:

$$\frac{\partial \sigma}{\partial t} = -i[H(t),\sigma(t)] , \qquad [14]$$

where H represents the Hamiltonian, including chemical shift terms, coupling terms and the interaction with the external rf field. The time evolution can be expressed by Equation [15]:

$$\sigma(t)= \exp\{-iHt\}\ \sigma(0)\ \exp\{+iHt\} \qquad [15]$$

The observable magnetization components can be evaluated from the trace relationship:

$$M_y(t) \propto Tr\{I_y\ \sigma(t)\} , \qquad [16]$$

where M_y is observable magnetization (suppose that the signal is detected along the Y axis) and I_y is the observable operator.

For the evaluation of Equation [16] The density operator σ may be expressed as a linear combination of base operators B_s:

$$\sigma(t) = \Sigma\ b_s(t)\ B_s , \qquad [17]$$

where $b_s(t)$ is the coefficient, so that the time dependence of $\sigma(t)$ is expressed in the coefficient $b_s(t)$. The complexity of such calculations greatly depends on the choice of the base operators B_s. In product operator formalism, the product operators are used as base operators, as shown in Equation [18].

$$B_S = 2^{(q-1)} \prod_{k=1}^{N} (I_{kv})^{a_{ks}} \qquad [18]$$

where I is a single spin operator, N is the total number of spin-1/2 nuclei in the spin system, k is the index of nucleus, v stands for the spatial coordinates, x, y or z, and q is the number of single spin operators used in the product; a is equal to 1 for q nuclei and 0 for the N-q remaining nuclei.

This choice greatly simplifies the interpretation of pulse experiments, because the destiny of individual operator terms can be followed throughout the experiment. Thus, POF deals with the time evolution of individual product operator terms instead of the state of the spin system. The important transformations of product operators can be obtained by using equation [15], under the conditions of a weakly-coupled two spin system and ignoring relaxation processes, and are presented in Table 6.

Table 6 Important Transformations of Product Operators (Ref. 65)*

Pulses	Chemical Shifts
$I_z \xrightarrow{\beta_{y,x}} I_z \cos\beta \pm I_{x,y} \sin\beta$	$I_z \xrightarrow{\Omega t I_z} I_z$
$I_{x,y} \xrightarrow{\beta_{x,y}} I_{x,y}$	$I_{x,y} \xrightarrow{\Omega t I_z} I_{x,y} \cos\Omega t \pm I_{y,x} \sin\Omega t$
$I_{x,y} \xrightarrow{\beta_{y,x}} I_{x,y} \cos\beta + I_z \sin\beta$	

Scalar Coupling

$$I_z \xrightarrow{\pi J t 2 I_{kz} I_{lz}} I_z$$

$$2I_{kx}I_{ly} \xrightarrow{\pi J t 2 I_{kz} I_{lz}} 2I_{kx}I_{ly}$$

$$I_{kx,ly} \xrightarrow{\pi J t 2 I_{kz} I_{lz}} I_{kx,ly} \cos\pi J t \pm 2I_{ky,lx} I_{lz} \sin\pi J t$$

$$2I_{kx,ly}I_{lz} \xrightarrow{\pi J t 2 I_{kz} I_{lz}} 2I_{kx,ly}I_{lz} \cos\pi J t \pm I_{ky,lx} \sin\pi J t$$

* Here β represents the tip angle and J the coupling constant between spin k and l.

b) COSY (chemical shift COrrelation SpectroscopY) experiments

The basic COSY experiment consists of two 90° pulses separated by a time t_1, as shown in Figure 17A. Considering a spin k weakly coupled to another spin l, the sequence of events occurring to I_k under the pulse sequence can be described by a cascade of transformations.

$$I_{k0} \xrightarrow{90^\circ_x} I_{k1} \xrightarrow{\Omega_k t_1 I_{kz}} \xrightarrow{\pi J t_1 2 I_{kz} I_{lz}} I_{k2} \xrightarrow{90^\circ_x} I_{k3} \qquad [19]$$

The indices of the operator I_k refer to the numbers on the time axis in Figure 17A. Equations 20-23 show the development of spin operators in various stages of the sequence using the information given in Table 6, starting at the equilibrium state.

$$I_{k0} = I_{kz} \qquad [20]$$

$$I_{k1} = -I_{ky} \qquad [21]$$

$$I_{k2} = -[I_{ky} \cos \pi J t_1 - 2 I_{kx} I_{lz} \sin \pi J t_1] \cos \Omega_k t_1 + [I_{kx} \cos \pi J t_1 + 2 I_{ky} I_{lz} \sin \pi J t_1] \sin \Omega_k t_1 \qquad [22]$$

$$I_{k3} = -[I_{kz} \cos \pi J t_1 + 2 I_{kx} I_{ly} \sin \pi J t_1] \cos \Omega_k t_1 + [I_{kx} \cos \pi J t_1 - 2 I_{kz} I_{ly} \sin \pi J t_1] \sin \Omega_k t_1 \qquad [23]$$

The first term in Equation [23] including longitudinal magnetization (I_{kz}) and double quantum coherence ($I_{kx}\ I_{ly}$) would not be detected in the following t_2 period. The in-phase term, I_{kx}, will evolve during the detection time, t_2, with the same chemical shift Ω_k as that in t_1, which means that the signal detected will be located on the diagonal in the resulting 2D contour plot. It is noted that the anti-phase term of spin I_k, i. e. $2I_{ky}\ I_{lz}$, in Equation 22 is transferred to the anti-phase term of spin I_l, i.e. $2I_{kz}\ I_{ly}$, by the second 90° pulse (or mixing pulse). This coherence transfer between the two spins, $2I_{ky}I_{lz} \rightarrow 2I_{kz}I_{ly}$, is the origin of the cross peak. This anti-phase term of spin I_l, $2I_{kz}I_{ly}$, will develop to an observable I_{ly} with the coefficient of $-\sin \Omega_l t_2 \sin \Omega_k t_1 \ \sin \pi J t_1 \ \sin \pi J t_2$, and other terms which do not contain any observable magnetization. Thus, this signal with the chemical shift of Ω_l in F_2 is modulated with a chemical shift of Ω_k during t_1, which results in the cross peak located at the coordinate of (Ω_l, Ω_k) in the contour plot, assuming that the J-splittings are not resolved. The peak intensities are proportional to the amplitudes of coherence transfer. Similarly, spin I_l will show two signals. One is on the diagonal and the other is a cross peak located at (Ω_k, Ω_l), as shown in Figure 17B.

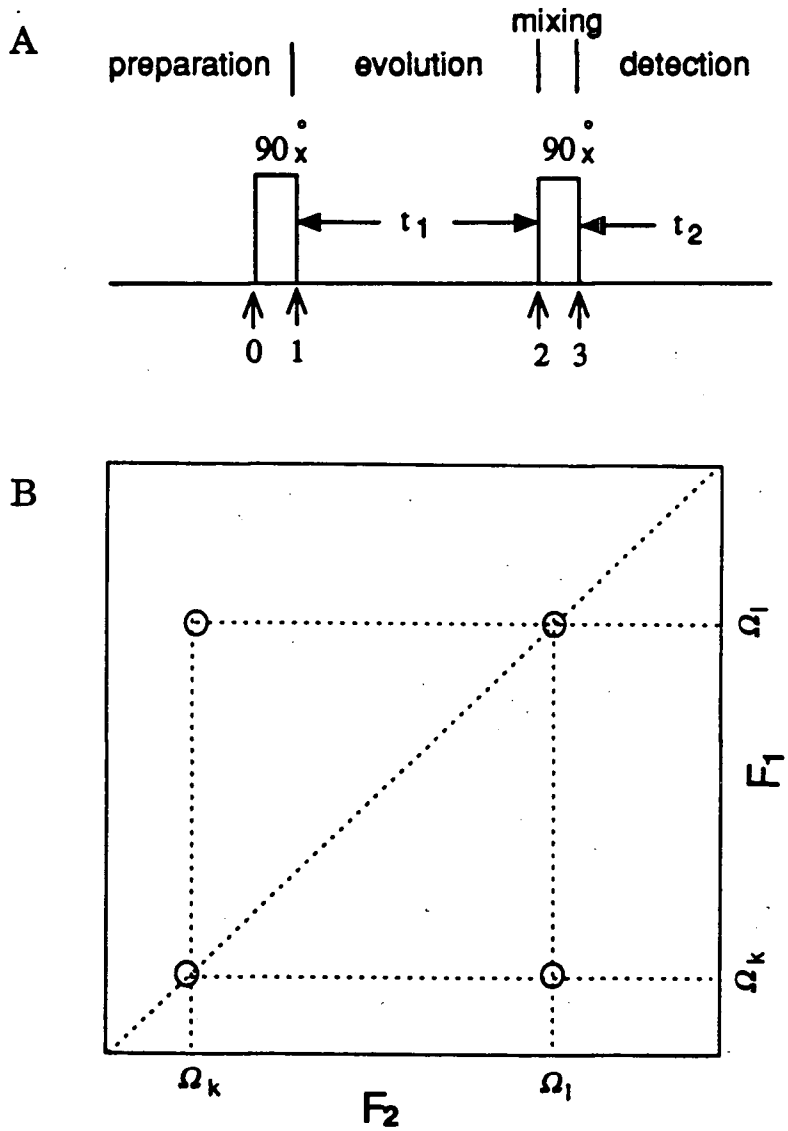

Figure 17 (A) Schematic representation of the pulse sequence used for COSY experiments. (B) Schematic contour plot of COSY experiment on a weakly coupled two spin system.

c) INADEQUATE (Incredible Natural Abundance DoublE QUAntum Transfer Experiment) experiments

The INADEQUATE experiment was first suggested by Bax and Freeman[66], and uses the pulse sequence given in Figure 18A. The excitation of double quantum coherence is achieved by a pulse 'sandwich' at the end of the preparation period. This double quantum coherence develops during the evolution time and is then converted into observables during the detection period. Using a similar POF treatment as described for the COSY experiment above, the evolution of product operators, I_k and I_l, at the various times indicated in the figure can be obtained, and explained as follows.

$$I_{k0} + I_{l0} = I_{kz} + I_{lz} \qquad [24]$$

$$I_{k1} + I_{l1} = -I_{ky} - I_{ly} \qquad [25]$$

During the 2τ period, where $\tau = 1/4$ J, only the J coupling interaction has to be considered, because the spin echo sequence refocuses the effect of chemical shift.

$$I_{k2} + I_{l2} = I_{ky} \cos \pi J 2\tau - 2I_{kx}I_{lz} \sin \pi J 2\tau + I_{ly} \cos \pi J 2\tau - 2I_{lx}I_{kz} \sin \pi J 2\tau$$
$$\xrightarrow{\tau=1/4J} -2(I_{kx}I_{lz} + I_{lx}I_{kz}) \qquad [26]$$

$$I_{k3} + I_{l3} = 2(I_{kx}I_{ly} + I_{lx}I_{ky}) \qquad [27]$$

Therefore the double quantum coherences, $I_{kx}I_{ly}$ and $I_{lx}I_{ky}$, are created at the end of the preparation period. Their intensities reach the maximum when $\tau = 1/4J$. The double quantum coherence does not develop under the interaction of J coupling according to Table 6. Thus only the chemical shift term is

considered during the evolution time. The double quantum coherence evolves at the double quantum frequency $\Omega_k + \Omega_l$ as indicated in Equation 28.

$$\begin{aligned} I_{k4} + I_{l4} &= 2(I_{kx} \cos \Omega_k t_1 + I_{ky} \sin \Omega_k t_1)(I_{ly} \cos \Omega_l t_1 - I_{lx} \sin \Omega_l t) \\ &+ 2(I_{lx} \cos \Omega_l t_1 + I_{ly} \sin \Omega_l t_1)(I_{ky} \cos \Omega_k t_1 - I_{kx} \sin \Omega_k t_1) \\ &= 2[(I_{kx}I_{ly} + I_{ky}I_{lx}) \cos(\Omega_k + \Omega_l)t_1 \\ &+ (I_{ky}I_{ly} - I_{kx}I_{lx}) \sin(\Omega_k + \Omega_l)t_1 \end{aligned} \quad [28]$$

$$\begin{aligned} I_{k5} + I_{l5} &= -2(I_{kx}I_{lz} + I_{kz}I_{lx}) \cos(\Omega_k + \Omega_l)t_1 \\ &+ 2(I_{kz}I_{lz} - I_{kx}I_{lx}) \sin(\Omega_k + \Omega_l)t_1 \end{aligned} \quad [29]$$

The last 90° pulse converts the double quantum coherence into the anti-phase coherences of I_k and I_l, i.e., $I_{kx}I_{lz}$ and $I_{kz}I_{lx}$ respectively. Then they evolve to be detectable in t_2 with chemical shifts Ω_k and Ω_l respectively, if the couplings are not resolved. It is clear now that a coupled spin pair shows two signals in the INADEQUATE experiment which are present at chemical shifts of Ω_k and Ω_l in the F_2 dimension respectively, while they appear at the chemical shift, $\Omega_k + \Omega_l$, in F_1, the two signals occurring equally-spaced on both sides of the diagonal of the plot, as shown in Figure 18B. The frequency in F_1 , $\Omega_k + \Omega_l$, is referred to as the 'double quantum frequency'.

As discussed above, a series of cross-peaks in the plots of COSY and INADEQUATE experiments reflects the bonding interactions, and makes it possible to deduce the connection patterns both in molecular structures and lattice frameworks.

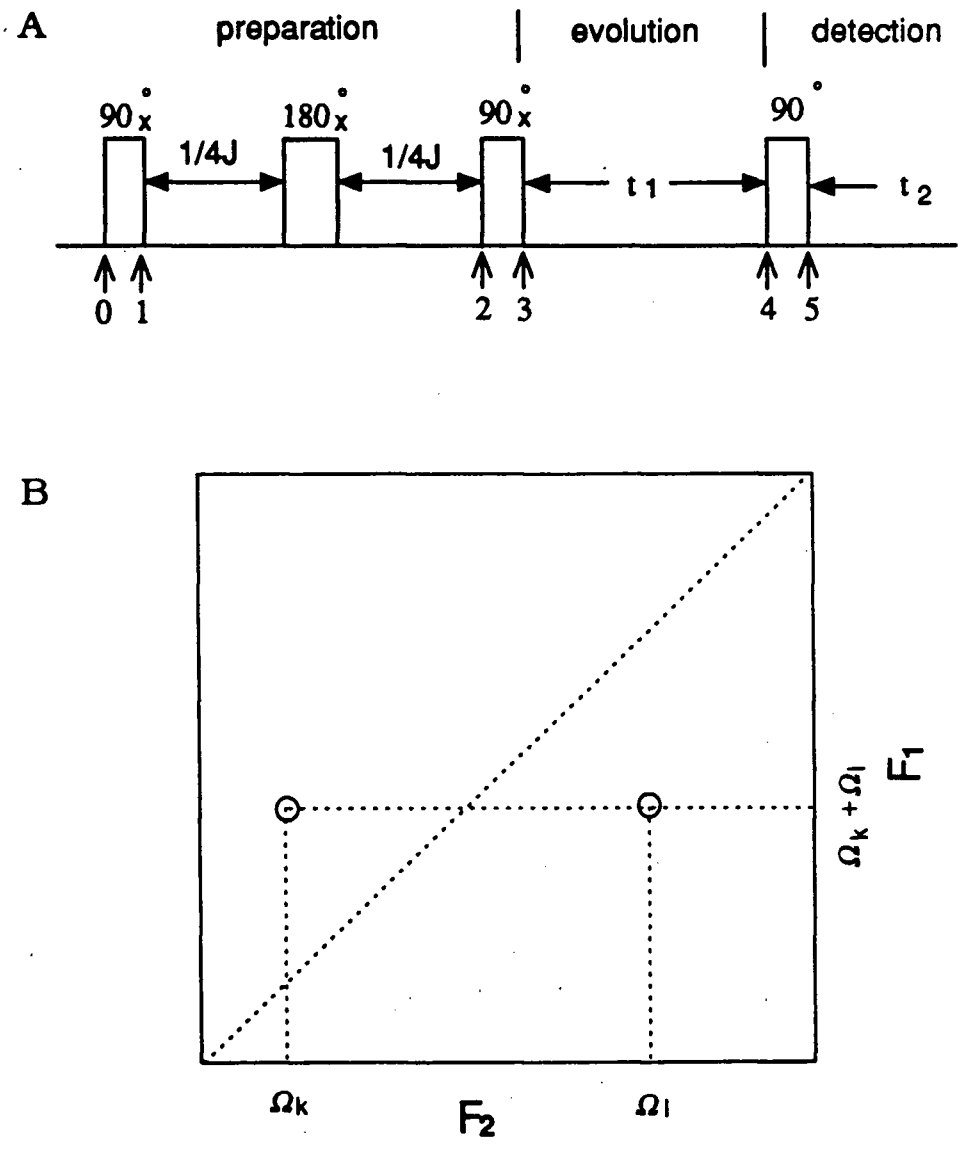

Figure 18 (A) Schematic representation of the INADEQUATE pulse sequence. (B) Schematic contour plot of an INADEQUATE experiment on a weakly-coupled two spin system.

B. APPLICATIONS OF 2D HOMONUCLEAR CORRELATION EXPERIMENTS TO ZEOLITES

I. GENERAL CONCEPTS

In the past decade, a number of 2D NMR experiments have been introduced in high resolution solid state NMR studies. There are two kinds of 2D experiments in the solid state. One is a straightforward analogue of 2D experiments in solution. For example, Szeverenyi[67] investigated the chemical exchange process, Vega[68] has demonstrated a method to establish $^{29}Si/^{1}H$ heteronuclear chemical shift correlations in silicas and zeolites and Benn and co-workers[69] have recently established $^{13}C/^{13}C$ connectivities using the INADEQUATE sequence for the plastic crystal camphor and have used the COSY sequence to establish $^{29}Si/^{29}Si$ connectivities in the reference molecule Q_8M_8 (cubic octamer silicic acid trimethylsilyl ester). Although identical or slightly modified versions of the pulse sequences used in solution NMR were used with the addition of the resolution and sensitivity enhancement techniques discussed in Chapter One, the situation in solids is often much more complicated than in solution due to the anisotropic nature of the spin interactions. A second type of 2D solid state experiments has no analogue in solution NMR. These experiments are used to study some special interaction in solids, and the 2D spectra obtained usually present isotropic chemical shifts in the F_2 dimension and some spatial interactions in the F_1 dimension. For example, such experiments have been used to retrieve chemical shift anisotropies[70], dipolar couplings[71-72], and to probe spin-diffusion processes[73].

The 2D NMR experiments used to investigate the structures of zeolites in this thesis belong to the first category. Due to the nature of the spin interactions in solids, it is usually impossible to predict the feasibility of the application of a specific experiment to a given system. This was true in the case of zeolites before this work was begun although it was felt that 2D NMR techniques could well be used to establish connectivities in zeolites.

II. BACKGROUND INFORMATION

Harris and co-workers[75] have reported a series of studies of the ^{29}Si NMR spectra of aqueous silicate solutions. The combined use of ^{29}Si isotopic enrichment and ^{29}Si -{^{29}Si} homonuclear decoupling made it possible to deduce the structures of the silicate anions present and to measure the $^{2}J_{Si\text{-}O\text{-}Si}$ couplings, which appear to be in the range of 3-10 Hz and dependent on ring size. Furthermore, this group has presented 2D J-resolved and shift- correlated ^{29}Si NMR of silicate solutions[76]. The $^{2}J_{Si\text{-}O\text{-}Si}$ values derived from these 2D experiments are consistent with those from the 1D experiments. In related work, Knight[77] has described 1D and 2D ^{29}Si NMR of germanosilicate solutions. The $^{2}J_{Si\text{-}O\text{-}Si}$ couplings are 7.5 Hz in the double four-membered ring system and 4.3 Hz in the double three-membered ring system. In solid silicates and aluminosilicates, only one example of J coupling has been reported so far, that is a $^{2}J_{Si\text{-}O\text{-}Al}$ value of 9 Hz deduced from a variable frequency MAS NMR study of the mineral Albite[78].

1D ^{29}Si MAS NMR techniques have been widely used to investigate the structure and properties of zeolites, as discussed in Chapter One. However, the matching of an NMR resonance with a particular silicon atom in the crystal

structure is difficult even in the highly siliceous cases unless the peak intensities of the resonances and related population parameters are unique. The assignment of resonances using geometric information from XRD experiments has been reported recently[17], but these methods are empirical and very ambiguous when the chemical shift differences are small. In addition, very few accurate XRD studies of zeolites are available and it becomes attractive to consider alternative NMR methods of obtaining the information, which in turn will also give detailed structural information on the systems.

III. OUTLINE OF PROPOSED RESEARCH

The work presented in this thesis, for most part, is directed towards the application of ^{29}Si 1D and 2D NMR spectroscopy to the investigation of zeolite structures. The rest of this chapter is concerned with the experimental aspects of both sample preparation and the NMR experiments. Chapter Three describes in detail the application of 2D COSY techniques to isotopically enriched, relatively simple zeolites of known structure, ZSM-39 and zeolite DD3R. Successful results from these experiments showed the potential of this approach for establishing the ^{29}Si-O-^{29}Si connectivities in zeolites. Further work extended these studies to the natural abundance samples, ZSM-12 and ZSM-22, and the results are presented in Chapter Four. Both 2D COSY and INADEQUATE experiments were successfully performed on these zeolites. Chapter Five deals with the most complex zeolite structure known, in terms of the large asymmetric unit in its unit cell, zeolite ZSM-5, both in its low-temperature monoclinic phase and the orthorhombic forms to which it is converted by the action of temperature and/or *p*-xylene. The 24 T-sites in the asymmetric unit and 48 connectivities of the

structures present a real challenge to the 2D NMR techniques. Some poorly-characterized zeolites, ZSM-11 and ZSM-23, are treated in Chapter Six. These successful experiments demonstrate the considerable potential of 2D NMR experiments for solving structural problems in zeolites when combined with XRD techniques.

C. EXPERIMENTAL CONSIDERATIONS FOR OBTAINING 2D SOLID STATE NMR SPECTRA

NMR spectroscopy has developed, through the introduction of two-dimensional methods, into the most important method for the investigation of the structure and dynamics of molecules in solution. The general application of 2D techniques to solids is considerably more difficult, principally because of dipolar interactions and chemical shift anisotropies which produce the broad lines typical of solid state NMR and make the interactions of spins in the solid more complex than in solution. In addition, the short T_2 relaxation times restrict the use of long evolution times which are required in some experiments. In the case of zeolites, the experiments are also insensitive, because of the low natural abundance of ^{29}Si, and the porous nature of the structures. Thus, the 2D experiments are very demanding and time consuming, both in terms of sample preparation and the spectroscopy involved. The important factors in the experiments will be briefly discussed.

I. PREPARATION OF HIGHLY SILICEOUS ZEOLITES

a) Zeolite Synthesis

Although zeolites were first discovered in natural form as minerals, it was the production of synthetic zeolites with novel framework structures which eventually led to their widespread application. Zeolites are hydrated aluminosilicates usually synthesized under hydrothermal conditions[4,79]. The term 'hydrothermal' is used in a broad sense and includes the crystallization of

zeolites from aqueous systems, often at elevated temperatures. Generally a zeolite synthesis is achieved by crystallization from an inhomogeneous gel, created from a silica source, an alumina source and various cations combined with water under high pH conditions. The cations are usually considered to act as structure-directing agents, called templates. How all the parameters, e.g. the ratios of the components, temperature and templates, can be manipulated to create different zeolites is a complex problem, not yet understood in any detail. The choice of parameters to obtain a particular lattice structure is largely a matter of trial and error. Each as-synthesized material used in the present work was examined by powder XRD techniques, and the very best ones according to XRD results were calcined in air at 550°C to drive off templates and water molecules included in the zeolite lattice, and also to heal any possible defects in the structure.

b) Dealumination

Although the synthesis of materials used in this work were carried out in the absence of any Al sources, there are still traces of Al as impurities introduced with the reactants used. It was desirable to effect complete dealumination to yield an 'aluminum free' sample. Essentially there are two major methods of dealumination: i) hydrothermal treatment of the ammonium or hydrogen-exchanged form of the zeolite; ii) chemical treatment of zeolites with suitable reagents (e.g. acid, chelating agents)[80].

The hydrothermal treatment adopted in this work was first demonstrated by McDaniel and Maher[81]. A calcined sample is ammonium-exchanged with a 1 M aqueous solution of NH_4F and then this ammonium exchanged sample is

subjected to the steaming treatment, by passing water vapor over the sample at ~750°C for several days. A schematic representation of a possible dealumination mechanism is presented in Figure 19. The first step is the 'deammoniation' to form an acidic H- form, then hydrolytic splitting of Si- O- Al bonds occurs, Al is released from the framework as (intermediate) $Al(OH)_3$ and four SiOH groups are formed at each vacant site of the framework. The mechanism of Step 3 can be explained by migration of the 'vacancies' within and out of the framework by exchanging places with neighbouring Si- sites (82).

The whole process of preparing highly siliceous zeolite samples was monitored by XRD and NMR measurements, and only those materials giving very narrow NMR lines were used for the 2D NMR experiments.

II. OPTIMIZATION OF THE NMR EXPERIMENT

To obtain well-resolved spectra with a good signal to noise ratio in the shortest possible measurement time, some practical aspects in performing the NMR experiments have to be considered. First, the proper setting of the "Magic Angle" is especially important to obtain high-resolution solid-state NMR spectra. This was done by observing the ^{79}Br resonance of a sample of KBr (83). The number and intensities of the sidebands in the ^{79}Br resonance are very sensitive to the angle of the spinning axis and maxima are reached when the angle is set to exactly 54.7°. Good homogeneity of the static field is also important factor for obtaining good resolution in the resulting spectra. In order to obtain the maximum S/N, the probeheads must be precisely tuned to resonance. The stability of the whole system during the experiment is crucial, since fluctuations

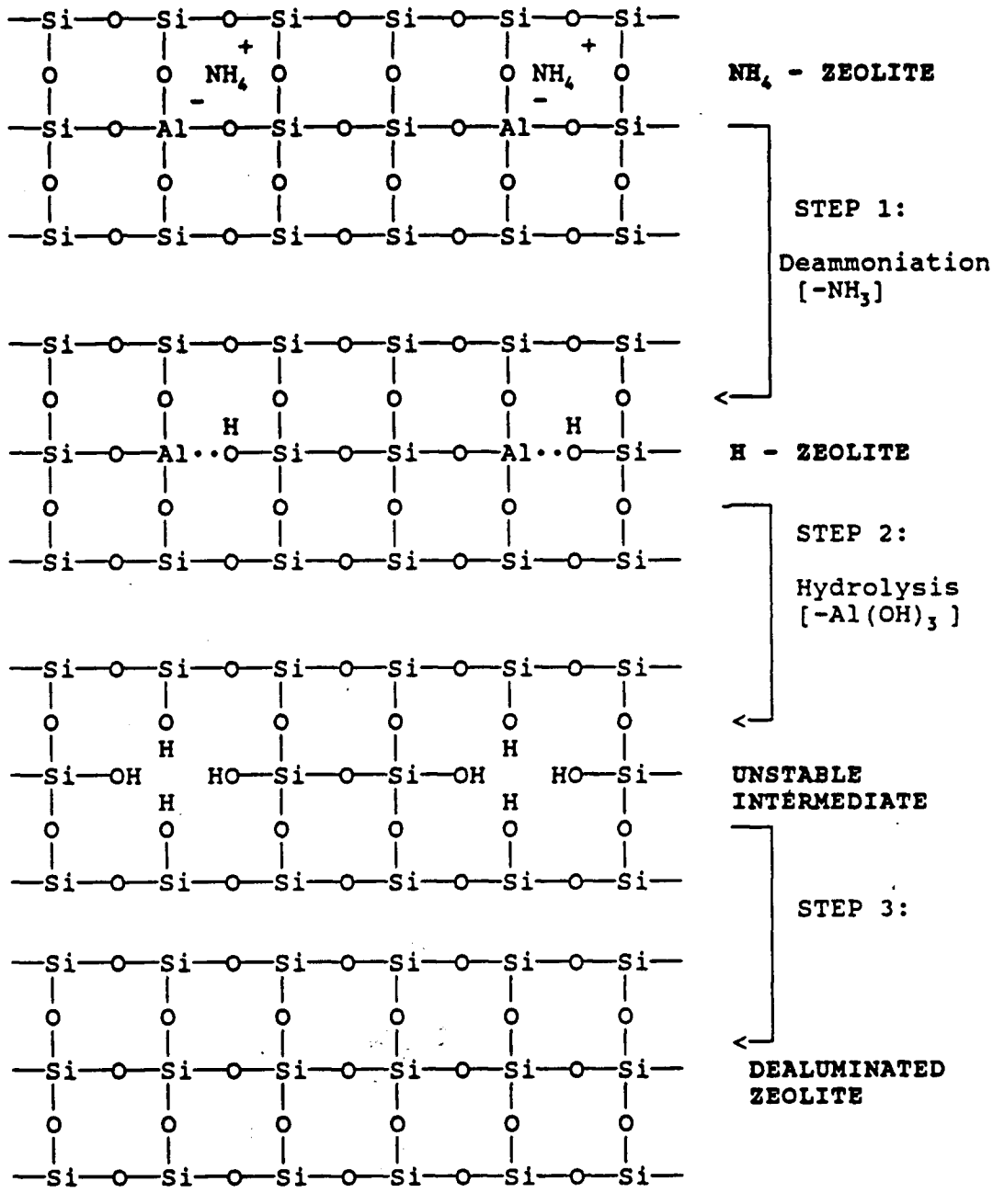

Figure 19 A schematic representation for a possible mechanism of hydrothermal dealumination of the zeolite framework. (ref. 17)

in temperature, sample spinning and field strength can considerably decrease the resolution and sensitivity and could generate artifacts.

It is good practice to check the system performance using a standard sample in standard conditions, whenever the spectrometer (Bruker MSL-400 in the current work) is reset to ^{29}Si MAS NMR experiments from other probes or nuclei. A sample of Q_8M_8 (cubic octamer silicic acid trimethylsilyl ester) was used as a standard. There are methyl groups attached to some of the silicon atoms in Q_8M_8, so it is a suitable sample for setting the Hartmann-Hahn condition for CP experiments and the spectum is also a measure of field homogeneity. It gives sharp, well separated resonances and a reasonable S/N ratio for easy and quick data accumulation. Figure 20 shows ^{29}Si CP MAS NMR spectrum of Q_8M_8. The S/N ratio for the strongest resonance and the linewidth of the highest field resonance indicate the sensitivity and resolution of the current performance of the spectrometer. The major factors affecting linewidth are shimming, decoupling power and setting of the magic angle. The factors affecting the S/N ratio are probehead tuning, amplifier tuning, setting of the Hartmann-Hahn condition, the cleanliness of the coil and any defects in the preamplifier or later stages of electronics. All ^{29}Si chemical shifts indicated in this thesis are indexed with respect to TMS, using Q_8M_8 as intermediate standard and taking the highest field resonance in the ^{29}Si spectrum to be -109.7 ppm [17].

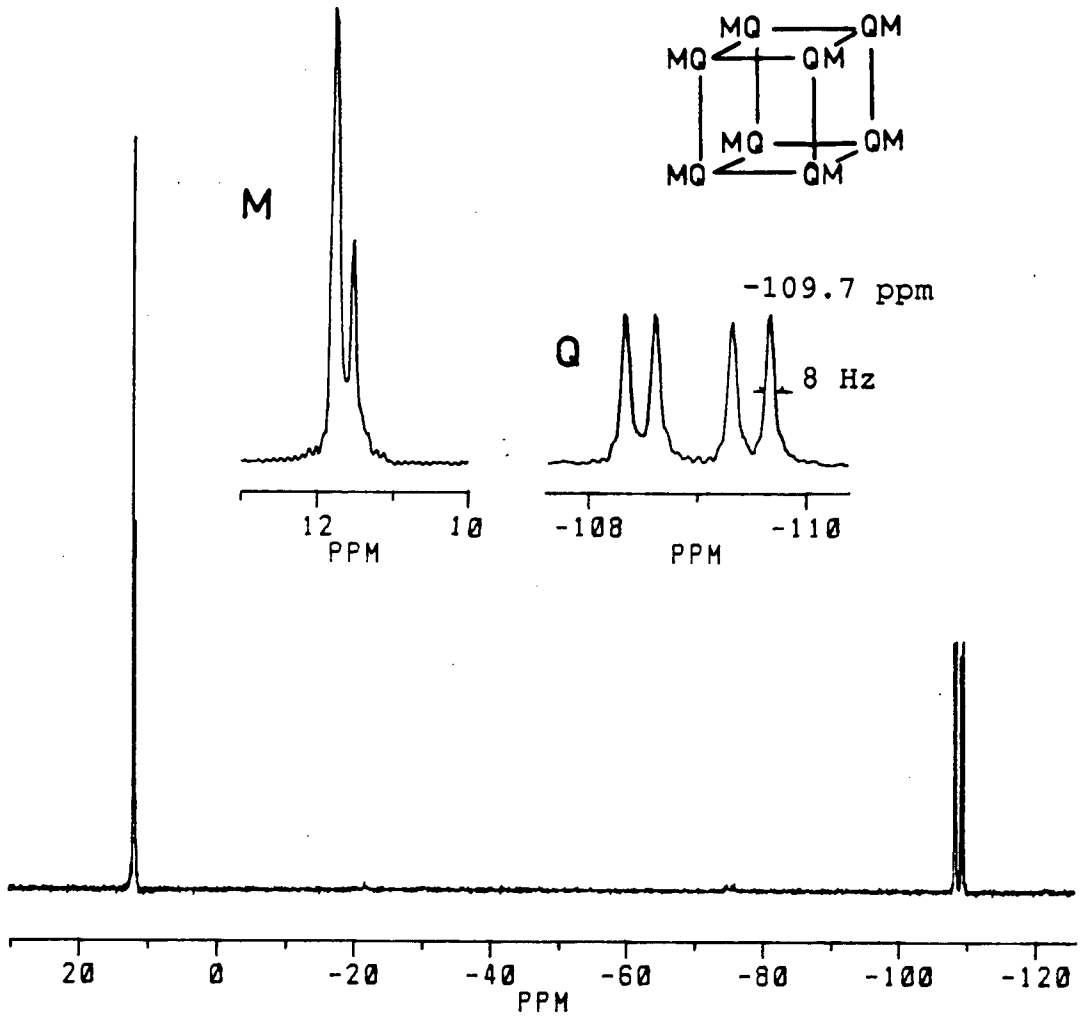

Figure 20 ^{29}Si CP MAS NMR spectrum of Q_8M_8 (M : trimethylsilyl silicons; Q : silicons of the silicate backbone). The spectrum was obtained at 79.5 MHz, using 4K data points and zero filling to 8K with the spectral width of 12.8 kHz. There are 4 scans with the contact time of 20 ms and recycle time of 10 s.

a) 2D Data Acquisition Parameters

As discussed in section A, each interferogram obtained from the first Fourier transformation can be considered and treated in the same way as a 1D FID. This means that parameters in the F_1 dimension such as acquisition time, spectral width, and digital resolution can be controlled in analogous ways as in the conventional F_2 dimension.

-Digital resolution in the F_1 domain

The digital resolution required in F_1 has a crucial bearing on the time requirement of a 2D experiment. If very high-resolution information is desired, a large number of spectra would be required, demanding in terms of total experimental time and also disk storage space. In the case of ^{29}Si 2D correlation experiments on zeolites, a great number of transients are needed to achieve a good enough S/N ratio because of the low natural abundance of ^{29}Si. In a compromise between these two factors, a digital resolution of ~40 Hz/point (before zero filling) in F_1 was found to be generally acceptable in the present studies.

-Pulse Calibration

Pulse calibration is important in that without accurately calibrated pulses even the simplest NMR experiments requiring a specific flip angle cannot be performed properly. In particular, pulse sequences using 180° pulses for inversion or refocusing are very sensitive to pulse imperfections or missetting. Furthermore, in some 2D NMR experiments, the variation of length of a specific pulse can be used to suppress unwanted signals or to enhance the information of interest. For example, the second pulse in the COSY experiment (Figure 17) is set to 45° to make the cross peaks close to diagonal more easily observed, and the

fourth pulse length in INADEQUATE (Figure 18) is adjusted to 135° in order to provide quadrature detection in the F_1 domain (see Chapter Three). The method for pulse calibration was the determination of the 180° pulse length using a simple one pulse sequence. When the 180° condition is achieved, zero amplitude should be observed.

-Optimization of cross polarization experiments

Cross polarization (CP) is an important sensitivity enhancement technique in high-resolution solid state NMR when it can be used (see Chapter One). The critical part of the CP experiment is the setting of the Hartmann-Hahn condition, which controls the magnetization transfer from abundant to rare spins. A reference sample of Q_8M_8 was used for this purpose, since the low sensitivity of ^{29}Si precludes setting this condition on the zeolites themselves even with templates or sorbed molecules. The optimization was carried out by observing the ^{29}Si FID using a CP pulse sequence (see Figure 6) with the power of the proton channel fixed. The FID of a single scan can be seen clearly for Q_8M_8 and the power of the ^{29}Si rf field, B_{1x}, was carefully adjusted until a maximum FID was obtained. A cross check can be obtained by measuring the 90° pulse lengths of both nuclei, which should be very close in magnitude to each other.

b) Data Processing

After a 2D experiment has been completed, a disk file is stored with a set of n FIDs, each composed of k data points. The basic steps in processing 2D data involve zero filling, window multiplication, Fourier transformation, computation of magnitude or power mode spectra and finally symmetrization when desired.

Instrumentation time constraints dictate that most 2D spectra are acquired with coarse digital resolution in F_1. In addition, 2D spectra are normally

presented in either power- or magnitude mode. In these cases, the absorption and dispersion parts of the transformed spectrum become intermingled. The resulting line-shape has a very wide base, which dramatically reduces the base-line separation between individual signals. There are two ways to improve the resolution after acquiring the data: One is by 'zero filling' and the other is 'window multiplication'. If the genuine data points are m, then 2^n data points can be obtained by adding proper points, each containing only a zero, to the end of the FID before Fourier transformation. This is called zero filling. In this work, the total data points (after zero filling) are in most cases 512 and 256 in the F2 and F1 dimensions respectively, which is 2 to 8 times the number of genuine data points.

Window multiplication is the important part of the 2D data processing. The time-domain data are multiplied by a window function for the purposes of enhancing resolution or of optimizing sensitivity. Figure 21 shows some examples of the window functions commonly used. Taking the sine-bell window (see the right curve in Figure 19C) as an example, this window starts and finishes close to zero and is symmetrical about the middle-point. The application of the window multiplication is to produce the desirable absorptive line-shape in a magnitude spectrum[52]. The spectra with and without sine-bell window treatments are given in Figure 22 taking a COSY experiment of zeolite ZSM-39 as an example. The sine-bell window is commonly used in 2D data processing and is optionally phase shifted and/or squared (Figure 19C and D) according to the degree of line narrowing required and the degree of acceptable degradation of S/N ratio. The particular parameters used for both

data acquisition and processing are presented in the figure captions for all of the 2D experiments reported in the thesis.

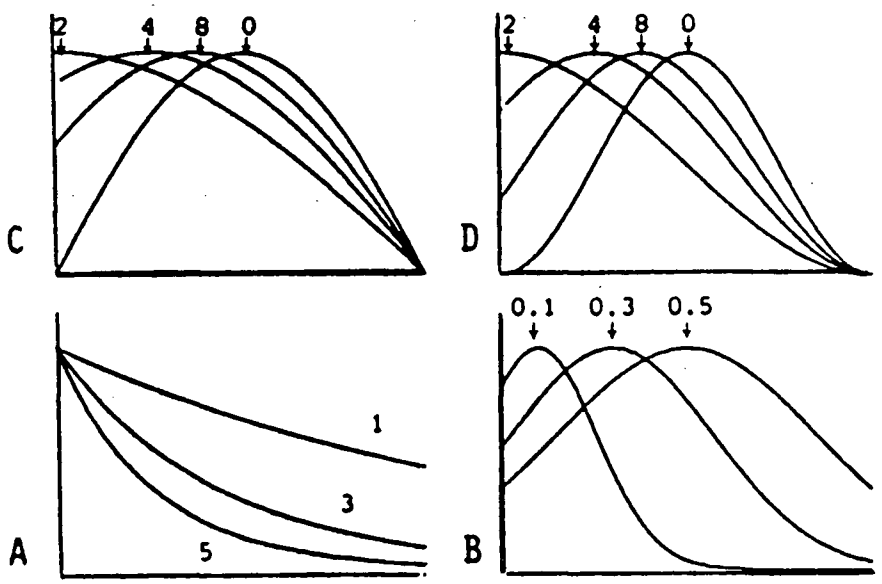

Figure 21 Comparison of some time-domain window functions. The time domain is 0.256 s. (A) Exponential multiplication with LB=1,3,5 Hz. (B) Gauss function with LB= -5 Hz and GB= 0.1, 0.3, 0.5 times the time domain. (C) Sine-bell shifted by 0, $\pi/2$, $\pi/4$, $\pi/8$ (labeled at the max. with 0,2,4,8, respectively). (D) Sine-bell squared shifted by 0, $\pi/2$, $\pi/4$, $\pi/8$. (ref. 84)

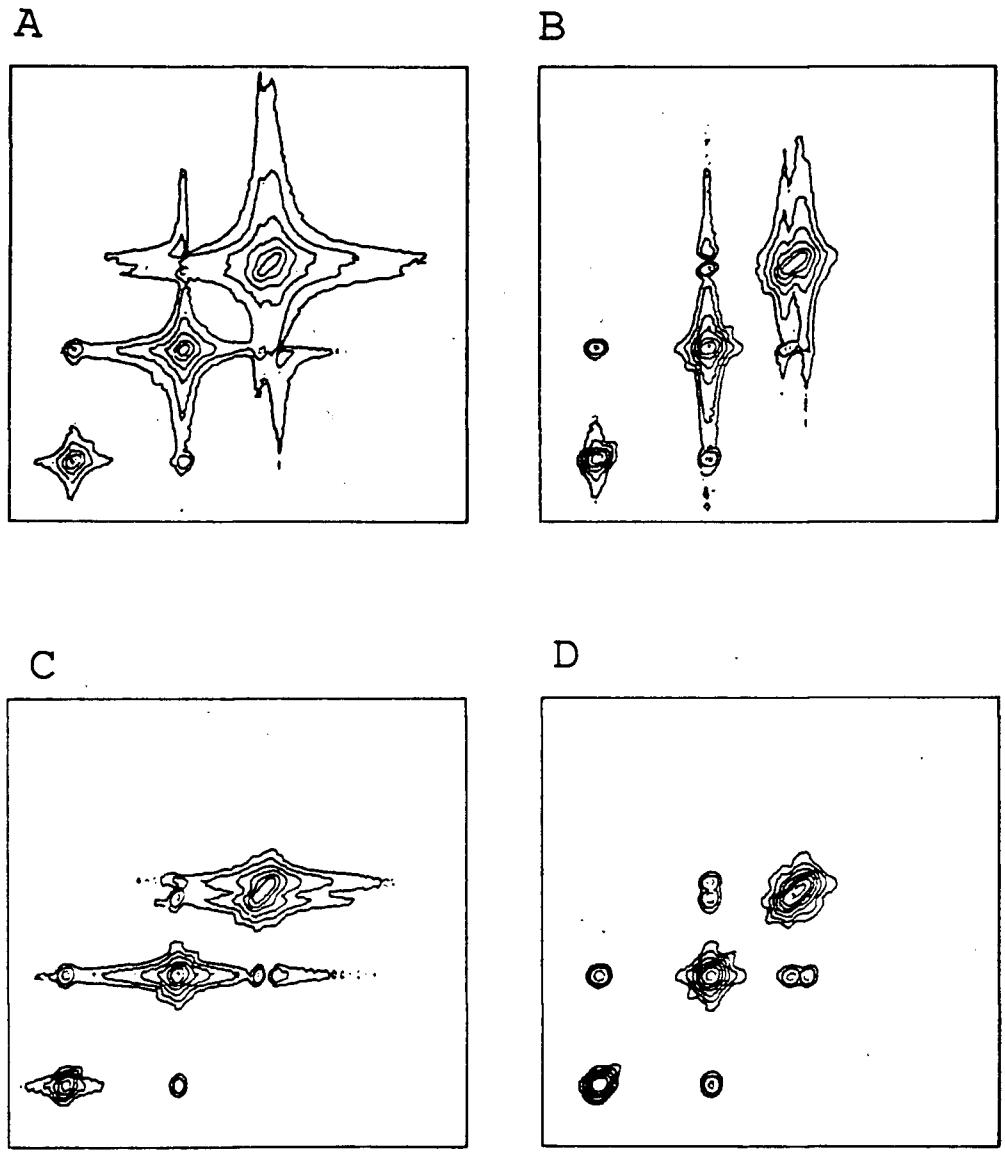

Figure 22 Contour plots of a 2D ^{29}Si COSY experiment (see Chapter Three). (A) Without any window function treatment. (B) With sine-bell window multiplication in F_2 dimensions. (C) With sine-bell window multiplication in F_1 dimensions. (D) With sine-bell window multiplication in both dimensions.

V. MEASUREMENT OF RELAXATION TIMES

a) Introduction

In all two dimensional NMR sequences, it is necessary to allow the spin system to relax back towards equilibrium between the acquisition of one FID and the start of the next pulse train. If this is not done, then at best the signal intensity will be less than optimum, and at worst, artifacts will appear. In addition, multipulse sequences for 2D NMR have a finite length of evolution and fixed delays during which transverse magnetization decays due to spin-spin relaxation (T_2). In the case of the spin diffusion experiments, (which will be discussed in Chapter Three) the perturbed longitudinal magnetization grows back toward its equilibrium value at the rate of $1/T_1$ during the mixing period. Therefore, the amount of transverse magnetization available for detection could be significantly reduced by the relaxation process, perhaps even making it impossible to carry out the experiments. Thus, it is desirable to measure the relaxation times for each sample before performing 2D experiments. Throughout this thesis, the italic forms T_1 and T_2 will be used to denote the spin-spin and spin-lattice relaxation times respectively, to avoid confusion with the indexing used for the T sites of zeolites.

b) Experimental

^{29}Si and ^{1}H relaxation time (T_1 and T_2) measurements were performed on a Bruker MSL-400 spectrometer at 79.49 MHz, using the pulse sequences listed in Table 7.

Table 7 The Pulse Sequences Used for T_1 and T_2 Measurements

relaxation time	name of the sequence	pulse sequence	equation for calculation
T_1	inversion-recovery (Ref. 61)	180°- τ- 90° (FID)	$\ln[S(\infty)-S(t)]=\ln 2+\ln S(\infty)- \tau/T_1$
T_2	CPMG (Ref. 85 A)	$90°_x$-[τ-$180°_y$-τ]$_n$(FID)	$\ln S(t)-\ln S(0)= -t/T_2$
T_1 of ^{1}H with CP		^{1}H: 180°-τ-90°-CP-HPD ^{29}Si: CP(FID)	$\ln[S(\infty) -S(t)]= \ln 2+ \ln S(\infty) - \tau/T_1$
T_1 of ^{29}Si with CP	(Ref. 85 B)	^{1}H: 90°-CP—τ——HPD ^{29}Si: CP90°-τ-90°(FID) phase cycle:180° shift of ^{1}H pulse	$\ln S(t)= \ln 2+ \ln S(0) - \tau/T_1$

* S(t) represents the intensity of a resonance at the time of t.

c) Results and discussion

The results of T_1 measurements on some representative siliceous zeolites are given in Figure 23. The T_1 values at ambient temperature of the T-sites in pure highly siliceous zeolites (in comparison with the forms with templates or organic molecules in the cavities and channels) are mostly in the range of 3 - 11 s. It is generally assumed that the dominant spin-lattice relaxation mechanism in synthetic zeolites is the direct interaction between the ^{29}Si nucleus and the electron spin of atmospheric paramagnetic dioxygen[86]. This mechanism is a satisfactory explanation of the present results. For example, in the case of ZSM-12, the second highest field resonance has the longest T_1 among the seven resonances, because this T site is the only one in the system which is not part of a channel surface (see Chapter Four) and thus will not be in direct contact with adsorbed oxygen. At elevated temperatures, the amount of absorbed oxygen

will be decreased, and as a consequence, the T_1 values should be longer. This has been observed in the case of ZSM-5 at 403 K. When the internal voids of a zeolite are filled with templates or organic molecules, the T_1 can be lengthened to 70 s or more due to the displacement of oxygen from the intracrystalline space by the guest molecules. ZSM-5 loaded with 8 molecules *p*-xylene per unit cell is an example, as shown in Figure 23.

Figure 24 shows the results of a series T_2 experiments on the same zeolites. The T_2 values fall in the range of 100 ms - 1 s except for the very long T_2 values of ZSM-12. The effect of T_2 on the 2D experiments used in current work will be discussed in Chapter Three.

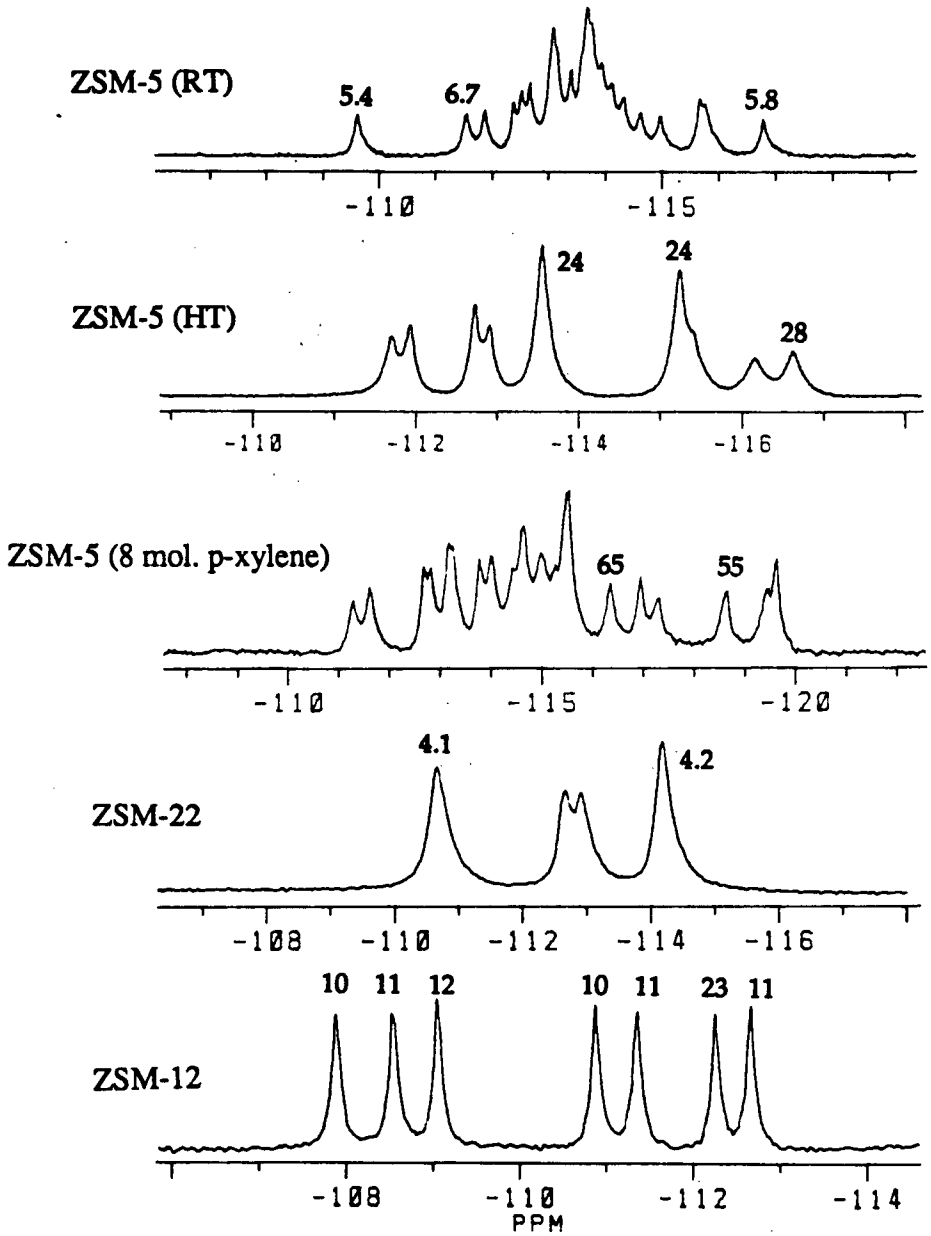

Figure 23 ^{29}Si spin-lattice relaxation times T_1 (in seconds) of some of the T-sites in some highly siliceous zeolites.

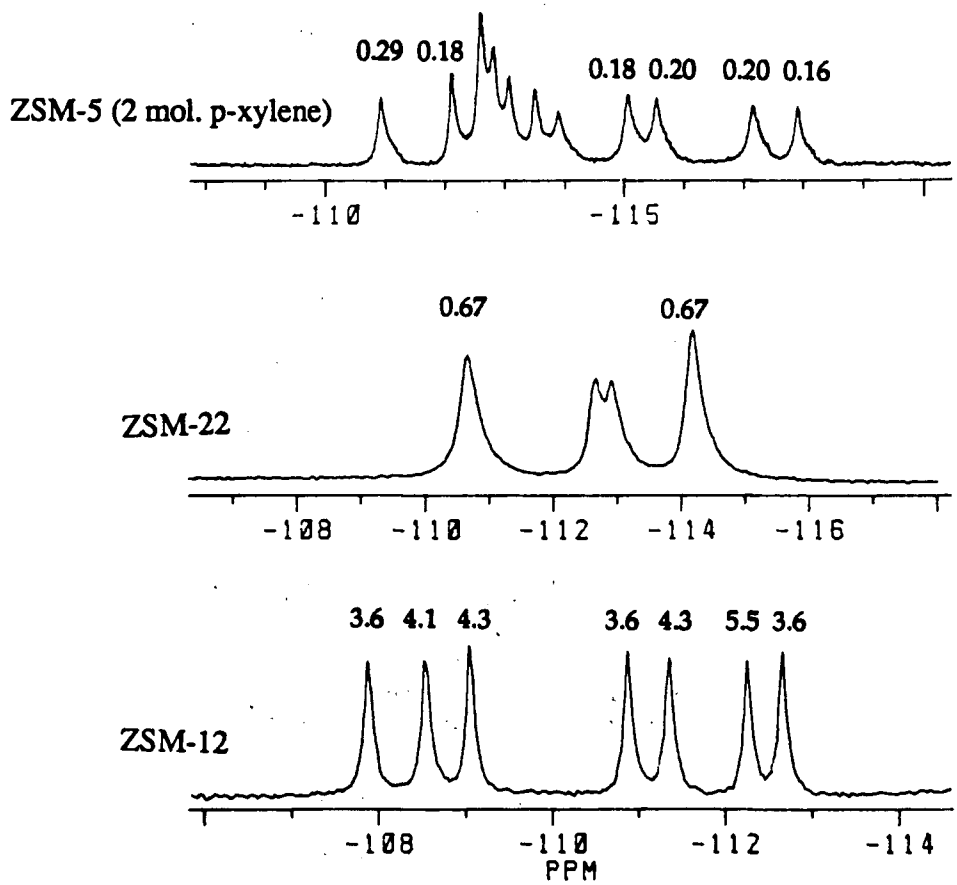

Figure 24 ^{29}Si spin-spin relaxation times T_2 (in seconds) of some of the T-sites in some highly siliceous zeolites.

CHAPTER THREE

APPLICATION OF TWO-DIMENSIONAL ^{29}SI HIGH-RESOLUTION SOLID STATE NMR TO INVESTIGATION OF THE SILICATE LATTICES OF THE ^{29}SI-ENRICHED ZEOLITES ZSM-39 AND DD3R

A. TWO-DIMENSIONAL ^{29}SI HIGH-RESOLUTION SOLID STATE NMR INVESTIGATION OF THE LATTICE STRUCTURE OF ^{29}SI-ENRICHED ZEOLITE ZSM-39

I. INTRODUCTION

In order to develop the relationship between high-resolution solid-state NMR data and the three-dimensional structures of zeolites, a sample of known structure, zeolite ZSM-39, was chosen as a probe material. The structure of ZSM-39 is well characterized and relatively simple. To facilitate the application of 2D experiments, the sample was prepared from ^{29}Si enriched sources (approximately 80% in ^{29}Si) and used in the as-synthesized form containing template so that the CP technique (see Chapter One) could be applied. The term 'ZSM-39' will be used in the following text instead of 'ZSM-39 with piperidine template' for reasons of simplicity, but in all instances template was present in the sample.

Zeolite ZSM-39 (clathrasil dodecasil-3C) is a highly siliceous tectosilicate first synthesized by Jenkins and Dwyer [87]. The crystal structure was determined by Schlenker et al[88] and refined in detail by Gies[89] and consists of layers of face-sharing pentagonal dodecahedra (5^{12}). The space group symmetry of the high-temperature form of the compound is Fd3, and a schematic representation of its lattice framework is given in Figure 25. There are 136 T-atoms in the unit cell distributed over three crystallographically inequivalent sites T_1, T_2 and T_3 of relative proportions 1:4:12. The room temperature form of the as-synthesized material is tetragonal and deviates from cubic symmetry by the absence of the 3-fold axis[90]. Therefore, there are a total of five T-sites: $8T_1$, $32T_2$, $32T_3'$, $32T_3''$ and $32T_3'''$. The connectivities of the T-sites are given in Table 8 for the ideal cubic form.

Table 8 T-sites, Their Occupancies, and Connectivities for the Asymmetric Unit in Zeolite ZSM-39 (Ref. 89)

T-site	occupancy	connectivity
T_1	1	$4T_2$
T_2	4	$1T_1: 3T_3$
T_3	12	$1T_2: 3T_3$

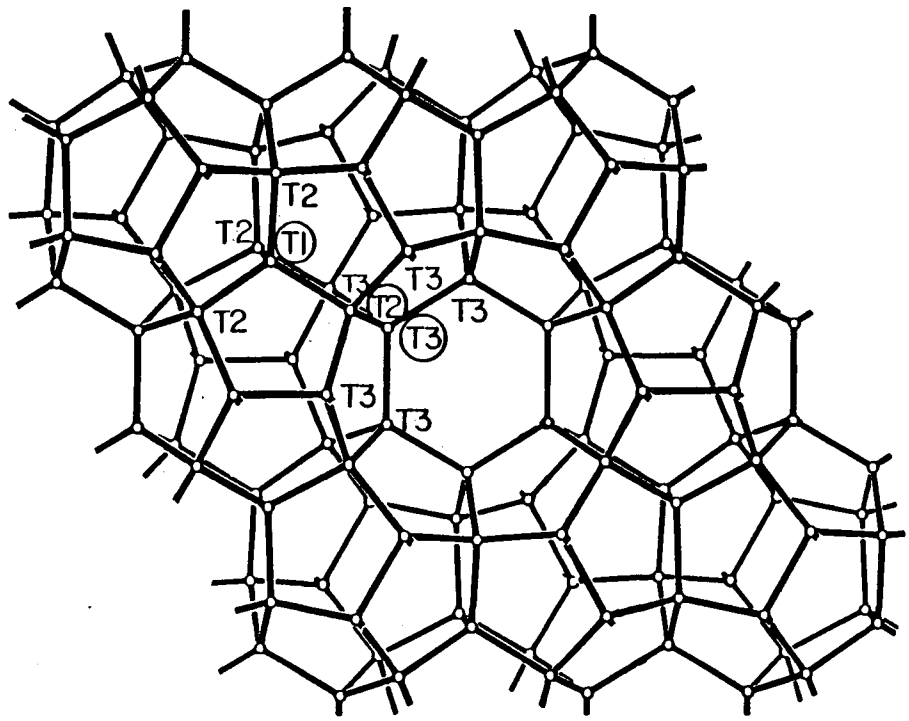

Figure 25. Schematic representation of the zeolite ZSM-39 lattice framework in the high temperature form. The three crystallographically inequivalent tetrahedral lattice sites are indicated by T_1, T_2, and T_3 (inside circles), and in each case the identities of the four nearest neighbors are shown. (ref. 95)

II. EXPERIMENTAL

^{29}Si CP MAS NMR spectra were obtained at 79.49 MHz on a Bruker MSL-400 spectrometer using the techniques previously described. 2D COSY experiments were performed using a modified version of the sequence used in solution with the initial 90° pulse replaced by the cross-polarization pulse scheme. Besides the use of the CP technique, a fixed delay (FD) was introduced before and after the second 90° pulse to emphasize the effect of small couplings [52], as shown in Figure 26C. The value of FD was optimized by trial and error. 2D spin diffusion experiments were carried out as described by Maciel and co-workers[96] using a standard ^{1}H to ^{29}Si cross-polarization to initiate the sequence (Figure 26B). 1D Spin diffusion experiments from individual resonances were performed as described by VanderHart[97] using a DANTE (Delays Alternating with Nutation for Tailored Excitation) sequence to invert the selected resonance[98], as shown in Figure 26A. Since magic angle spinning is sufficient to suppress the effects of ^{1}H-^{29}Si dipolar interactions in these experiments, no heteronuclear decoupling needed to be used during the detection periods. Nevertheless, this interaction remains active in the magnetization- transfer process.

A small quantity of a highly siliceous sample of ZSM-39 was synthesized hydrothermally by Dr. Hermann Gies, U. Bochum, Germany, in a sealed silica glass tube in 8 days at 200°C using piperidine as template. The silica source was enriched to approximately 80 % in ^{29}Si.

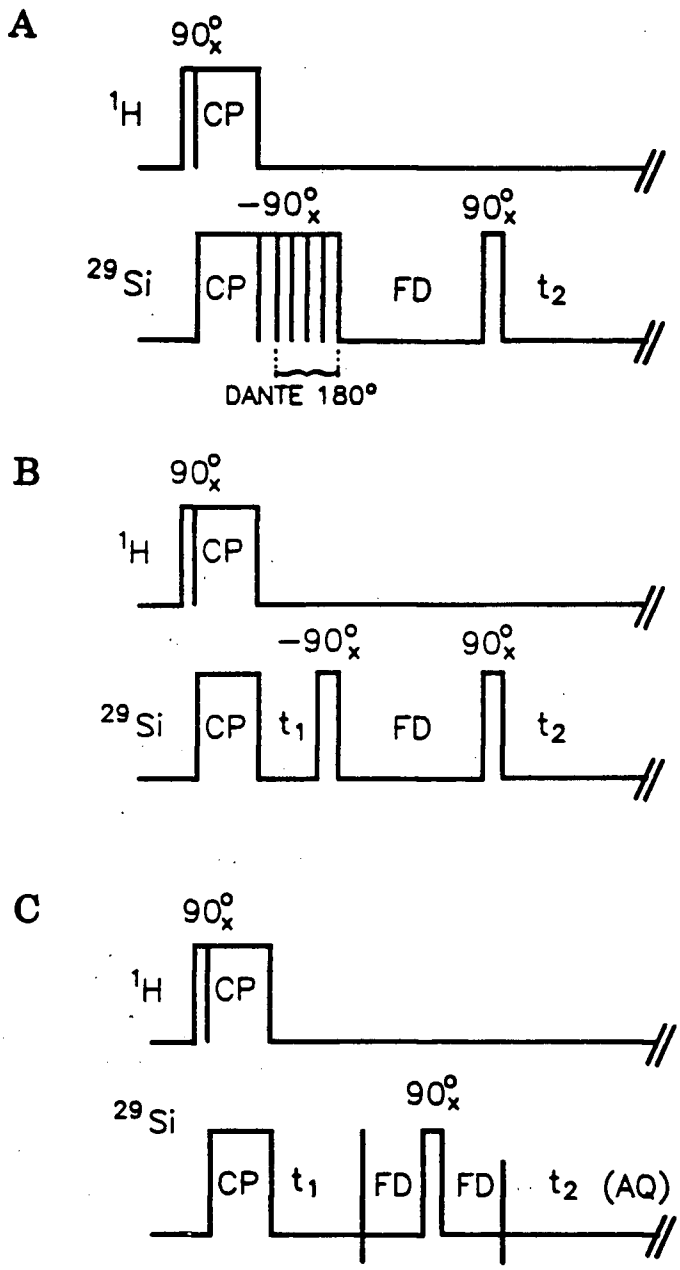

Figure 26. Schematic representation of the pulse sequences relevant to the 2D CP MAS NMR experiments.
(A) one-dimensional spin-diffusion pulse sequence with selective inversion of one resonance using a DANTE sequence.
(B) two-dimensional spin-diffusion pulse sequence.
(C) two-dimensional modified COSY pulse sequence.

III. RESULTS AND DISCUSSION

a) 1D Experiments

The 1D ^{29}Si CP MAS NMR spectra of ZSM-39 which are presented in Figure 27 show good resolution and are similar to those previously reported [90-94]. The three T sites are clearly resolved, and the structure of the T_3 resonance reflects the absence of a 3-fold symmetry axis. The resonances are quite narrow, indicating that the system is both highly siliceous and highly crystalline.

b) Spin-Diffusion Experiments

Spin diffusion can be understood as an energy-conserving 'flip-flop' process between two dipolar coupled nuclear spins. This phenomenon is responsible for the fact that a uniform spin temperature is obtained for abundant spins throughout a solid[54]. Due to its dipolar origin, the spin diffusion rate is proportional to r^{-6}. Thus, the spin diffusion experiments provide information on the spatial proximity of nuclei. Since ^{29}Si-O-^{29}Si distances are all approximately 3Å, while ^{29}Si-O-Si-O-^{29}Si distances are around 5.5Å in these systems, it was hoped that the two would be clearly differentiated. The pulse sequences used are shown in Figures 26A and B. During the mixing period (FD), spin diffusion takes place. The maximum mixing time (FD) will be limited by the spin-lattice relaxation time T_1 of the ^{29}Si nuclei, usually the FD $\leq T_1$. In the present instance, T_1 is of the order of 650 s and imposes no limitation on the experiments. However, the recycle time between pulse sequences is determined only by the spin-lattice relaxation time T_1 of the protons due to the use of the cross polarization technique. The proton T_1 in this sample is ~4 s, which makes the experiments very efficient.

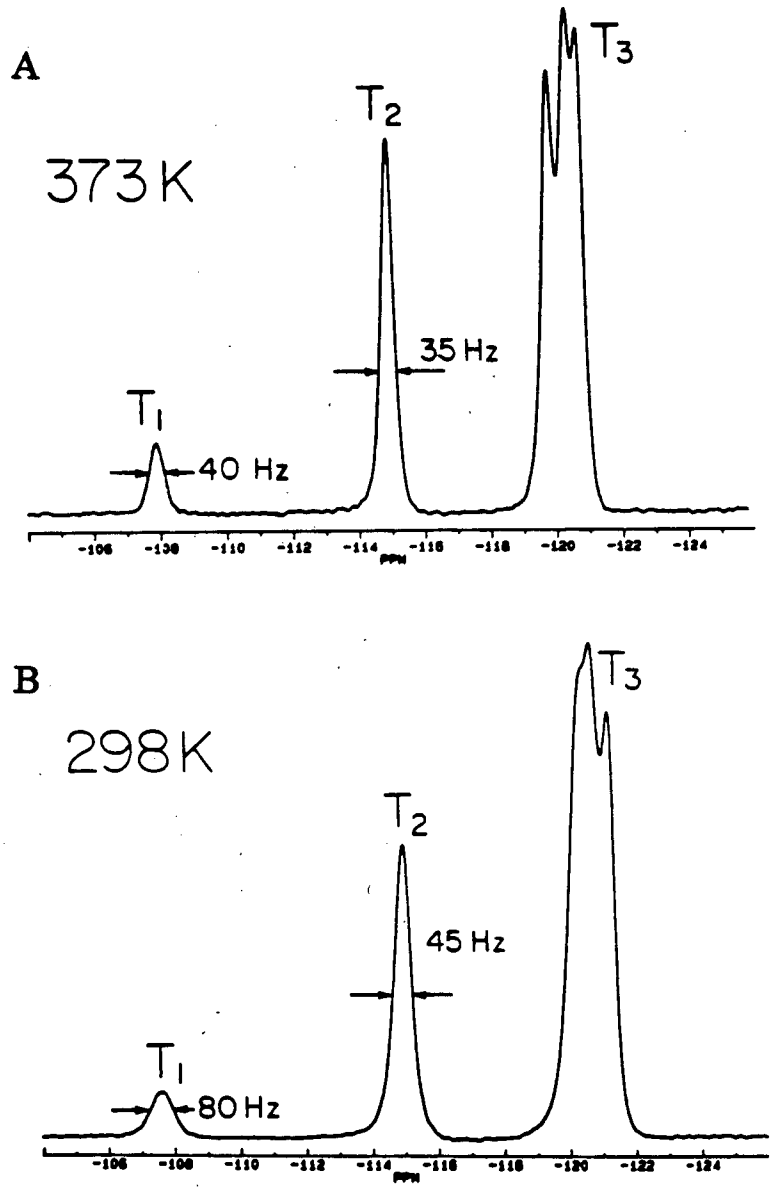

Figure 27. (A) ^{29}Si CP MAS NMR spectrum of zeolite ZSM-39 at 373K.
(B) ^{29}Si CP MAS NMR spectrum of zeolite ZSM-39 at 298K.

One-dimensional spin diffusion experiments were carried out using a DANTE sequence to selectively excite a specific resonance (Figure 26A). In this experiment, the magnetization of the ^{29}Si nuclei is generated in the xy plane by the CP technique, and stored back along z axis by a 90° pulse. Then one of the individual magnetizations is inverted by a DANTE sequence. After a mixing time (FD), where spin-diffusion takes place, application of a 90° pulse reestablishes the magnetization in the xy plane where the FID is recorded. The results of 1D spin diffusion experiments inverting T_3 and T_2 respectively are shown in Figure 28 and 29 with mixing times of 1s and 5s. Curve **a** represents the spectrum using the pulse sequence in Figure 26A. Curve **b** is the spectrum using the same sequence as curve **a** except that the transmitter of the ^{29}Si channel was gated off during the DANTE period, and curve **c** is the difference between **b** and **a**, which reflects the progress of the spin-diffusion process. As can be seen from the figures, there is relatively rapid spin diffusion between T_2 and T_3 and between T_1 and T_2, while the diffusion process between T_1 and T_3 is very much slower, in agreement with the known connectivities in the structure.

The spin-diffusion experiment can also be performed in a two-dimensional format using the sequence shown in Figure 26B. Figure 30 shows the result of a ^{29}Si 2D NMR experiment with a mixing time of 10 s, in which the expected connectivities T_1T_2 and T_2T_3 are clearly observed while that between T_1 and T_3 is not observed under these experimental conditions. It is known that the motion generated by the MAS technique decreases the dipole-dipole interactions of the spins and therefore the efficiency of the spin-diffusion process increases as the spinning rate is lowered. At either longer spin-diffusion periods

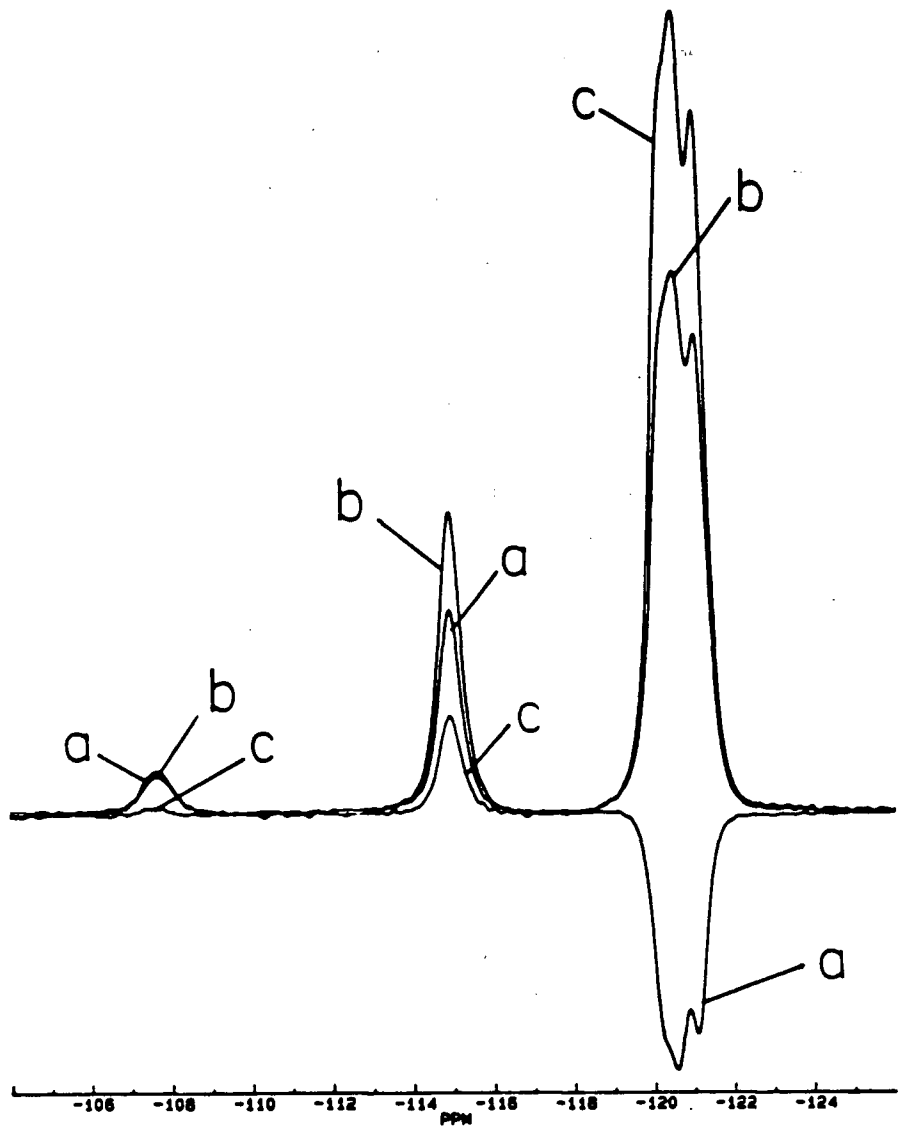

Figure 28 One-dimensional experiments using the pulse sequence of Figure 26A illustrating spin diffusion from the T_3 resonance, fixed delay 1 s. 8 scans were taken in each experiment with a contact time of 20 ms.

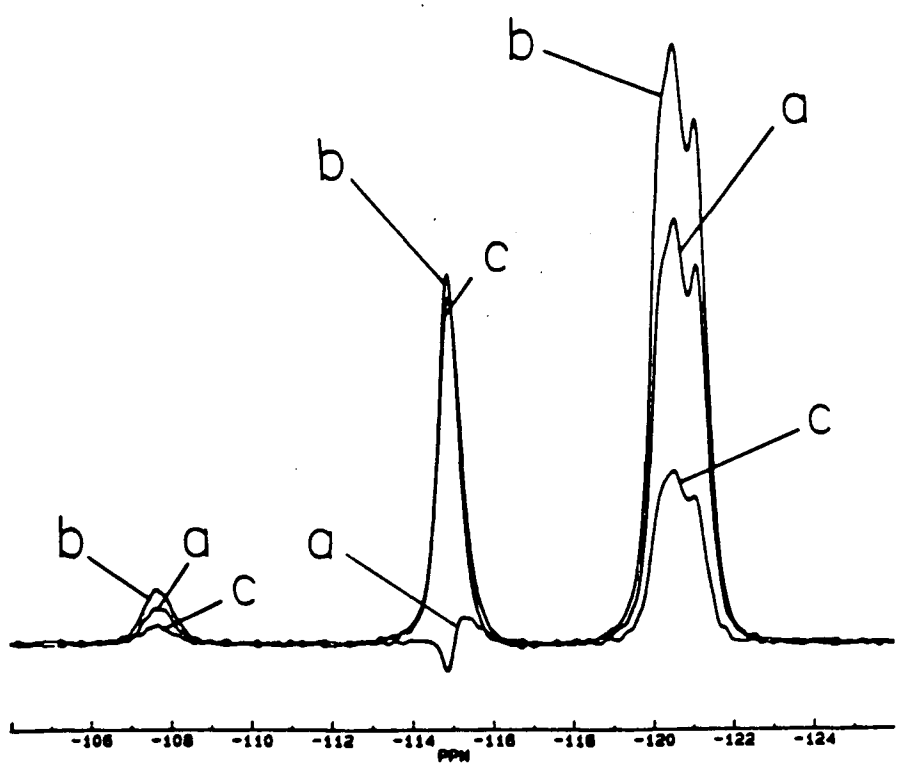

Figure 29 One-dimensional experiments using the pulse sequence of Figure 26A illustrating spin diffusion from the T_2 resonance, fixed delay 5 s. 8 scans were taken in each experiment with a contact time of 20 ms.

(25 s at 2 kHz spinning frequency) or shorter times at lower spinning rates (5-10s at 1 kHz rotor frequency), spin diffusion between T_1 and T_3 is eventually observed, as would be expected. Although the spin-diffusion rate is strongly dependent on the internuclear distance, it is also related to the chemical shift anisotropies and the isotropic shift differences of the interacting nuclei[99,100]. Since the atoms involved all have tetrahedral co-ordinations and the chemical shifts are well separated in this case, these non-distance dependent effects could well be minimal.

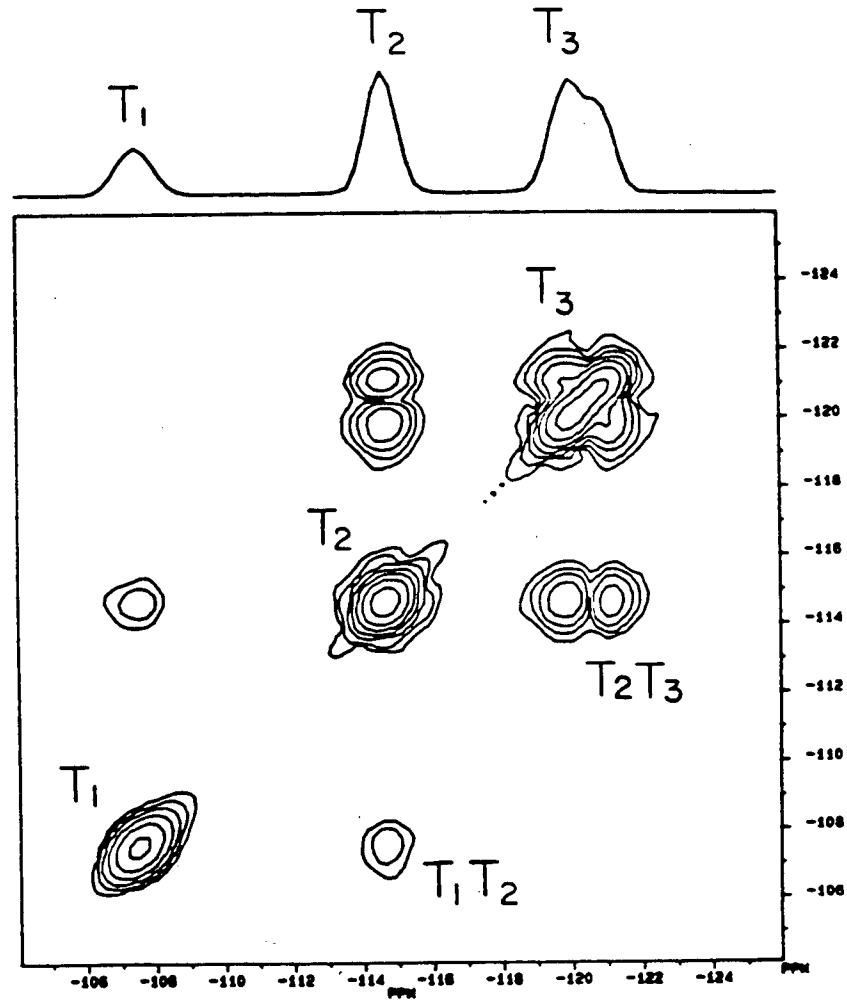

Figure 30 Contour plot of a 2D spin-diffusion experiment on ZSM-39 using the pulse sequence of figure 26B, with 128 experiments, 8 scans in each experiment, sweep width of 5 kHz, and 256 data points collected during acquisition. The fixed delay during which spin diffusion occurs was 10 s, the spinning rate 2 kHz, and the total time for the experiment approximately 6 h. Sine bell squared apodization was used, and the plot has been symmetrized.

c) COSY Experiments

An alternative and more reliable and unambiguous method is the COSY experiment. The pulse sequence used is shown in Figure 26C. The total evolution time is the sum of t_1 and FD due to the introduction of the fixed delay. A preliminary series of 2D COSY experiments were first carried out at room temperature. It was difficult to optimize the experimental conditions even in this simple system, because the lack of information on the magnitudes of the J couplings, and the values from solution NMR are not directly transferable to the solid state (see on). Either none or a single pair of cross peaks were observed in this series of experiments. Figure 31 shows the best results obtained in these preliminary experiments. A clear connectivity is established between T_2 and T_3 but the expected interaction between T_1 and T_2 is not observed. Although the intensity of the T_1 resonance is considerably less than the others and the number of interactions is 3 times lower than for T_2T_3, the S/N of the 2D plot is such that the T_1T_2 cross-peak should have been observable if it had had a similar growth profile. The major factors effecting the profile could be the J coupling and the T_2^* relaxation time. That is, the amount of magnetization transfer detected is proportional to $\exp(-t_1/T_2^*)\cdot\sin \pi J t_1$ [55]. It reaches a maximum at the time of $t_{max} = (1/\pi J)\tan^{-1}\pi J T_2^*$. For small J ($JT_2^* < 1$), $t_{max} = \sim T_2^*$. Thus an encoding time $\equiv 2T_2^*$ is needed. In solution, the major contributions to the line-width are field inhomogeneity and the natural spin-spin relaxation time. However the present situation is more complicated, and there are several other factors which will broaden the line: i) dispersion of isotropic chemical shifts due to structural disorder including residual aluminum and the disorder of templates; ii) unaveraged dipolar interactions of the ^{29}Si nucleus with ^1H; iii) the presence of

paramagnetic impurities in the sample; iv) overlapped multiplet splittings due to the ^{29}Si-O-^{29}Si couplings in this enriched sample. Therefore, the best encoding time is expected to be longer than $2T_2^*$, but is not attainable in practice.

Inspection of Figure 27B reveals that the width of the T_1 resonance is approximately twice that of the other signals (~80 vs ~45 Hz), which could affect the detection of the cross peaks involving this resonance. In an attempt to narrow the resonances, the sample temperature was raised[90,93]. The linewidth of the T_1 resonance at 373 K was reduced to one half of that at room temperature (Figure 27), which would make the COSY experiments more efficient. Therefore a second series of experiments were performed at 373 K and the results of the best one under the conditions indicated in figure caption are shown in Figure 32 . In addition to the T_2T_3 cross peaks previously observed, T_1T_2 connectivities are now clearly visible. The doubling of the T_2T_3 cross peak is caused by the partial resolution of the T_3 resonances due to the absence of cubic symmetry. These results are in exact agreement with the known connectivities of the structure. In an attempt to optimize the encoding times, variable fixed delay experiments were carried out, keeping all other parameters constant. The results are listed in Table 9, in which the intensities of the T_1T_2 cross peak are presented relative to the T_2 diagonal peak intensities . When the encoding time is increased from 31-46 ms the intensities of the T_1T_2 cross peak decease dramatically, confirming the importance of T_2^* in the solid state experiments. The T_1 resonance has a linewidth of ~40 Hz and thus T_2^* is approximately 8 ms calculated from the equation: $T_2^* = 1/(\pi \cdot \Delta\nu_{1/2})$. The best encoding time from these experiments is ~31 ms, being around $4T_2^*$, in agreement with expectations.

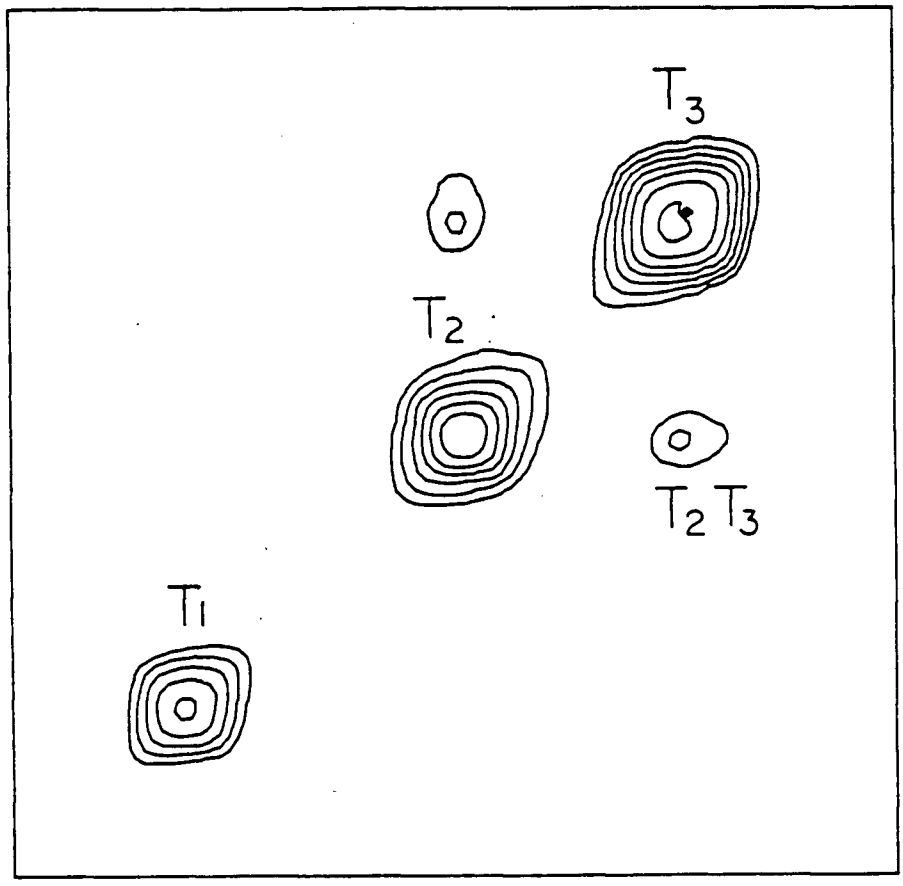

Figure 31 Contour Plot of COSY experiment on ZSM-39 carried out at ambient temperature with 128 experiments, 48 scans in each experiment, sweep width of 5 kHz, and 256 data points collected during the acquisition. The fixed delay was 15 ms and the total experimental time approximately 17 h. Sine bell squared apodization was used and the plot symmetrized.

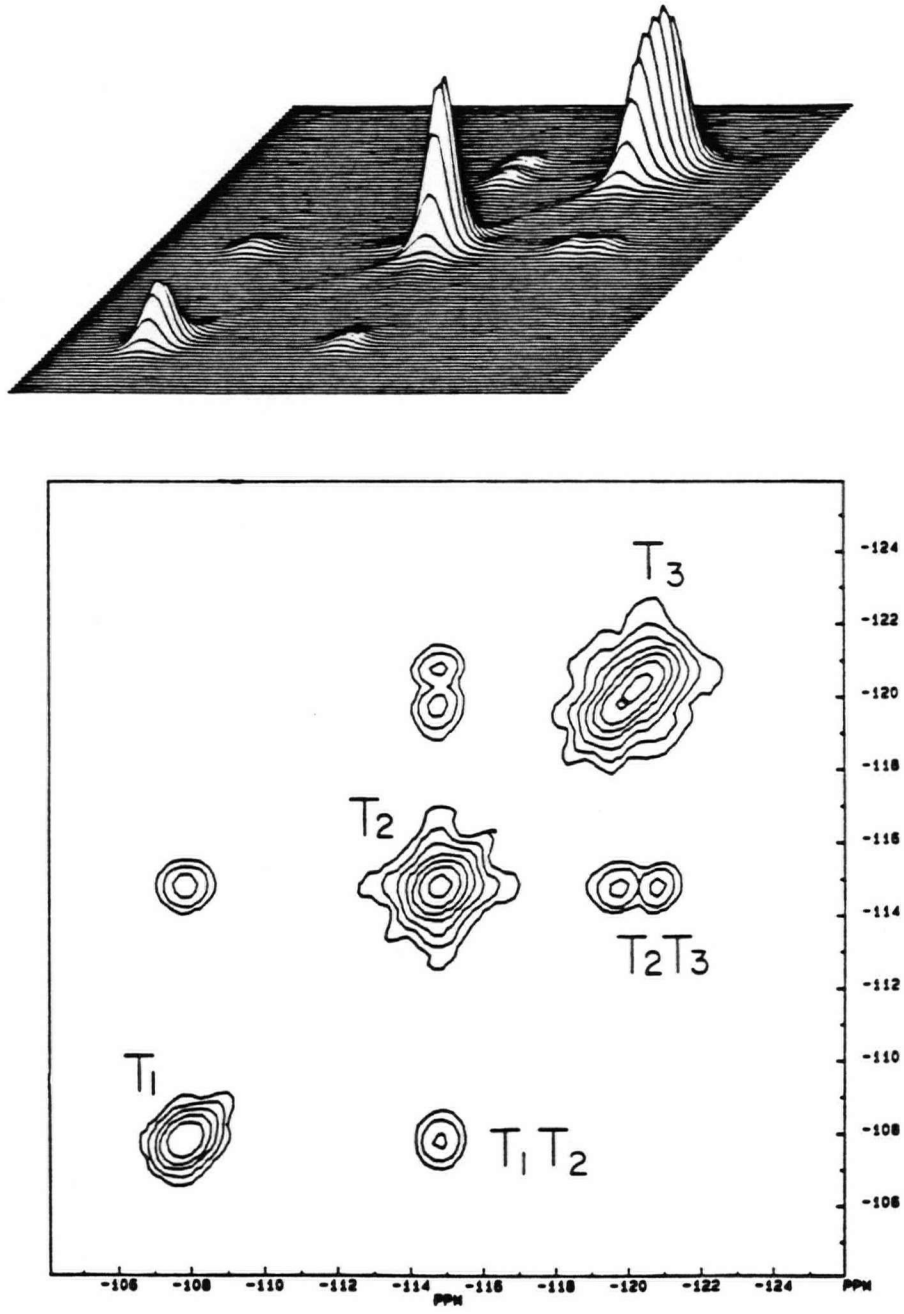

Figure 32 Contour and stacked plots of a COSY experiment on ZSM-39 carried out at 373k, with 128 experiments, 64 scans in each experiment, sweep width of 5 kHz, and 256 data points collected during the acquisition. The fixed delay was 5 ms and the total experimental time approximately 23 h. Sine bell apodization was used, and the data are presented without symmetrization.

Table 9 The results of variable fixed delay experiments.

fixed delay (ms)	total encoding time(ms)	cross peaks visible (pair)	relative intensity ratio* of T_1T_2/T_2
20	46	1	0
15	41	2	0.15
10	36	2	0.5
5	31	2	1
2	28	2	~1

* The intensity ratio of T_1T_2/T_2 at 5 ms fixed delay is taken as unity.

With the experience in the experiments at 373K and the knowledge of the importance of the T_2^*, an attempt of performing COSY experiments at ambient temperature was made again with the number of experiments reduced to 64, to reduce the encoding time to one half. The best result is shown in Figure 33 and was obtained at the total encoding time of 15 ms, which is again ~$4T_2^*$. Both T_1T_2 and T_2T_3 correlations are clearly observed over a range of total encoding times of 13-18 ms. The resolution and sensitivity of these experiments are worse than those at 373 K. The degradation in the quality of the correlations at ambient temperature may be recovered to some extent by the use of double quantum filtered (DQF) COSY experiments. A conventional DQF-COSY pulse sequence was used except that a CP sequence was used to excite the ^{29}Si magnetization. A suitable choice of the phase cycle is used to separate out single quantum signals from the signals which come from coupled pairs. Figure 34 shows the results of a DQF COSY experiment where the quality of the connectivities is almost completely recovered. It is even possible to observe both connectivities when the number of frequency encoding experiments is reduced to 32 for this system.

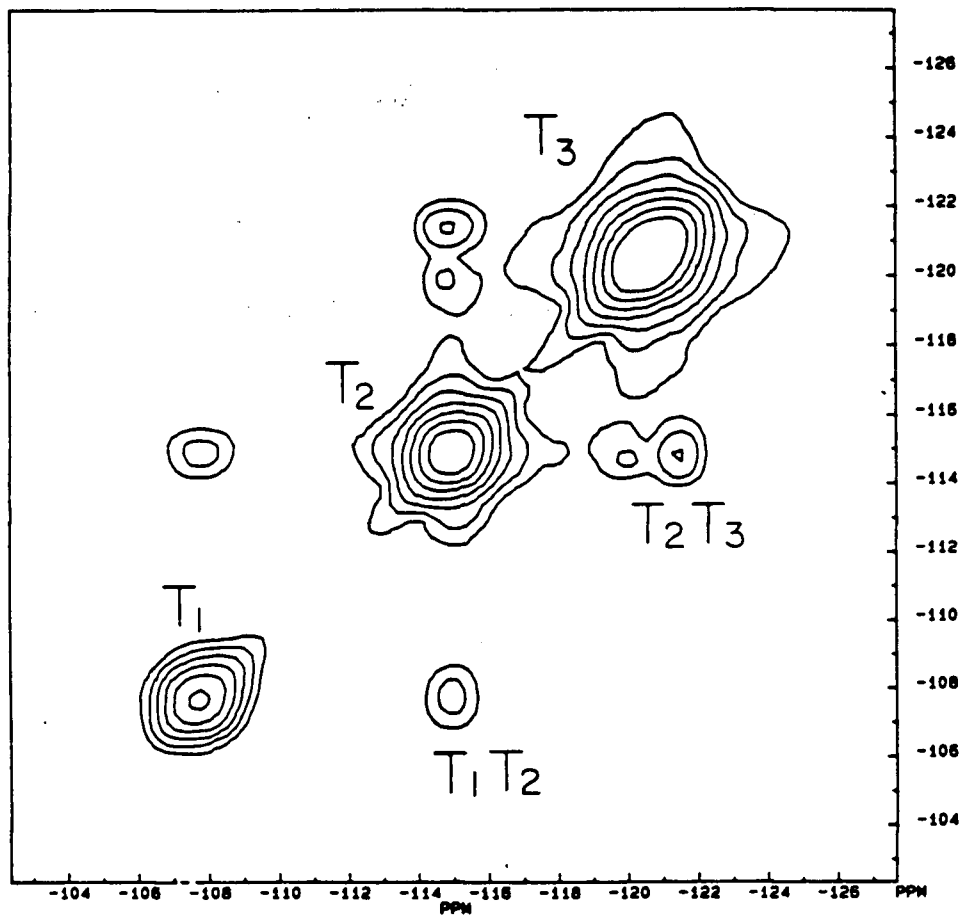

Figure 33 Contour plot of a COSY experiment on ZSM-39 carried out at 298k, with 64 experiments, 80 scans in each experiment, sweep width of 5 kHz, and 256 data points collected during the acquisition. The fixed delay was 2 ms and the total experimental time approximately 14 h. Sine bell apodization was used, and the data were symmetrized and a smoothing function applied.

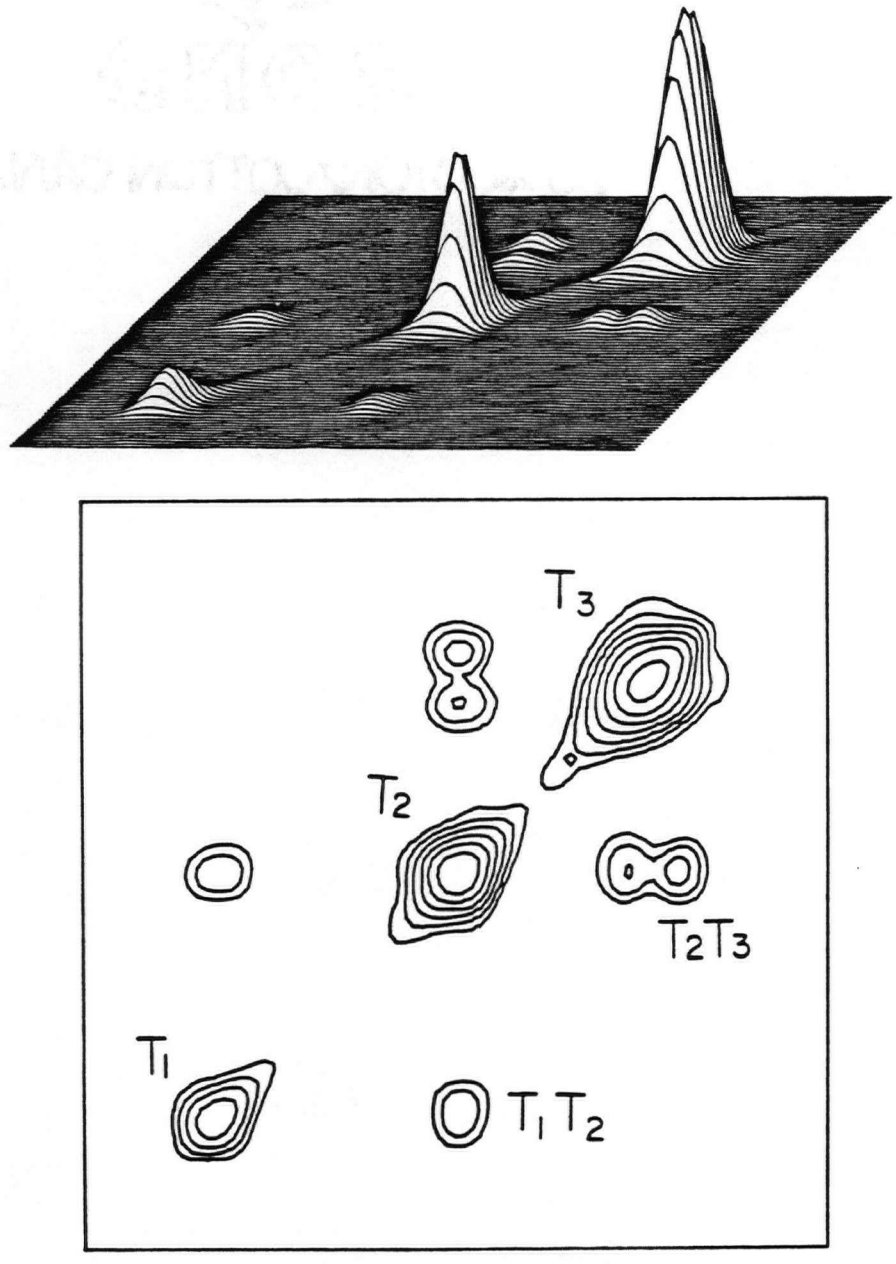

Figure 34 Contour and stacked plots of a DQF COSY experiment on ZSM-39 carried out at 298k, with 64 experiments, 128 scans in each experiment, sweep width of 5 kHz, and 256 data points collected during the acquisition. The fixed delay was 2 ms and the total experimental time approximately 23 h. Sine bell apodization was used, and the data are presented without symmetrization.

B. TWO-DIMENSIONAL ^{29}SI HIGH-RESOLUSION SOLID STATE NMR INVESTIGATION OF THE LATTICE STRUCTURE OF ^{29}SI-ENRICHED ZEOLITE DECA-DODECASIL 3R (DD3R)

I. INTRODUCTION

Deca-dodecasil 3R (DD3R) was first synthesized by Gies[101] in 1986, by crystallization from an alkaline silicate solution with 1-aminoadamantane as template. The sample used in the present work was prepared from ^{29}Si enriched sources again to increase the number of ^{29}Si-O-^{29}Si interactions. The silica host framework of DD3R is related to the framework types of the dodecasil series [102], one example of which is ZSM-39 (see section A). In ZSM-39, layers of pentagonal dodecahedra are directly stacked in an ABCABC sequence. However, in DD3R, the same layers are stacked in an ABCABC sequence, but interconnected by additional SiO_4 tetrahedra. The space group of DD3R was determined by Gies[101] as R3m from a single crystal diffraction study of template-containing material. The schematic representation of the DD3R lattice framework is shown in Figure 35A. The T-site 5 cannot be shown in this figure because it is located between the layers and acts as a linkage. Figure 35B shows the [100] projection of the structure and in this projection T-site 5 is clearly visible. The structure has a unit cell of 120 T-atoms distributed over seven sites in the relative proportions 6: 3: 3: 3: 3: 1: 1. The expected connectivities for the T-sites are presented in Table 10. Compared to ZSM-39, 2D correlation experiments on DD3R will be a more demanding test of the techniques because of the larger number of signals and more complex connection pattern expected.

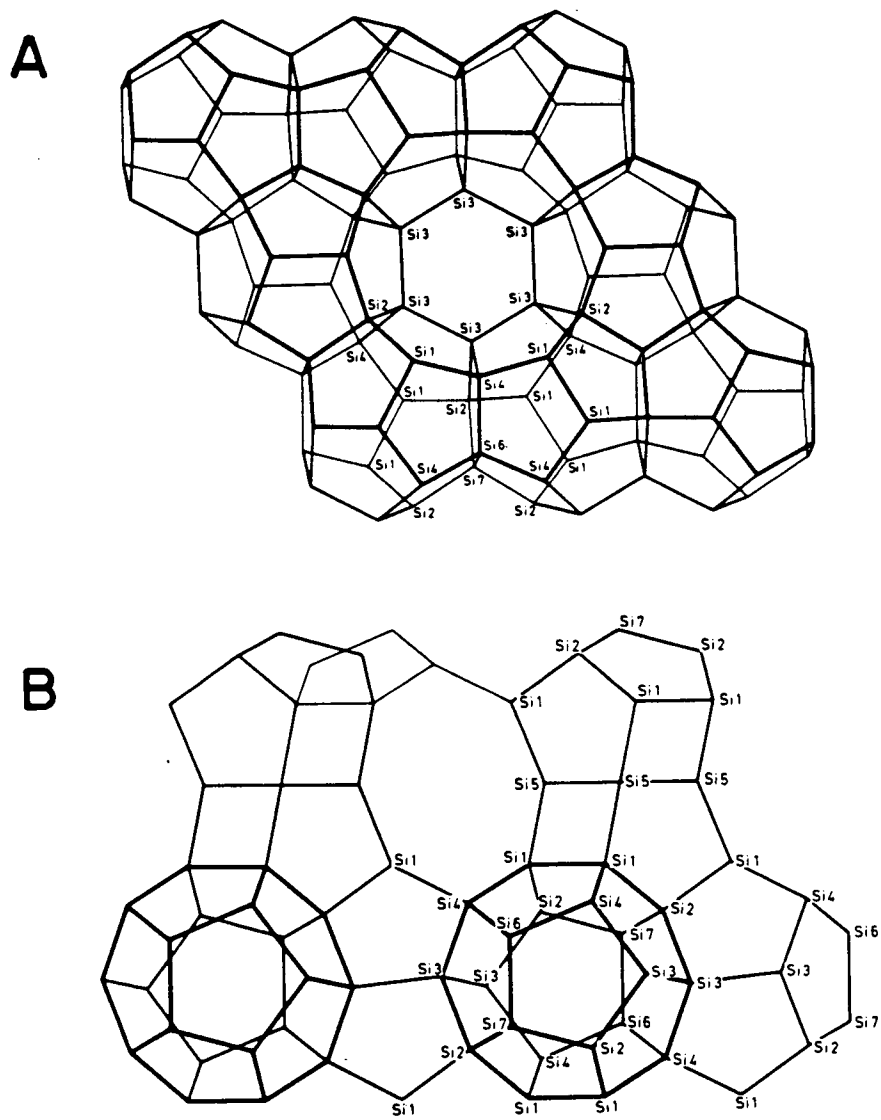

Figure 35 (A) Schematic representation of the zeolite DD3R lattice framework viewed along c axis.
(B) The projection along the a axis of the structure. The seven crystallographically inequivalent tetrahedral T-sites are indicated by Si1 etc. (ref. 95)

Table 10 T-sites, Their Occupancies, and Connectivities for the Asymmetric Unit in Zeolite DD3R (Ref. 101)

T-site	occupancy	connectivity
T_1	6	$1T_1$: $1T_2$: $1T_4$: $1T_5$
T_2	3	$2T_1$: $1T_3$: $1T_7$
T_3	3	$1T_2$: $2T_3$: $1T_4$
T_4	3	$2T_1$: $1T_3$: $1T_6$
T_5	3	$2T_1$: $2T_5$
T_6	1	$3T_4$: $1T_7$
T_7	1	$3T_2$: $1T_6$

II. EXPERIMENTAL

^{29}Si MAS NMR spectra were obtained at 79.49 MHz on a Bruker MSL-400 spectrometer using the techniques previously described. 2D COSY-45 experiments were performed using the pulse sequence shown in Figure 36A. The replacement of the second 90° pulse (Figure 17A) with a 45° pulse simplifies the appearance of the spectrum around the diagonal to make the cross peaks close to the diagonal more easily observed. The fixed delay is used to enhance small couplings. The sample as-synthesized showed broad lines and had to be investigated in its calcined form and thus CP and proton decoupling techniques could not be used. 2D INADEQUATE experiments were performed using the pulse sequence shown in Figure 36B. The replacement of the last 90° pulse (Figure 18A) with a 135° pulse provides quadrature detection in the double quantum frequency domain (103).

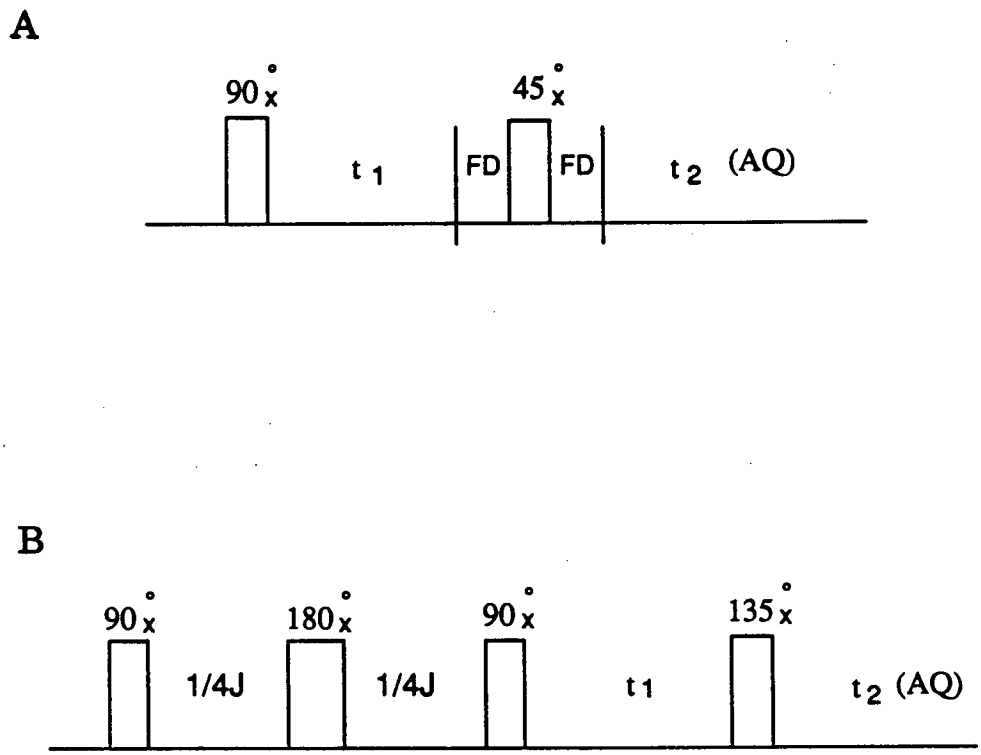

Figure 36. Schematic representation of the pulse sequences used in the 2D MAS NMR experiments:
(A) 2D COSY-45 pulse sequence,
(B) 2D INADEQUATE pulse sequence.

A highly siliceous sample of DD3R was synthesized hydrothermally by Dr. Hermann Gies, U. Bochum, Germany, in a sealed silica glass tube in 14 days at 160°C using 1- aminoadamantane as template, and the silica source was enriched to ~80% in ^{29}Si.

III. RESULTS AND DISCUSSION

a) 1D Experiments

The 1D ^{29}Si MAS NMR spectrum is shown in Figure 37A, in which the assignments of the T-sites come from the 2D studies (see on). Figure 37B shows the computer simulation of the spectrum as seven peaks. The relative intensities of the peaks are 1:3:3:3:6:3:1 as expected. The linewidths are around 40 Hz, which is of the same order as those in ZSM-39 and the previous results were used as a guide for the choice of parameters in the present work.

b) 2D COSY Experiments

According to the results obtained from the experiments on ZSM-39, the total encoding time was chosen to be ~$4T_2^*$ because both samples were ^{29}Si enriched and the sources of line broadening should be similar. Figure 38 shows the results of a COSY experiment carried out using the experimental parameters given in the figure caption. To facilitate the discussion, the seven resonances are denoted as A-G from high to low field, as indicated in the F_2 projection. Although a number of cross-peaks are clearly observed, it is difficult to make an assignment of the spectrum from this data alone because the postulated structure is not completely correct for this sample (see on) and the low field resonances are

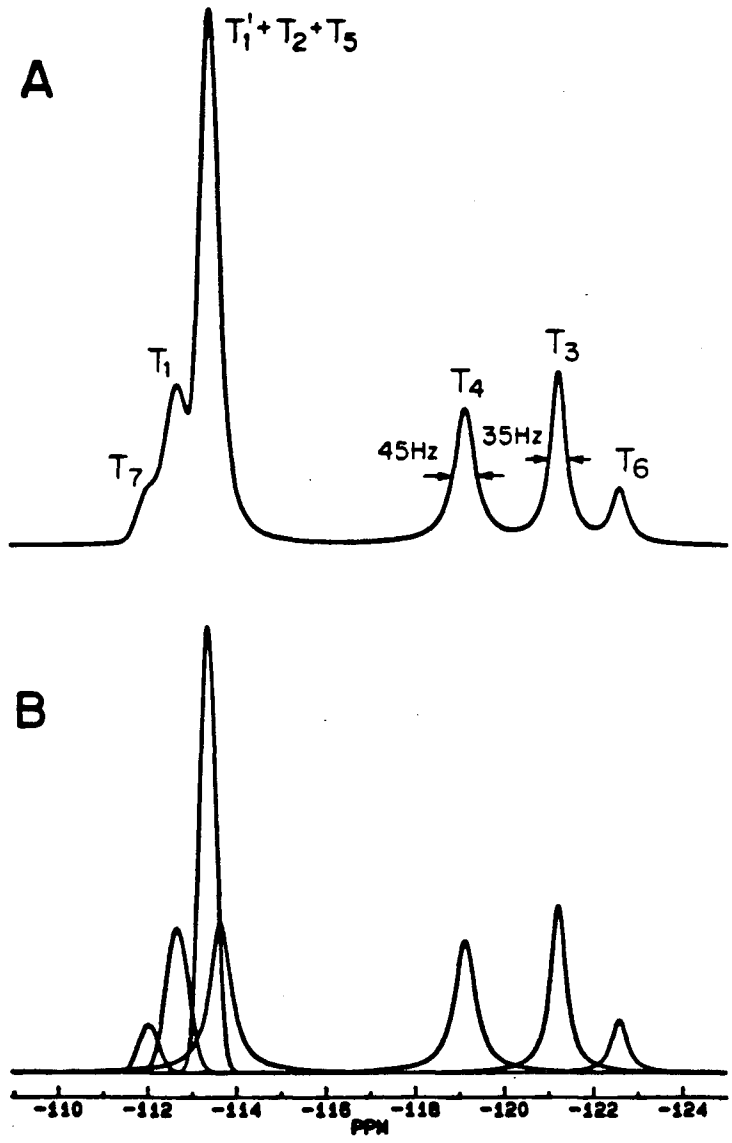

Figure 37 (A) ^{29}Si MAS NMR spectrum of ^{29}Si enriched DD3R at 300 K.
(B) Combined Lorentzian-Gaussian curves used in the computer simulation of spectrum A.

overlapped. The assignment may be obtained by combining the NMR results with XRD data in such way that the T- sites with longer mean T- T distances will be associated with the resonances at the lower field[117] (see Section E, Chapter Five). The resonances A and G of unit intensity can be assigned to T_6 and T_7, which are connected to each other as expected. Resonance A can be assigned as T_6 due to the longer average T-T distances than that of T_7[101]. It should be noted that there are very substantial errors in the XRD derived parameters. However in the present instance the chemical shift difference is thought to be large enough that the assignment is reliable. From Figure 38 and Table 10, T_6 is connected to T_4 as well as T_7, thus assigning G $\rightarrow T_7$ and C $\rightarrow T_4$. T_7 is connected to T_2 as well as T_6 and therefore the T_2 resonance is within D/E. In order to develop the connectivity network, Table 11 lists the connectivities of T_4, T_2 and C, D/E. The assignment of B $\rightarrow T_3$ can be readily made. Thus some complexity is removed by the fact that two resonances, F and one in D/E are associated to T_1. No connectivity between T_2 and T_1 is visible, which can be understood since their resonances are too close to be resolved and the cross peaks will be buried in the strong diagonal signals. This experiment was repeated a number of times to confirm the 'doublet' structure of T_4T_1. A possible explanation is that the symmetry of the structure is lower and there are two inequivalent T_1 sites. The only resonance unassigned until now ,T_5, must be within D/E, and the complete assignment is shown in Figures 37 and 38. Thus, it is deduced that there are 8 resonances in the NMR spectrum, which is not clear from the 1D data. This illustrates the advantages of 2D experiments in determining the contents of the asymmetric unit of an unknown sample.

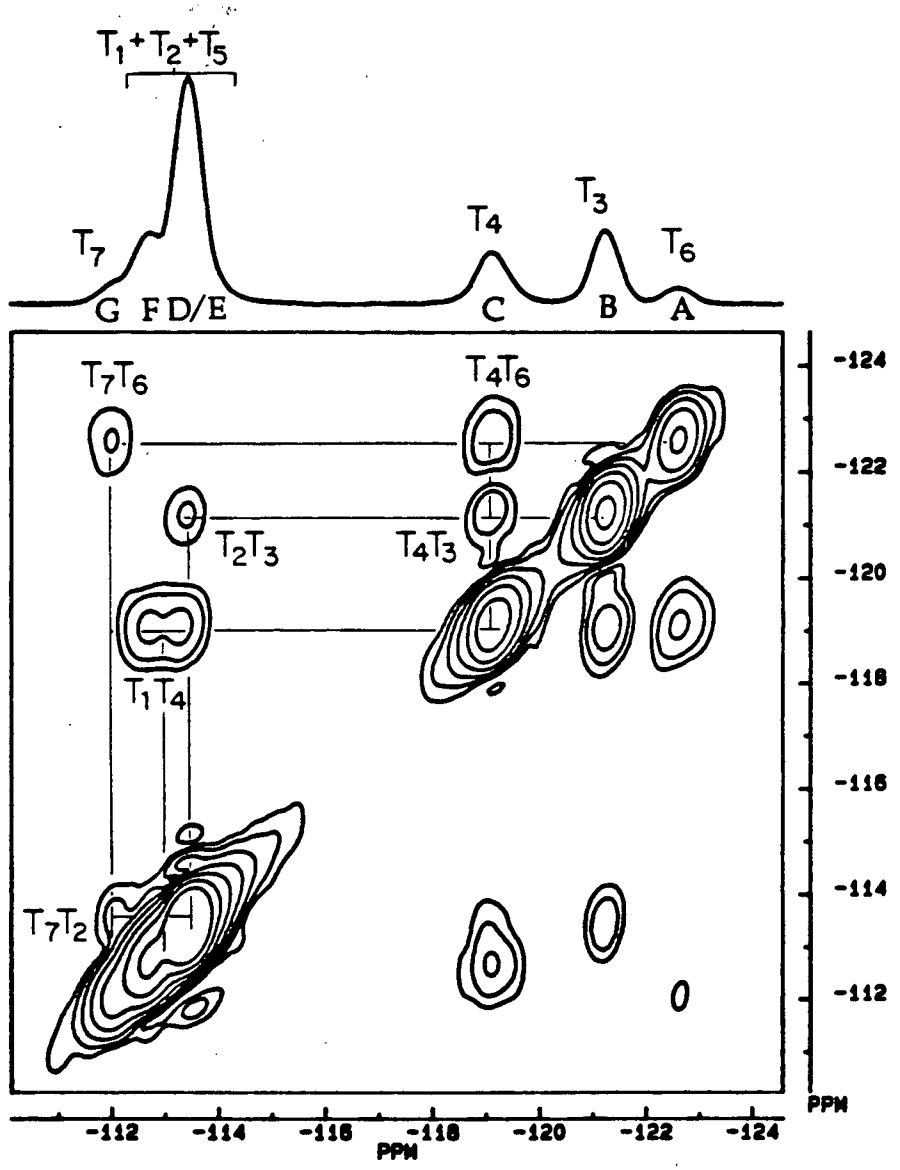

Figure 38 Contour plot of a COSY experiment with the projection on the top, carried out at 300K with 64 experiments, 992 scans in each experiment, a sweepwidth of 2500 Hz and 256 data points collected during the acquisition. The fixed delay was 2 ms and the total encoding time was 28 ms. Sine-bell squared apodization was used and the plot is unsymmetrized.

Table 11 Connectivities Related to T-sites 4, 2 and Resonances C, D/E in the DD3R Structure

T_4	T_1	T_1	T_3	T_6
C	D/E	F	B	A

T_2	T_1	T_1	T_3	T_7
D/E			B	G C

c) 2D INADEQUATE experiments

Figure 39 shows the results of a 2D INADEQUATE experiment on the same sample. 2D INADEQUATE experiments will be discussed in more detail in Chapter Four, but this one example is included here for completeness of the discussion of zeolite DD3R structure. All of the connectivities previously observed in the COSY experiment are clearly seen as indicated by the assignments in the figure. The existence of the T_2T_7 connection is confirmed. In addition, the T_1T_2 coupling pair within the low field signals can be observed. The 'doublet' structure of the T_1T_4 pair is very clearly and unambiguously seen confirming the results of the COSY experiment. The same observation in two different types of experiments indicates that the existence of two inequivalent T_1's is real.

NMR spectroscopy is known to be more sensitive to local environments than diffraction techniques and can be used as a subtle probe of the contents of asymmetric units. As a working hypothesis, it is postulated that the T_1 sites are split into two types T_1 and T_1' due to the loss of some symmetric element or elements. From subgroup-supergroup relationships, R3 is the only space group

which can explain the splitting of the T_1 position. It should be noted that the XRD study of the single crystal of DD3R was performed on its uncalcined form containing template, while the NMR measurements were carried out on a calcined sample. There are some known examples where calcined samples have lower symmetry, eg. zeolite ZSM-5. The templates are trapped inside channels and cavities of zeolites during preparation and the total energy of the system could be lower because of the interaction between templates and frame work, and the symmetry could be higher[104]. A recent refinement [105] on the calcined sample prompted by these results supports the lower space group symmetry in agreement with the present NMR data.

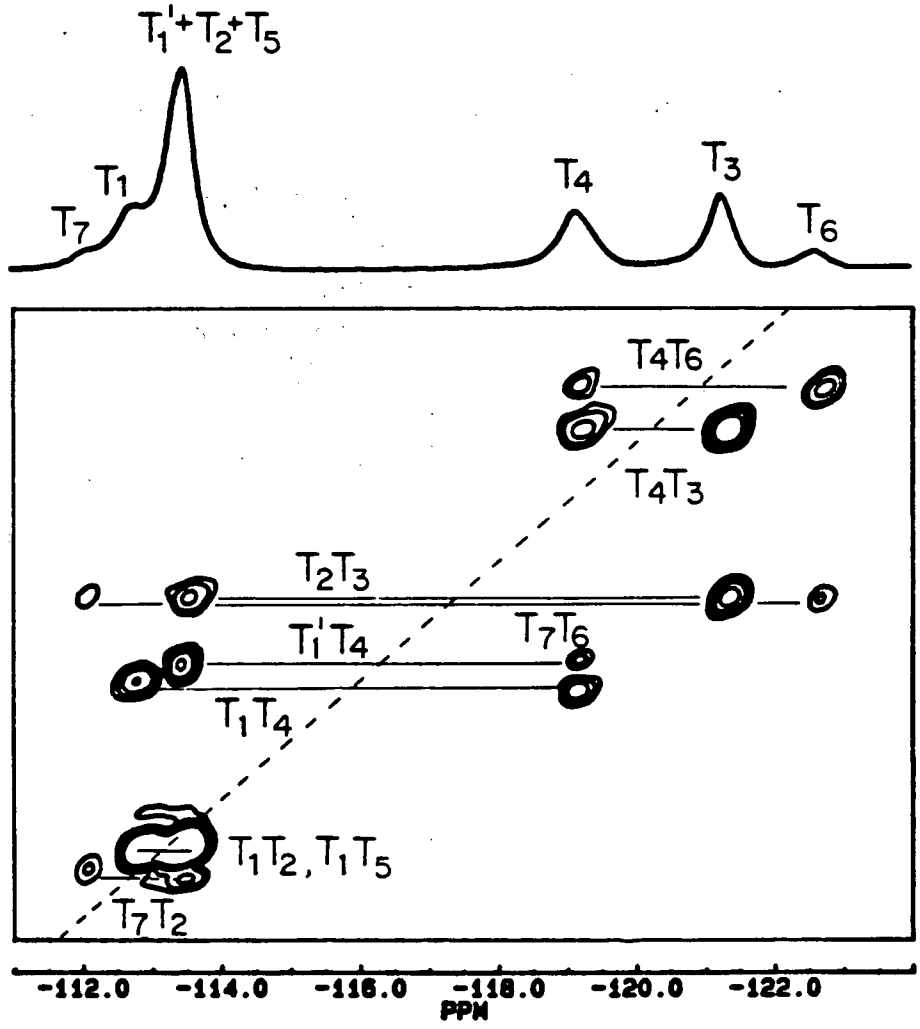

Figure 39 Contour plot of an INADEQUATE experiment on DD3R at 300 K with 44 experiments, 448 scans per experiment, 1285 Hz sweepwidth, a fixed delay of 20 ms, and 128 data points collected during the acquisition. Trapezoidal and shifted sine bell apodization were used for F_1 and F_2 dimensions, respectively.

CHAPTER FOUR

NATURAL-ABUNDANCE TWO-DIMENSIONAL SOLID STATE ^{29}SI NMR INVESTIGATION OF THE THREE-DIMENSIONAL LATTICE CONNECTIVITIES IN ZEOLITES ZSM-12 AND ZSM-22

A. INTRODUCTION

Our initial 2D NMR studies of zeolites ZSM-39 and DD3R (see Chapter Three) have demonstrated that homonuclear correlation spectroscopies including COSY, INADEQUATE and spin-diffusion experiments yield the correct (known) connectivities of the lattice structures. The results of these experiments thus lay the groundwork for subsequent investigations. However, these two samples were prepared by using an 80% ^{29}Si enriched silica source to increase the signal to noise ratio and enhance the connectivities due to the ^{29}Si-O-^{29}Si interactions. Such high degrees of isotopic enrichment are too expensive and difficult for routine use. In order that these techniques can be widely used to investigate the lattice structures of zeolites it must be possible to perform them on natural abundant samples. Sensitivity could be considered to be the most serious problem in the 2D work because of the low ^{29}Si natural abundance of 4.7%. The probability of a ^{29}Si nucleus being involved in a ^{29}Si-O-^{29}Si pair will be ~19%. Therefore, ~81% among the 4.7% ^{29}Si nuclei are not coupled, and 19% will be in coupled pairs. Fortunately, there are some advantages in using natural

abundance samples. Firstly, only the very best samples need be chosen for 2D NMR work due to the lower expense in synthesis. They are usually very highly crystalline and 'aluminum-free', giving very sharp peaks in their NMR spectra, usually with linewidths of 10- 30 Hz. Thus the resolution will be better and the intensity left after the encoding time may be improved due to the longer T_2^*. Secondly, the interactions involved between ^{29}Si nuclei will be simpler than enriched samples since they are dilute. The zeolites chosen for starting this study were zeolite ZSM-12 and ZSM-22, whose structures are well defined and which were considered reasonably typical of these systems in terms of complexity.

B. NATURAL-ABUNDANCE TWO-DIMENSIONAL ^{29}SI HIGH-RESOLUTION SOLID STATE NMR INVESTIGATION OF THE LATTICE STRUCTURE OF ZEOLITE ZSM-12

I. INTRODUCTION

Zeolite ZSM-12 was first synthesized by Rosinski and Rubin[106]. The general lattice structure was proposed by LaPierre[46]. Fyfe and Gies [47] have recently determined the space group of ZSM-12 as C2/c by a combination of synchrotron powder X-ray data with solid state NMR measurements (see Chapter One). ZSM-12 is high silica zeolite with 12-membered ring channels along the c axis. A schematic representation of the lattice framework is shown in Figure 40. The asymmetric unit consists of seven crystallographically inequivalent T sites as indicated in the figure. The connectivity scheme of ZSM-12 is given in Table 12. There are a total of ten connectivities, of which nine are

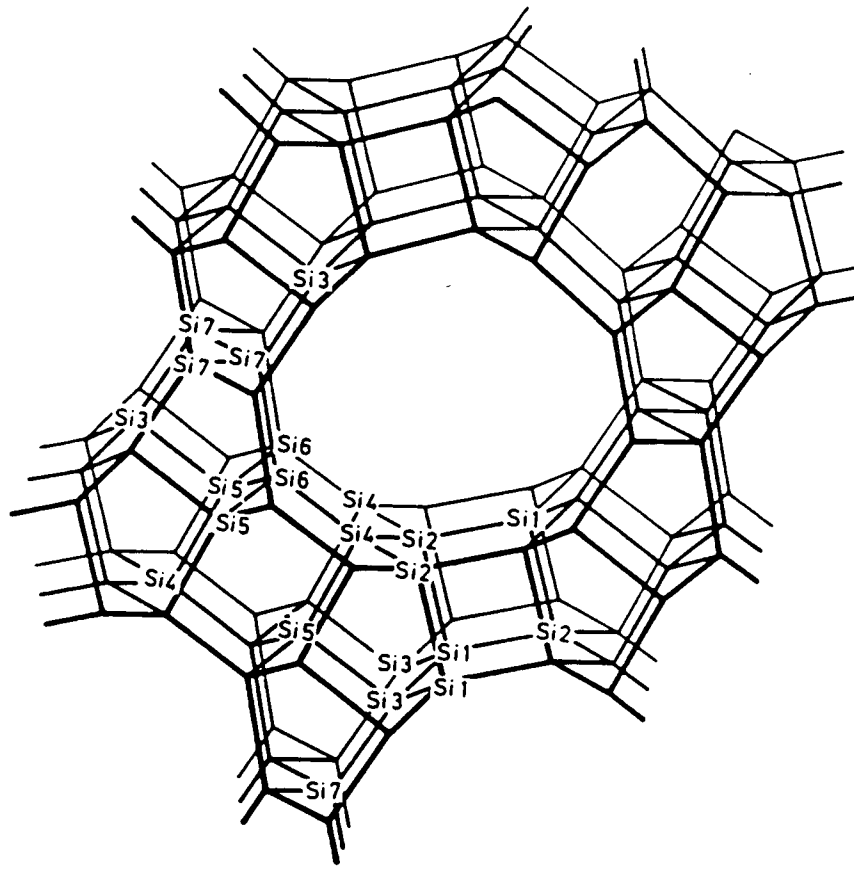

Figure 40 Schematic representation of the lattice structure of zeolite ZSM-12. The seven crystallographically inequivalent T-sites are indicated by Si1, Si2,...,Si7. (ref. 108)

expected to be observable in 2D experiments. The link between the equivalent silicons at the site 7 can obviously not be detected directly in NMR experiments.

Table 12 T-sites, Their Occupancies, and Connectivities for the Asymmetric Unit in Zeolite ZSM-12 (Ref. 47)

T-site	occupancy	connectivity
T_1	1	$2T_2$: $2T_3$
T_2	1	$2T_1$: $2T_4$
T_3	1	$2T_1$: $1T_5$: $1T_7$
T_4	1	$2T_2$: $1T_5$: $1T_6$
T_5	1	$1T_3$: $1T_4$: $2T_6$
T_6	1	$1T_4$: $2T_5$: $1T_7$
T_7	1	$1T_3$: $1T_6$: $2T_7$

II. EXPERIMENTAL

^{29}Si MAS NMR spectra were obtained at 79.49 MHz on a Bruker MSL-400 spectrometer using the techniques previously described. In the COSY experiments, samples were spun at frequencies equal to, or a multiple of, the spectral sweep width. The pulse sequences used are shown in Figure 36. Since the linewidths of ~9 Hz (Figure 41) are of the order of those obtained in solution spectra and the coupled pairs are isolated, it is considered that field inhomogeneity is the major source of the linewidths. Thus $\sim 2T_2^*$ value of 58 ms was chosen for the total encoding time in COSY experiments.

A highly siliceous sample of ZSM-12 was synthesized hydrothermally by Gwyneth Barlow, U. of Guelph, using methyltriethyl ammonium chloride as a template according to the literature[74].

III. RESULTS AND DISCUSSION

a) COSY experiments

The 1D ^{29}Si MAS NMR spectrum shown in Figure 41 is composed of seven well-resolved resonances with ~9 Hz linewidths. The number and intensities of the resonances are in agreement with the proposed structure and previously published spectra[47].

2D COSY 45 experiments were carried out first, and Figure 42 shows contour plots from a typical one. As can be seen, all 9 expected connectivities between the resonances are clearly observed in the plot. The assignments of the resonances can be deduced unambiguously from the connectivities given in Table 12 in several different ways. The most important thing is to identify a starting point for tracing the coupling patterns. One starting point is the observation that three T sites have only two connectivities which can be obtained in a COSY experiment, i.e. T_1, T_2 and T_7. By drawing vertical lines through every peak in the projection, three lines hit cross-peaks twice and the others three times. The three resonances showing two connectivities are A, C and D, which are thus associated with these three T sites. From the fact that T_1 and T_2 are connected to each other and T_1 and T_7 are simultaneously connected to T_3, the following associations can be made: A→ T_2, D→ T_1, C→ T_7 and G→ T_3. T_2 has double connectivities to both T_4 and T_1, and since T_1 is known, the resonance F must be T_4. Similarly, the assignments of B→ T_5 and E→ T_6 can be made. The complete assignment is shown in the figure. An alternative starting point comes from the differences in spin-lattice relaxation times, T_1, of the seven nuclei.

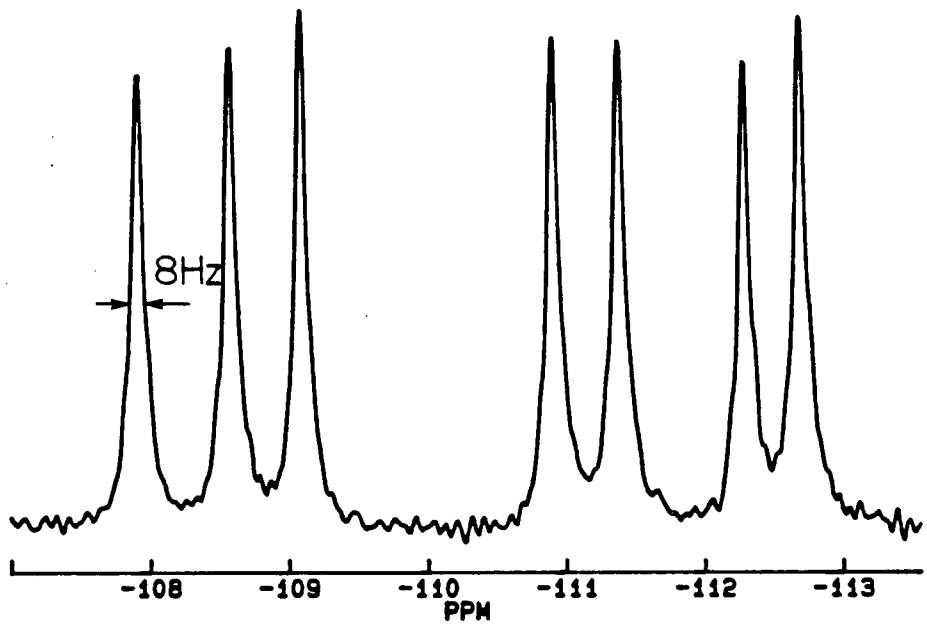

Figure 41 ^{29}Si MAS NMR spectrum of zeolite ZSM-12. The spectrum were obtained at room temperature with 128 scans and 1 K data points before zero-filling.

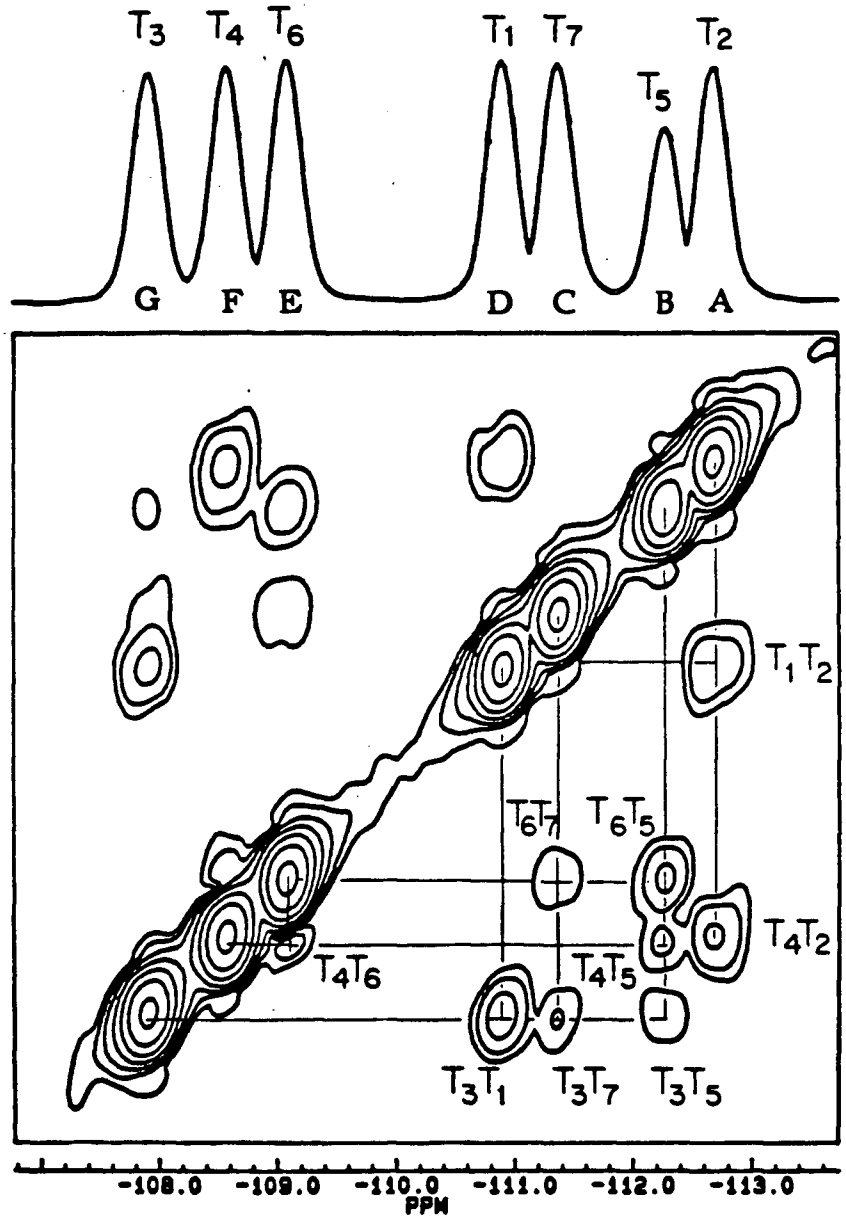

Figure 42 Contour plot of a COSY experiment on zeolite ZSM-12 with a projection in the F_2 dimension carried out at 300 K with 64 experiments, 160 scans in each experiment, sweep width of 1200 Hz, and a fixed delay of 5 ms. 256 data points in F_2 before zero-filling, sine bell squared apodization and magnitude calculation were used for data processing.

All T_1 values of ^{29}Si nuclei in ZSM-12 are ~ 10 s except that of the nucleus associated with resonance B (see Figure 23), which is almost double this value. As discussed in Chapter Two, T_5 site is the only one that is not in the surface of the channel and, therefore, will not be in direct contact with adsorbed oxygen which provides the mechanism for the spin- lattice relaxation of ^{29}Si nuclei. In the NMR experiments, the resonance B is always of low intensity if the repeat delay for the pulse sequence is not long enough for complete recovery of the magnetization. Obviously, this COSY experiment with a delay time of 15 s is the case and the intensity of resonance B is much less than the others, as shown in the projection. From the starting point of B→ T_5, resonances of E, F and G could be associated with T_3, T_4 and T_6. Among them, T_4 and T_6 are connected to each other, and T_3 and T_6 are linked to T_7 simultaneously. Therefore, the assignments of E→ T_6, F→ T_4, G→ T_3 and C→ T_7 can be made. The remaining resonances are easily assigned, and the whole assignment is in exact agreement with the previous result. Another possible starting point is the relative intensities of the cross-peaks. There are four double connectivities in Table 12, i.e. T_1T_2, T_1T_3, T_2T_4 and T_5T_6, whose intensities, in general, are expected to be stronger than those from single connectivities. The four strongest cross-peaks in both the upper left and lower right parts in the contour plot (Figure 42) are AD, AF, BE and DG. It is easy to see that A and D are associated to T_1 and T_2, B, E to T_5, T_6, and F, G to T_3, T_4. The only one left, C, must be T_7. Both T_5 and T_6 have a connection to T_4, thus F→ T_4, G→T_3, A→T_2 and D→T_1 can be made. All these assignments are self-consistent. These methods plus those discussed in the case of zeolite DD3R provide the basic 'techniques' for making assignments, and were used in subsequent studies.

b) Direct observation of ^{29}Si- O- ^{29}Si couplings

In the 2D COSY experiments discussed in the previous section, 512 data points were collected during detection period for each experiment. However, only 256 points were used in the Fourier transformation in order to obtain a better S/N ratio in the 2D spectrum (Figure 42). When the number of points in F_2 is increased to 450 before zero filling, the 2D plot (Figure 43) shows the same connectivities, with the signal to noise ratio being traded for extra resolution. A power calculation was used to compensate, to some degree, for the loss of sensitivity. Doublet splittings are observed for almost all the cross peaks in the F_2 dimension, as shown in the figure. In principle, four peaks should be observed in each 'cross peak', but the real digital resolution in F_1 without zero filling is only ~40 Hz/point and is not sufficient to resolve the splittings in this dimension. The magnitudes of the apparent couplings are in the range of 10-16 Hz, and they are symmetrical about the diagonal as expected. The structure of the cross-peaks can be clearly observed in plots of cross sections from the 2D spectrum as shown in Figure 44. These values must be considered as only approximate due to the limited real digital resolution of ~5 Hz per point before zero filling. On the other hand, the experiments are not phase sensitive, which will tend to increase the observed splittings[55]. The mechanism for the splitting is thought to be scalar coupling. However, possible dipolar interactions within each ^{29}Si-O-^{29}Si pair must also be considered since a similar connectivity pattern to that from scalar couplings could be produced. The expression for the dipolar splitting, R, in a powder sample is given in Equation 27[28],

$$R = \frac{\hbar\, \gamma_1 \gamma_2\, \mu_0}{4\pi\ \ r^3\ \ 4\pi} \qquad [27]$$

where μ_0 is permeability constant; r the internuclear distance and $\gamma_1 = \gamma_2 = \gamma$ (^{29}Si) the magnetogyric ratio. In the case of zeolites, the value of R for ^{29}Si-O-^{29}Si is calculated to be around 170 Hz by assuming r= 3Å. The spinning rates used in these experiments are ~2.4 kHz and are rapid enough to eliminate the dipolar interactions. However, an experiment was carried out at rotor frequency of 1.2 kHz to make sure that the splitting is not due to a dipolar interaction, since the magnitude of any observed coupling from the dipolar interaction will depend inversely on the spinning rate. No differences in the magnitudes of the couplings were observed, which ruled out the dipolar interaction being the source of the splitting of the cross peaks. In addition, in COSY experiments, scalar couplings must be present. The observed splittings are of the correct magnitude when compared with solution data of 3-10 Hz [75] (see Chapter Two). Most silicate species in solution contain a substantial number of three and four membered rings, while in zeolites five and six membered rings are dominant. The couplings are very dependent on ring size, and the larger the size of the rings, the greater the J values for the silicons. With the knowledge of these J couplings, the 1D spectrum (Figure 41) could be reexamined. The line shapes could not be fitted by standard Lorentzian curves, there being `bumps' on both sides of the base of each peak, which could be the satellites of those coupled pairs. Thus the main intensity of each peak comes from the uncoupled $^{29}Si$ and the satellites separated by 10-16 Hz are buried within both side wings, resulting in `distorted' line-shapes.

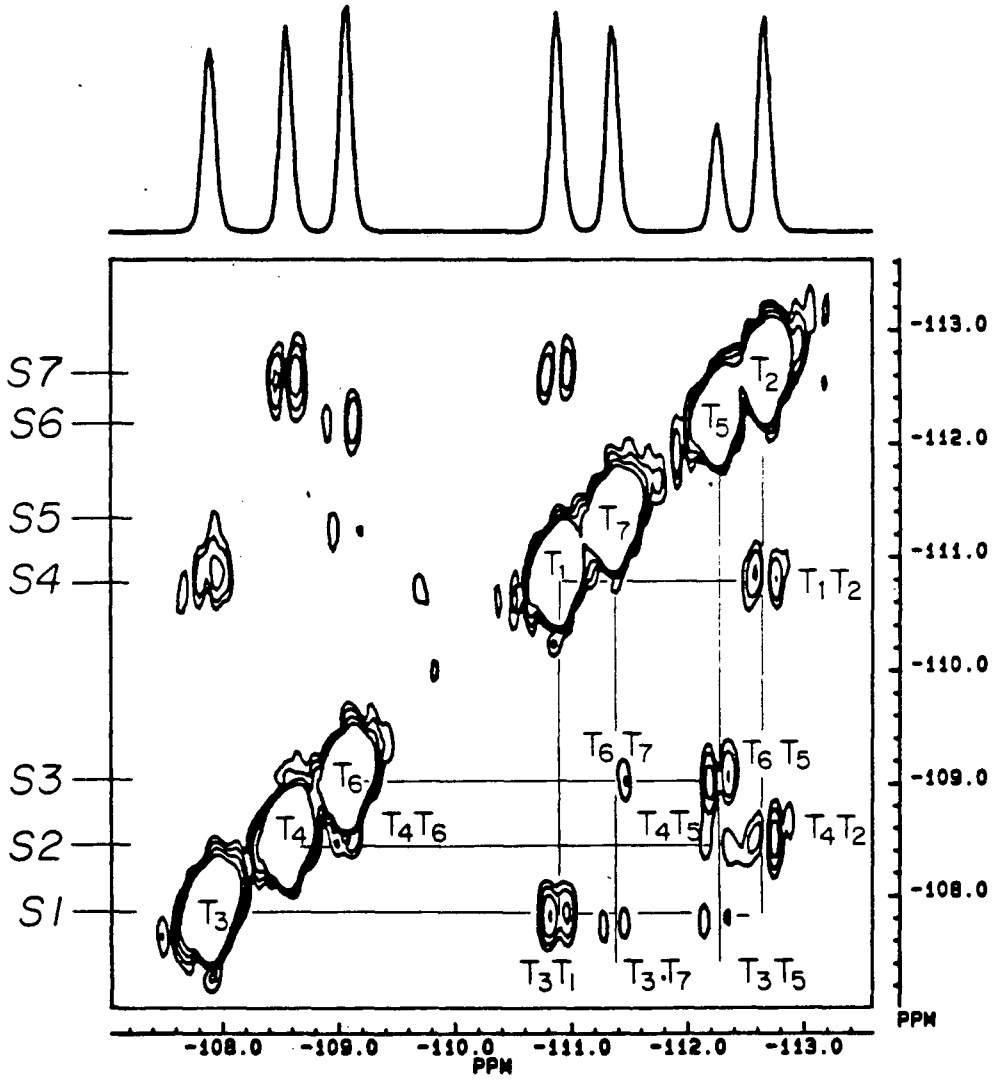

Figure 43 Contour plot with projection in F_2 of a COSY experiment on ZSM-12 obtained under the same conditions as in Figure 42, except that there are 80 scans in each experiments and 450 data points and power calculation were used in the data processing.

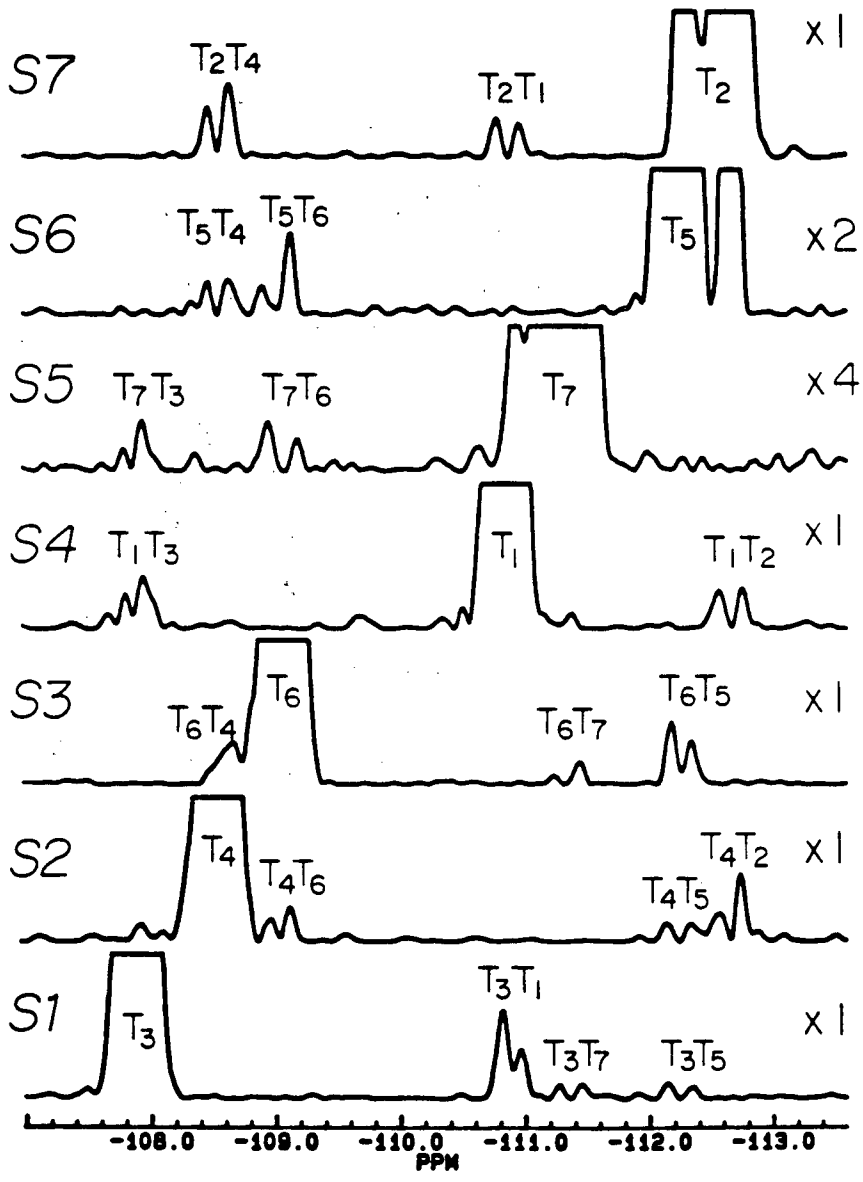

Figure 44 Cross section plots from Figure 43. The sections correspond to those indicated in Figure 43.

c) 2D INADEQUATE experiments

The INADEQUATE pulse sequence was proposed by Bax, Freeman and Kempsell[66] in 1980 to directly determine the carbon skeletons of organic molecules through J-couplings. The INADEQUATE experiments of ^{13}C are considered to be of low sensitivity due to the ~1% natural abundance. Although it seems a little easier to perform this kind of experiment on ^{29}Si of 4.7% abundance, no work regarding this has been reported in either solution or solid state NMR to date. With the knowledge of the J coupling values of 10-16 Hz, obtained from the COSY experiment, a fixed delay of ~16 ms (1/4J) was used in INADEQUATE experiments to optimize the intensities of J-coupled signals (see Chapter Two). A one-dimension INADEQUATE experiment was first performed on ZSM-12. The spectrum was not easy to interpret because the residual main signals and the satellites are overlapped due to the similar magnitudes of the linewidths of the residual main signals and the separations of satellites, but substantial signal intensity was observed. Considering the advantages of two dimensional experiments, a 2D INADEQUATE experiment was undertaken (Figure 45). All of the connectivities found in the previous COSY experiments were confirmed, including that between T_4 and T_6, which is clearly resolved here but was somewhat ambiguous in the COSY experiment due to the close proximity of these cross-peaks to the diagonal. All of the assignments made from the COSY experiments could have been made from the INADEQUATE experiment as well. The doublet structures are clearly observed in this experiment, again confirming the previous results. Figure 46 shows plots of slices from the 2D contour plot corresponding to the maxima of the signals, where the fine structure is clearly observable.

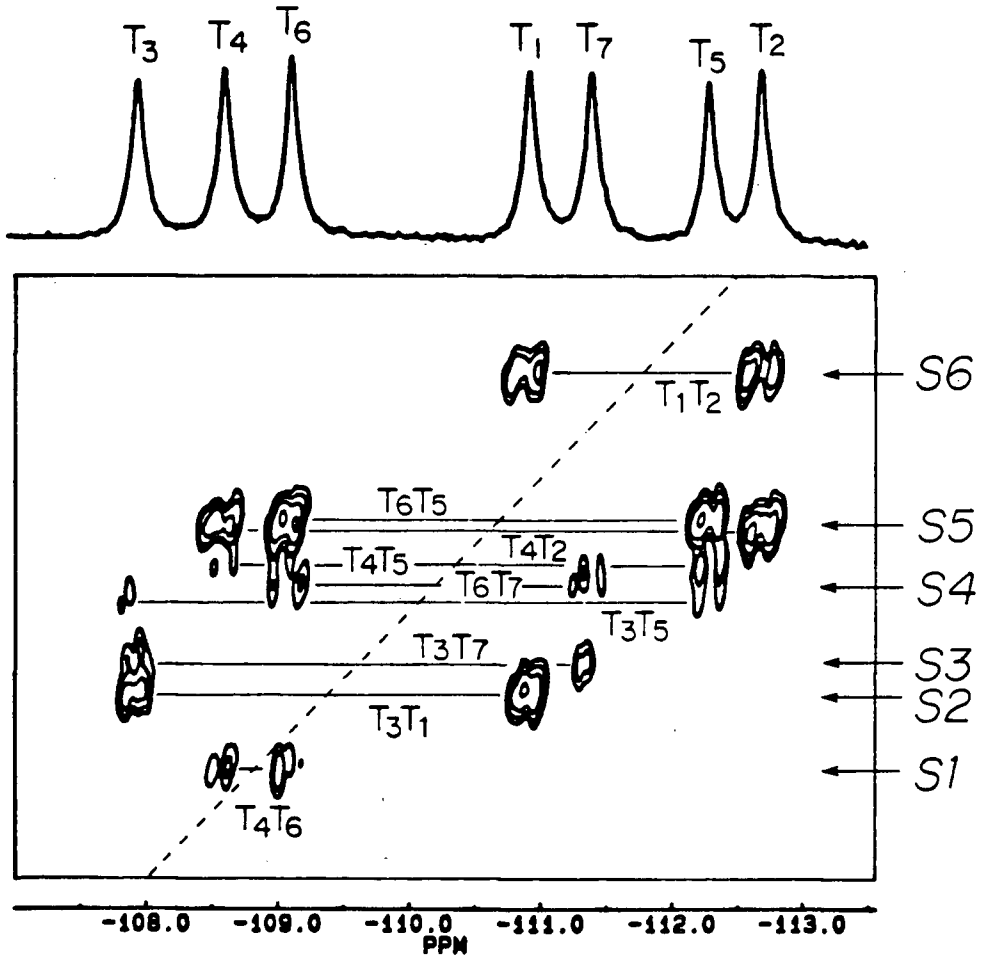

Figure 45 Contour plot of an INADEQUATE experiment on ZSM-12 at 300 K with the 1D MAS NMR spectrum shown above , with 52 experiments carried out, 64 scans per experiment, 800 Hz sweep width, fixed delay of 20 ms 450 data points collected during the acquisition, sine bell apodization and power calculation were used in the data precessing.

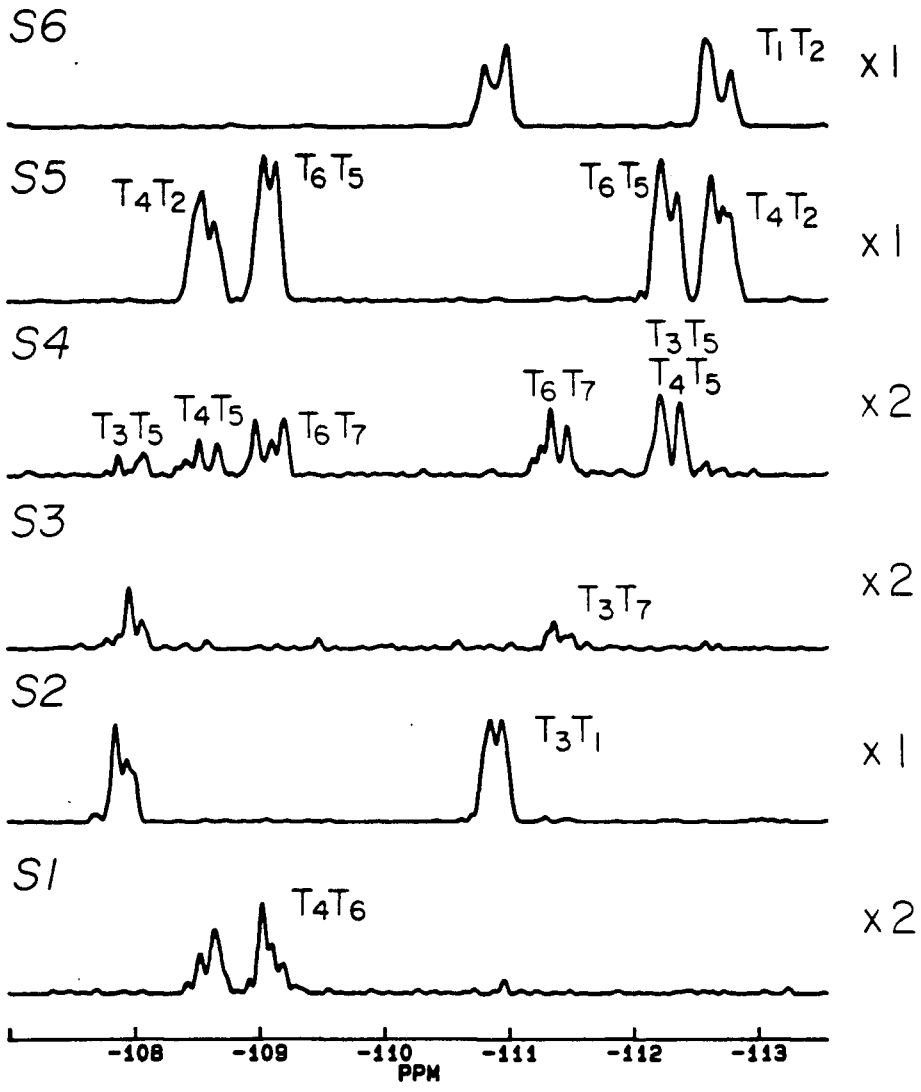

Figure 46 Cross section plots from Figure 45. The numbers of the rows correspond to those indicated in Figure 45.

A symmetrical INADEQUATE experiment[109], a simple modification of the standard INADEQUATE procedure was also performed. By applying a 90° pulse in the middle of the evolution period in the normal sequence (see Figure 36B), the resulting correlation spectrum has a COSY-like appearance, but without intense diagonal signals. Figure 47 shows the results of a symmetrical INADEQUATE experiment with a projection in the F_2 dimension, where again all the connectivities are clearly observed. Compared with the results of the corresponding COSY experiment (Figure 42), this spectrum is neater and unambiguous. Since the correlations are now symmetrical relative to the diagonal, the symmetrization routine could be used as for COSY experimets to remove some artifacts and increase the signal to noise ratio.

d) Comparison of 2D INADEQUATE and COSY experiments

Both INADEQUATE and COSY experiments contain essentially the same information, i.e. homonuclear connectivities via J-coupling. The major advantage of INADEQUATE is that the spectrum lacks the diagonal peaks due to the single quantum resonances from uncoupled nuclei. Thus, for complex systems, it may be possible to trace correlations in the 2D INADEQUATE spectrum which would be lost close to the diagonal of the COSY experiment. The uncoupled ^{29}Si nuclei could produce strong single quantum coherences during the detection period in both experiments, but in INADEQUATE, these unwanted conventional signals are filtered out based on the different phase properties between the single and double-quantum signals [66]. If the phase of the read pulse (see Figure 36) is cycled in the x-direction in the first step and in the y-direction in the second, the phase of the transverse signal generated from single quantum coherence will cycle in the same sense. In contrast, the signal

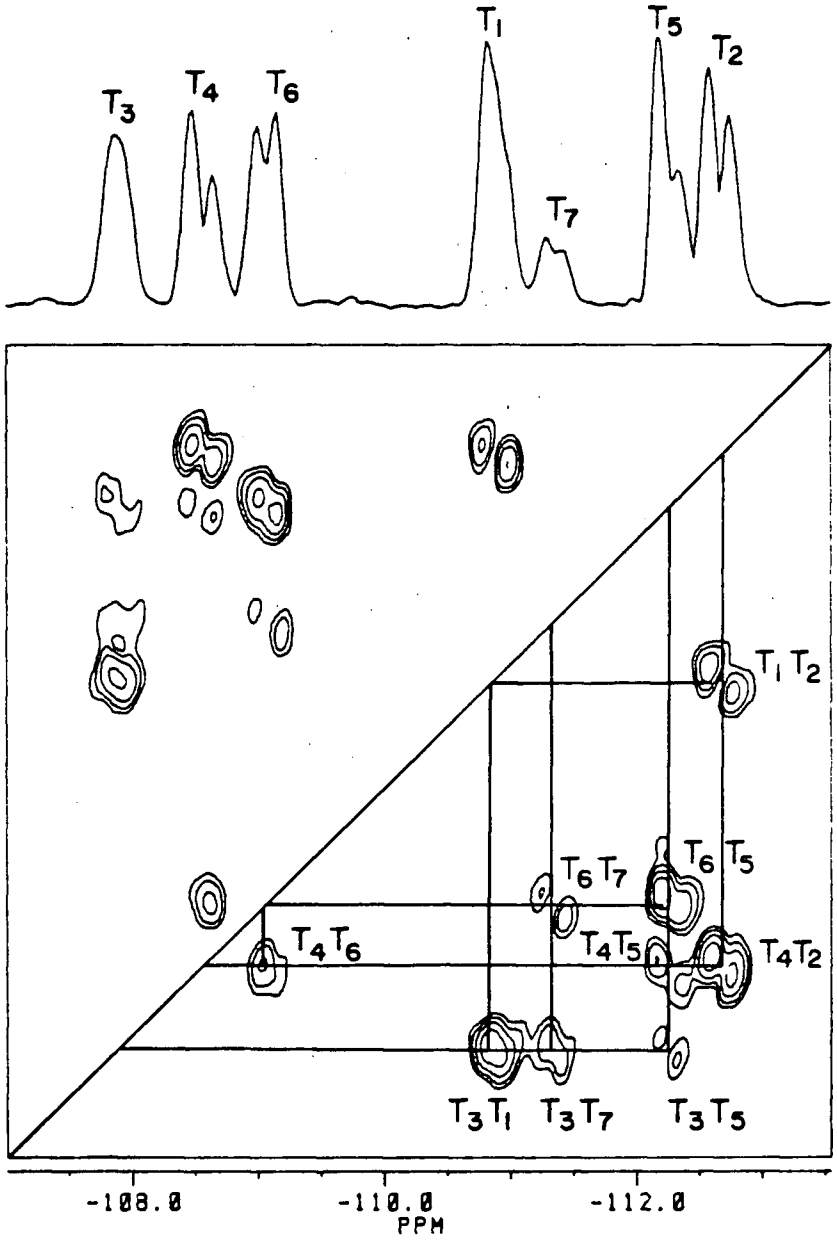

Figure 47 Contour plot of a symmetrical INADEQUATE experiment on ZSM-12 at 300 K with the projection in the F_2 dimension, with 26 experiments carried out, 64 scans per experiment, 522 Hz sweep width, fixed delay of 20 ms. 256 data points collected during the acquisition, sine bell apodization and power calculation were used in the data processing.

generated from double quantum coherence shifts by 270° for each 90° step in the read pulse, i.e. in the x-direction in the first step and in the -y direction in the second. The receive phase can be adjusted such that the weak signals from coupled pairs are accumulated and the single quantum signals as well as the spinning sidebands from these signals are not present in the final spectrum. Unfortunately, in the case of COSY experiments, both diagonal and cross peaks come from single quantum coherences, and there is no simple way to discriminate between them. In addition, the suppression of the spinning sidebands is very important in solid state 2D experiments, because the presence of spinning sidebands and their fold-back signals makes the spectrum difficult to interpret. In order to eliminate the interference from these unwanted peaks and other artifacts in COSY experiments, all resonances are put within either the left or right half of the spectral range, resulting in half the possible digital resolution in both dimensions compared to the corresponding INADEQUATE experiments. Furthermore, the samples must be spun at frequencies equal to, or a multiple of, the spectral sweep width in COSY experiments so that any spinning sidebands in F_1 are exactly coincident with the main signals. The lack of intense single quantum signals in INADEQUATE experiments gives a better dynamic range for the connectivities, and the weak coupled signals can be readily detected. Another advantage of INADEQUATE is that a better S/N may anticipated. The generation of double quantum coherences during the preparation period is optimized for each t_1 incremented experiment. It is obvious that each experiment makes an efficient contribution to the final results. In addition, since the final signal is more constant in time, a much efficient window function can be used in the data manipulation. However, in cases of P-

type selection COSY experiments used in this thesis work, the echoes shift substantially during the experiment, which makes it difficult to apply a single window function which is efficient for every t_1 incremented experiment.

The major disadvantage of INADEQUATE experiments is that a reasonable estimate of the J coupling must be made to choose an appropriate fixed delay, during which the double quantum coherence is generated. If the J coupling is not known, it is hard to make the experiments work properly, whereas the corresponding COSY experiment will usually yield some information . In addition, the INADEQUATE pulse sequence involves a long preparation period, and the situation may arise where the values of the relaxation times and couplings are such that it is not possible to carry out this kind of experiment due to the restriction of short T_2 or T_2^*. In this work, the J coupling doublets are directly observed in the COSY experiments, and the J coupling values are measured to be within a narrow range of 10-16 Hz because all silicon atoms are in similar chemical environments in the highly siliceous samples. Hence, the INADEQUATE experiments are very efficient. The linewidths of the resonances are in range of 9-30 Hz for highly siliceous zeolite samples. Consequently, there are no severe restraints on the experiments.

Thus, the INADEQUATE experiment can be carried out very efficiently, with no interferences from signals originating from the majority of uncoupled ^{29}Si nuclei and their sidebands and with improved S/N. This technique will usually be the method of choice in the investigation of zeolite structures.

C. NATURAL-ABUNDANCE TWO-DIMENSIONAL ^{29}SI HIGH-RESOLUTION SOLID STATE NMR INVESTIGATION OF THE LATTICE STRUCTURE OF ZEOLITE ZSM-22

I. INTRODUCTION

Zeolite ZSM-22 was synthesized quite independently by different groups using different reaction conditions and templates and is also described as KZ-2, Theta-1 and NV-10 [110-114]. A crystal structure of space group $Cmc2_1$ was proposed based on powder XRD studies[115,116]. There are 24 silicons in a unit cell distributed over four crystallographically inequivalent sites, and there is a one-dimensional 10-membered ring channel system running along the c axis (Figure 48). A single crystal structural refinement of a completely siliceous ZSM-22 sample has been presented by Marler[16], giving better geometric parameters for the structure. Table 13 presents the connection scheme of ZSM-22. Four connectivities between the pairs T_1T_2, T_1T_4, T_2T_3 and T_3T_4 are expected to be observed in 2D NMR experiments.

Table 13 T-sites, Their Occupancies, and Connectivities for the Asymmetric Unit in Zeolite ZSM-22 (Ref. 115)

T-site	occupancy	connectivity
T_1	1	$2T_2$: $2T_4$
T_2	1	$2T_1$: $2T_3$
T_3	2	$1T_2$: $2T_3$: $1T_4$
T_4	2	$1T_1$: $1T_3$: $2T_4$

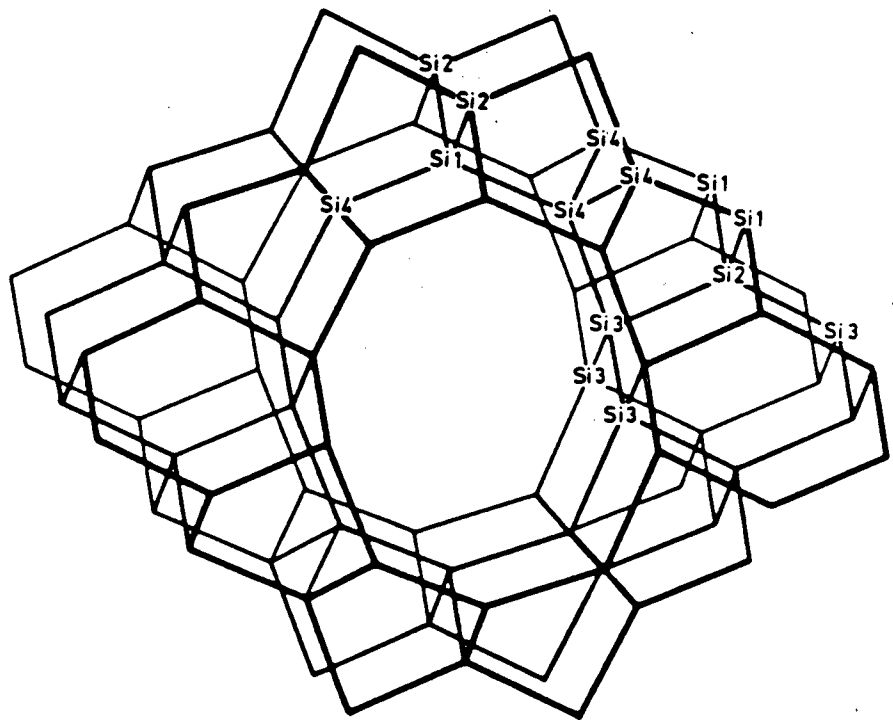

Figure 48 Schematic representation of the zeolite ZSM-22 lattice framework, the four crystallographically inequivalent T-sites indicated by Si1, Si2, Si3 and Si4. (ref.108)

II. EXPERIMENTAL

A highly siliceous sample of ZSM-22 (GEB 100) was previously prepared by Gwyneth Barlow, U. Guelph, using diethylamine as a template according to reference 112. The high-resolution ^{29}Si MAS NMR spectra were acquired at 79.5 MHz using the equipment and techniques previously described.

III. RESULTS AND DISCUSSION

a) 2D COSY experiments

The 1D ^{29}Si MAS NMR spectrum of highly siliceous ZSM-22 is shown in Figure 49. The four resonances of relative intensities 2:1:1:2 are in excellent agreement with the diffraction-determined structure and previously published NMR spectra[50].

2D COSY experiments were performed in a similar way to those discussed for ZSM-12. The results are shown in Figure 50, and three cross-peak pairs are clearly observed. The resonances may be divided into two groups A, D and B, C on the basis of their relative intensities in the 1D spectrum. The resonances A and D with double intensities are assigned to the pair T_3 and T_4, while B and C to the pair T_1 and T_2. A connectivity between T_1 and T_2 is expected, but the cross-peaks are too close to the diagonal to be resolved. Because of the intrinsic symmetric nature of the structure of ZSM-22, there are two possible assignments starting from B $\rightarrow$ T_1 and B $\rightarrow$ T_2 respectively (Table 14), both of which can satisfy the connectivity pattern indicated in Table 13. There are two ways to solve the problem. One is based on the difference of T_1 relaxation times. It can be seen from the structure of ZSM-22 (Figure 48) that the 10-membered ring is formed by 2 T_1 atoms, 4 T_3 and 4 T_4 atoms. Therefore, T_2 is not on the surface of

Table 14 Two Possible Assignments of the Spectrum of ZSM-22

	Assignment I	Assignment II
Resonance	A B C D	A B C D
T-sites	4 2 1 3	3 1 2 4

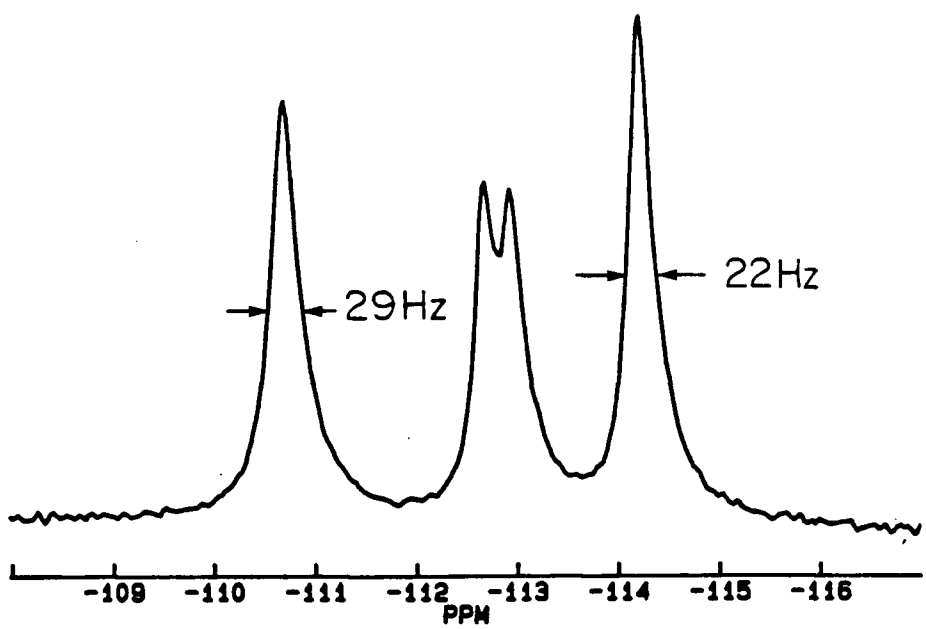

Figure 49 1D ^{29}Si MAS NMR spectrum of zeolite ZSM-22 obtained at room temperature with 280 scans and 512 data points.

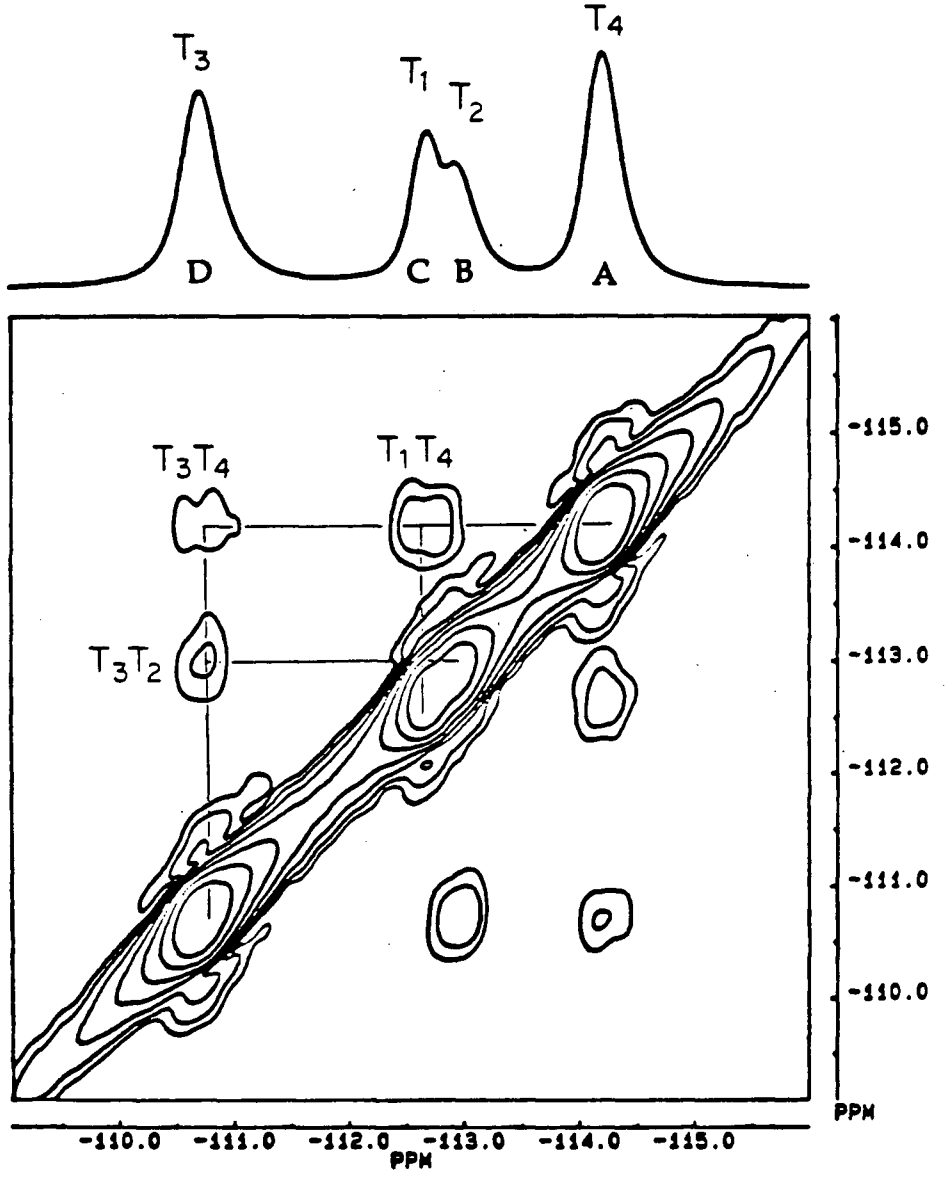

Figure 50 Contour plot with projection in the F2 dimension of a COSY experiment on zeolite ZSM-22 carried out at 300 K, 64 experiments, 592 scans per experiment, 1200 Hz sweep width, fixed delay of 0.5 ms. 256 data points were used during the data processing and sine-bell-squared apodization and magnitude calculation employed.

the channels, which results in it having a longer T_1 relaxation time than any other nuclei. The 1D spectrum in Figure 50 shows that the intensity of resonance B is smaller than A if the repeat time is < 5 T_1. Thus a assignment of B→ T_2 can be made and a complete assignment is obtained as indicated in Figure 50. The other way is by combining the NMR results with X-ray structural data, i. e. from the correlation between average T-T distances and ^{29}Si chemical shifts. In general, the resonances of ^{29}Si associated T site with shorter T-T distances are located to lower field (117). In the present case, the average T-T distances of T_3 and T_4 are 3.08 and 3.11 Å respectively (16). Thus, the resonances of A and D may be assigned such that the lowest field resonance D is associated with T_3 and the resonance A is T_4. The large difference in chemical shift between the resonances makes the assignment reliable, and yields exactly the same assighments as the T_1 method.

When 512 data points are used in F_2 dimension before zero-filling, the doublet structure is observed in the cross-peaks as in the case of ZSM-22. The results is shown in Figure 51. The values of the splittings are again in the range of 10-15 Hz.

b) 2D INADEQUATE experiments

Figure 52 shows the results of the INADEQUATE experiment on zeolite ZSM-22. Again the connectivities previously observed are confirmed, and the T_1T_2 coupling not observed at all in the COSY experiments is now clearly seen. The S/N ratio is better than in COSY experiment although less experimental time was used. All of the signals exhibit a doublet structure, and the interactions have values similar to those previously observed in the COSY experiments.

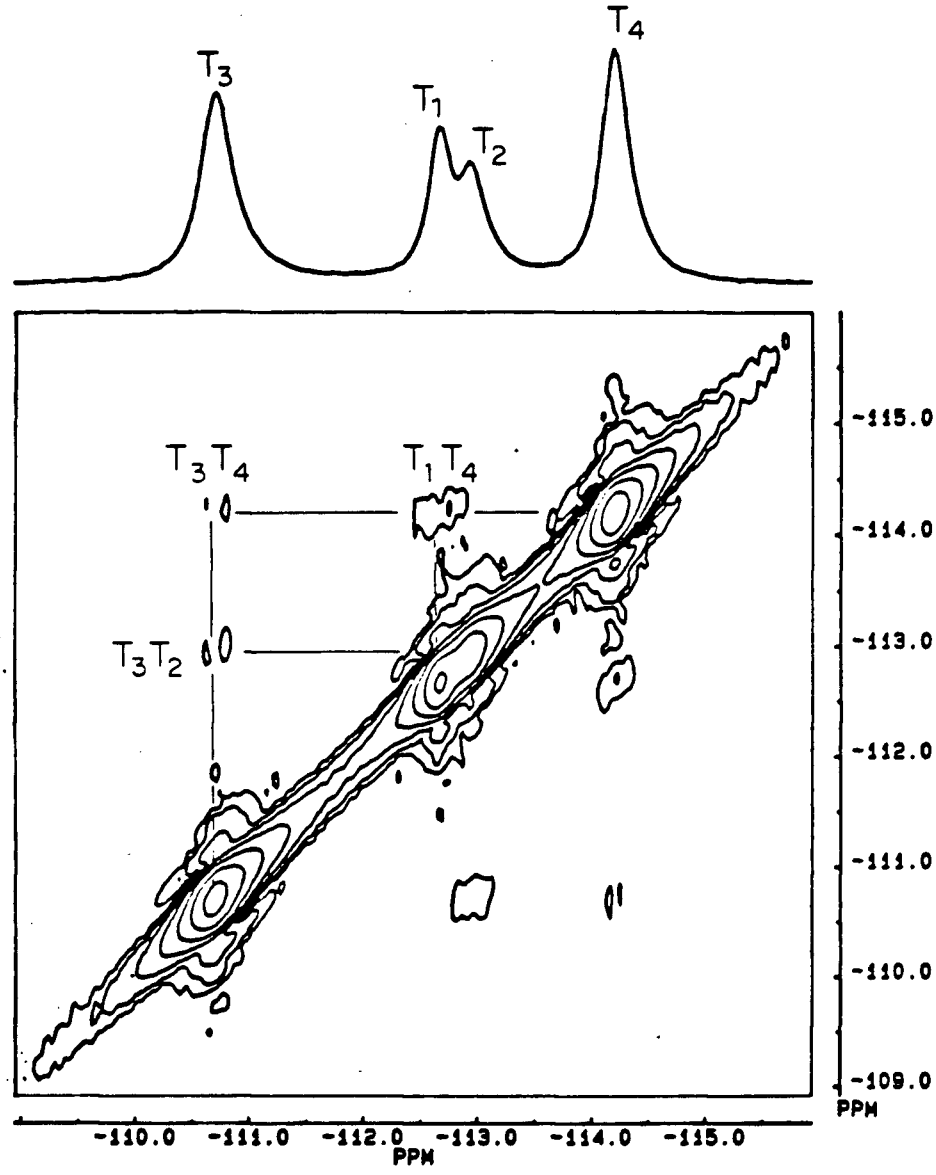

Figure 51 Contour plot of a COSY experiment on zeolite ZSM-22 with a projection in the F2 dimension. Conditions were the same as employed in Figure 50 except that 512 data points and sine bell apodization were used in the data processing.

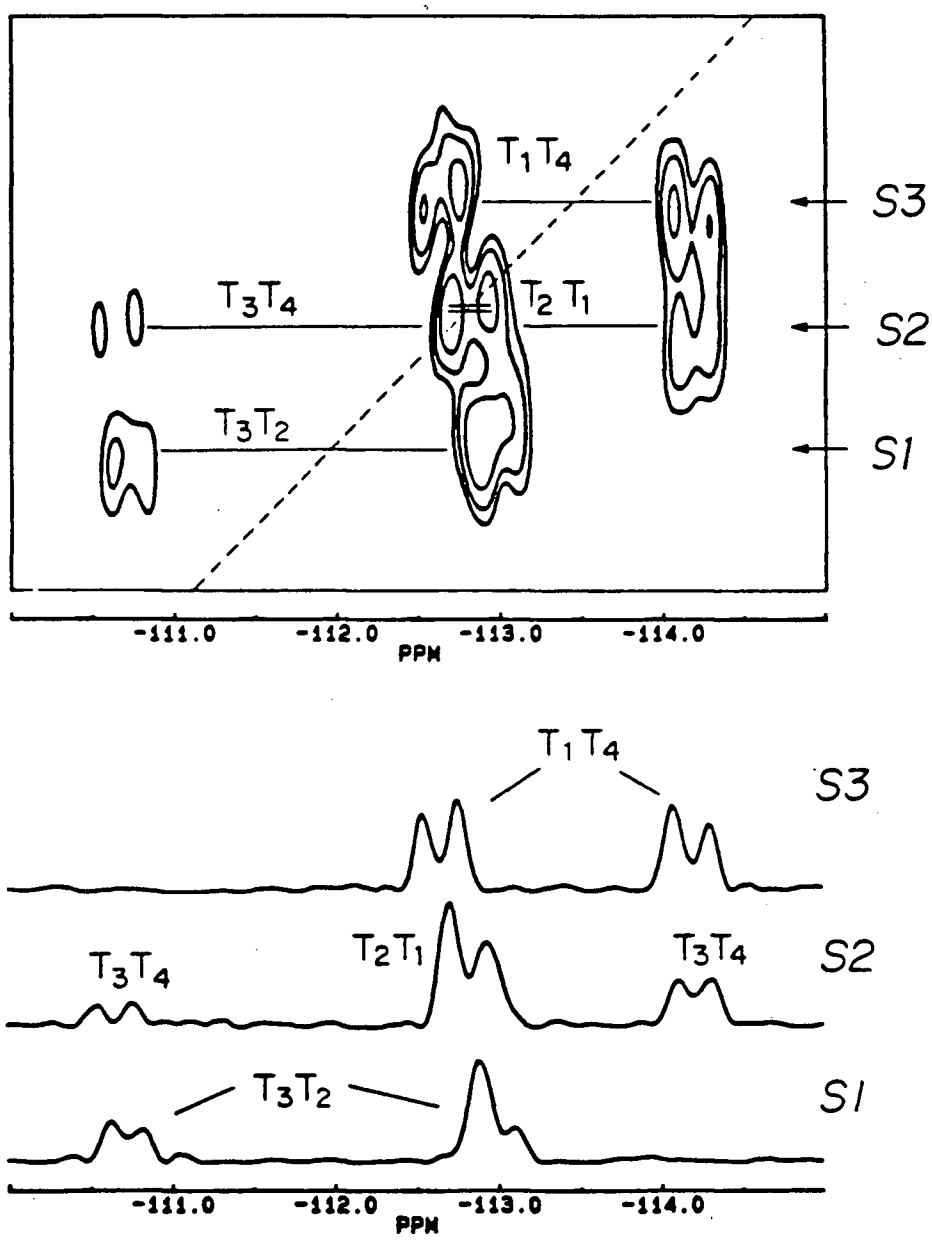

Figure 52 Contour plot of INADEQUATE experiment on zeolite ZSM-22 with three individual rows shown as indicated. The experiments were carried at 300 K, 16 experiments, 256 scans for each experiment, 750 Hz sweep width, and fixed delay of 20 ms. 200 data points before zero-filling and sine bell and trapezoidal apodization for F_2 and F_1 dimensions respectively were used in the data processing.

CHAPTER FIVE

NATURAL-ABUNDANCE TWO-DIMENSIONAL SOLID STATE ^{29}SI NMR INVESTIGATIONS OF THE THREE-DIMENSIONAL BONDING CONNECTIVITIES IN THE DIFFERENT STRUCTURAL FORMS OF THE ZEOLITE CATALYST ZSM-5

A. INTRODUCTION

Zeolite ZSM-5 has been of particular interest in recent years because of its high catalytic activity and extreme size and shape selective adsorption properties. Examples of its use include the conversion of methanol to high-quality gasoline, paraffin cracking, olefin interconversion, ethylbenzene synthesis, xylene isomerization and toluene disproportionation[118-119].

Zeolite ZSM-5 is the best known of a whole family of zeolites called "pentasils", which are characterized by closely related structures[120,121]. The pentasil framework can be constructed from a secondary building unit (SBU) of the 5-1 type shown in Figure 53A. Pairs of 5-1 units are joined to form a building unit of the framework (Figure 53B), which is the asymmetric unit of the phase with the space group Pnma or half of the asymmetric unit of the other phases (see on). These units can be linked to form chains (Figure 53C), and such chains interconnected to form a layer, as shown in Figure 54A. Different ways of linking the sheets form different members of the pentasil family. When the sheets are connected such that neighboring pairs are related by an inversion

center, the ZSM-5 framework with 96 T-sites per unit cell (u.c.) is formed (Figure 54B). The structure of ZSM-5 is characterized by two interconnected channel systems (Figure 54C). There is a straight channel parallel to the **b** axis with a nearly circular cross-section varying from approximately 5.3 to 5.6 Å in diameter , and a zigzag channel along the **a** axis with an elliptical cross-section of approximately 5.1 X 5.5 Å. The shape and size of the three-dimensional pore system together with the high thermal stability and unique catalytic and adsorption properties make ZSM-5 a commercially significant zeolite.

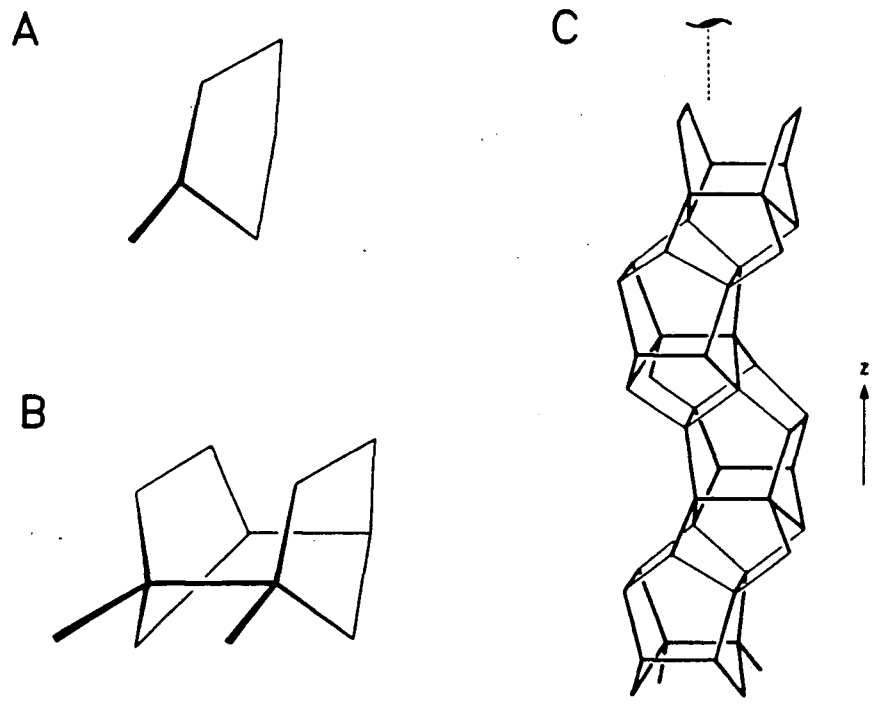

Figure 53 (A) A secondary building unit of the 5-1 type.
(B) An asymmetric unit of orthorhombic form with the space group Pnma.
(C) Chain-type building block. (ref. 121)

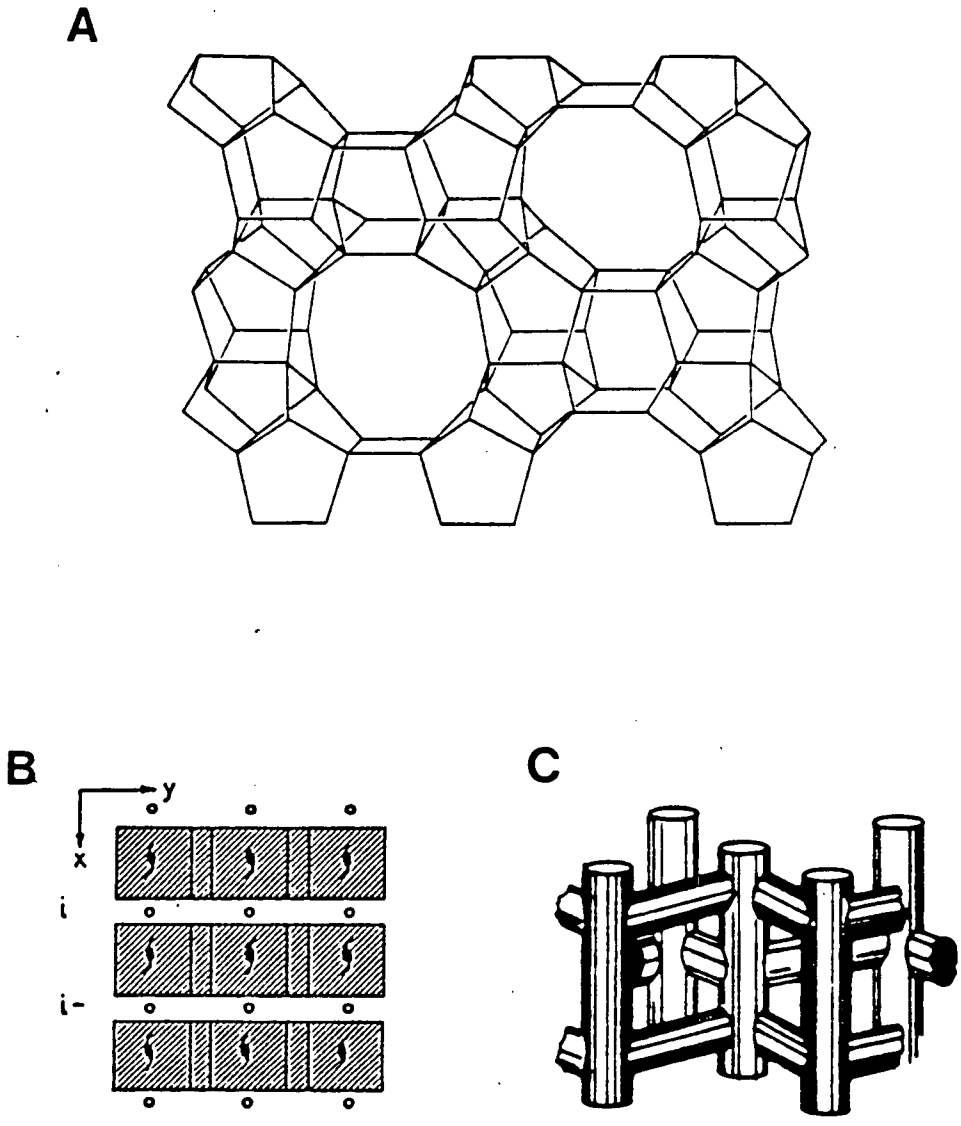

Figure 54 (A) Skeletal diagram of a pentasil layer linked by the chain-type building blocks.
(B) Stacking sequence of layers in ZSM-5 (layers shaded).
(C) The channel system in ZSM-5. (ref. 120)

The structure of ZSM-5 was first deduced from powder diffraction studies by Kokotailo and co-workers[120] in an "as-synthesized form" containing templates and has orthorhombic symmetry and space group Pnma. Removal of the template molecules by calcination produces a reduction of the symmetry of the framework to monoclinic, space group $P2_1/n$[121]. Recently, several single crystal studies of the ZSM-5 system have been reported by van Koningsveld and co-workers, including the as-synthesized form[122], the calcined forms at both room temperature and high temperature [104,123], and the phase induced by adsorption of eight *p*-xylene molecules per unit cell [124]. Synchrotron X-ray powder studies of highly siliceous samples at both low and high temperatures have also been carried out[125,126].

High resolution ^{29}Si MAS NMR studies have also demonstrated that the room temperature form of the completely siliceous ZSM-5 is monoclinic with 24 T-sites and that a structural change to the orthorhombic form with 12 T-sites is induced by increasing the temperature or by the addition of two molecules of *p*-xylene or *p*-dichlorobenzene[44,127-131]. In the sorbate-induced case, the change is gradual, both monoclinic and orthorhombic forms being crystalline and co-existing at the intermediate state, while for the thermally-induced change, the monoclinic 24 to orthorhombic 12 T-site turnover occurs over a very small temperature range. These phase transitions are reversible. Recently, Fyfe and co-workers have presented an extensive study of these conversions [49].

In this chapter, the investigation by one-dimensional NMR techniques of a phase transition of ZSM-5 induced by more than two molecules p-xylene per unit cell will be reported. Then the application of 2D correlation experiments to the phases whose structures are known will be described and finally, some less well- definded structures of ZSM-5 will be examined.

B. INVESTIGATION OF THE HIGH-LOADED FORM OF ZEOLITE ZSM-5 WITH *P*-XYLENE BY HIGH-RESOLUTION SOLID STATE ^{29}SI NMR SPECTROSCOPY

I. INTRODUCTION

The adsorption properties of ZSM-5 have attracted a number of studies, especially, the adsorption of *p*-xylene due to its industrial importance. These studies have indicated that four molecules of *p*-xylene can readly sorb into a unit cell of ZSM-5 and up to eight molecules of *p*-xylene per unit cell may be incorporated into the ZSM-5 lattice under certain conditions [121,132-133]. For average sorbate loadings greater than four molecules per unit cell a sudden increase of the adsorption from 4 to ~7 molecules per unit cell is observed and a phase transition occurs. A X-ray powder diffraction analysis of the location of adsorbed *p*-xylene in the high-loaded form was carried out by assuming orthorhombic Pnma symmetry [134]. A detailed single crystal X-ray diffraction study was recently reported by van Koningsveld and co-workers [124], and a structure of orthorhombic symmetry $P2_12_12_1$ with an asymmetric unit cell of 24 T-sites was found for this "high-loaded" form of ZSM-5.

Previous NMR studies of this degree of *p*-xylene loading were characterized by broad and featureless resonances with no clear indications of the presence of a new phase [17,135]. Stimulated by the new reported structure, experiments to investigate this phase using high resolution NMR techniques were carried out.

II. EXPERIMENTAL

^{29}Si MAS NMR spectra were obtained at 79.49 MHz on a Bruker MSL-400 spectrometer using the conditions discribed in Chapter Two. The highly siliceous samples of ZSM-5 used in the present work were previously synthesized using tetrapropylammonium ion as a template [49] and dealuminated by Gwyneth Barlow, U. Guelph. The *p*-xylene loaded samples were prepared by activating highly siliceous zeolite ZSM-5 at 500°C for four hours. After the sample was cooled to room temperature, various amounts of liquid *p*-xylene were added to weighed amounts of ZSM-5 in a glass vial. The samples were cooled to liquid nitrogen temperature and then fire-sealed under vacuum. They were then kept in an oven at 100°C for one day to ensure an equilibrium distribution of the sorbate through the sample.

III. RESULTS AND DISCUSSION

A series of single pulse MAS experiments were carried out without proton decoupling. Figure 55A shows the ^{29}Si MAS spectra of ZSM-5 loaded with *p*-xylene from 2 to 8 molecules per unit cell. The spectrum at 2 molecules per u.c. is identical to that in the literature and indicates clearly that the asymmetric unit contains 12 T-sites [49]. As more *p*-xylene is added, there is a gradual broadening of the spectra, most noticeable in the bases of the resonances, as previously reported [17,135]. Although it can be seen that the position of the resonance with the highest intensity shifts when the loading is increased from 2 to 8 molecules, there is no clear indication of a phase transition due to the severe line-broadening. Possible reasons for the broadening of the resonances could be: a) The crystallites are partially destroyed due to adsorption, resulting in a lower

Figure 55 (A) ^{29}Si MAS NMR spectra of ZSM-5 with increasing concentrations of *p*-xylene. The numbers indicate the numbers of *p*-xylene molecules sorbed per u. c.
(B) ^{29}Si MAS NMR spectra of the same samples with proton decoupling during acquisition. A 350 s delay time between pulses ensures the spectra are quantitative.
(C) ^{29}Si CP MAS NMR spectra of the same samples with a 20 ms contact time and 5 s delay time.

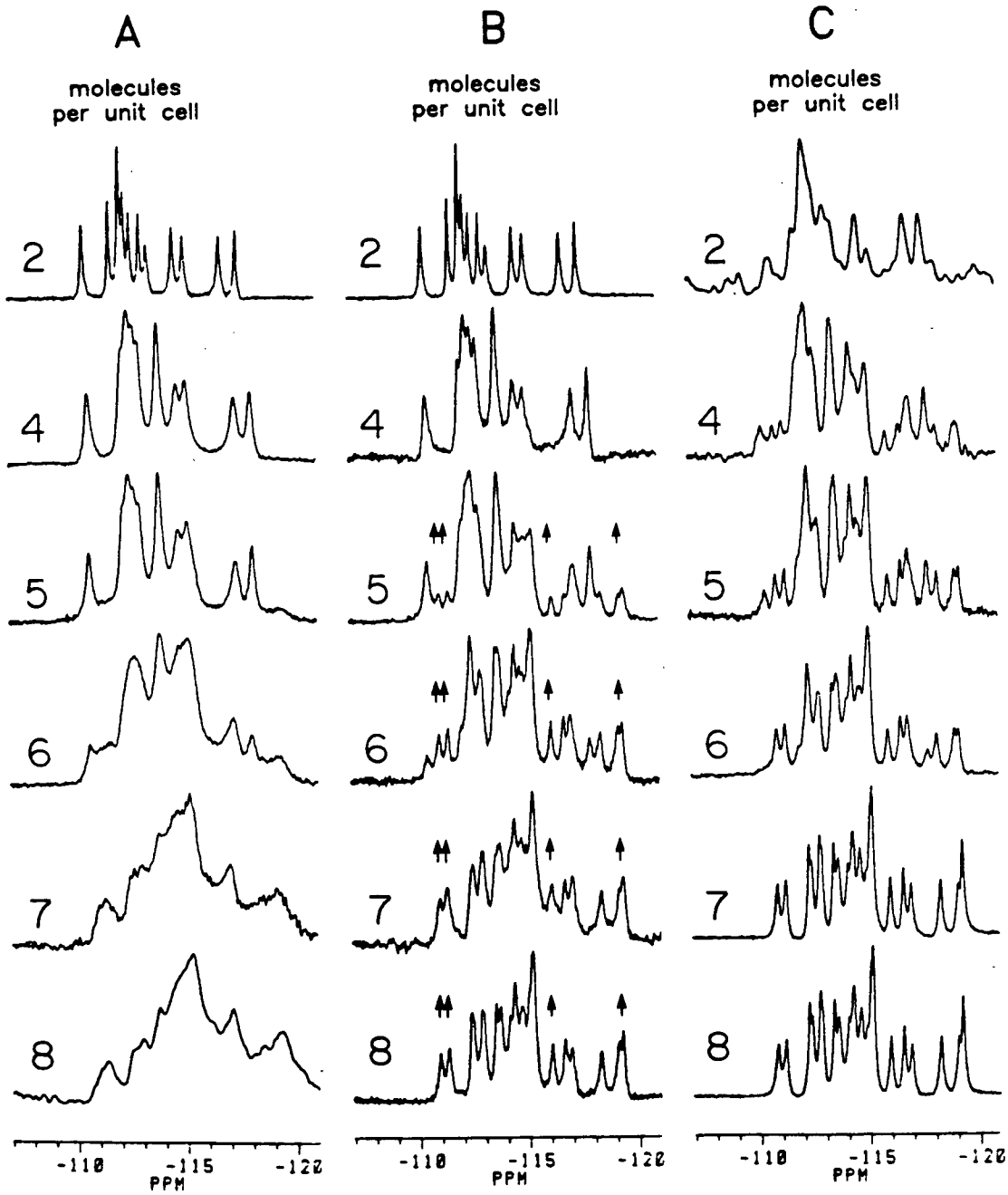
A
molecules
per unit cell
2
4
5
6
7
8
-110
-115
-120
PPM
B
molecules
per unit cell
2
4
5
6
7
8
-110
-115
-120
PPM
C
molecules
per unit cell
2
4
5
6
7
8
-110
-115
-120
PPM

degree of crystallinity; b) The distribution of sorbates in the lattice is not uniform, creating a distribution of various local chemical environments; c) The dipolar interactions between ^{29}Si and the ^{1}H nuclei of the sorbed molecules become significant when the amount of *p*-xylene is increased. To investigate this further, a second series of single pulse experiments with proton decoupling during acquisition were performed on the same series of samples. There is a substantial narrowing of the resonances, as shown in Figure 55B, indicating that dipolar interactions from protons are the main source of the line broadening. A second species is clearly observed at loadings greater than 4 molecules per unit cell as indicated by the vertical arrows. This new "high-loaded" form is the only species present at loadings greater than 7 molecules per u.c. and clearly indicates that there has been a change of phase. The delay times between pulses are sufficiently long, so that these spectra can be considered to be quantitatively reliable. The spectra at loadings of 5 and 6 molecules per u. c. can be represented as a sum of the spectra at loadings of 4 and 8 molecules present in different proportions, and the relative proportion of the "high-loaded" phase gradually increases with increasing *p*-xylene concentration as shown in Figure 56. Both low-loaded and high-loaded forms are simultaneously present and the resonances all remain sharp, indicating that both are highly ordered and crystalline. The NMR results suggest that from 2 to 4 molecules per unit cell, the ^{29}Si spectra are in principle consistent with a orthorhombic symmetry of 12 T-sites. When the loading is increased, part of the sample is transformed to the high-loaded form, and the rest remains in the low-loaded form, resulting in a lower total energy, in agreement with the results found in sorption studies (121,133).

The need for proton decoupling indicates that there are significant dipolar interactions between the ^{1}H nuclei in the organic molecules and the ^{29}Si nuclei in the lattice, which suggests that at least some of the *p*-xylene molecules are immobile in the channels. Thus the cross-polarization technique might be reasonably efficient for this "high-loaded" structure. Figure 55C shows the ^{29}Si CP MAS NMR spectra corresponding to the spectra in Figure 55A and B. The results are as expected: For the '8 molecules' case, the total experimental time was ~10 min, while the spectrum on the same sample in Figure 55B took approximately 14 hours to obtain acceptable S/N.

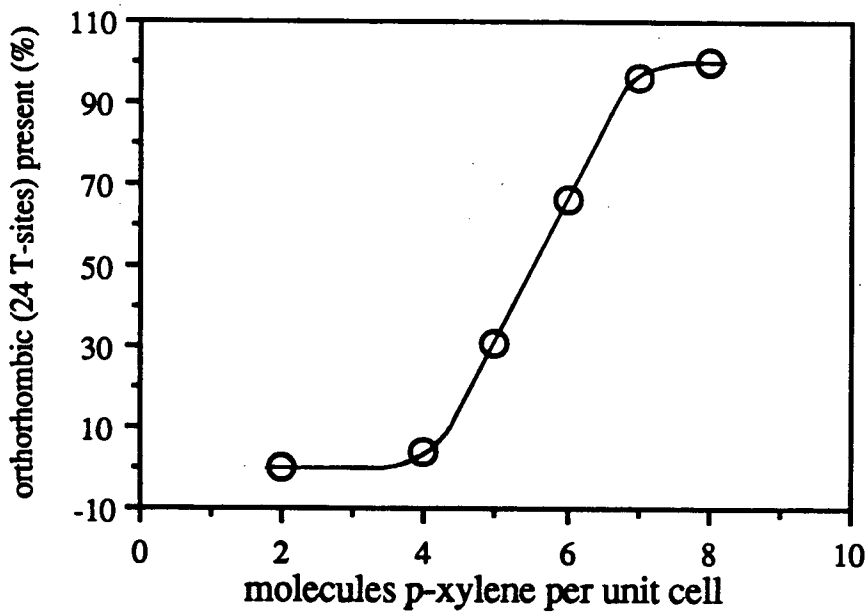

Figure 56 The effect of *p*-xylene loading on the proportion of high-loaded form in the sample.

In contrast, cross polarization is very inefficient for the low-loaded form. This may be due to the motion of the adsorbed molecules relative to the lattice and/or the longer distances between the ^{1}H and ^{29}Si nuclei. Figures 57A and B show the ^{1}H MAS NMR spectra of absorped *p*-xylene in ZSM-5 at loadings of 2 and 8 molecules per u.c. respectively and reflect the different motions in the two cases. The broad featureless peak with a 20 kHz linewidth in the '8 molecules' case reflects strong dipolar interactions between the ^{1}H nuclei and suggests that at least some of the *p*-xylene are immobile. In contrast, the spectrum of the '2 molecules' case shows much narrow central lines (~ 400 Hz linewidth for the highest peak) and a series of spinning sidebands, indicating that the adsorbed *p*-xylene molecules show some motional freedom. In the figure, the resonances associated with aromatic protons are indicated by '*' and aliphatic ones, '•'. These results are in agreement with deuterium solid-state NMR studies [136, 137]. Because of the lack of geometric information on the 'low loaded' form, it is difficult to estimate the contribution of ^{1}H-^{29}Si distances to the dipolar interaction.

Figure 58A shows the ^{29}Si MAS spectrum with proton decoupling of the sample loaded with 8 molecules of *p*-xylene per u.c. with a long relaxation delay ($\geq$ 5 times the longest ^{29}Si T_1). The Lorentzian peaks from the deconvolution are shown in Figure 58B, and indicate that the asymmetric unit contains 24 T-sites. This is in agreement with the recent single crystal X-ray study by van Koningsveld and co-workers[124].

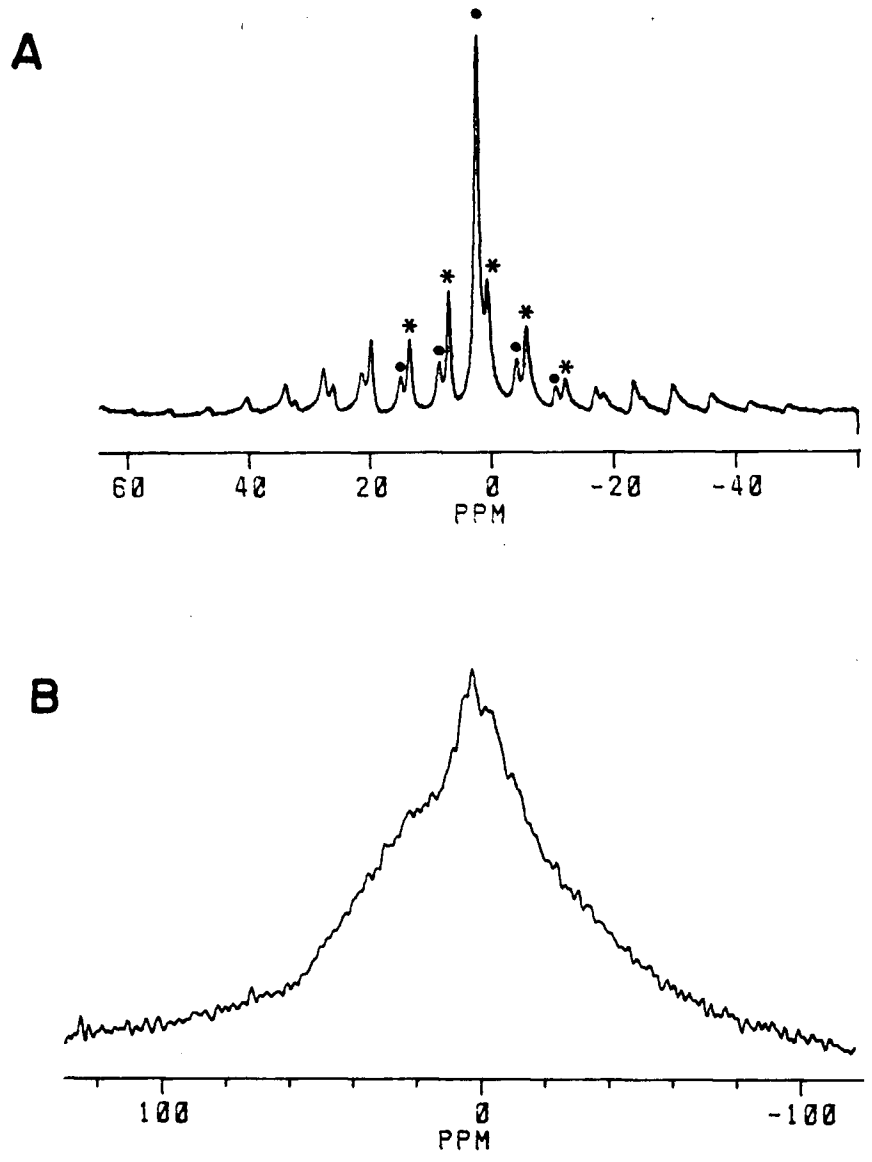

Figure 57 (A) ^{1}H MAS NMR spectrum of ZSM-5 loaded with 2 molecules of *p*-xylene per u.c., with a spinning rate of 2.5 kHz.
(B) ^{1}H MAS NMR spectrum of ZSM-5 loaded with 8 molecules of *p*-xylene per u.c., with a spinning rate of 2.5 kHz.

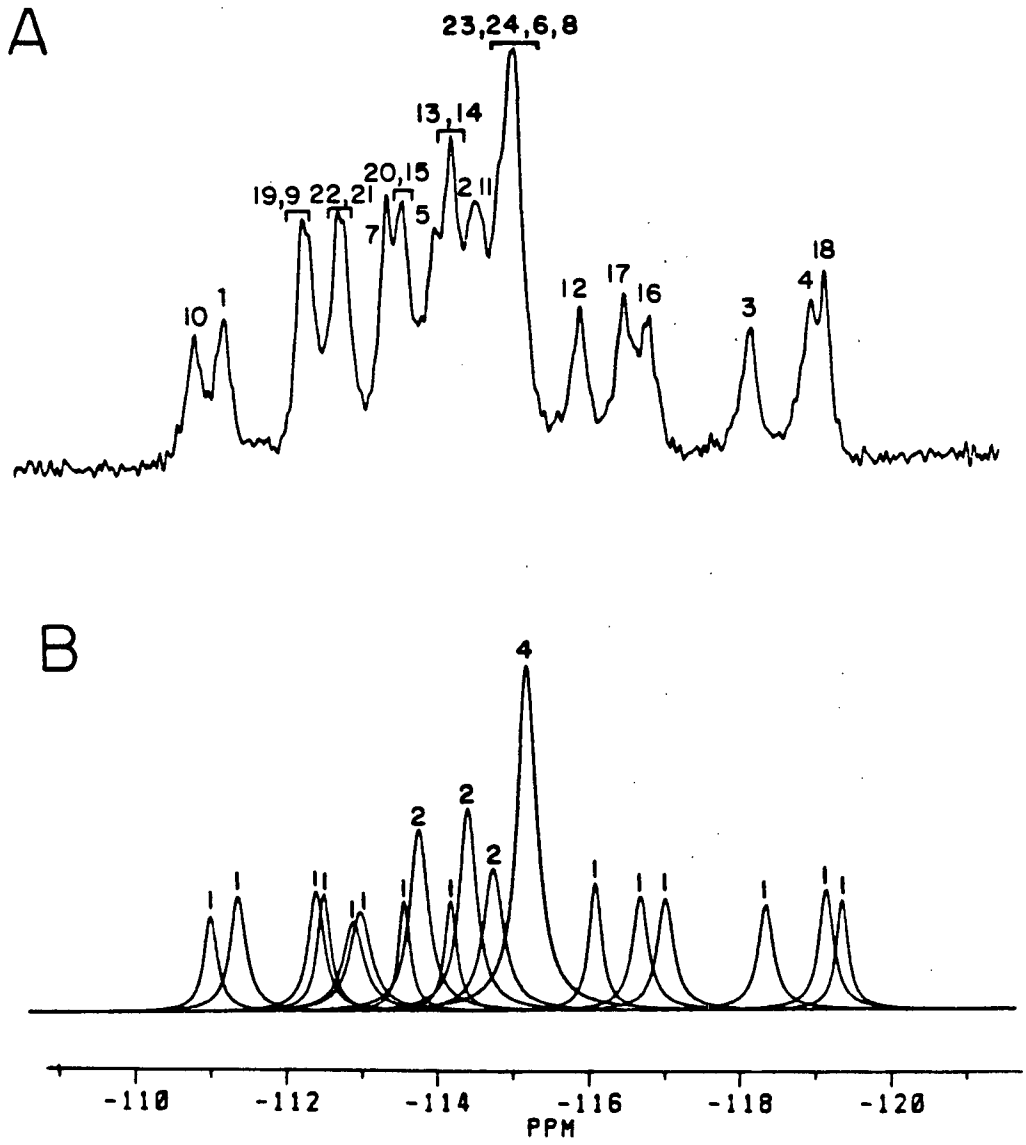

Figure 58 (A) ^{29}Si MAS NMR spectrum of the ZSM-5 sample with 8 molecules per u.c. with proton decoupling during acquisition and a recycle time of 375 s.
(B) The individual Lorentzian curves from a deconvolution of Figure 58A. The numbers above the curves indicate relative peak areas.

C. NATURAL-ABUNDANCE TWO-DIMENSIONAL ^{29}SI HIGH-RESOLUTION SOLID STATE NMR INVESTIGATIONS OF THE KNOWN LATTICE STRUCTURES OF ZEOLITE ZSM-5

I. INTRODUCTION

The ZSM-5 structure is a particularly difficult one to investigate by 2D NMR connectivity experiments and represents the most demanding test possible of these techniques to date. First, zeolite ZSM-5 is the most complex known zeolite in the terms of the size of the asymmetric unit. There are 12 T-sites for the Pnma structure and 24 T-sites for the other structures. As many as 48 ^{29}Si-O-^{29}Si connectivities will occur within the 2D plots, which means that 96 peaks will appear in a contour plot if every one is well- resolved. Secondly, there is no readily available starting point, which can be used to begin working through the connectivity scheme. All of the T-sites have equal occupancies and occupy positions on the surface of the channels, precluding the assignment of any of the resonance on the basis of either their relative intensities or their spin-lattice relaxation times as was done previously for zeolites ZSM-12 and ZSM-22. However, in all of the different phases of ZSM-5 investigated, the overall topology is unchanged. It may thus be possible to trace the changes of the resonances in the 1D ^{29}Si MAS NMR spectra induced by raising temperature and/or sorbed *p*-xylene, and use this to relate some resonances in the different spectra to each other. In this way the assignments of the different 2D spectra may be checked for self-consistency.

In this section, four samples of highly siliceous zeolite ZSM-5 are investigated by 2D NMR correlation experiments. They are the low-temperature monoclinic phase or the orthorhombic phases to which it is converted by the action of temperature and/or absorption of *p*-xylene. A summary of the different phases investigated is given in Table 15. The schematic representations of the asymmetric units of the phases are shown in Figure 59, and the expected connectivities for each of them are presented in Tables 16-18 after references 104, 122 and 124.

Table 15 Description of the four samples investigated

Sample	Conditions	Space group (ref)	T-site (in a.u.*)	Name given in the discussion
ZSM-5	ambient temperature (300K)	monoclinic form $P2_1/n$ (104)	24	monoclinic phase
	high temperature (403K)	orthorhombic form Pnma (123)	12	orthorhombic phase (12 T-sites)
ZSM-5 with sorbed *p*-xylene	low-loaded form 2 molecules /u.c. 300K	Pnma (121)		
	high-loaded form 8 molecules / u.c. 293K	orthorhombic form $P2_12_12_1$ (124)	24	orthorhombic phase (24 T-sites)

* 'a. u.' Stands for asymmetric unit.

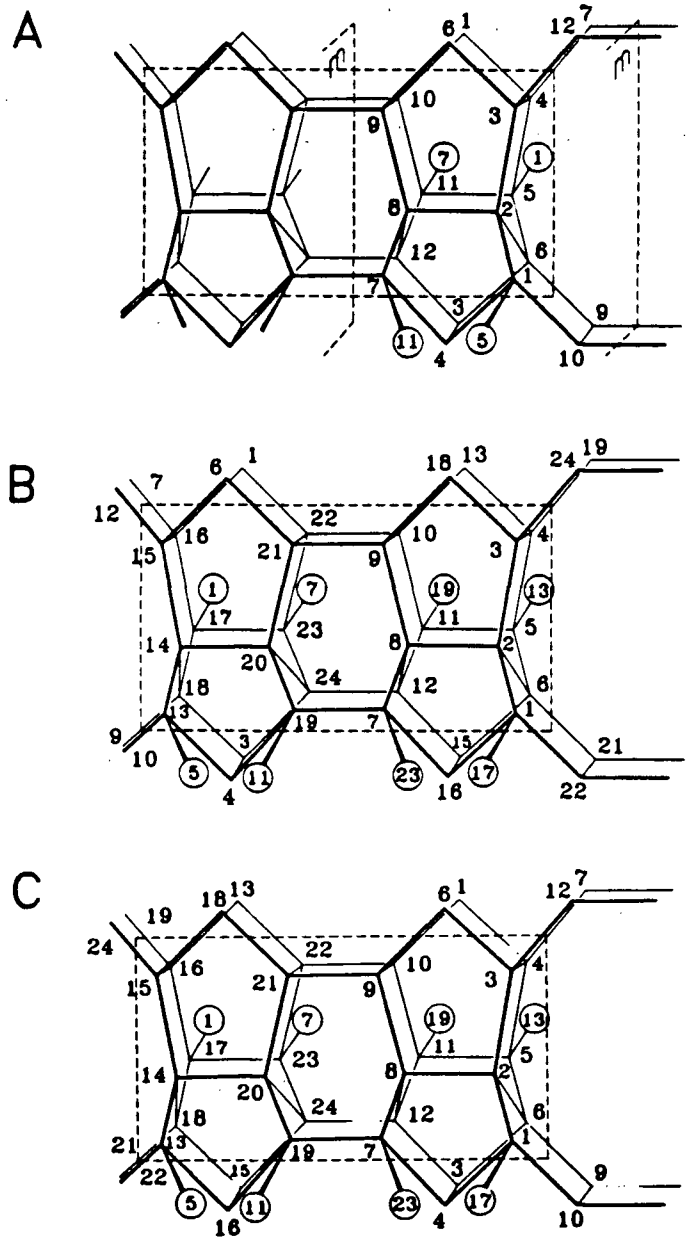

Figure 59 Schematic representations of the structures of ZSM-5 in:
(A) the orthorhombic phase (12 T-sites);
(B) the monoclinic phase (24 T-sites);
(C) the orthorhombic phase (24 T-sites).
(refs. 122, 104 and 124 respectively)

Table 16 T-sites, Their Occupancies, and Connectivities for the Asymmetric Unit in the Orthorhombic Phase (12 T-sites) of Zeolite ZSM-5 (Ref. 121)

T-site	occupancy	connectivity
T_1	1	$1T_2$: $1T_4$: $1T_5$: $1T_{10}$
T_2	1	$1T_1$: $1T_3$: $1T_6$: $1T_8$
T_3	1	$1T_2$: $1T_4$: $1T_6$: $1T_{12}$
T_4	1	$1T_1$: $1T_3$: $1T_5$: $1T_7$
T_5	1	$1T_1$: $1T_4$: $1T_6$: $1T_{11}$
T_6	1	$1T_2$: $1T_3$: $1T_5$: $1T_9$
T_7	1	$1T_4$: $\underline{1T_7}$: $1T_8$: $1T_{11}$
T_8	1	$1T_2$: $1T_7$: $1T_9$: $1T_{12}$
T_9	1	$1T_6$: $1T_8$: $\underline{1T_9}$: $1T_{10}$
T_{10}	1	$1T_1$: $1T_9$: $\underline{1T_{10}}$: $1T_{11}$
T_{11}	1	$1T_5$: $1T_7$: $1T_{10}$: $1T_{12}$
T_{12}	1	$1T_3$: $1T_8$: $1T_{11}$: $\underline{1T_{12}}$

Table 17 T-sites, Their Occupancies, and Connectivities for the Asymmetric Unit in the Monoclinic Phase of Zeolite ZSM-5 (Ref. 104)

T-site	occupancy	connectivity
T_1	1	$1T_2$: $1T_{16}$: $1T_{17}$: $1T_{22}$
T_2	1	$1T_1$: $1T_3$: $1T_6$: $1T_8$
T_3	1	$1T_2$: $1T_4$: $1T_{18}$: $1T_{24}$
T_4	1	$1T_3$: $1T_5$: $1T_{13}$: $1T_{19}$
T_5	1	$1T_4$: $1T_6$: $1T_{11}$: $1T_{13}$
T_6	1	$1T_2$: $1T_5$: $1T_{15}$: $1T_{21}$
T_7	1	$1T_8$: $1T_{16}$: $1T_{19}$: $1T_{23}$
T_8	1	$1T_2$: $1T_7$: $1T_9$: $1T_{12}$
T_9	1	$1T_8$: $1T_{10}$: $1T_{18}$: $1T_{21}$
T_{10}	1	$1T_9$: $1T_{11}$: $1T_{13}$: $1T_{22}$
T_{11}	1	$1T_5$: $1T_{10}$: $1T_{12}$: $1T_{19}$
T_{12}	1	$1T_8$: $1T_{11}$: $1T_{15}$: $1T_{24}$
T_{13}	1	$1T_4$: $1T_5$: $1T_{10}$: $1T_{14}$
T_{14}	1	$1T_{13}$: $1T_{15}$: $1T_{18}$: $1T_{20}$
T_{15}	1	$1T_6$: $1T_{12}$: $1T_{14}$: $1T_{16}$
T_{16}	1	$1T_1$: $1T_7$: $1T_{15}$: $1T_{17}$
T_{17}	1	$1T_1$: $1T_{16}$: $1T_{18}$: $1T_{23}$
T_{18}	1	$1T_3$: $1T_9$: $1T_{14}$: $1T_{17}$
T_{19}	1	$1T_4$: $1T_7$: $1T_{11}$: $1T_{20}$
T_{20}	1	$1T_{14}$: $1T_{19}$: $1T_{21}$: $1T_{24}$
T_{21}	1	$1T_6$: $1T_9$: $1T_{20}$: $1T_{22}$
T_{22}	1	$1T_1$: $1T_{10}$: $1T_{21}$: $1T_{23}$
T_{23}	1	$1T_7$: $1T_{17}$: $1T_{22}$: $1T_{24}$
T_{24}	1	$1T_3$: $1T_{12}$: $1T_{20}$: $1T_{23}$

Table 18 T-sites, Their Occupancies, and Connectivities for the Asymmetric Unit in the Orthorhombic Phase (24 T-sites) of Zeolite ZSM-5 (Ref. 124)

T-site	occupancy	connectivity
T_1	1	$1T_2$: $1T_4$: $1T_{10}$: $1T_{17}$
T_2	1	$1T_1$: $1T_3$: $1T_6$: $1T_8$
T_3	1	$1T_2$: $1T_4$: $1T_6$: $1T_{12}$
T_4	1	$1T_1$: $1T_3$: $1T_5$: $1T_7$
T_5	1	$1T_4$: $1T_6$: $1T_{11}$: $1T_{13}$
T_6	1	$1T_2$: $1T_3$: $1T_5$: $1T_9$
T_7	1	$1T_4$: $1T_8$: $1T_{19}$: $1T_{23}$
T_8	1	$1T_2$: $1T_7$: $1T_9$: $1T_{12}$
T_9	1	$1T_6$: $1T_8$: $1T_{10}$: $1T_{21}$
T_{10}	1	$1T_1$: $1T_9$: $1T_{11}$: $1T_{22}$
T_{11}	1	$1T_5$: $1T_{10}$: $1T_{12}$: $1T_{19}$
T_{12}	1	$1T_3$: $1T_8$: $1T_{11}$: $1T_{24}$
T_{13}	1	$1T_5$: $1T_{14}$: $1T_{16}$: $1T_{22}$
T_{14}	1	$1T_{13}$: $1T_{15}$: $1T_{18}$: $1T_{20}$
T_{15}	1	$1T_{14}$: $1T_{16}$: $1T_{18}$: $1T_{24}$
T_{16}	1	$1T_{13}$: $1T_{15}$: $1T_{17}$: $1T_{19}$
T_{17}	1	$1T_1$: $1T_{16}$: $1T_{18}$: $1T_{23}$
T_{18}	1	$1T_{14}$: $1T_{15}$: $1T_{17}$: $1T_{21}$
T_{19}	1	$1T_7$: $1T_{11}$: $1T_{16}$: $1T_{20}$
T_{20}	1	$1T_{14}$: $1T_{19}$: $1T_{21}$: $1T_{24}$
T_{21}	1	$1T_9$: $1T_{18}$: $1T_{20}$: $1T_{22}$
T_{22}	1	$1T_{10}$: $1T_{13}$: $1T_{21}$: $1T_{23}$
T_{23}	1	$1T_7$: $1T_{17}$: $1T_{22}$: $1T_{24}$
T_{24}	1	$1T_{12}$: $1T_{15}$: $1T_{20}$: $1T_{23}$

II. RESULTS AND DISCUSSION

a) Orthorhombic phase (12 T-sites)

Figure 60 shows the 1D ^{29}Si MAS NMR spectra for the four samples studied with the assignments of the individual resonances from the 2D experiments (see on). The linewidths of all the resonances are approximately 12 Hz except those in the high temperature spectra which are ~15 Hz . The broadening at high temperature may be caused by field inhomogeneity because the static magnetic field was shimmed at room temperature or perhaps by small lattice distortions. The sharpness of all resonances indicates that all of the materials being examined are both highly ordered and crystalline. The numbering of the different resonances in each spectrum comes from the 2D NMR spectroscopy of the present work (see later). The substantial changes observed in the peak positions reflect clearly the changes in local T-site geometries induced in the structure by these transformations.

Since the orthorhombic phase (12 T-sites) is more symmetric and has a less complicated structure, it was investigated first. The phase transition from monoclinic to orthorhombic symmetry can be induced either by raising the temperature or by adsorbing *p*-xylene. The 1D NMR spectrum of ZSM-5 loaded with 2 molecules per u.c. and that of pure ZSM-5 at 403K are shown in Figures 60B and C respectively, and they are quite distinct. Although it is possible to trace some lines though a series of spectra at 373 K from samples containing various amounts of *p*-xylene and variable-temperature experiments on a sample with 2 molecules of *p*-xylene per u. c., an unambiguous correlation between all of the peaks in the two spectra cannot be established from 1D spectra alone due to

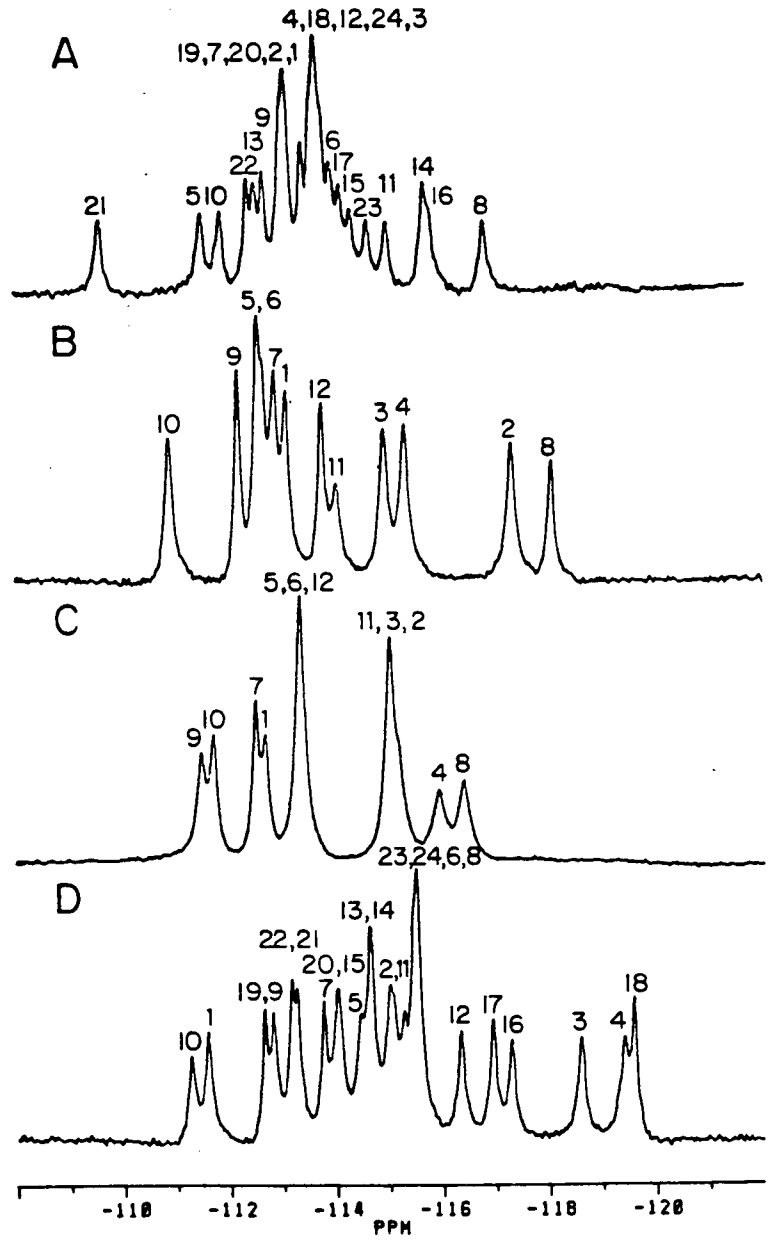

Figure 60 (A) ^{29}Si MAS NMR spectrum of ZSM-5 at 300 K.
(B) ^{29}Si MAS NMR spectrum of the low-loaded form of ZSM-5 (2 molecules of *p*-xylene per u.c.) at 300 K.
(C) ^{29}Si MAS NMR spectrum of ZSM-5 at 403 K.
(D) ^{29}Si MAS NMR spectrum of the high-loaded form of ZSM-5 (8 molecules of *p*-xylene per u.c.) at 293 K.

peak crossing and/or overlap, and both species were investigated in detail by 2D experiments

A series of ^{29}Si 2D COSY experiments were carried out on the *p*-xylene loaded form (2 molecules per u.c.) and the results from a typical experiment are shown in Figure 61 . There are clear indications that a number of connectivities between different silicons exist, 12 of the expected 22 being clearly observed in the figure. However, there is not enough information available from this experiment to assign individual resonances. In part, this is due to there being no unique signals in terms of either relative intensities or spin-lattice relaxation times with which to begin assignments, as discussed above. In addition, the very large intensities which occur along the diagonal obscure those cross peaks close to it, limiting the number which can be observed and subsequently used in the spectral assignment. In an attempt to solve this problem, ^{29}Si 2D experiments using an INADEQUATE sequence were carried out. Figure 62 shows the results of such an experiment carried out on the same low-loaded material using the parameters indicated in the figure caption. As can be seen, many more connectivities are observed, 21 in all, which from Table 16 means that almost every single possible ^{29}Si-O-^{29}Si bonding interaction has been detected, although some of them are not well defined in terms of the two source resonances because of limited spectral resolution. The problem in assigning the resonances arises from the difficulty in finding a starting point as noted above. Careful inspection of Table 16 reveals that only four silicon atoms of the total of 12 have self-connectivities, which are underlined in the table. Two of them are in the four-membered rings (T_9 and T_{10}) and the others are T_7 and T_{12}. Because self connectivity is not detected, these resonances will show only three connectivities

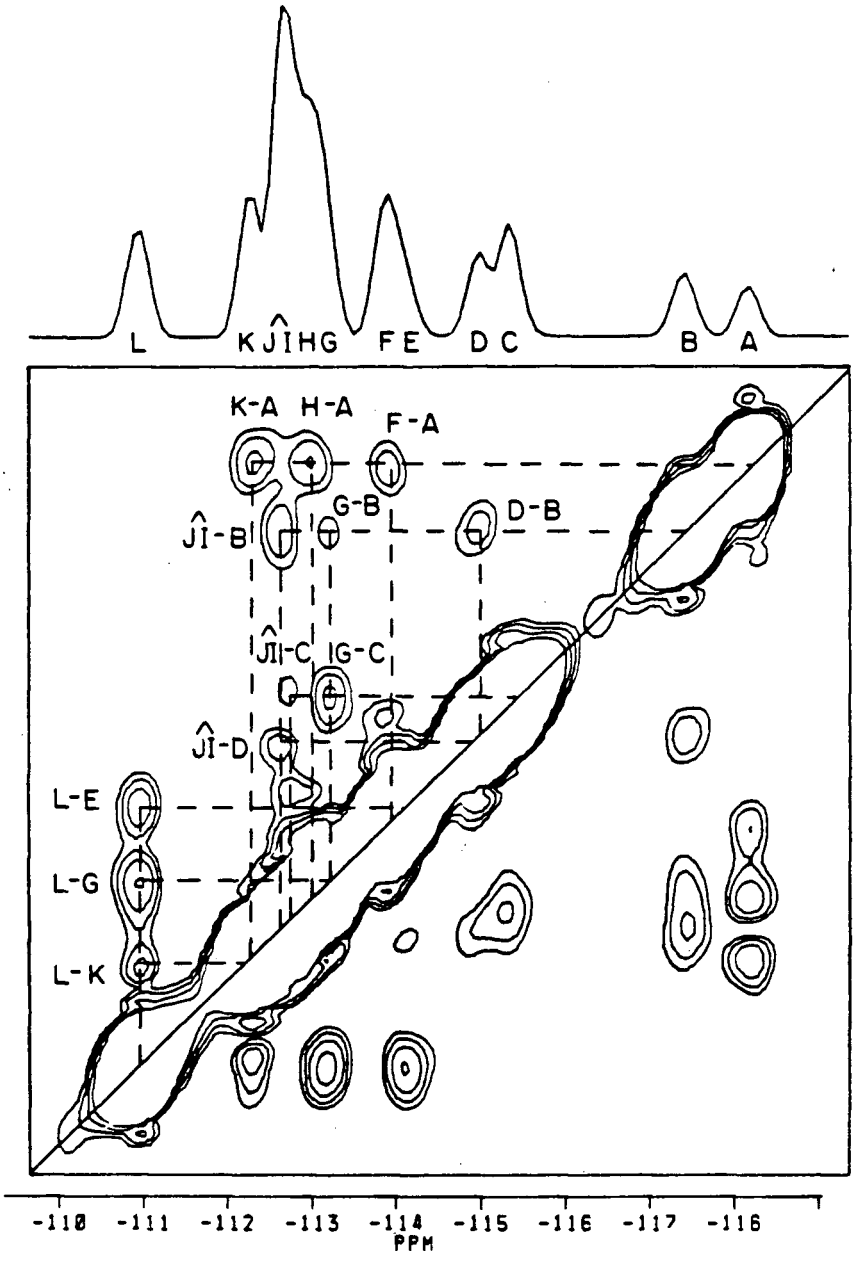

Figure 61 Contour plot of a COSY 45 experiment on ZSM-5 with 2 molecules of *p*-xylene per unit cell with the projection in the F_2 dimension shown on top. The temperature was 300K and 64 experiments were carried out with 576 scans in each experiment. A sweepwidth of 1700 Hz, a fixed delay of 10 ms and 220 real data points were used. Sine bell squared apodization and power calculation were used for the data processing.

in the 2D plots. From this, these four signals can be identified as the resonances F, H, K and L, as indicated by the arrows in Figure 62. The two silicons in the four-membered ring are directly bonded and thus show a connectivity between them, identifying them as resonances K and L. There are two possibilities for starting the assignment from this point, i. e., $T_9 \rightarrow$ K or $\rightarrow$ L. Each of these leads to a complete set of assignments of resonances, both of which are consistent with the connectivitiy scheme shown in Table 16. One complete assignment from $T_9 \rightarrow$ K is shown in the figure. The other assignment can be obtained from this one by the following Equation:

$$T_i \leftrightarrow T_{7-i}, \text{ when } 1 \leq i \leq 6$$
$$T_i \leftrightarrow T_{19-i}, \text{ when } 7 \leq i \leq 12 \qquad [28]$$

Having two possible assignments is the case for all phases of ZSM-5, which is similar to ZSM-22 as discussed in Chapter Four, reflecting the symmetry of the structure and a discrimination between these assignments cannot be, in general, made from the NMR data alone. Additional information which would help discriminate in favour of one assignment could be gained by combining the NMR data with geometric information from diffraction studies, as in the case of ZSM-22. Unfortunately, the present powder diffraction data[126] is not considered accurate enough to use for this purpose and the choice of the correct assignment will be postponed until the discussion of the orthorhombic phase (12 T-sites) induced by high temperature.

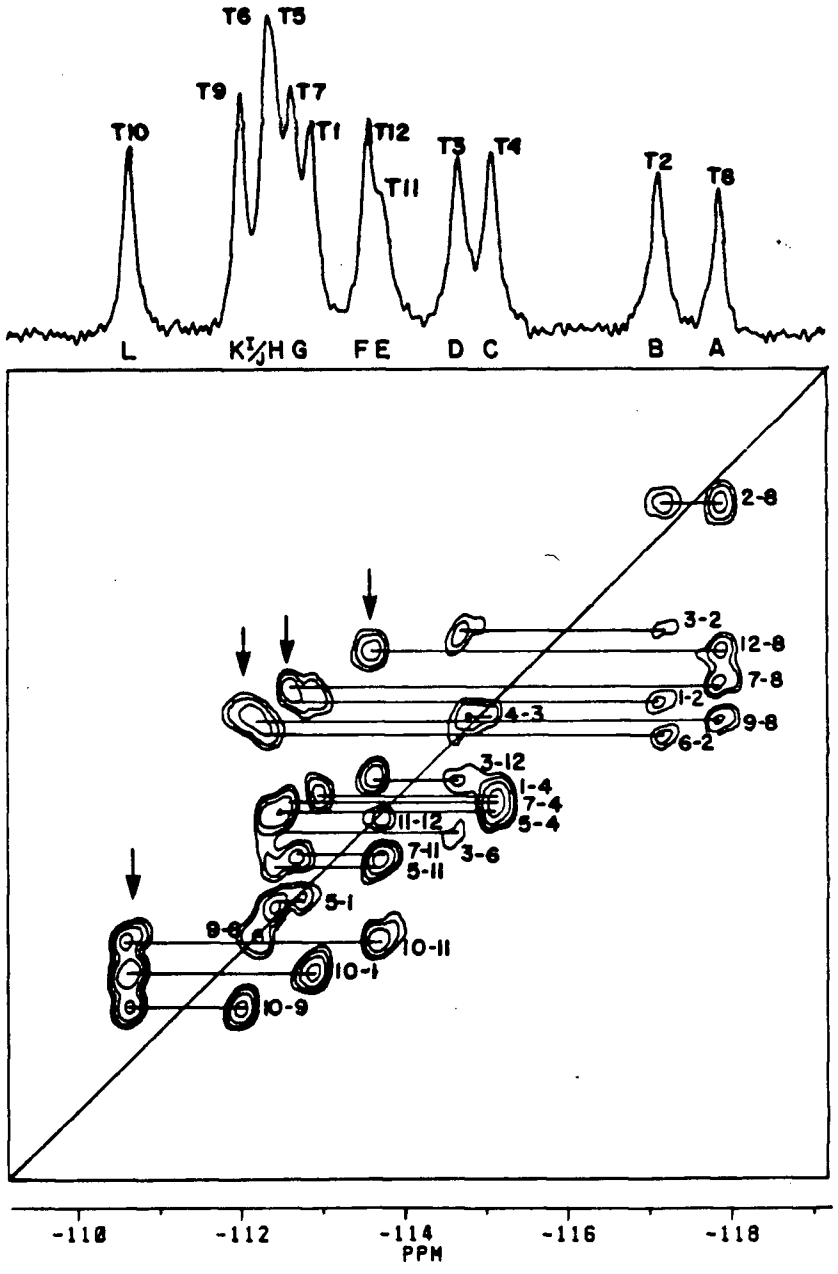

Figure 62 Contour plot of an INADEQUATE experiment on ZSM-5 with 2 molecules *p*-xylene per unit cell carried out at 300K with a 1D MAS NMR spectrum above. 36 experiments with 512 scans in each experiment were performed with a recycle time of 14 s. and the total experimental time was approximately 72 h. A sweepwidth of 800 Hz, fixed delay of 15 ms. and 140 real data points were used. Sine- bell and trapezoidal apodizations in the F_2 and F_1 dimensions respectively and a power calculation were used for the data processing.

On raising the temperature, a phase transition from the monoclinic to the orthorhombic phase (12 T-sites) occurs for pure ZSM-5. Figure 63 shows the results of a 2D INADEQUATE experiment on ZSM-5 at 403K. The assignment can be initiated at the same point as the case of the low-loaded form of *p*-xylene/ ZSM-5 described above, and the resonances J, K and L indicated by arrows in the figure are associated with three T-sites among the four which have self-connections. The assignment of K and L to T_{10} and T_9 can be made due to the connection between them. In this spectrum, the overlap of some resonances is more severe and only 18 connectivities out of the 22 are observed, making it more difficult to obtain a complete assignment. An effort to determine the relationship of some resonances between the high temperature spectrum of ZSM-5 and that of the low-loaded sample was made from the published literature[49], because two possible assignments of the low-loaded form of *p*-xylene/ ZSM-5 were obtained. Careful inspection of the spectra of ZSM-5 in the low-loaded form at various temperatures and the spectra with increasing concentration of *p*-xylene at 373 K[49] reveals that the highest field peak in all cases is due to the same T-site. With this information and the assignment of resonances K, L and J, it is now possible to obtain two complete sets of assignments (Table 19), which are related to each other by Equation 28.

In this case, combining the NMR and the X-ray diffraction data allows a completely unambiguous choice between the two possible assignments. Thus, a highly accurate single crystal refinement of the high temperature form of ZSM-5 has recently been carried out by van Koningsveld and co-workers [123]. The very low errors in the positional parameters obtained in this study mean that it

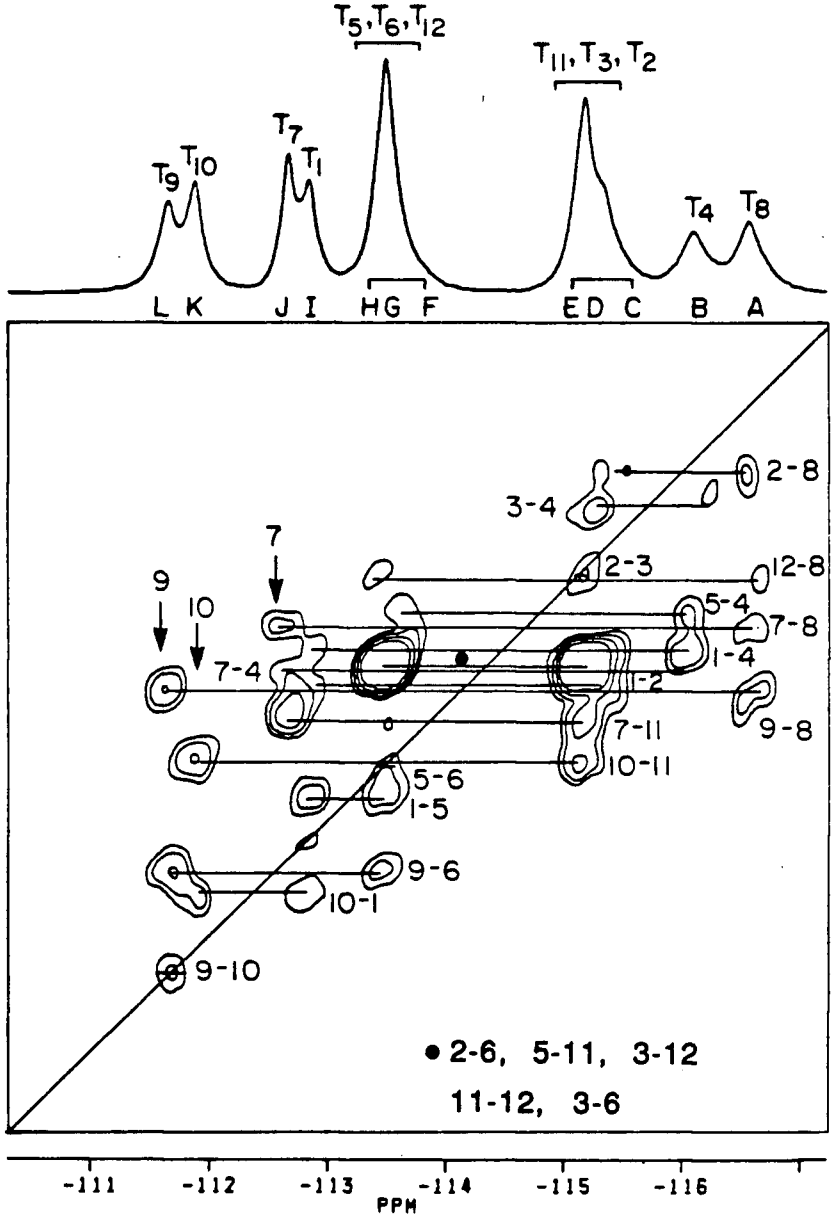

Figure 63 Contour plot of an INADEQUATE experiment on ZSM-5 at 403K with a 1D MAS NMR spectrum above. 32 experiments with 352 scans in each experiment were carried out with the recycle time of 50 s. and the total time for the experiment was approximately 157 h. A sweepwidth of 550 Hz, fixed delay of 15 ms and 108 real data points were used. Sine-bell and trapezoidal apodizations in the F_2 and F_1 dimensions respectively and a power calculation were used for the data processing.

may reliably be used to distinguish between the two possible assignments. The chemical shifts are plotted as a function of average T-T distances for both assignments, as shown in Figure 64. As can be seen the linear correlation is much better for assignment I, and this one is considered to be unique and is that presented with the 1D spectrum in Figure 63. Consequenly, the unambiguous assignment for the low-loaded p-xylene/ZSM-5 can be deduced as shown in figure 62.

Table 19 T-sites and Two Possible Assignments of the Resonances in the Orthorhombic Phase (12 T-sites) of Zeolite ZSM-5 at 403 K

T-site	Assignment I	Assignment II
T_1	I	F-H
T_2	C-E	F-H
T_3	C-E	B
T_4	B	C-E
T_5	F-H	C-E
T_6	F-H	I
T_7	J	F-H
T_8	A	C-E
T_9	L	K
T_{10}	K	L
T_{11}	C-E	A
T_{12}	F-H	J

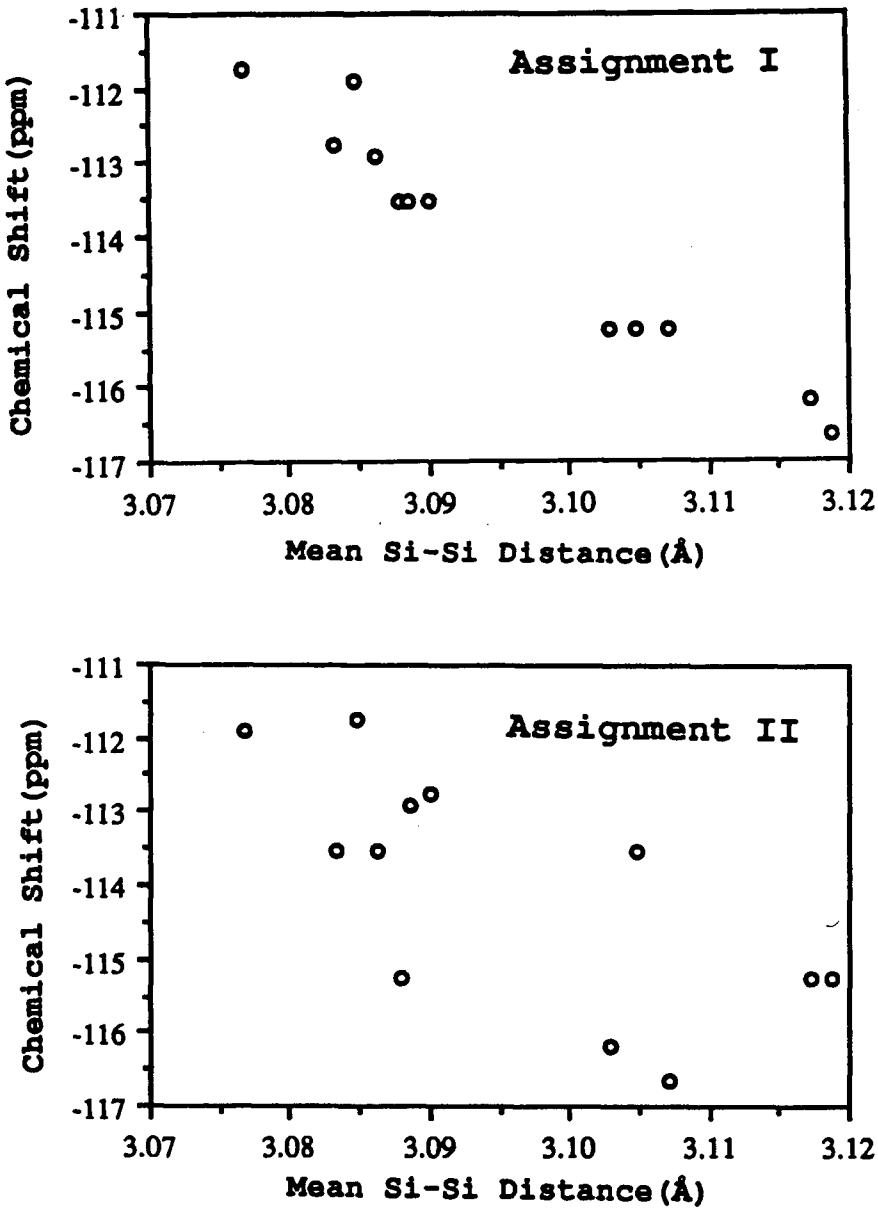

Figure 64 Plots of the ^{29}Si chemical shifts as functions of the average T-T distances calculated from the data of reference 123 for the two possible assignments of the high temperature form of ZSM-5.

B) Monoclinic Phase (24 T-sites)

It is well known that the structure of pure ZSM-5 at room temperature is monoclinic $P2_1/n$, with 24 crystallographically inequivelant silicons in an asymmetric unit. Inspection of its 1D spectrum (Figure 60A) shows that most of the spectral intensity occurs in the centre of the spectrum. It can be anticipated that in COSY experiments on this form, most of the cross peaks would be obscured by the large diagonal peaks. Thus INADEQUATE experiments were chosen to investigate this phase. The result of such an experiment is presented in Figure 65, and 38 of the total 48 expected connectivities are observed. In this phase, each silicon is bonded to four different silicons through oxygen bridges in addition to having the same occupancy and similar T_1 relaxation times. Hence, it is again difficult to find any starting point to the assignment. On raising the temperature from ambient, there are gradual changes in the frequencies of the different resonances and then a more abrupt change at the transition temperature [49]. In the low field region, four resonances tend towards the frequencies of the two lowest field signals of the orthorhombic form (12 T-sites), as shown in Figure 66. Making specific connections between the two phases cannot be absolutely justified because of the discontinuity at the transition temperature, but it was felt that the resonances corresponding to the silicon atoms in the four membered ring in the monoclinic phase were probably amongst those at lower field and particular attention was paid to those signals in this regard. As seen in Figure 65 there are 6 resonances at lower field (to the left of the large central peaks) and these were examined first. The connectivities of the four silicons in the four-membered ring, i.e. T_9, T_{10}, T_{21} and T_{22}, are presented in Table 20A, the diagonal pairs connecting simultaneously to the other pairs. The connectivities of the six resonances are listed in Table 20B.

Figure 65 Contour plot of an INADEQUATE experiment on ZSM-5 at 300K with a 1D MAS NMR spectrum above. 36 experiments with 448 scans in each experiment were carried out with a recycle time of 12 s. and the total time for the experiment was approximately 54 h. A sweep width of 700 Hz, fixed delay of 15 ms and 160 real data points were used. Sine-bell and trapezoidal apodizations in F_2 and F_1 dimensions respectively and a power calculation were used for the data processing.

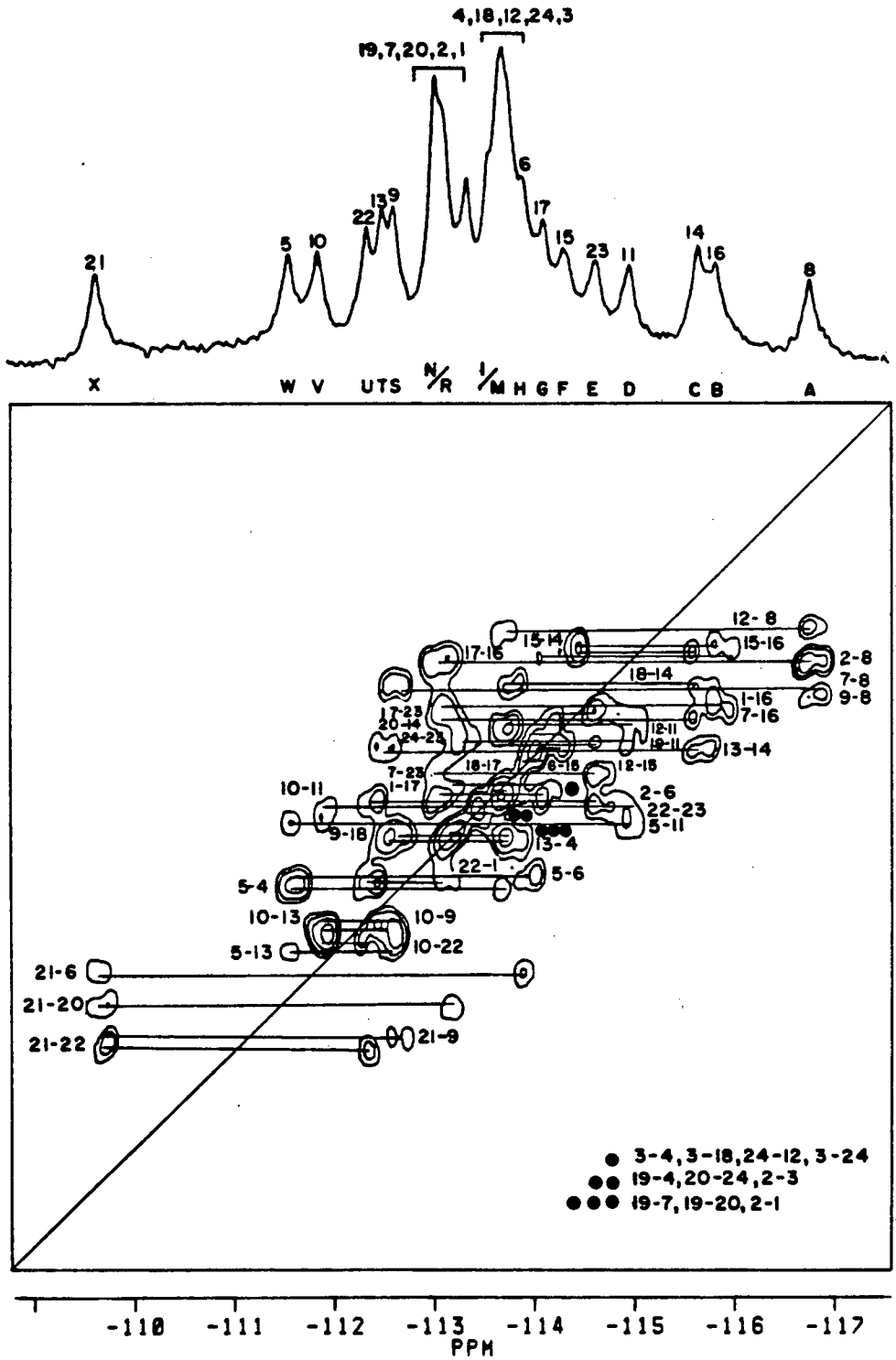
4,18,12,24,3
19,7,20,2,1
6
17
15
23
11
14
16
8
5
10
22
13
9
21
X
W V
UTS
N/R
I/M
H G F E D
C B
A
12-8
15-14
15-16
17-16
2-8
18-14
7-8
1-16
9-8
17-23
20-14
24-23
7-16
12-11
19-11
13-14
18-17
6-15
12-15
7-23
1-17
10-11
2-6
22-23
5-11
9-18
13-4
22-1
5-6
5-4
10-13
10-9
5-13
10-22
21-6
21-20
21-22
21-9
3-4,3-18,24-12,3-24
19-4,20-24,2-3
19-7,19-20,2-1
-110
-111
-112
-113
-114
-115
-116
-117
PPM

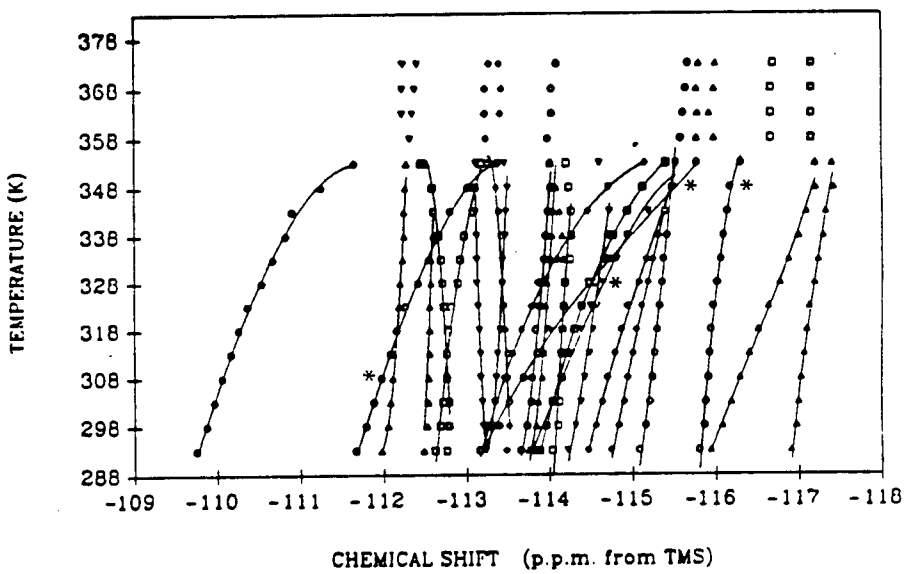

Figure 66 A graphical representation of the variation of chemical shift with temperature for zeolite ZSM-5. (ref. 138)

Table 20 A. Known Connectivities of the Four Membered Ring T-Sites in the Monoclinic Phase of ZSM-5 (From Table 17)

T-site	Connectivities			
9	8	10	18	21
10	9	11	13	22
21	6	9	20	22
22	1	10	21	23

B. Observed Connectivities of the Six Lowest Field Resonances From NMR Experiments (From Figure 65)

Resonance	Connectivities			
S	A	I/M	V	X
T	C	I/M	V	W
U	E	N/R	V	X
V	D	S	T	U
W	D	H	I/M	T
X	H	N/R	S	U

From those connectivities underlined, it can be deduced that silicons 9, 22 and 10, 21 are the (S, U) and (V, X) pairs. There are again two possible assignments which are related to each other by Equation [29].

$$T_i \leftrightarrow T_{i+12}, \quad \text{when } i \leq 12$$

$$T_i \leftrightarrow T_{i-12}, \quad \text{when } i > 12 \qquad [29]$$

In order to facilitate discussion, the resonances V and X are assigned to be T_{10} and T_{21} at this stage. In Table 20B the resonances V and W show the same connectivities to D and T. T_{10} and T_{21} are connected to T_{11}, T_{13} and T_6, T_{20} respectively besides T_9 and T_{22}. Table 17 shows that T_5 is connected to T_{11} and T_{13} too, while only T_{21} is connected to T_6 and T_{20}. Thus the assignments, V $\rightarrow$ T_{10}, W $\rightarrow$ T_5 and X $\rightarrow$ T_{21} can be made, so resonance H corresponds to T_6. By trial and error, the assignments of D $\rightarrow$ T_{11} and T $\rightarrow$ T_{13} follow. At this point, almost all of the lower field resonances are assigned. When the process is traced to the higher field part, it is more difficult to make progress because of the severe overlapping of resonances and the lower resolution of the 2D experiment than that shown in the 1D spectrum on the top of the 2D plot. In order to get a reliable connectivity scheme of resonances, the experiments were repeated by carefully optimizing all of the NMR experimental variables and using different temperatures to improve the resolution of specific signals. The data obtained were processed using different numbers of data points and window functions to help identify the connected signals and resonances from which they originate. Figure 65 shows the result of one of these experiments and both the resolution and sensitivity are good enough to continue tracing the connection pattern. The

remaining assignments were accomplished mainly by trial and error. The second possible assignment from the alternative starting point can be obtained by exchanging pairs of T-sites as described in Equation 29. During the course of this study, a single crystal refinement of the room temperature structure of ZSM-5 was reported by van Koningsveld and co-workers [104]. As in the case of high temperature form, the chemical shifts are plotted as a function of the average T-T distance for both assignments, as shown in Figure 67. The linear correlation of Assignment I, which is the one presented in Figure 65, is much superior and this assignment is considered to be the correct one.

From the results of the 2D experiments at room temperature and high temperature (Figures 63 and 65 respectively), the relationships between the resonances of the two forms can be made, as shown schematically in Figure 68. It can be seen that the changes of chemical shifts for most resonances are small. Variable temperature 1D experiments[138], as mentioned before, show that there are gradual changes in the frequencies of the different resonances and then a more abrupt change at the transition temperature (Figure 66). However the results of this 2D work (Figure 68) show that the interruption is small. Although it is impossible to make specific connections between the two forms from the 1D variable temperature experiments, it may be acceptable to link the resonances in groups. In fact, the shift trend of the individual resonance in Figure 66 is in general correct except that the lines marked '*' could lead wrong connections. Thus most of the connections obtained from 1D variable temperature experiments are reliable. This will be useful in future studies of unknown systems which have this kind of linkage to some known structure.

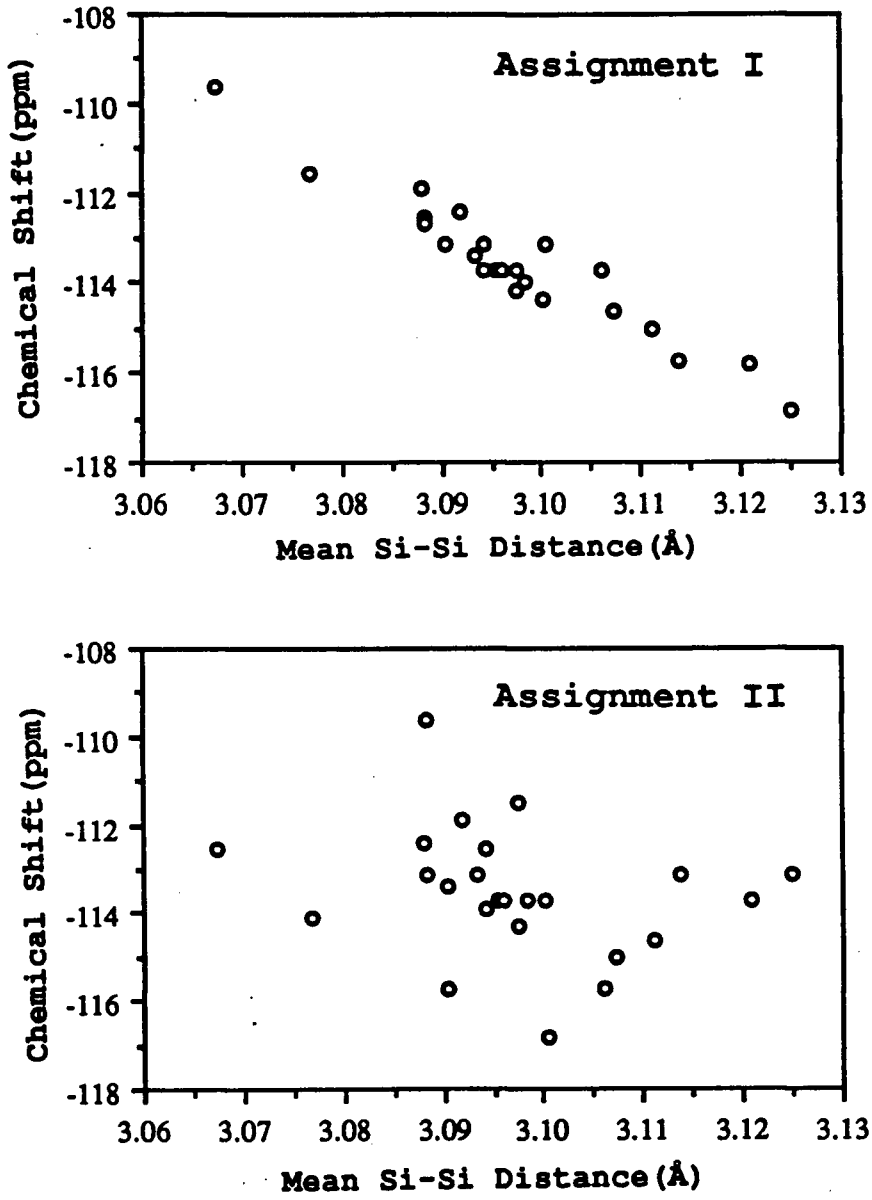

Figure 67 Plots of the ^{29}Si chemical shifts as functions of the average T-T distances for the two possible assignments of the room temperature form of ZSM-5.

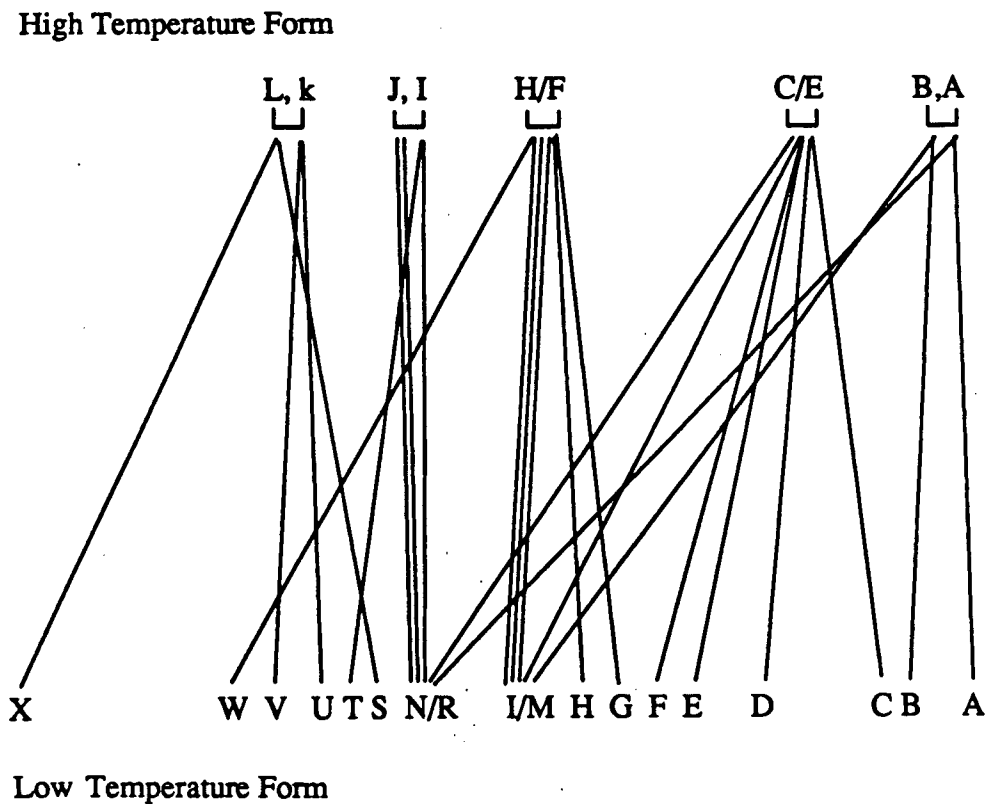

Figure 68 Relationship of the resonances between the room- and high- temperature forms of ZSM-5.

C) Orthorhombic Phase (24 T-sites)

As discussed earlier, when the loading of *p*-xylene is increased from 2 to 7 molecules per unit cell, another phase transition occurs. The new phase has orthorhombic symmetry with space group of $P2_12_12_1$ with the connectivity pattern presented in Table 18. 2D experiments were performed on the high loaded sample using the basic pulse sequence shown in Figure 36B and the cross polarization sequence to excite ^{29}Si nuclei. The results of an INADEQUATE experiment are shown in Figure 69. All but one of the 48 connectivities are clearly observed in this case, but not every connectivity is well defined in terms of the two resonances from which it originates because of the limited resolution of the spectrum. There is nothing known regarding the relationship of the various chemical shifts between this phase and the other phases, and thus no help can be obtained from all of the assignments discussed above except that the resonances of four-silicons in the four membered ring might well again be expected to appear at lower field. Particular attention was paid to resonances X and W, which are the only two better resolved resonances at lower field. The connectivities of the other resonances associated with W are given in Table 21A. The first row in this table shows the resonances associated with W and each column presents the association of each of these resonances to other resonances in the spectrum. It can be seen from the table that B and L are simultanously connected with C and the resonances L and E may or may be not linked to the same resonance within the overlapped peaks, G/J. Then, the first 12 T-sites are analysed according to Table 21A on the basis of diffraction data (Table 18) and 6 T-sites, T_1, T_4, T_5, T_8, T_{10} and T_{12}, present this kind of connectivity pattern.

Figure 69 Contour plot of a CP-INADEQUATE experiment on ZSM-5 with 8 molecules of *p*-xylene per unit cell with a 1D CP MAS NMR spectrum on top. 64 experiments with 1088 scans in each experiment were carried out with a recycle time of 3 s and the total time for the experiment was approximately 58 h. A sweepwidth of 846 Hz, contact time of 20 ms., fixed delay of 16 ms. and 100 real data points were used. Sine-bell apodization and a power calculation were used for the data processing.

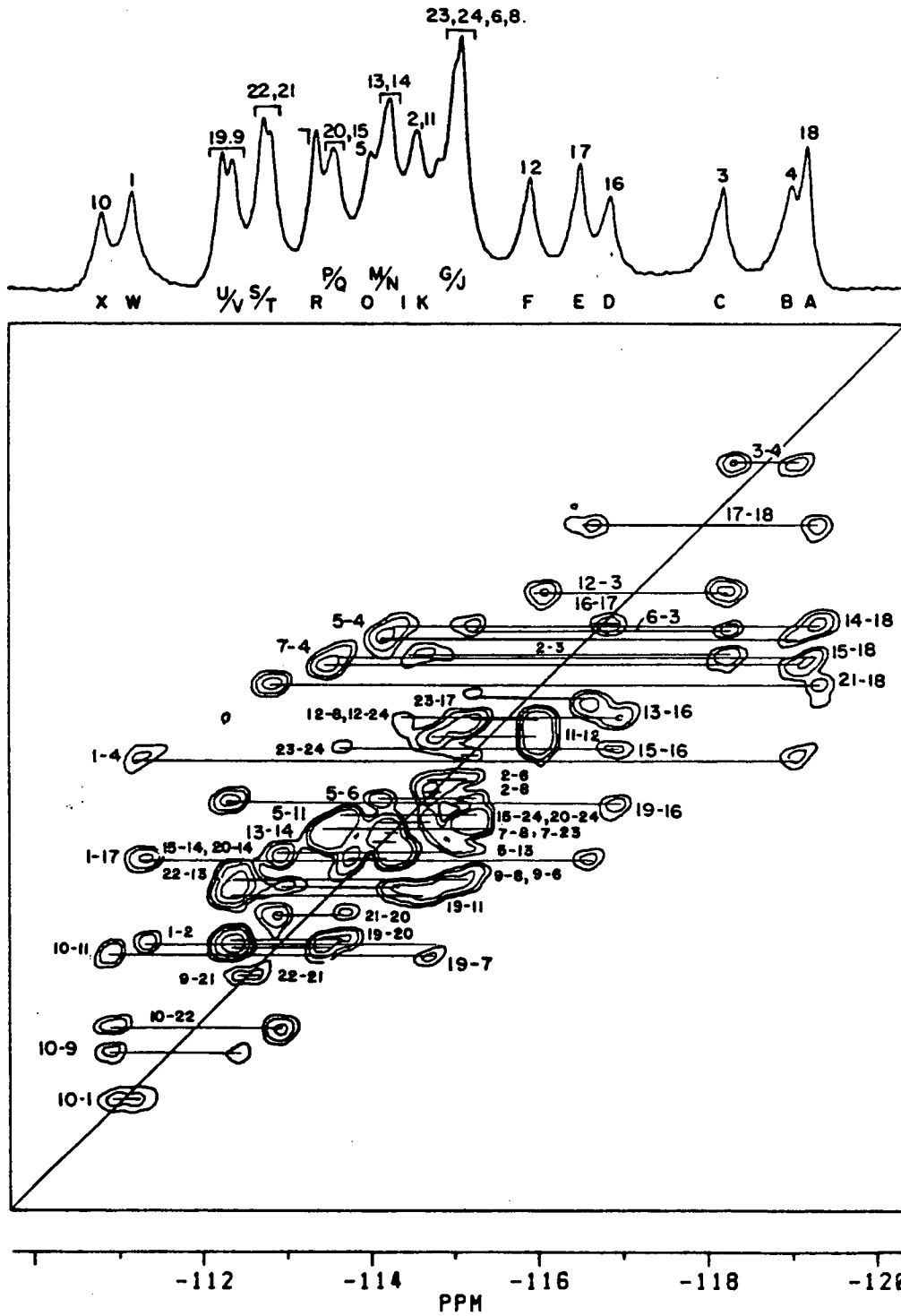
23,24,6,8.
22,21
13,14
19.9
20,15
5
2,11
18
17
12
16
3
4
10
1
X W
U/V S/T
P/Q
R
M/N
O I K
G/J
F
E D
C
B A
3-4
17-18
12-3
16-17
5-4
6-3
14-18
7-4
2-3
15-18
21-18
23-17
12-8,12-24
13-16
11-12
1-4
23-24
15-16
2-6
2-8
5-6
5-11
19-16
15-24,20-24
13-14
7-8, 7-23
1-17
15-14, 20-14
6-13
22-13
9-8, 9-6
19-11
21-20
1-2
19-20
10-11
19-7
9-21
22-21
10-22
10-9
10-1
-112
-114
-116
-118
-120
PPM

Table 21 Connectivities Related to Resonance W and T-site 1 in the High Loaded *p*-Xylene Form of ZSM-5.

A. Observed Connectivities related to resonance W

W	L	B	X	E
	W	W	W	W
	C	C	K	A
	G/J	O	S/T	D
	G/J	R	U/V	G/J

B. Connectivities of T_1 from Diffraction Data (Table 18)

1	2	4	10	17
	1	1	1	1
	3	3	9	16
	6	5	11	18
	8	7	22	23

In the present orthorhombic phase (24 T- sites) two possible assignments can be made as in the monoclinic phase. Thus only the first 12 T-sites are considered. Resonance W is at lower field and is connected with only one other lower field resonance X. Thus W could not be a silicon in the four membered ring, while X might be. Among the 6 possible T-sites only T_1 is connected with one of the four membered ring silicons. The assignment can thus be started at this point, W→ T_1. The connectivities related to T_1 are given in Table 21B. By comparison with Tables 21A and B, the following assignments can be made: X→ T_{10}, E→ T_{17}, C→ T_3, (L, B) → (T_2, T_4), (A, D) → (T_{16}, T_{18}) and (O, P) → (T_5, T_7). In addition, T_6, T_8 and T_{23} are among the resonances of G/J. The process of assignment continues without much difficulty yielding the complete assignment shown in Figure 69. There are two possible assignments with the same exchange rules as in the monoclinic form (Equation 29). The solution to this problem again lies in combining the NMR results with single crystal diffraction data[124]. The chemical shifts are plotted as a function of average T-T distances for both assignments, as shown in Figure 70. The linear correlation of Assignment I, which is the one presented in Figure 69, is much better and this one is considered to be unique.

The method based on listing the connectivity patterns both of resonances from NMR experiments and of T-sites on the XRD data, as shown in Table 21, can be generally used in assignments. For the cases where all or almost all connectivities are resolved, the assignments can be made without any additional information, such as intensities of signals, T_1 values of nuclei, etc. Zeolites ZSM-39, ZSM-12 and ZSM-22 are such cases, though the methods of assignment discussed in previous chapters are more easy and direct. However, in situations

where the resonances are severely overlapped, such as the cases of pure ZSM-5 in the room temperature and high temperature forms, it is hard to apply this method. Firstly, there is considerable uncertainty in the connections of resonances. Secondly, the clues needed to propagate the assignments quickly disappear due to peak overlap, even if a starting point can be found. Nevertheless, with the help of some other information it may be possible to make an assignment to this kind of 2D spectrum, as described in the high loaded form of ZSM-5.

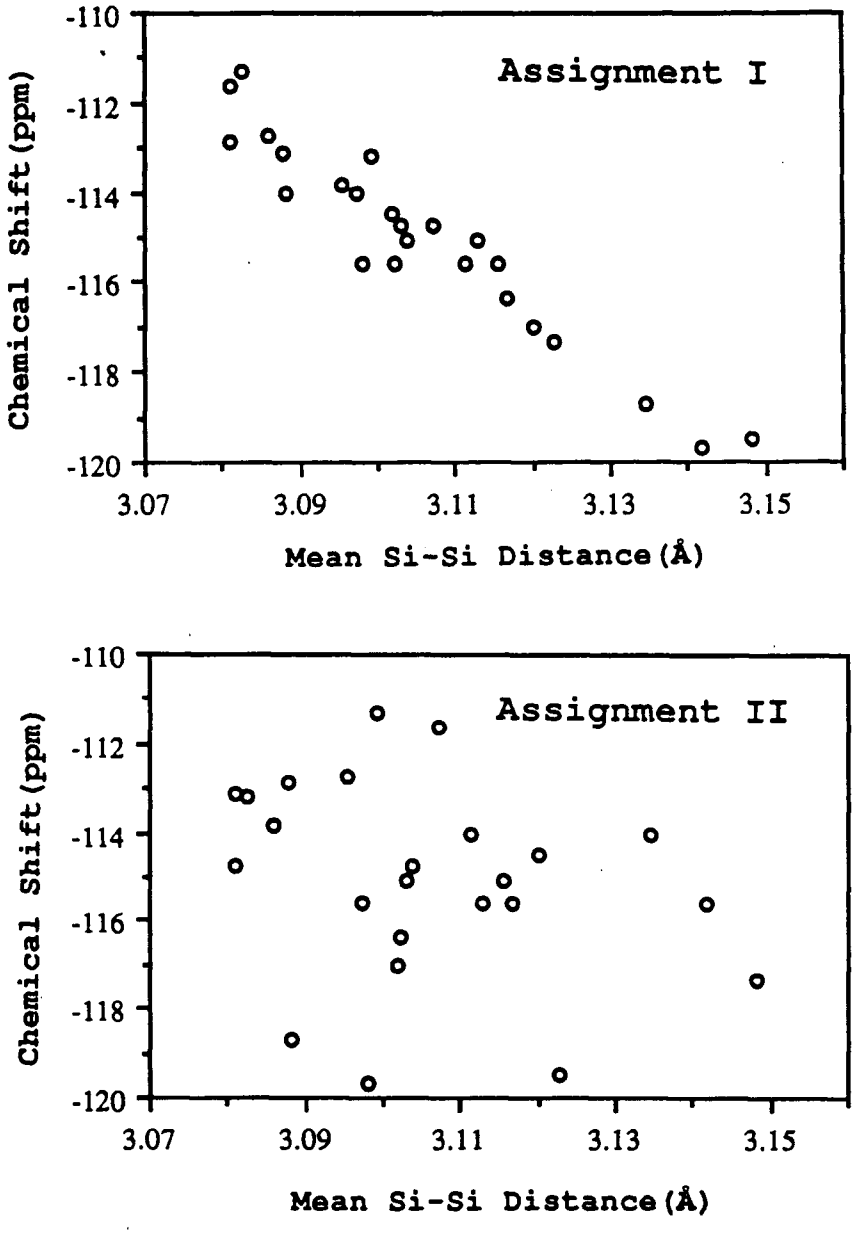

Figure 70 Plots of the ^{29}Si chemical shifts as functions of the average T-T distances for the high loaded *p*-xylene form of ZSM-5.

D. TWO-DIMENSIONAL ^{29}SI HIGH-RESOLUSION SOLID STATE NMR INVESTIGATION OF THE LATTICE STRUCTURES OF ZEOLITE ZSM-5 LOADED WITH *P*-DICHLOROBENZENE

I. INTRODUCTION

It has been reported by Fyfe and co-workers [51] that the compounds *p*-xylene, *p*-chlorotoluene and *p*-dichlorobenzene, at a loading of 2 molecules per unit cell, induce essentially identical changes in the 1D ^{29}Si MAS NMR spectrum of zeolite ZSM-5, as mentioned in Chapter One. This result indicates that the major contribution to the phase transition from the monoclinic phase (24 T-sites) to the orthorhombic phase (12 T-sites) in these cases is the size and shape of the sorbed organic molecules. This conclusion is based on the appearance of 1D NMR spectra and has been confirmed by the powder X-ray diffraction patterns of these systems. 2D correlation NMR techniques have provided more detail and reliable information about the zeolite structures, as can be seen in the previous discussion, and thus can also be used to confirm the conclusions drawn from the 1D NMR results.

As discussed in Section B of this chapter, the dynamic behavior of *p*-xylene molecules adsorbed in the channels of ZSM-5 is dependent on the loading. In the low-loaded form, *p*-xylene molecules are mobile on the NMR time scale, while they are relatively 'fixed' in the high-loaded form. If this is true in the case of *p*-dichlorobenzene, it is expected that the dipolar and electronic interactions between the adsorbed *p*-dichlorobenzene and the framework of ZSM-5 will be more efficient at high loadings. Therefore, the changes both in

NMR spectra as well as in the structure of ZSM-5 induced by very high loadings *p*-dichlorobenzene are not easily predictable. Thus 1D and 2D NMR investigations of the structure of ZSM-5 with different loadings of *p*-dichlorobenzene were carried out to further investigate the interactions between sorbates and the host zeolite ZSM-5.

II. RESULTS AND DISCUSSION

a) 1D MAS NMR experiments

Similar results to those obtained for the '*p*-xylene case' (see Figure 56) are observed for ZSM-5 with various loadings of *p*-dichlorobenzene, as shown in Figure 71. The ^{29}Si spectra at loadings of both 2 and 4 molecules per unit cell show that the asymmetric units contain 12 T-sites, except that the '4 molecule' one shows a trace of extra intensities. This second species is clearly present at loadings of 6 and 8 molecules which has more than 12 independent T-sites. The CP sequence is much more efficient in the high loaded form, as in the case of *p*-xylene. Figure 72 shows the deconvolution of the spectrum of the '8 mol./u.c.' system indicating that the asymmetric unit contains 24 silicon atoms with at least 15 independent T-sites. However, the spectrum at this loading of *p*-dichlorobenzene appears somewhat different from that observed in the case of *p*-xylene except for the highest field portion. It is, therefore, not possible to draw any conclusions at this stage about the dominant interactions in the adsorption of 8 molecules of *p*-dichlorobenzene contributing to the phase transition as mentioned in the '2 molecule' case. Another difference between absorption of *p*-xylene and *p*-dichlorobenzene is the behavior when raising the temperature.

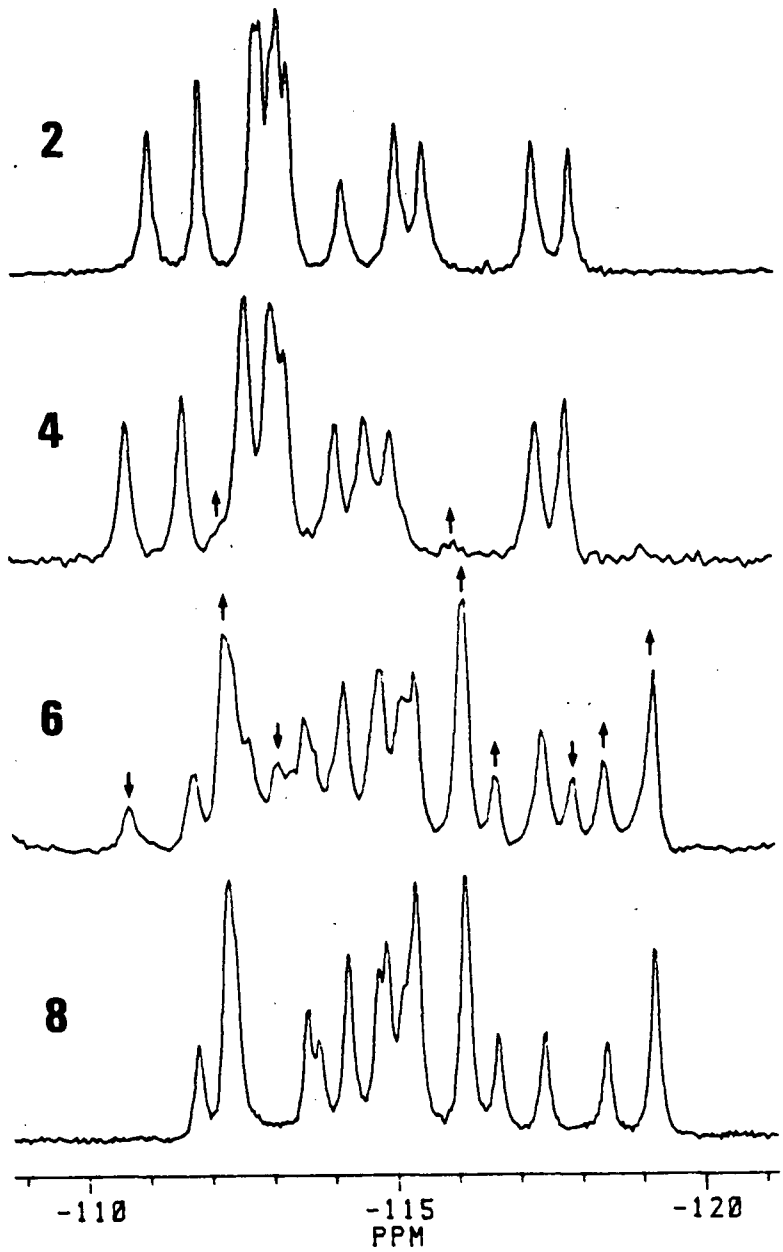

Figure 71 ^{29}Si MAS NMR spectra of ZSM-5 with proton decoupling during acquisition with increasing concentrations of *p*-dichlorobenzene . The numbers indicate the numbers of *p*-dichlorobenzene molecules sorbed per u. c.

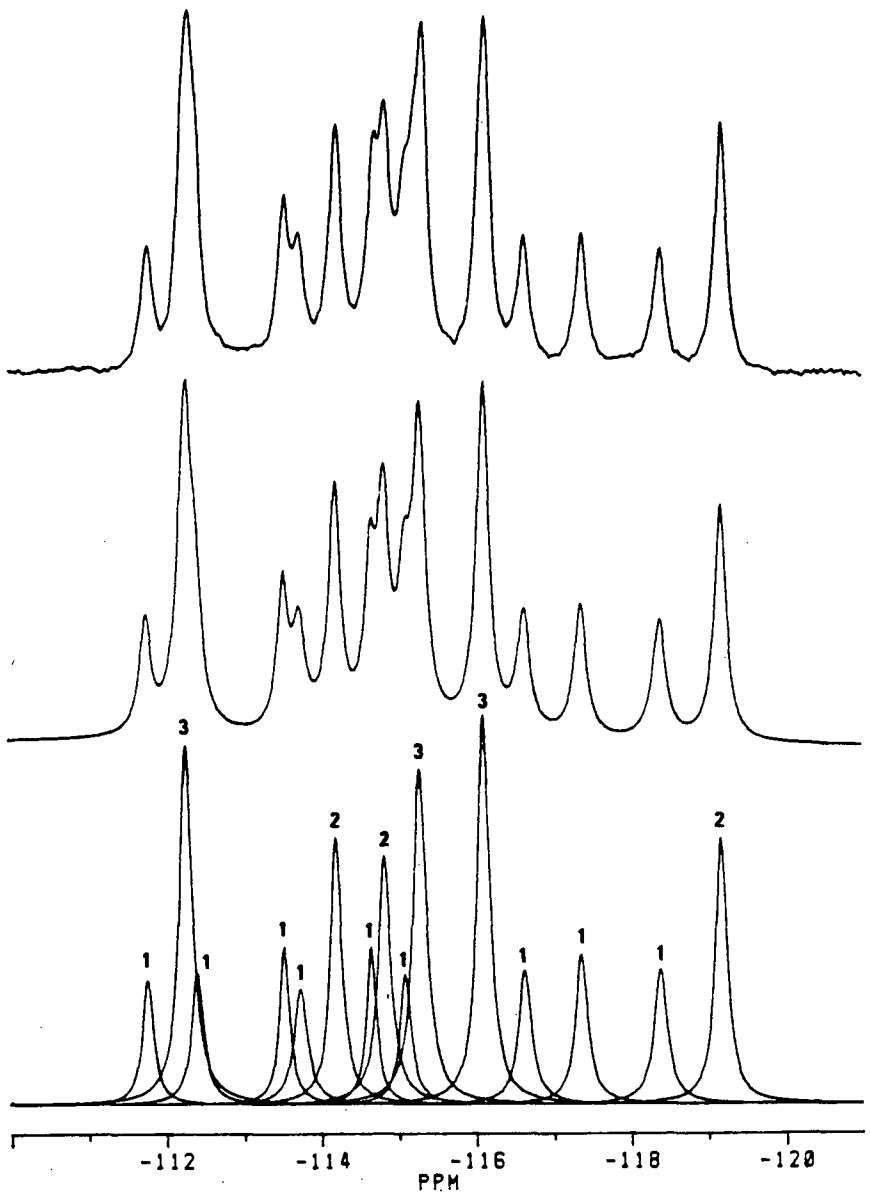

Figure 72 (A) ^{29}Si MAS NMR spectrum of ZSM-5 loaded with 8 molecules *p*-dichlorobenzene per u.c. with proton decoupling during acquisition.
(B) Computer simulation of the experimental spectrum as the sum of fifteen Lorentzian curves.
(C) The individual Lorentzian curves. The numbers above the curves indicate relative peak areas.

Figure 73 shows the results of variable temperature experiments at a loading of 8 molecules of *p*-dichlorobenzene per unit cell, indicating that this phase is stable at least up to 370 K, while in the case of *p*-xylene, the sorbate desorb at elevated temperatures, and the spectrum of the 4 molecules form is found at a temperature of 373K. These results indicate the interactions involving *p*-dichlorobenzene molecules with each other and the internal surface of ZSM-5 are stronger than in the *p*-xylene case.

b) 2D INADEQUATE experiments

The result of an INADEQUATE experiment on ZSM-5 loaded with 2 molecules of *p*-dichlorobenzene per unit cell is shown in Figure 74. A similar connectivity pattern to that found for *p*-xylene (Figure 62) was observed as expected. Two equally valid assignments based on Pnma symmetry are obtained, as in all other ZSM-5 cases. One of the two assignments is compatible with the result obtained for the *p*-xylene case, and this is considered the unique one as shown in the figure. These 2D results for the '2 molecule' case confirm the conclusion obtained from the 1D studies that the two organic molecules induce the same phase transition on ZSM-5 and since they have similar geometries the nature of the interaction at least for this form is primarily based on the size and shape of the organic molecules.

An INADEQUATE experiment on ZSM-5 loaded with 8 molecules of *p*-dichlorobenzene per unit cell was carried out, and the results are presented in Figure 75. The structure of this form has not been reported yet, and thus the space group of the high loaded form of *p*-xylene was considered first in order to

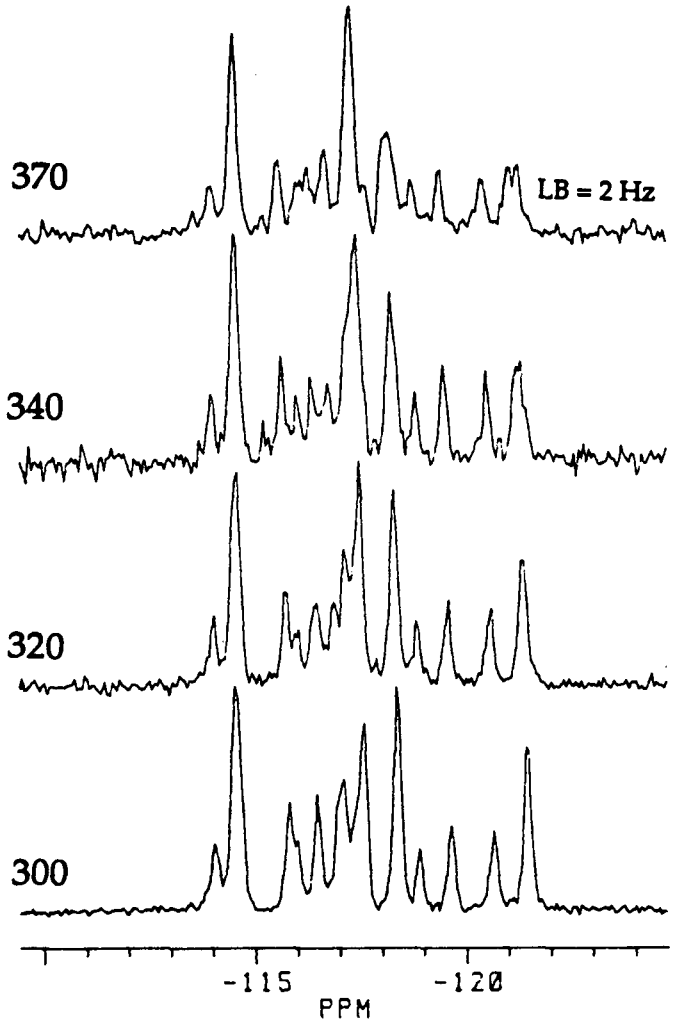

Figure 73 Variable temperature ^{29}Si CP MAS NMR spectra of ZSM-5 loaded with 8 molecules *p*-dichlorobenzene per unit cell. The temperatures in K are indicated.

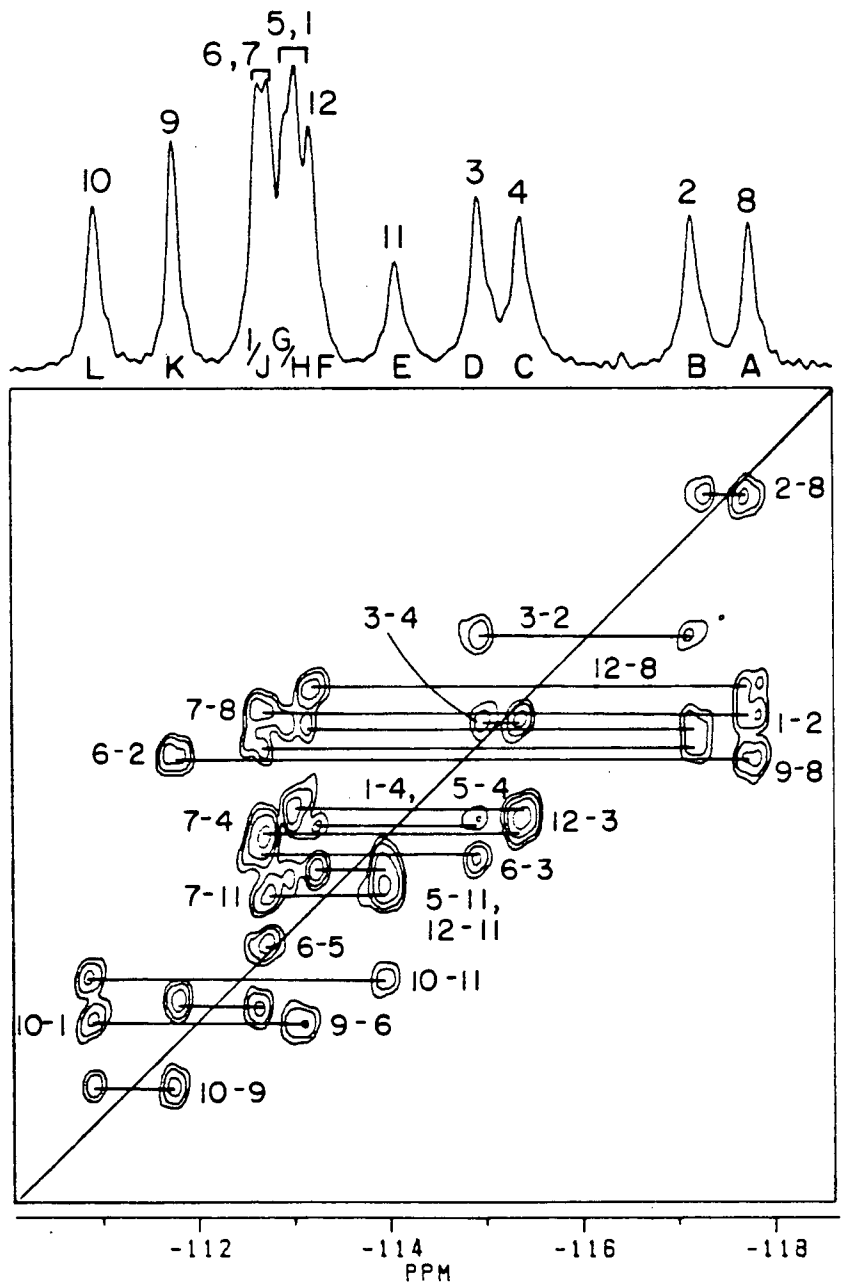

Figure 74 Contour plot of an INADEQUATE experiment on ZSM-5 with 2 molecules of *p*-dichlorobenzene per unit cell at 300 K with a 1D MAS NMR spectrum above. 32 experiments with 192 scans in each experiment were carried out and the total time for the experiment was approximately 20 h. A sweepwidth of 680 Hz, fixed delay of 16 ms. and 140 data points were used before zero filling. Shifted sine-bell apodizations in the F_2 and F_1 dimensions respectively and a power calculation were used for the data processing.

Figure 75 Contour plot of a CP-INADEQUATE experiment on ZSM-5 loaded with 8 molecules of *p*-dichlorobenzene per unit cell at 300 K with a 1D CP MAS NMR spectrum above. 56 experiments with 960 scans in each experiment were carried out. A sweepwidth of 737 Hz, fixed delay of 16 ms. and 100 real data points were used. Shifted sine-bell apodizations in the F_2 and F_1 dimensions respectively and a power calculation were used for the data processing.

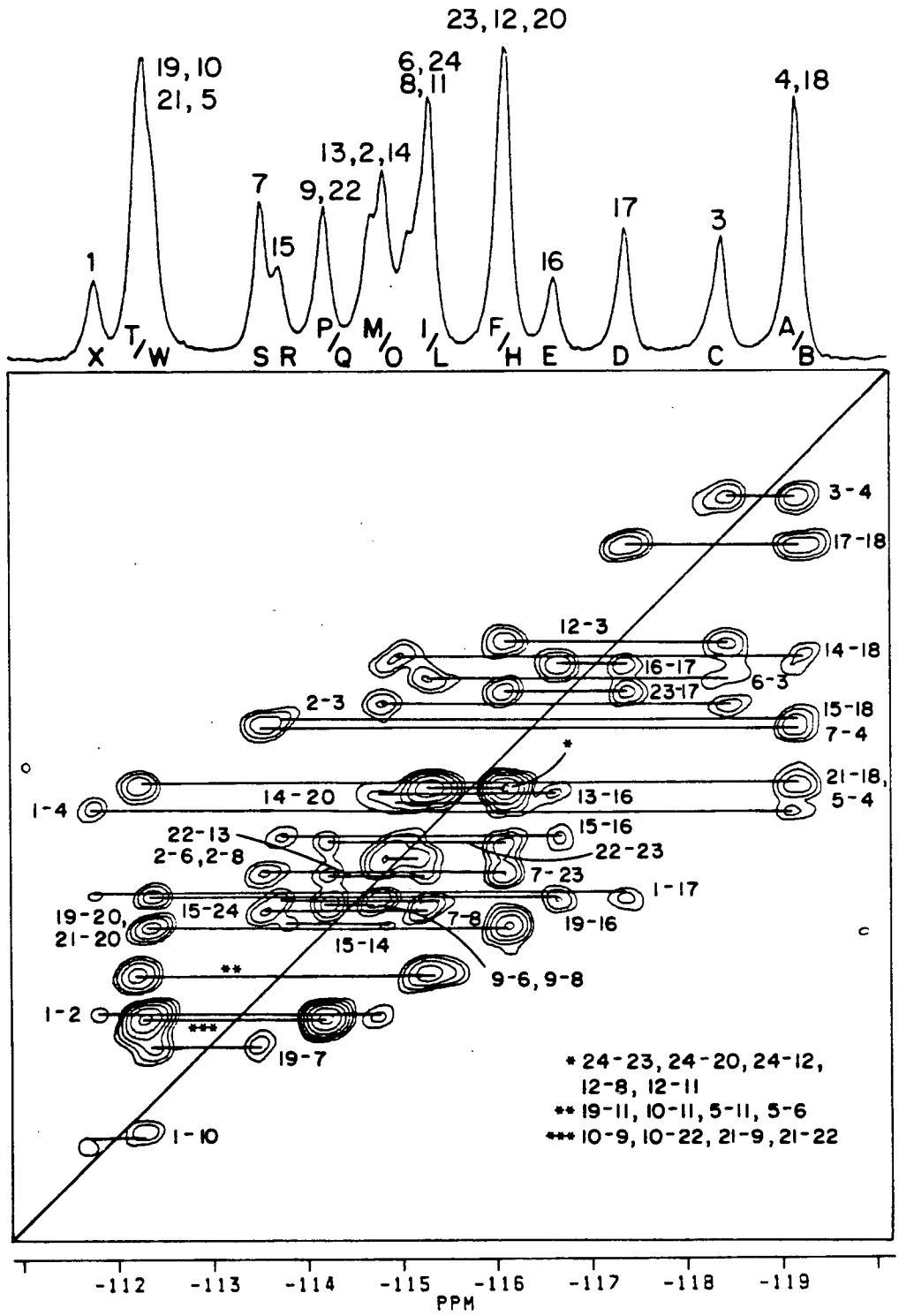
23,12,20
19,10
21,5
6,24
8,11
4,18
13,2,14
7
9,22
17
3
15
1
16
X
T/W
S R
P/Q
M/O
I/L
F/H
E
D
C
A/B
3-4
17-18
12-3
14-18
16-17
6-3
23-17
2-3
15-18
7-4
21-18,
5-4
14-20
13-16
1-4
15-16
22-13
2-6,2-8
22-23
7-23
1-17
19-20,
21-20
15-24
7-8
19-16
15-14
9-6, 9-8
1-2
19-7
1-10
* 24-23, 24-20, 24-12,
12-8, 12-11
** 19-11, 10-11, 5-11, 5-6
*** 10-9, 10-22, 21-9, 21-22
-112
-113
-114
-115
-116
-117
-118
-119
PPM

interpret the 2D NMR data. Based on the fact that the highest field part of the 2D plot is similar to that of the *p*-xylene case, it is possible that the resonances A and B in both cases are due to the same T-sites 18 and 4. The complete assignment can be obtained from this starting point and is shown in the figure. Other possible space groups were examined and were not compatible with the NMR data. Hence the structure of ZSM-5 with a loading of 8 molecules of *p*-dichlorobenzene per u. c. is associated with the orthorhombic space group $P2_12_12_1$. Comparing the results of the two assignments, it is found that the differences in chemical shift corresponding to the same T-site are generally small. Therefore, the major interactions between both *p*-xylene and *p*-dichlorobenzene and the lattice at various loadings again appear to be based on size and shape.

The fact that cross polarization from the ^1H nuclei in the *p*-dichlorobenzene sorbates to the ^{29}Si nuclei is efficient for the high loaded form provides a way to cross-check the proposed orthorhombic structure, $P2_12_12_1$. This is based on the fact that the magnetization transfer originates from the dipolar interaction between ^1H and ^{29}Si, and the efficiency of the CP process is very dependent on the internuclear distance. The XRD data from ZSM-5 with 8 molecules of *p*-xylene per unit cell[124] is used to calculate the positions of the H atoms attached to the benzene rings. Then the distances between ^1H and ^{29}Si can be calculated using the coordinates of silicons in this data set assuming the molecules are reasonably fixed in the positions indicated by XRD study. Table 22 lists all of the Si-H distances less than 4.0 Å., where H_1- H_4 represent the H atoms of the molecules in the channel intersections and H_5- H_8 those of the molecules in the sinusoidal channels (Figure 76).

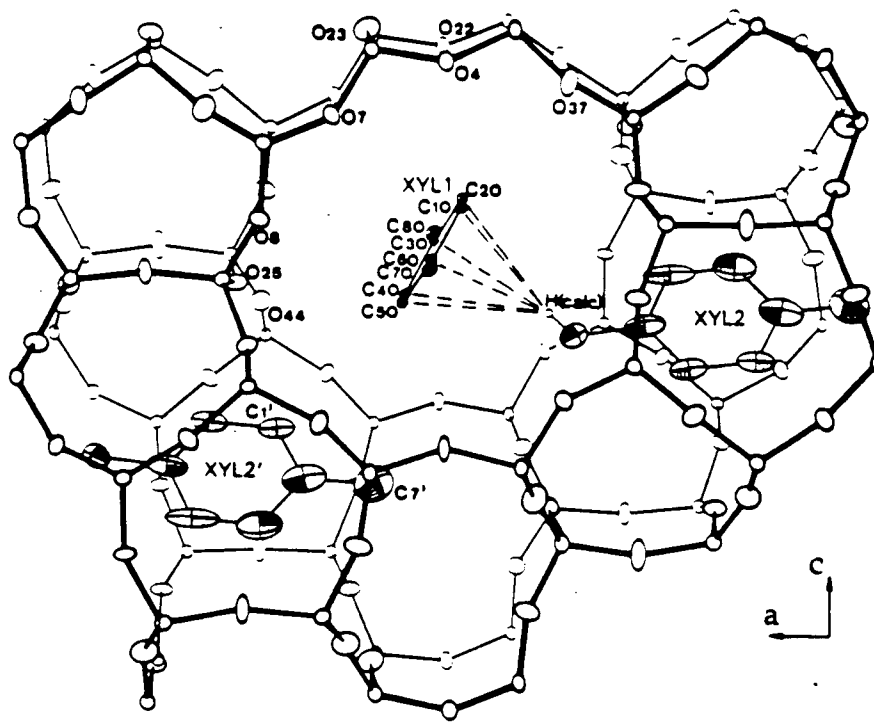

Figure 76 Positions of two independent *p*-xylene molecules in the channels of ZSM-5 in the form with 8 molecules per unit cell: XYL1 is located at the intersection of the straight and the sinusoidal, XYL2 lies in the sinusoidal channel. (ref. 124)

Table 22 Calculated Si- H distances (< 4Å) for ZSM-5 loaded with 8 *p*-xylene per unit cell (from Ref.124)

Si- atom	H- atom	Distance (Å)	Si- H interaction estimated*
T_1	no		W
T_2	H_7	3.8	M
T_3	H_7	3.1	S
	H_8	3.6	
T_4	H_8	3.0	S
T_5	no		W
T_6	H_4	3.9	M
T_7	H_8	3.4	S
	H_1	3.5	
T_8	no		W
T_9	H_4	3.6	M
	H_6	3.7	
T_{10}	no		W
T_{11}	H_2	3.4	S
T_{12}	H_7	3.2	S
	H_2	3.4	
T_{13}	no		W
T_{14}	H_2	3.4	S
T_{15}	no		W
T_{16}	no		W
T_{17}	H_3	3.6	M
	H_5	3.6	
T_{18}	H5	3.2	S
	H6	3.3	
	H3	3.5	
T_{19}	H2	3.6	M
T_{20}	no		W
T_{21}	H6	3.1	S
	H5	3.5	
	H3	3.7	
T_{22}	H6	3.7	M
T_{23}	H1	3.3	S
T_{24}	H1	3.4	S
	H7	3.7	

* dipolar interaction between Si and H, S: strong; M: median; W: weak.

Variable contact time CP NMR experiments on ZSM-5 with a loading of 8 molecules of *p*-dichlorobenzene were carried out to probe similarities in the geometries of the high loaded *p*-xylene form to the corresponding *p*-dichlorobenzene case and the correctness of the assignments. Figure 77 shows the results of the NMR experiments and Figure 78 displays the intensities of some of the T-sites from Figure 77 as functions of the contact time. Resonances A, B, C and S, whose intensities grow faster at beginning are indicated by '*',and are associated to T-sites 18, 4, 3, and 7. They all have stronger dipolar interactions with H as indicated in Table 22, while resonances E, R and X marked by '•' grow much more slowly and correspond to T_1, T_{16} and T_{15}, characterized by 'W'in the table. The good agreement between the NMR results on the 8 molecules of *p*-dichlorobenzene /ZSM-5 and the XRD data of the corresponding *p*-xylene/ZSM-5 system confirms that: i) The proposed orthorhombic structure of symmetry $P2_12_12_1$ for the high loaded form of *p*-dichlorobenzene/ZSM-5 is correct, ii) The positions of the organic molecules in the channels of ZSM-5 in both cases are very similar, i.e. one is in the channel intersections and the other in the sinusoidal channels.

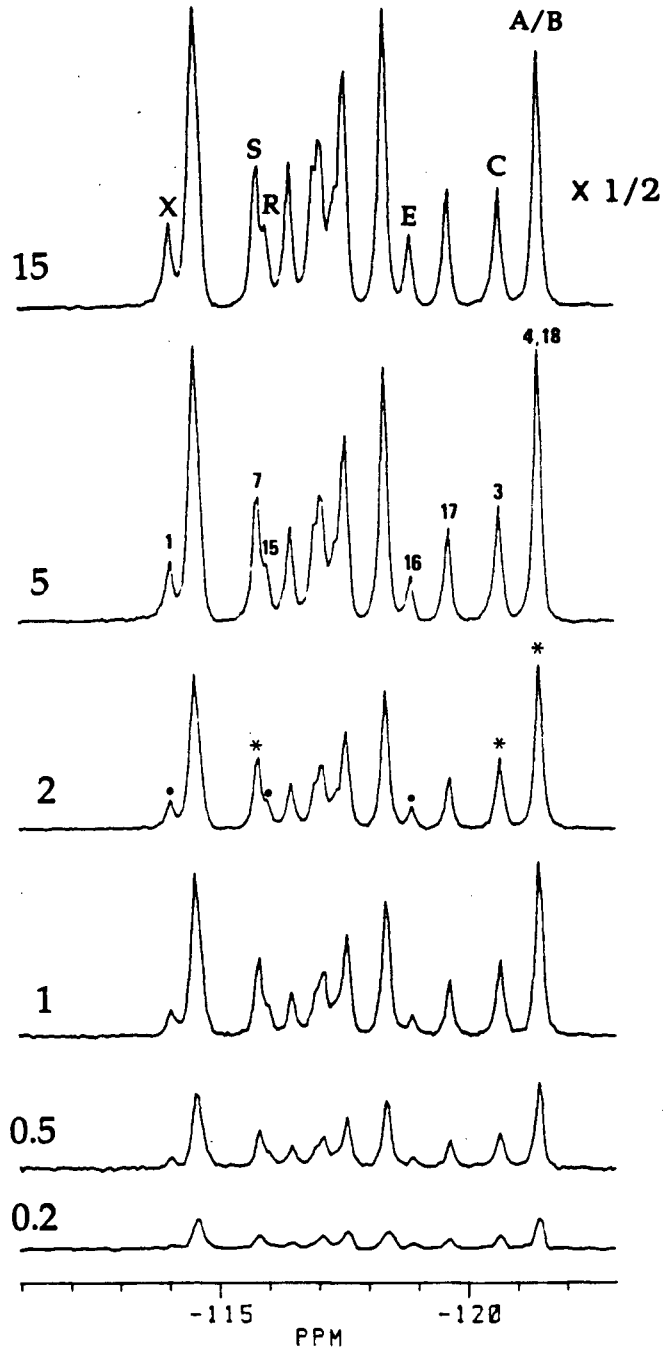

Figure 77 Variable contact time ^{29}Si CP MAS NMR spectra of ZSM-5 loaded with 8 molecules of *p*-dichlorobenzene per unit cell obtained with the contact times in ms indicated.

Figure 78 The intensities of some T-sites in the high *p*-dichlorobenzene loaded form of ZSM-5 as a function of the contact time.

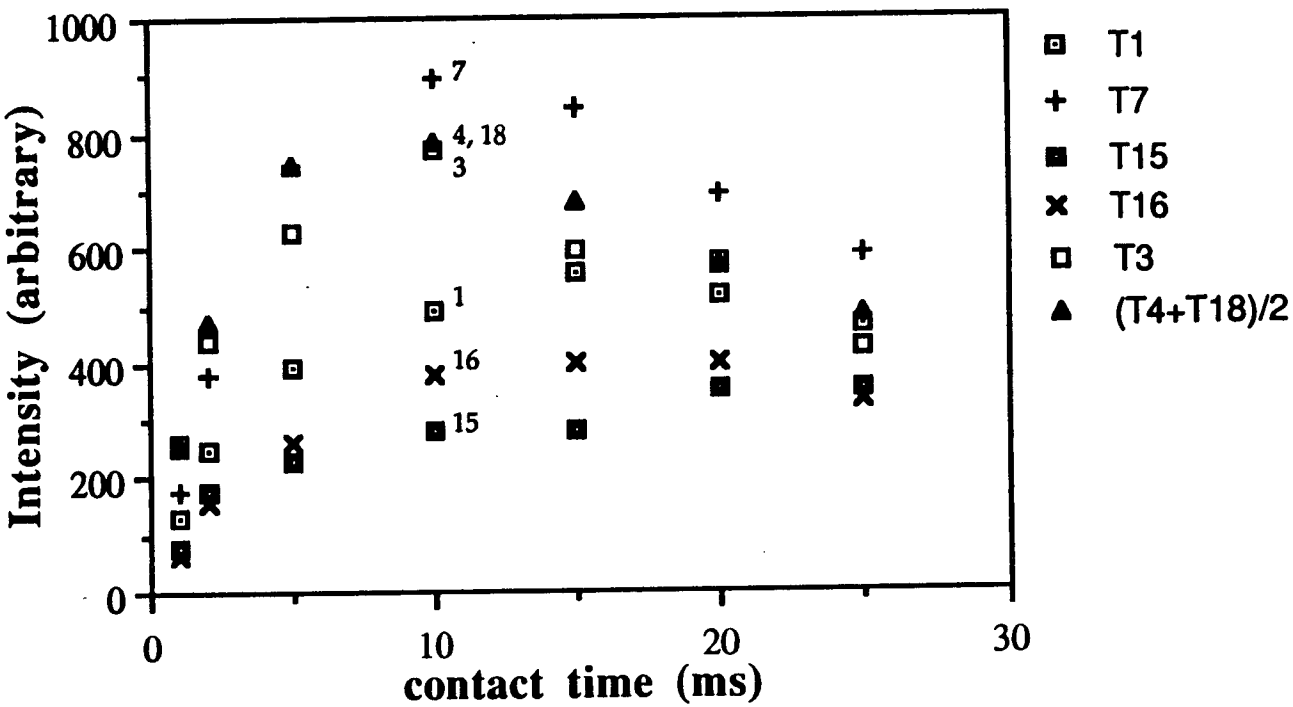
1000
800
600
400
200
0
Intensity (arbitrary)
0
10
20
30
contact time (ms)
7
4, 18
3
1
16
15
T1
T7
T15
T16
T3
(T4+T18)/2

E. CORRELATIONS BETWEEN ^{29}SI MAS NMR CHEMICAL SHIFTS AND X-RAY DIFFRACTION DATA FOR HIGHLY SILICEOUS ZEOLITES

I. INTRODUCTION

As has been shown earlier, high resolution ^{29}Si solid state MAS NMR spectroscopy has developed as an important complementary technique to diffraction studies for structural investigations of zeolites since the ^{29}Si NMR chemical shift is a very sensitive probe of the local structure surrounding the silicon nuclei. In order to interpret the ^{29}Si chemical shifts observed in structural studies more quantitatively, various linear correlations based on bond length [139,140], bridging bond angle [141,142], bond strength [143], mean TOT distance [144], group electronegativity [145], and s-orbital hybridization[146] have been previously presented. These relationships are of particular interest for highly siliceous zeolites, where all T-sites experience the same Si[0Al] chemical environment. The numbers and relative intensities of the resonances in these spectra provide direct information on the number of crystallographically inequivalent silicons, and their chemical shifts are sensitive to subtle changes in the local framework structures. The geometric parameters from X-ray diffraction data used for interpreting the ^{29}Si MAS NMR spectra of highly siliceous zeolites are: 1) the mean Si-O-Si bond angle, α, in different forms, e.g. α[142]; sin $\alpha/2$[144]; cos α /(cos α -1)[146,147], 2) the mean Si-Si distance[117], 3) the mean Si-O bond length[141]. The mean Si-O bond length in highly siliceous zeolites varies very little, from 1.592Å to 1.604Å with estimated standard deviations (ESD) of 0.005Å for the 24 T-sites in ZSM-5 with 8 *p*-xylene molecules per

u.c.[124]. Thus it is not sensitive enough for correlation studies. The cos α /(cos α -1) function is the most accepted parameter in the case of Si-O-Si angular dependence[146]. Correlations using mean Si-Si distances include the effects of both bond length and bond angle. In the study of structures with multiple T-sites, the matching of a NMR resonance in a 1D spectrum with a particular silicon atom in the crystal structure is ambiguous for structures with more than one T-site unless the resonance peak intensities and corresponding population parameters can be related uniquely because these correlations are basically empirical.

As can be seen in previous discussions, 2D correlation NMR experiments of highly siliceous zeolites provide unambiguous assignments of the resonances of NMR spectra to the corresponding T-sites directly if the assignment is unique and by combination with XRD data when two equivalent assignments are possible from the NMR data. Using the peak assignments which have been obtained from the 2D experiments discussed earlier, the reliability of various geometric correlations will be examined and discussed in more detail in this section. Four linear correlations will be considered, as presented in Equations 29- 32.

$$\delta = a\,[\text{mean (Si- Si)}] + b \qquad [29]$$

$$\delta = a\,(\text{mean } \alpha) + b \qquad [30]$$

$$\delta = a\,[\cos \bar{\alpha} / (\cos \bar{\alpha} - 1)] + b \qquad [31]$$

$$\delta = a\,\{\text{mean } [\cos \alpha / (\cos \alpha - 1)]\} + b \qquad [32]$$

where δ is the ^{29}Si isotropic chemical shift measured in ppm. with respect to TMS taking Q_8M_8 as a secondary reference (see page 68), the Si- Si distance is the

separation between the target ^{29}Si nucleus and its first neighbor Si atom, measured in Å and α is Si-O-Si angle. The measurement error in δ in the present study is estimated to be ±0.05 ppm for resolved peaks and ±0.15 ppm for overlapping peaks.

II. DISCUSSION

A synchrotron powder XRD refinement data set of ZSM-12[47] is taken as a first example for the correlation study as it represents the highest quality of powder data available, being derived from both a sample of the highest possible crystallinity and by using a synchrotron X-ray source. Figures 79A and B are the plots of chemical shift vs the mean T-T distance and the mean cos α /(cos α -1) respectively and the lines of regression are drawn as dashed lines for reasons which will be discussed below. As can be seen from the figures, the data points correlate but not very well. In general, this is because the estimated standard deviations (ESD) in the powder diffraction data are quite substantial, as indicated in the figure. The information which can be drawn from these figures is only semi-quantitative; that is, it is possible to divide the T-sites into two groups, one is T_5 T_7, T_2 and T_1 whose corresponding resonances should be at higher field and the second group T_4, T_3 and T_6 which should occur at lower field.

Single crystal X-ray diffraction studies of zeolites provide much more accurate and detailed structure information. As mentioned earlier, only a very few synthetic zeolites have been studied to date by these techniques due to the difficulty of growing large enough single crystals. A single crystal XRD refinement on a small crystal (45X 100X 225 μm) of ZSM-22 was reported[16] and taken for this study. Figures 80A and B present the NMR and XRD correlation

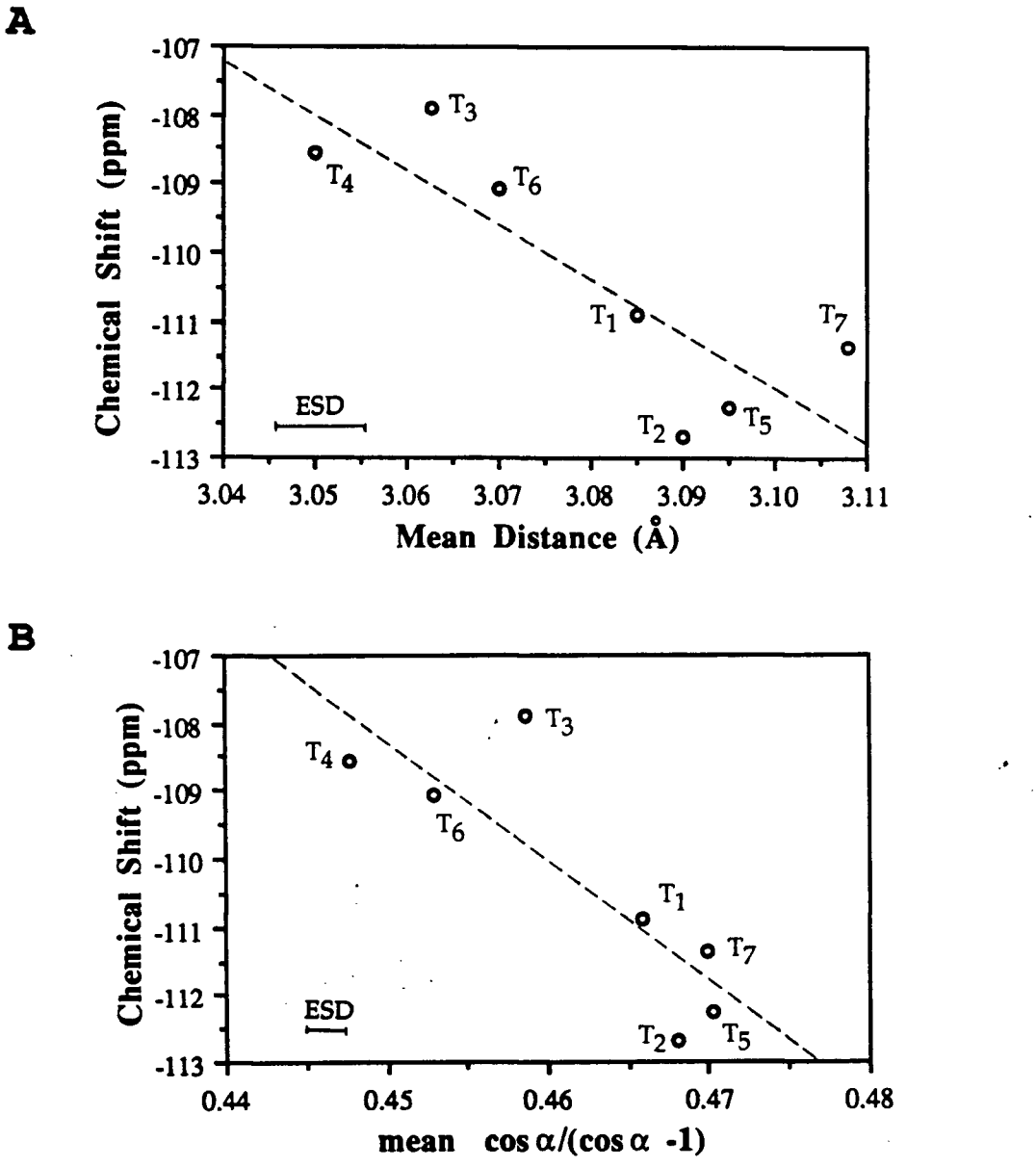

Figure 79 NMR and XRD correlation diagrams of zeolite ZSM-12:
(A) plot of chemical shift vs. the mean T-T distance;
(B) plot of chemical shift vs. the mean cosα/(cosα-1).
The estimated standard deviations in the geometric parameters are indicated by the horizontal lines.

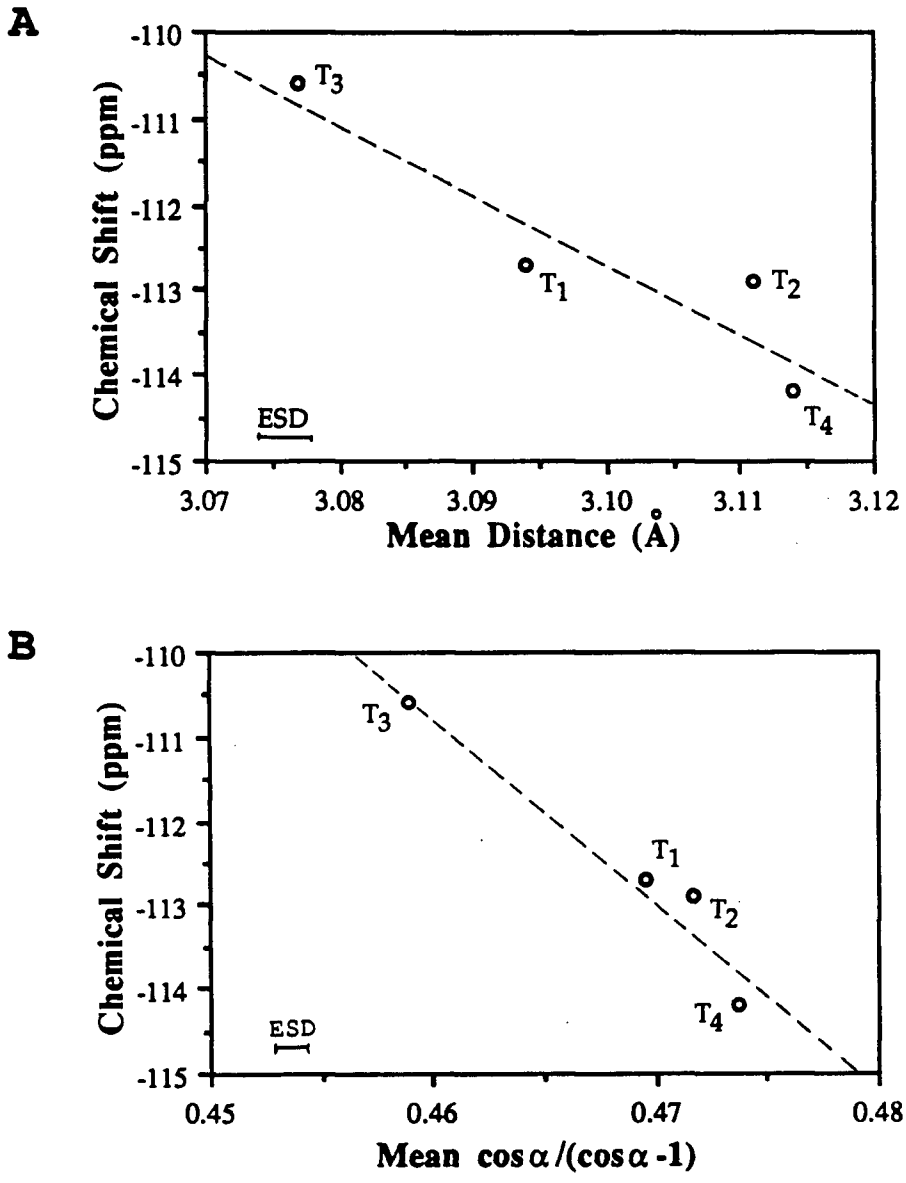

Figure 80 NMR and XRD correlation diagrams of zeolite ZSM-22:
(A). plot of chemical shift vs. the mean T-T distance;
(B). plot of chemical shift vs. the mean cosα/(cosα-1).
The estimated standard deviations in the geometric parameters are indicated by the horizontal lines.

diagrams between the ^{29}Si chemical shifts and the mean Si- Si distances and the mean cos α /(cos α -1) respectively for ZSM-22. Both show the correct trends, i.e. the T-sites with longer Si- Si distances or larger Si-O-Si angles correspond to the resonances at higher field. The linear relationships between the NMR and XRD data are much better than those from powder XRD data of ZSM-12, and can be used with some confidence to choose the correct assignment from two equally valid possibilities obtained from 2D NMR studies, as was done in Chapter Four.

Several highly accurate single crystal refinements of various forms of zeolite ZSM-5 are available,[104,123,124] where the ESDs in the Si- O- Si bond angles are approximately 0.3° and the ESDs in the Si-O bond lengths are ~0.004 Å. This is the highest quality data available to date for zeolite structures. Figures 81 and 82 show the correlation diagrams between the chemical shifts and the XRD derived parameters for the ZSM-5 room-temperature structure as indicated in the figure captions, and the bold lines in the figures are the results of the linear regression analysis. The results for the high temperature form of ZSM-5 and the high loaded form of *p*-xylene/ZSM-5 as well as the room temperature one are summarized in Table 23. In general, the four functions describe the variation of δ Si[4Si] for ZSM-5 in the RT and HT forms quite well, as reflected in the high linear correlation coefficients. However, for the high loaded sample the mean distance function shows a better linear trend. When the three data sets are presented together (Figure 83), only the mean distance function shows a good correlation. This function was used to discriminate between the two possible assignments valid for the NMR data of ZSM- 5 in various cases, as described in Section C. It is also possible using mean Si- Si distances to assign some

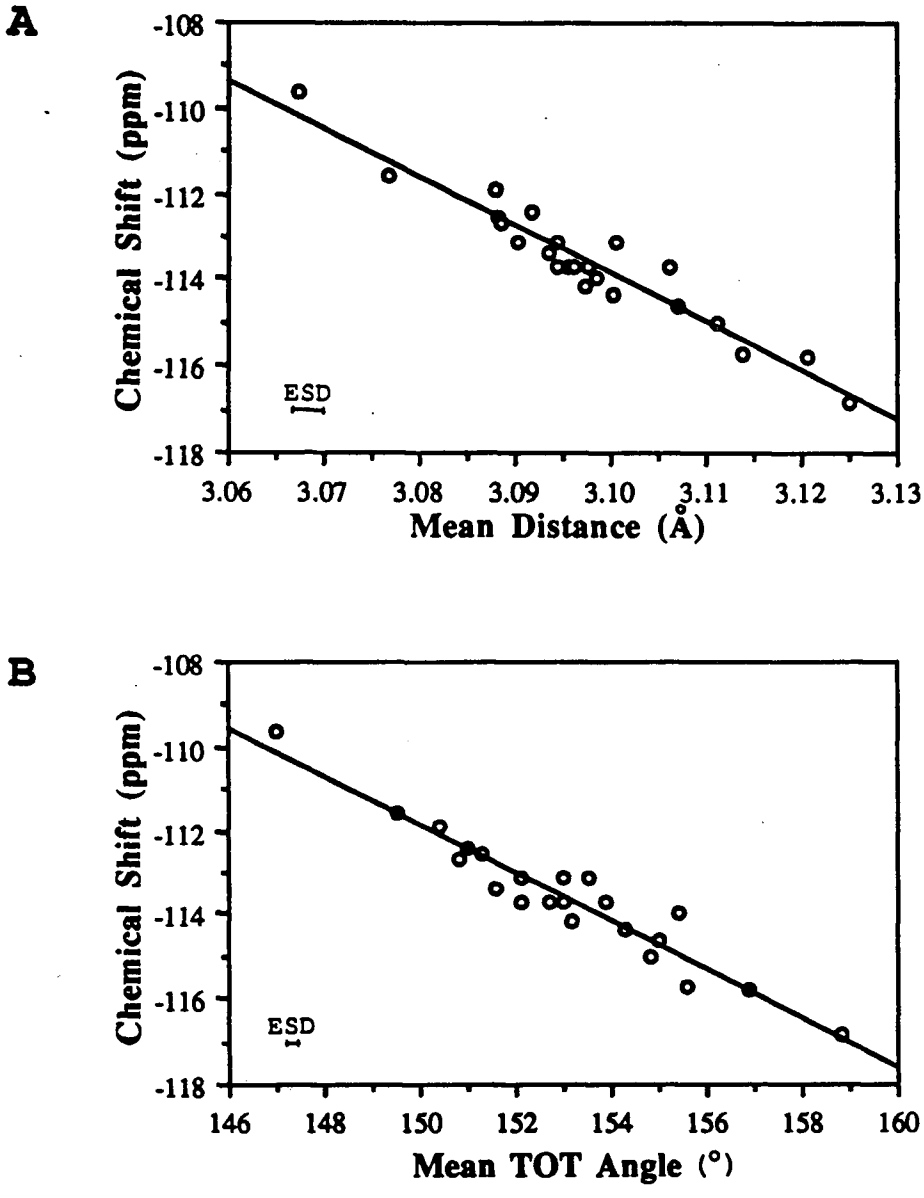

Figure 81 NMR and XRD correlation diagrams of zeolite ZSM-5 at room temperature:
(A) plot of chemical shift vs. the mean Si-Si distance;
(B) plot of chemical shift vs. the mean Si-O-Si angle.
The estimated standard deviations in the geometric parameters are indicated by the horizontal lines.

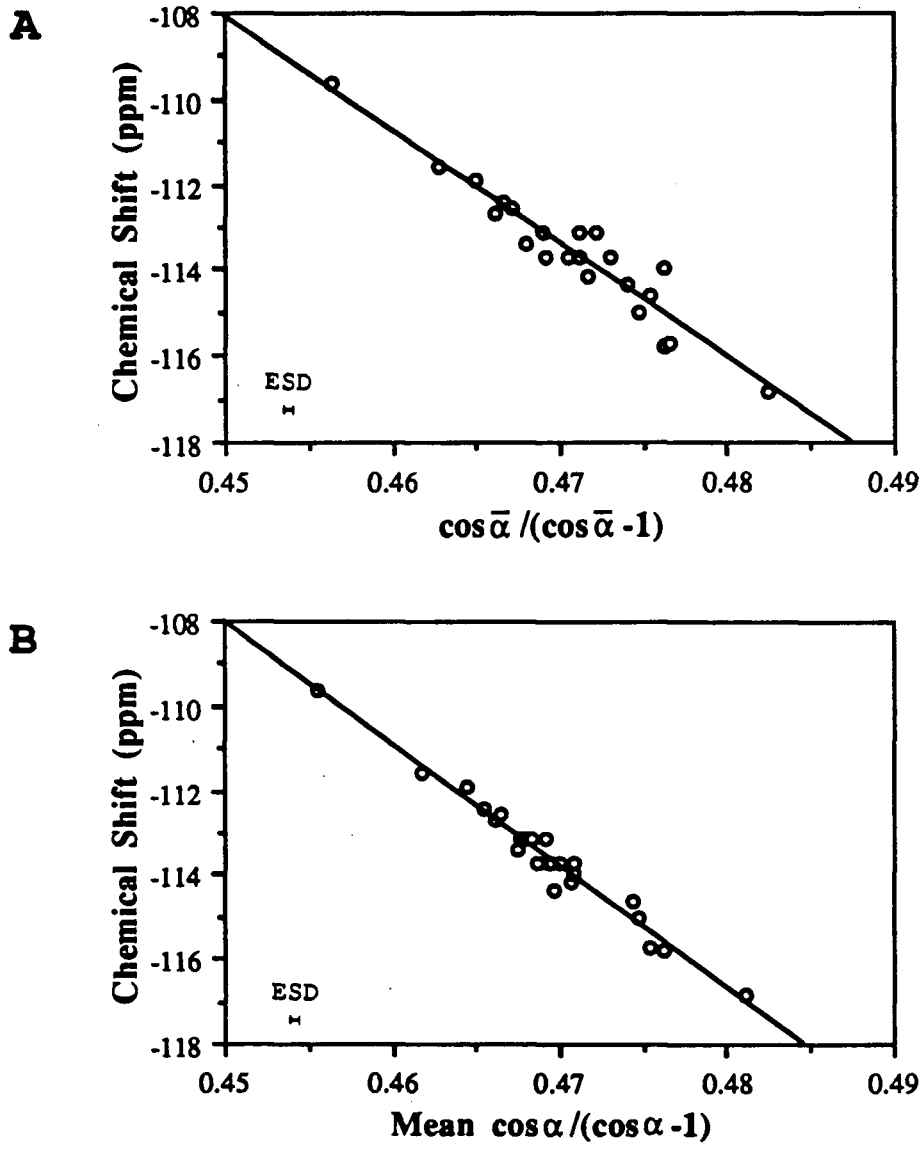

Figure 82 NMR and XRD correlation diagrams of zeolite ZSM-5 at room temperature:
(A) plot of chemical shift vs. cosᾱ/(cos ᾱ-1),
(B) plot of chemical shift vs. the mean cosα/(cosα-1).
The estimated standard deviations in the geometric parameters are indicated by the horizontal lines.

Table 23 Linear Regression Analysis of Chemical Shift Against Various Geometric Parameters for the Different forms of ZSM-5

X	Sample ZSM-5 (RT)	Sample ZSM-5 (HT)	Sample ZSM-5 (*p*-xylene)
$\overline{\text{Si-Si}}$	δ= 234.6-112.4X r*= 0.918	δ= 242.6-115.2X r= 0.952	δ= 243.3-115.4X r= 0.920
$\overline{\alpha}$	δ= -25.73-0.5739X r= 0.917	δ= -52.68-0.3932X r= 0.949	δ= -26.05-0.5755X r= 0.872
$\cos\overline{\alpha}$ /($\cos\overline{\alpha}$-1)	δ= 11.51-265.6X r= 0.909	δ= -12.45-213.0X r= 0.961	δ= 18.26-281.2X r= 0.853
$\overline{\cos\alpha}$ /($\cos\alpha$-1)	δ= 21.44-287.6X r= 0.969	δ= 6.583-254.4X r= 0.968	δ= 19.19-285.0X r= 0.876

* r stants for correlation coefficient

resonances in the highest and/or lowest fields if they are well separated. However, it is still very difficult to predict the chemical shifts of the T-sites from XRD data in multiple T-sites cases, such as ZSM-5, and vice versa. The reasons may be: a) The conditions including temperature and loading between XRD and NMR experiments might not be exactly the same. b) In the case of the high loaded form, the local environments of Si nuclei may depend not only upon the geometry, but also be affected by the presence of *p*-xylene molecules in the channels. Therefore errors are introduced, which can affect the accuracy of the correlation. Nevertheless, these correlations between ^{29}Si NMR chemical shifts and XRD data from 2D NMR and single crystal XRD studies are the most reliable ones to date for multiple T-sites zeolites and will be of use in future studies.

The accuracy of XRD data can substantially affect the precision of the correlation as shown above in three different kinds of data sets, i.e. ZSM-12, ZSM-22 and ZSM-5. Collecting all reliable XRD and NMR data sets as well as the data discussed above, general correlation maps can be obtained and are shown in Figures 84A and B. Both the mean Si-Si distances and mean $\cos \alpha / (\cos \alpha - 1)$ show a linear relationship and their correlation coefficients are approximataely 0.84. Better XRD and NMR data measured under the same conditions will be required in order to get more reliable correlations for the investigation of zeolite structures.

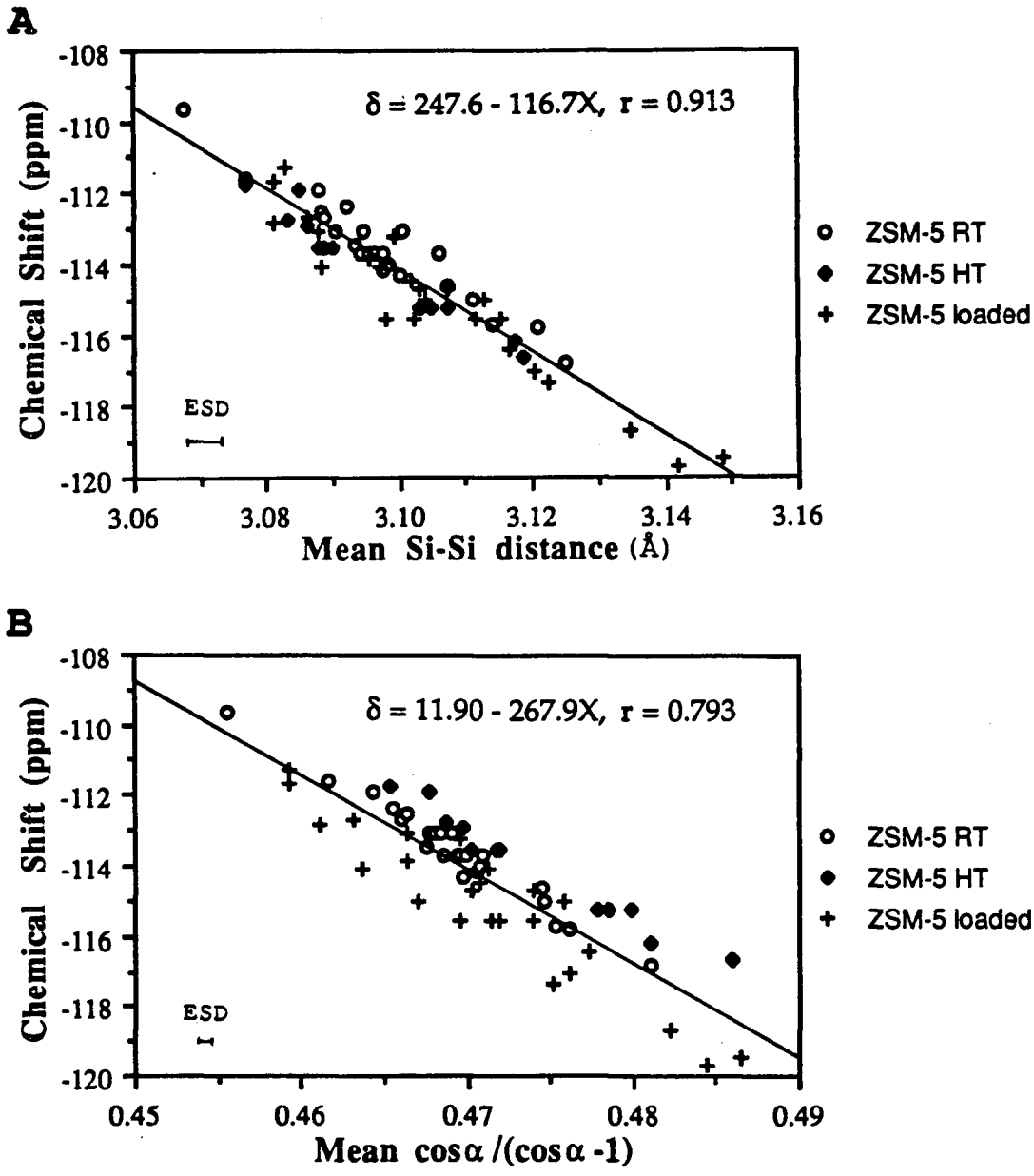

Figure 83 NMR and XRD correlation diagrams of zeolite ZSM-5 in the three cases:
(A) plot of chemical shift vs. the mean distance,
(B) plot of chemical shift vs. the mean cosα/(cosα-1).
The estimated standard deviations in the geometric parameters are indicated by the horizontal lines.

Figure 84 NMR and XRD correlation diagrams for all avaiable data sets:
A) plot of chemical shift vs. the mean distance,
B) plot of chemical shift vs. the mean $\cos\alpha/(\cos\alpha-1)$.

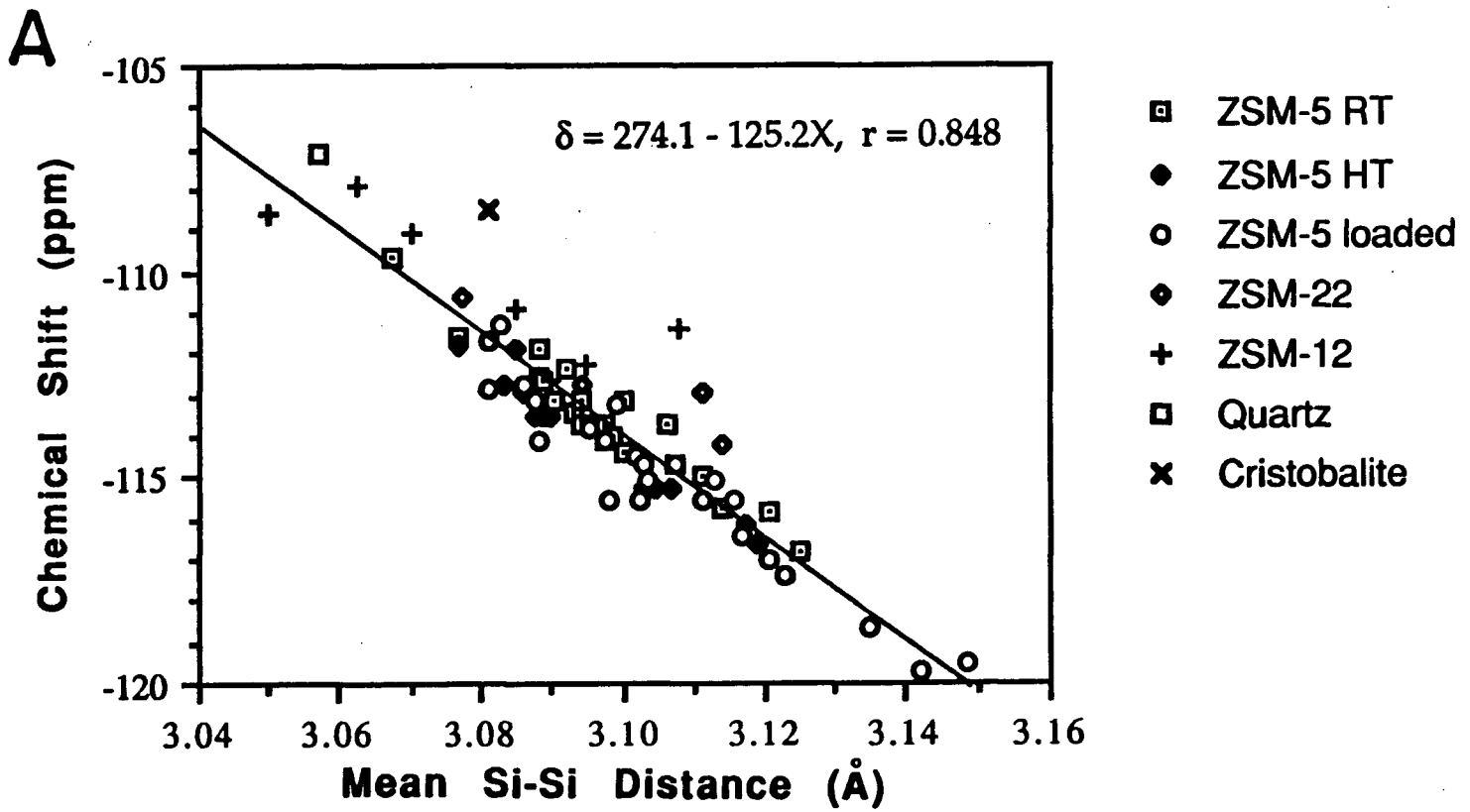
A
-105
-110
-115
-120
Chemical Shift (ppm)
δ = 274.1 - 125.2X, r = 0.848
3.04
3.06
3.08
3.10
3.12
3.14
3.16
Mean Si-Si Distance (Å)
ZSM-5 RT
ZSM-5 HT
ZSM-5 loaded
ZSM-22
ZSM-12
Quartz
Cristobalite

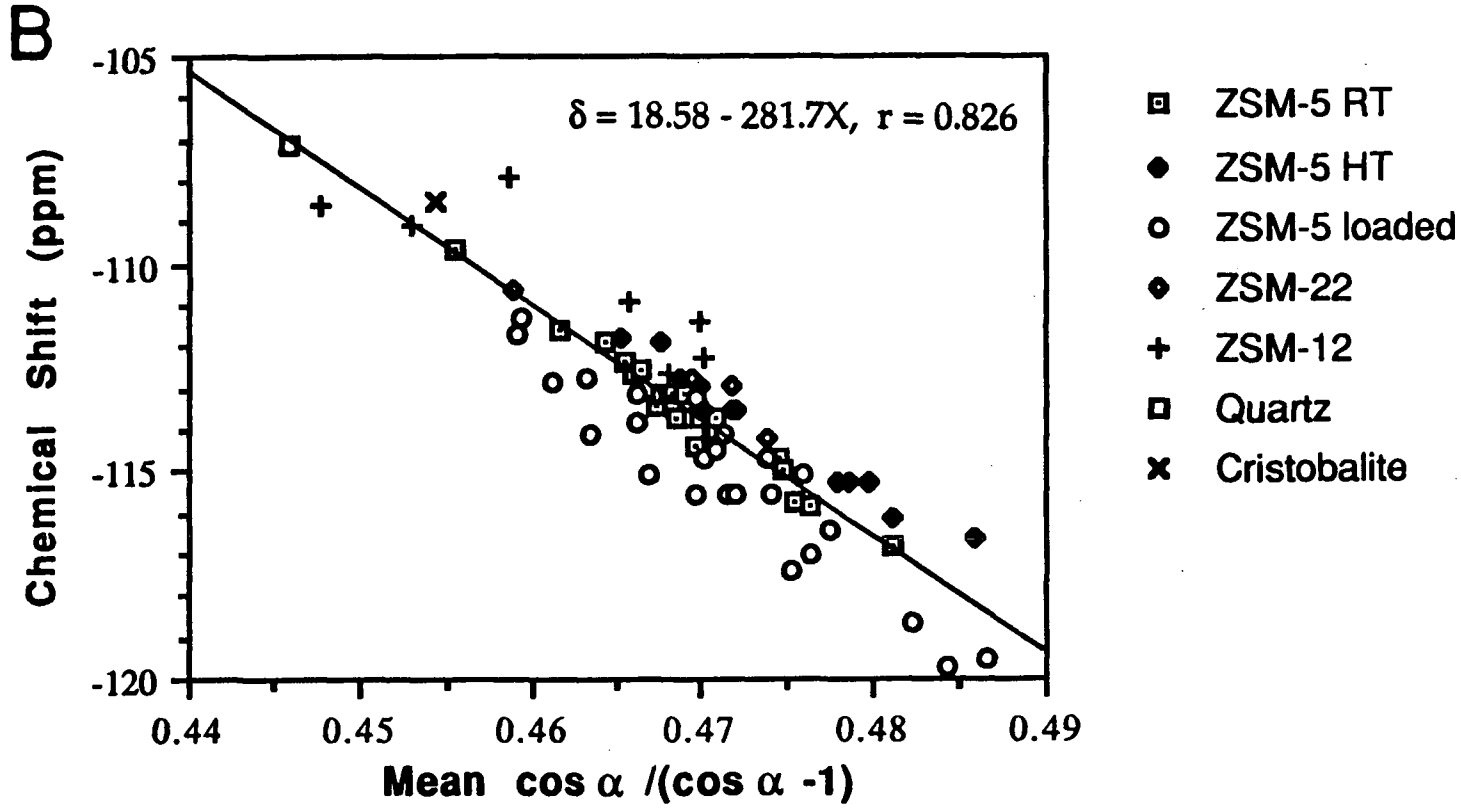
B
δ = 18.58 - 281.7X, r = 0.826
Chemical Shift (ppm)
-105
-110
-115
-120
0.44
0.45
0.46
0.47
0.48
0.49
Mean cos α /(cos α -1)
ZSM-5 RT
ZSM-5 HT
ZSM-5 loaded
ZSM-22
ZSM-12
Quartz
Cristobalite

CHAPTER SIX

APPLICATION OF TWO-DIMENSIONAL ^{29}Si MAS NMR TECHNIQUES TO THE STRUCTURAL INVESTIGATION OF LESS WELL CHARACTERIZED ZEOLITES

A. NATURAL-ABUNDANCE TWO-DIMENSIONAL ^{29}SI MAS NMR INVESTIGATION OF THE THREE-DIMENSIONAL BONDING CONNECTIVITIES OF THE HIGH AND LOW TEMPERATURE FORMS OF ZEOLITE ZSM-11

I. INTRODUCTION

ZSM-11 is one end member of a family of pentasil zeolites, of which ZSM-5 is the other member as discussed in Chapter Five. They are both shape-selective catalysts [149-151]. In the ZSM-11 structure, the pentasil layers are joined such that neighboring layers are related by a reflection plane, as shown in Figure 85-A, while in ZSM-5 they are related by an inversion centre. The ZSM-11 framework contains two straight intersecting channel systems with ten-membered ring openings with free diameters of 5.1 X 5.4 Å (Figure 85-B). Intergrowths between ZSM-11 and ZSM-5 are common and ZSM-5 may easily be obtained in pure form, but it is very difficult to synthesize ZSM-11 samples which are free both of intergrowths of ZSM-5 and of amorphous materials. For this reason, in comparison with ZSM-5, considerably less work has been done on ZSM-11, and the quality of the structural data available is limited.

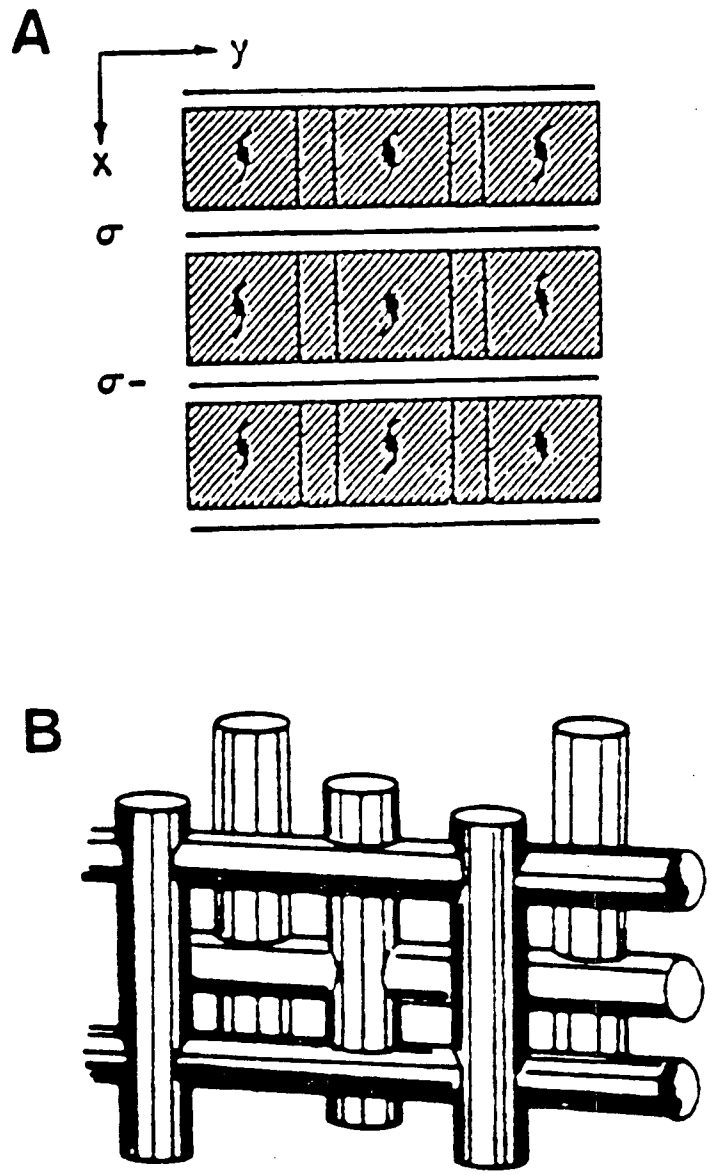

Figure 85 (A) Stacking sequence of layers in zeolite ZSM-11 (layers shaded). (B) The channel systems in ZSM-11. (ref. 152)

The structure of zeolite ZSM-11 originally proposed by Kokotailo and co-workers[152] was based on powder XRD studies and model building, and has a tetrahedral space group $I\bar{4}m2$. This tetrahedral symmetry implies that there are seven crystallographically inequivalent sites with relative occupancies of 1: 1: 2: 2: 2: 2: 2. A schematic representation of the structure is shown in Figure 86 with the T-sites in the asymmetric unit indicated by filled circles. An early ^{29}Si MAS NMR spectrum of zeolite ZSM-11 was presented by Nagy and co-workers[153], but the resolution was insufficient to resolve any crystallographically inequivalent silicons. Detailed studies of the zeolite ZSM-11 structure have recently been presented by Fyfe and co-workers [154,155] using a combination of solid state NMR and synchrotron X-ray diffraction techniques. This work demonstrated that the lattice structure of ZSM-11 is temperature dependent, changing from a tetrahedral form of space group $I\bar{4}m2$ to a lower symmetry form below ambient temperature. The higher symmetry form can be also induced by adsorption of some organic molecules, for example, *n*-octane, as is the case for ZSM-5 which was previously discussed in Chapter Five. Rietveld refinement of synchrotron powder x-ray diffraction data collected at 373 K proceeded smoothly in space group $I\bar{4}m2$ with 7 crystallographically inequivalent T-sites. However, the room temperature XRD data could not be smoothly refined to match the 1D NMR data which suggested 12 T-sites in the asymmetric unit, and the ZSM-11 structure at lower temperatures remains ill-defined at present.

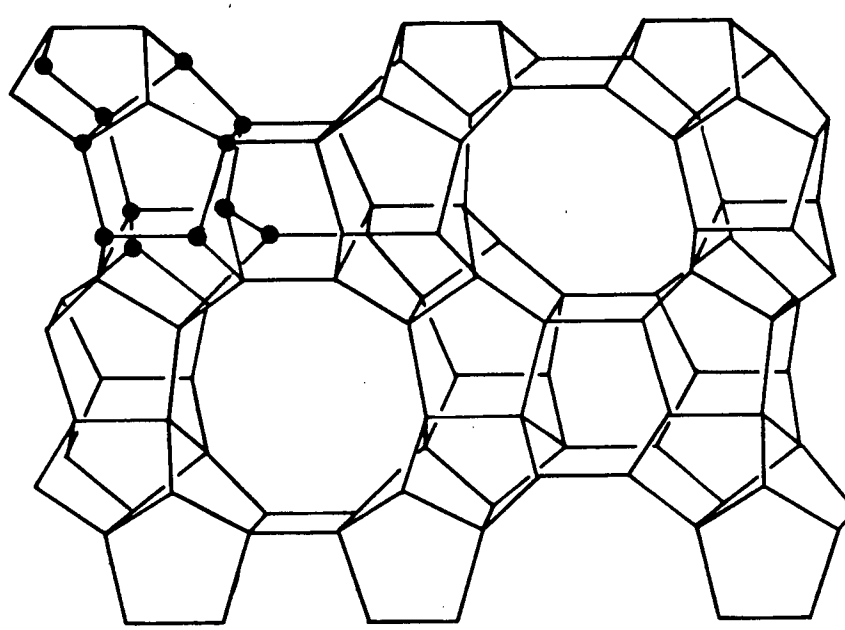

Figure 86 Schematic representation of zeolite ZSM-11 lattice framework with the T-sites in the asymmetric unit indicated by the filled circles. (ref. 152)

As demonstrated in the previous chapters, ^{29}Si 2D MAS NMR connectivity experiments have been successfully applied to investigate the three dimensional bonding in ^{29}Si enriched and natural abundance zeolites, most of whose structures are well defined. In this section, 2D ^{29}Si MAS NMR techniques are applied to the case of zeolite ZSM-11 in both its high and low temperature forms where the structures are less well-known.

II. EXPERIMENTAL

Highly siliceous zeolite ZSM-11 was synthesized hydrothermally based on a modification of the method reported by Chu[156]. The templates used were benzyltrimethyl ammonium hydroxide and tetrabutylammonium bromide. The calcined material was ion-exchanged with ammonium fluoride and then dealuminated by passing water vapor over the sample at 750°C for three days. After the exchange and dealumination procedures were carried out twice, the sample was treated with 0.6 N sodium hydroxide solution at 80°C for approximately five minutes to remove poorly crystalline materials, then filtered and activated at 500°C for 2 hours.

The 1D and 2D ^{29}Si MAS NMR spectra were obtained at 79.5 MHZ using a Bruker MSL-400 spectrometer as described previously. The *n*-octane loaded sample was prepared by adding 14 mg of n-octane to 250 mg of ZSM-11. The sample was sealed and then kept in an oven at 100°C for 2 hours in order to reach an equilibrium distribution of the sorbate within the host zeolite.

III. RESULTS AND DISCUSSION

a) 1D experiments on zeolite ZSM-11

i) Effect of sodium hydroxide treatment on ZSM-11

The effect of sodium hydroxide treatment on the resolution of the ^{29}Si NMR spectra is shown in Figure 87. Close examination of Figure 87A indicated that the sample consisted of two parts: One was highly crystalline ZSM-11, as represented by the sharp lines in the spectrum, and the other consisted of some less crystalline or highly disordered materials, which formed the broad base in the lower part of the spectrum. After sodium hydroxide treatment, the resolution is substantially improved (Figure 87B). The effectiveness of the base treatment may result from differences in the solubilities in alkaline solution between the highly crystalline ZSM-11 and less crystalline or amorphous materials[157]. The latter may be easier to dissolve, resulting in a more highly crystalline ZSM-11 sample after filtration. Some Si-O-Si defects and hydroxyl groups could be formed during the treatment, which could affect the resolution in the NMR spectra and the thermal treatment at 500°C "heals" these crystal lattice defects, leaving a highly siliceous and crystalline sample, whose spectrum is superior to those previously published.

ii) Variable-temperature NMR experiments

^{29}Si variable-temperature MAS NMR spectra have been previously published by Fyfe and co-workers[155] and 8 resonances could be resolved in the temperature range of 268-373 K, but the resolution was insufficient to indicate the exact temperature range of the phase transition or to determine the best temperature at which to investigate the low temperature structure.

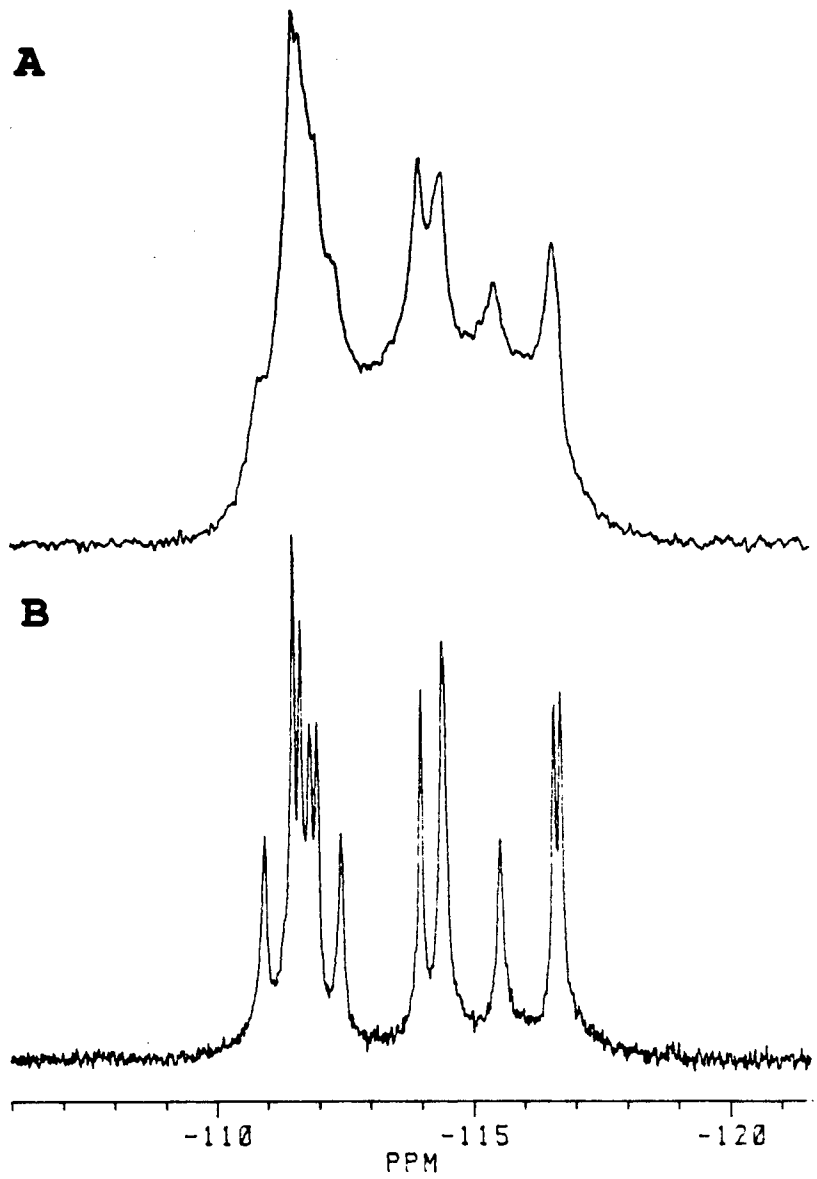

Figure 87 (A) ^{29}Si MAS NMR spectrum of zeolite ZSM-11 before sodium hydroxide treatment.
(B) ^{29}Si MAS NMR spectrum of zeolite ZSM-11 after sodium hydroxide treatment.

Two variable-temperature ^{29}Si MAS NMR experiments were carried out separately in the temperature ranges of 273-318 K and 298-342 K in order to determine the optimum temperatures for the investigation of the three dimensional bonding connectivities of the high and low temperature forms of ZSM-11. The results are shown in Figures 88 and 89 respectively, and clearly indicate the existence of two distinct phases. The very high resolution of the spectra confirms the highly siliceous and ordered nature of the sample and makes it possible to establish a relationship between the resonances of the two phases.

When the temperature is below 316 K, 11 or 12 resonances are clearly resolved in the spectra. There are only gradual shifts of some of the resonances, which probably reflect the general thermal expansion of the lattice and the corresponding changes induced in the local geometries of some of the silicons. The temperature for the best resolved spectrum is approximately 302 K, so this temperature was selected for the lower temperature 2D experiments. Between 316-329 K the resonances are broadened, reflecting some distortion of the lattice in the region of the phase change. The phase transition itself occurs between 320-327 K. It is clear from Figure 89 that another phase forms with seven well resolved resonances when the temperature exceeds 334 K and 342 K was chosen as an appropriate temperature to investigate this high temperature structure. Figure 90 shows the ^{29}Si MAS NMR spectrum obtained at 302 K together with its deconvolution in terms of Lorentzian curves. The linewidths are approximately 11 Hz without any resolution enhancement. Figure 91 shows a ^{29}Si NMR spectrum of ZSM-11 at 342 K, together with its deconvolution. The numbers above the curves indicate the relative peak intensities.

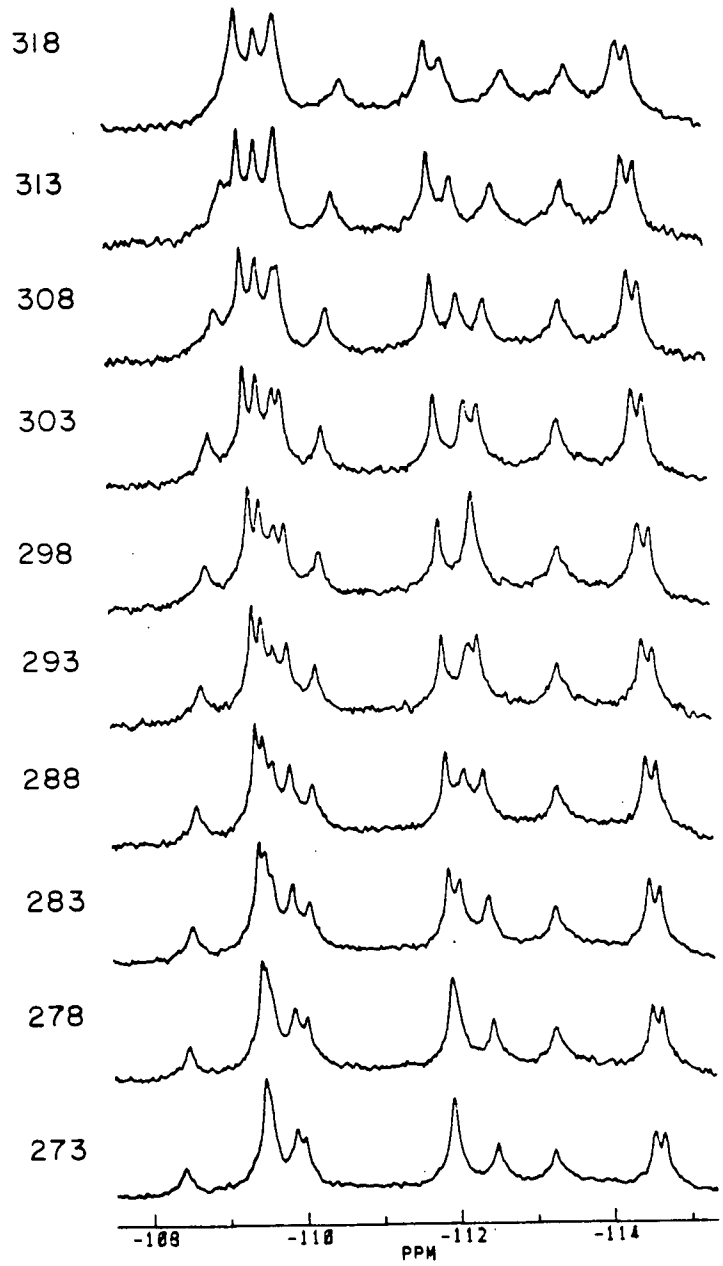

Figure 88 Variable temperature ^{29}Si MAS NMR experiments (273- 318 K) on ZSM-11.

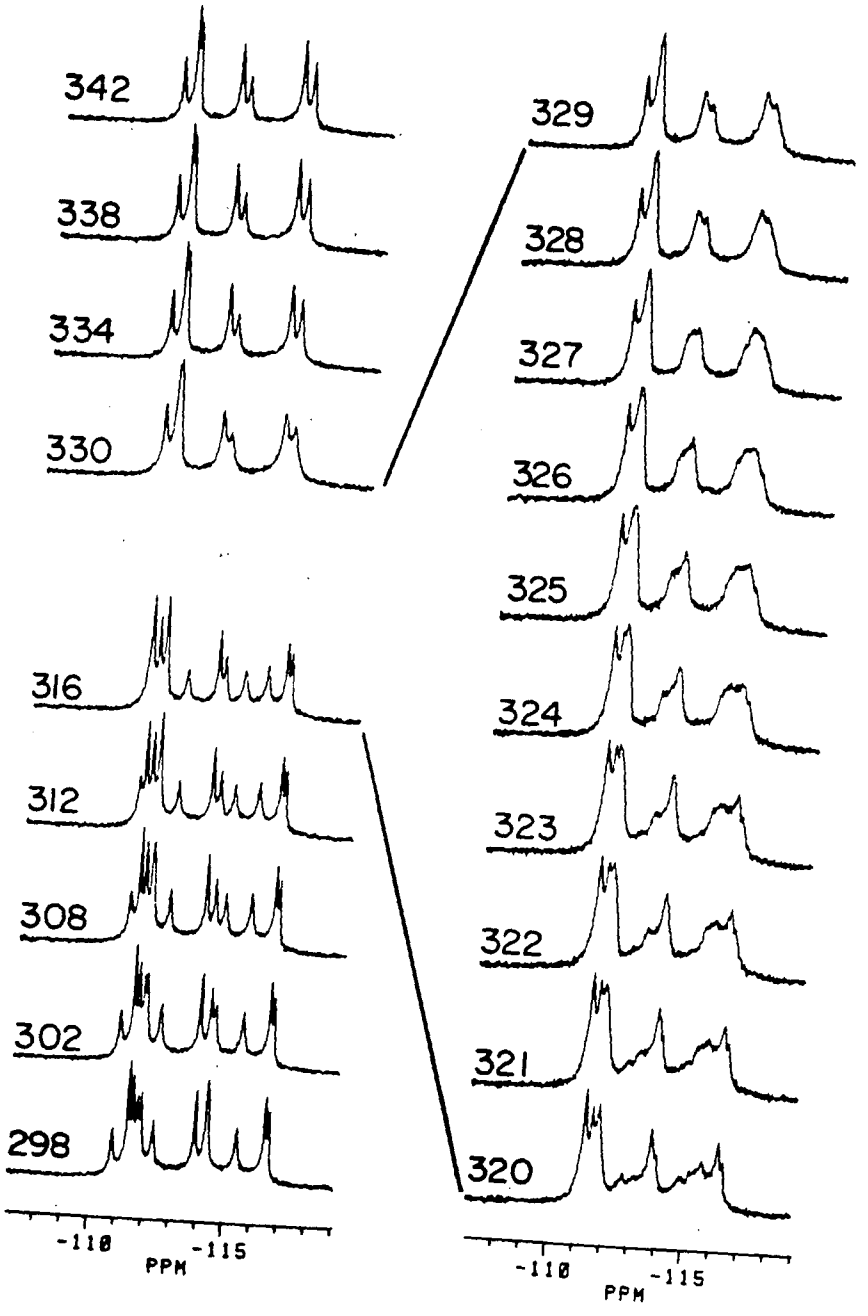

Figure 89 Variable temperature ^{29}Si MAS NMR experiments (298- 342 K) of ZSM-11.

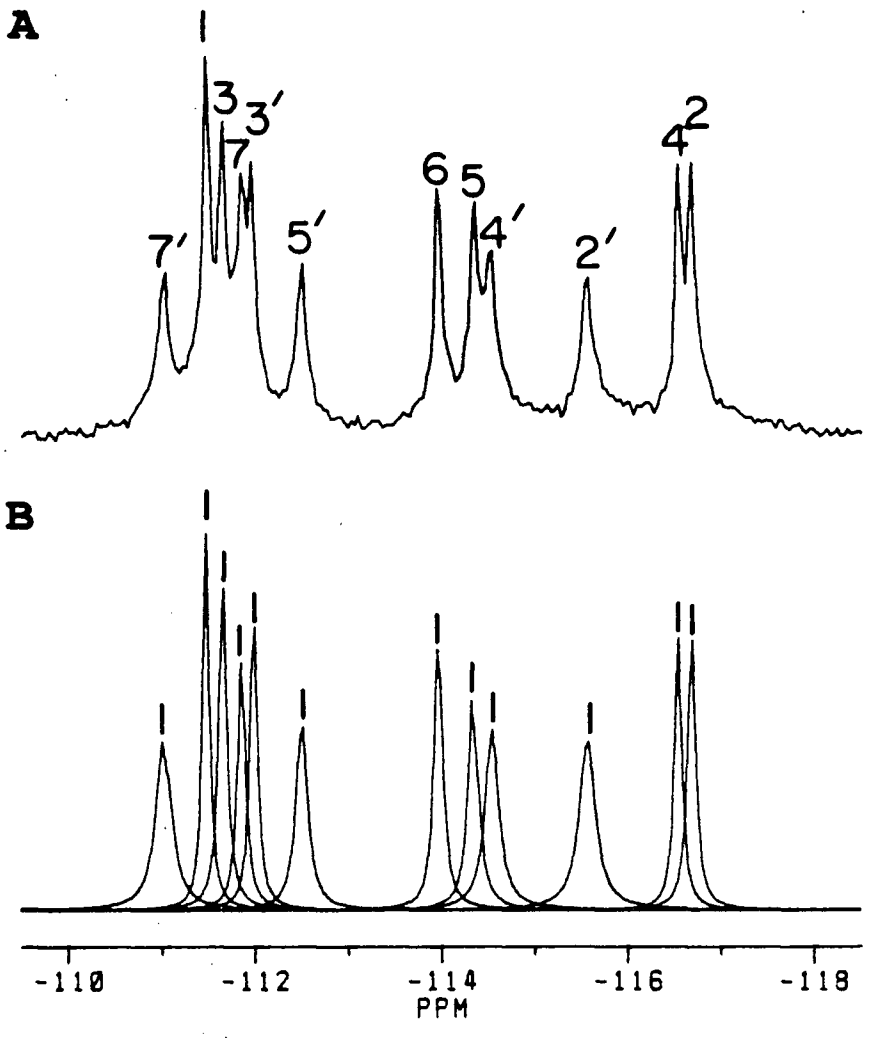

Figure 90 (A) ^{29}Si MAS NMR spectrum of ZSM-11 at 302K with one of the two possible peak assignments (see text).
(B) The individual Lorentzian curves used in the simulation of A. The numbers above the curves indicate the relative peak areas.

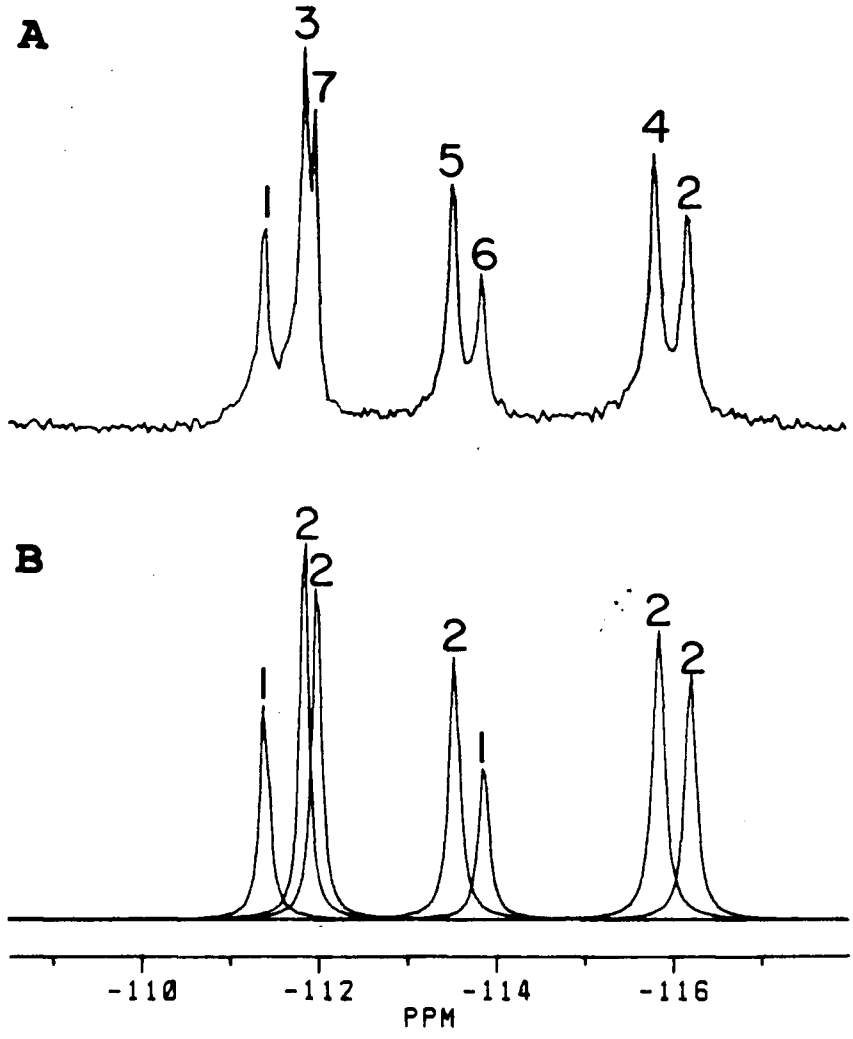

Figure 91 (A) ^{29}Si MAS NMR spectrum of ZSM-11 at 342K with the peak assignments (see text).
(B) The individual Lorentzian curves used in the simulation of A. The numbers above the curves indicate the relative peak areas.

b) 2D experiments on the high temperature and *n*-octane loaded forms of ZSM-11

The lattice structure of ZSM-11 in its high-temperature form has been refined from synchrotron X-ray data in detail in the space group of $I\bar{4}m2$[155]. The schematic representation of the structure is shown in Figure 92A and the expected Si-O-Si connectivities are presented in Table 24. Figure 93 shows the results of a ^{29}Si 2D INADEQUATE experiment carried out at 340 K. All nine of the expected connectivities are clearly observed, and the different occupancies of the T-sites provide a starting point for the assignment of the resonances and the interpretation of the 2D NMR data, restricting the assignment of resonances G and C which have unit intensities to the T-sites 1 and 6. Resonance G presents one connectivity with A, while C shows two connectivities in Figure 93. The assignment can be started at G → 1 and C → 6, and continued by A → 2, F → 3. The complete assignment is shown above the 1D spectrum in Figure 90, and is unique. The resonances of silicons 1, 3, and 7, which are in the four-membered rings, appear at low-field, which is in agreement with the previous observations in the case of zeolite ZSM-5.

Table 24 T-sites, Their Occupancies, and Connectivities for the Asymmetric Unit in Zeolite ZSM-11 in the Space Group $I\bar{4}m2$

T-site	occupancy	connectivity
T_1	1	$2T_1$: $2T_2$
T_2	2	$1T_1$: $1T_3$: $1T_4$: $1T_5$
T_3	2	$1T_2$: $1T_3$: $1T_6$: $1T_7$
T_4	2	$1T_2$: $1T_4$: $1T_5$: $1T_6$
T_5	2	$1T_2$: $1T_4$: $1T_5$: $1T_7$
T_6	1	$2T_3$: $2T_4$
T_7	2	$1T_3$: $1T_5$: $2T_7$

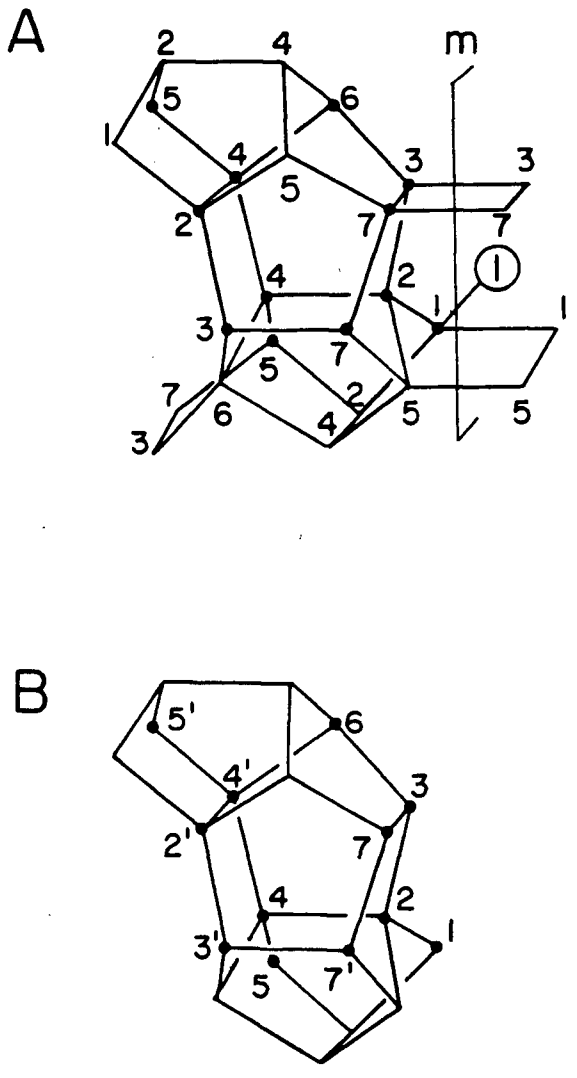

Figure 92 (A) Schematic representation of the high-temperature form of ZSM-11, space group $I\bar{4}m2$. The T-sites are indicated.
(B) Schematic representation of the low-temperature form of ZSM-11. The T-sites are indicated.

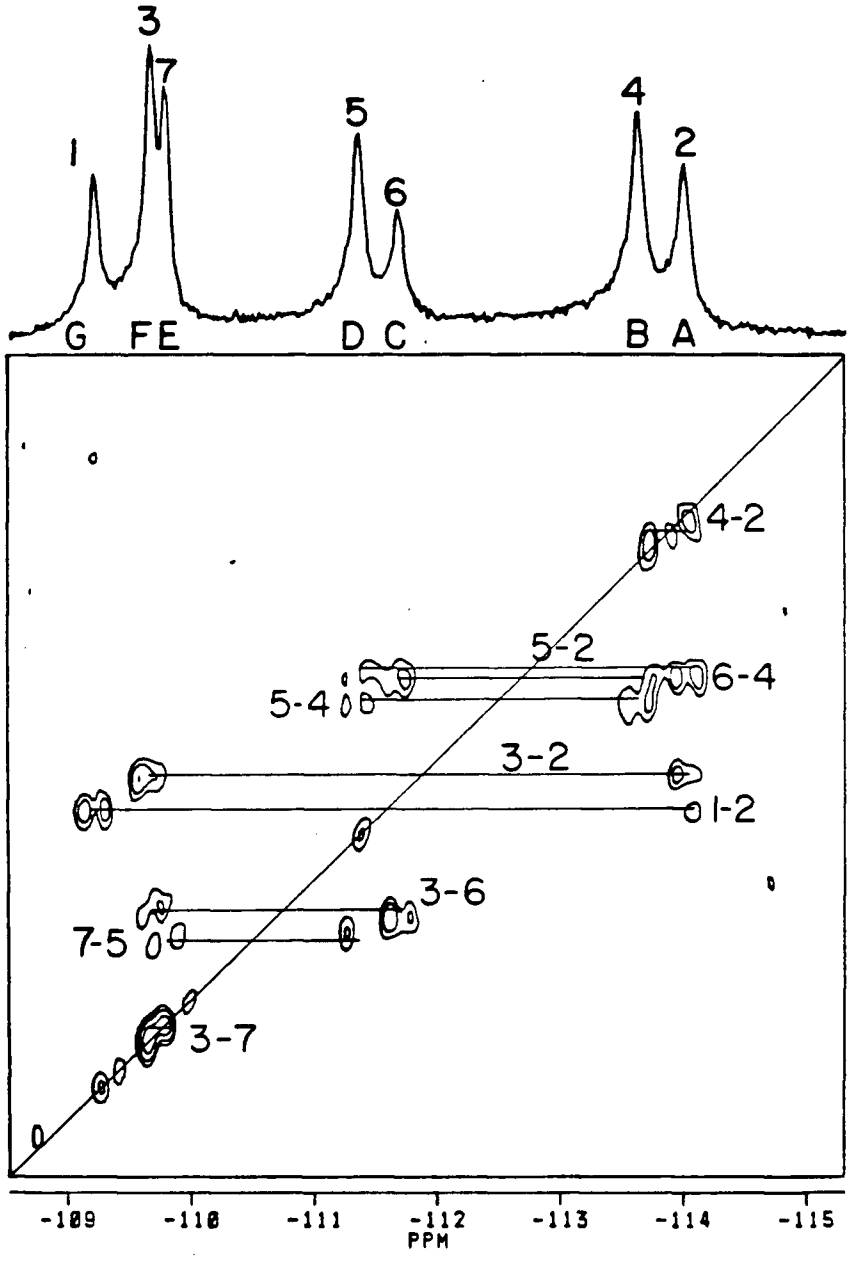

Figure 93 Contour plot of an INADEQUATE experiment on ZSM-11 at 340 K with a 1D MAS NMR spectrum on top. 32 experiments with 224 scans in each experiment were performed with a recycle time of 22 s. The total time for the experiment was approximately 44 h. A sweepwidth of 540 Hz, fixed delay of 16 ms and 160 data points were used. Sine-bell apodizations in both F_2 and F_1 dimensions and a power calculation were used in the data processing.

This high-symmetry phase observed at elevated temperatures can occur at ambient temperature when the sample is loaded with ~3 molecules of *n*-octane per 96 T- atoms unit cell of ZSM-11. The results of a 2D INADEQUATE experiment together with the 1D spectrum are shown in Figure 94. The 1D spectrum has a very similar appearance to that of high-temperature form and Table 25 lists the chemical shifts of the resonances for both cases. This similarity does not mean that the T-sites corresponding to the resonances are necessarily the same in both cases, although they may well be. The assignment of the 2D experiment (Figure 94) is obtained in a similar way to that discribed above for the high-temperature case, with the results shown in the figure. Identical assignments in both cases indicate that the two factors, temperature and adsorption of n-octane, have a similar effect on the lattice structure both in terms of symmetry and geometry.

Table 25 Chemical Shifts of the Resonances of ZSM-11 in the Two Cases of Symmetry I4m2

Form of ZSM-11	Chemical Shift (ppm)						
	Resonance						
	A	B	C	D	E	F	G
n-octane	-116.8	-116.5	-114.2	-113.7	-112.5	-112.5	-111.6
high temp.	-116.2	-115.8	-113.9	-113.5	-112.0	-111.7	-111.4

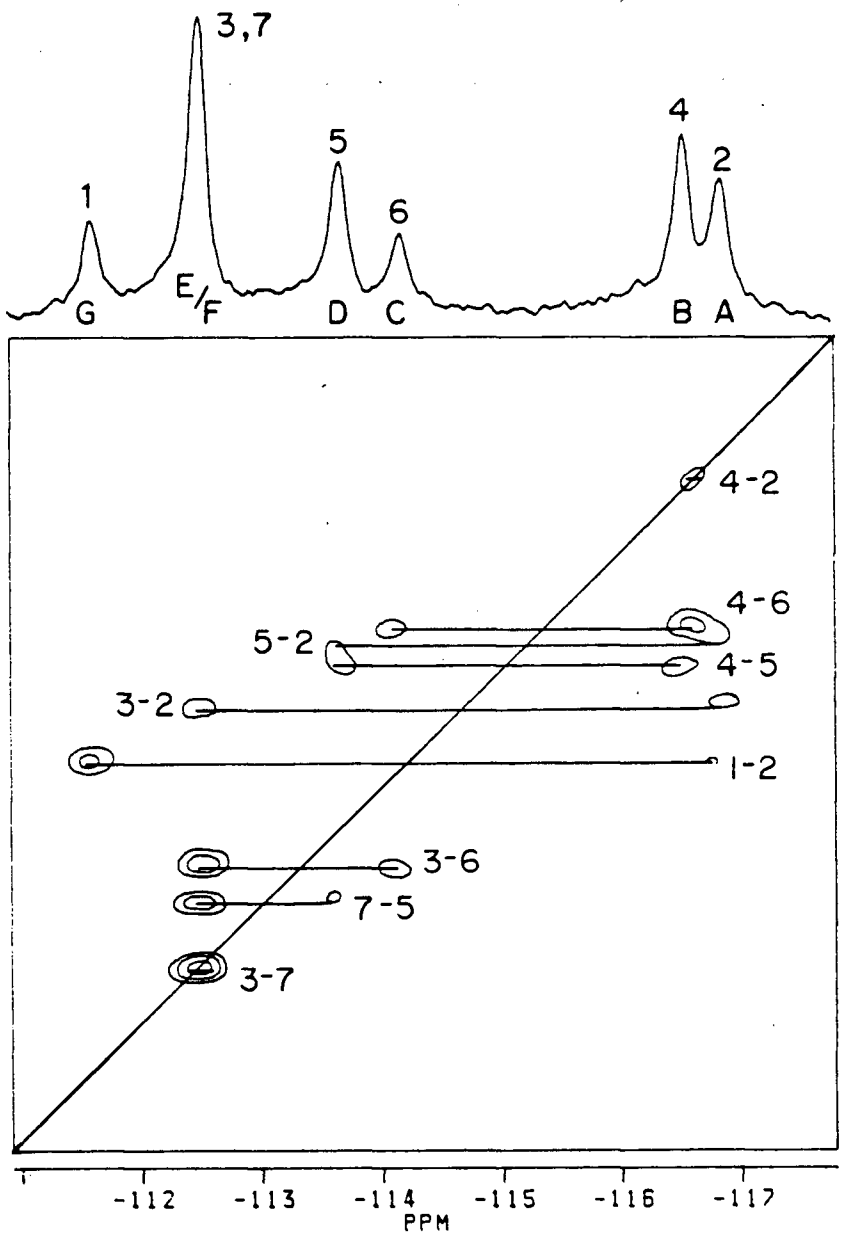

Figure 94 Contour plot of an INADEQUATE experiment on ZSM-11 loaded with 3 molecules *n*-octane per unit cell at 300 K with a 1D MAS NMR spectrum on top. 32 experiments with 128 scans in each experiment were performed with a recycle time of 12 s. The total time for the experiment was approximately 13 h. A sweepwidth of 545 Hz, fixed delay of 16 ms. and 80 data points were used. Sine-bell apodizations in both F_2 and F_1 dimensions and a power calculation were used in the data processing.

C) Investigation of the low-temperature lattice structure of ZSM-11

Step 1. Discussion of the 2D NMR spectra of the low-temperature form.

A 2D INADEQUATE experiment was performed at 303 K and the results are shown in Figure 95. There are a number of well-defined signals, and the splitting due to scalar coupling is observed in almost all of them. The range of ^{29}Si-O-^{29}Si J couplings in ZSM-11 from Figure 95 is between 9 and 16 Hz, which is consistent with those previously observed (see Chapter Four). From the discussion given in previous chapters, it is obvious that in the contour plot of a 2D INADEQUATE experiment, the connected signals occur equally spaced on both sides of the diagonal of the plot and the maximum number of connectivities that can occur for a single ^{29}Si resonance is four in the case of zeolites. From these restrictions, the connectivities of the resonances can be assigned and are presented in Table 26. Due to the small differences in chemical shifts, the connectivities among H, I and J are slightly ambiguous, and are indicated by '*' in Table 26.

An interpretation of the data may be made in the following manner. Firstly, the topology of the whole framework is assumed to remain the same except that the number of crystallographically inequivalent sites in the asymmetric unit is changed after the phase transition. The asymmetric unit in the low-temperature form has 12 distinct T-sites according to the 12 resonance lines observed in ^{29}Si NMR spectrum, which are defined as T_1, T_2,.....T_7 and $T_{2'}$, $T_{3'}$, $T_{4'}$, $T_{5'}$ and $T_{7'}$ as shown in Figure 92B. Further, the connectivities inside the asymmetric unit are fixed no matter what the space group is. The connectivities are shown in Table 27. A relationship of the resonances between the high and low temperature forms can be obtained through careful inspection

Figure 95 Contour plot of an INADEQUATE experiment of ZSM-11 at 303 K with a 1D MAS NMR spectrum on top. 32 experiments with 832 scans in each experiment were performed with a recycle time of 12 s. and the total time for the experiment was approximately 90 h. A sweepwidth of 622 Hz, fixed delay of 16 ms. and 200 data points were used. Sine-bell apodizations in both dimensions and a power calculation were used for the data processing. The inset in the lower right corner is an expansion of the region indicated by the dashed lines.

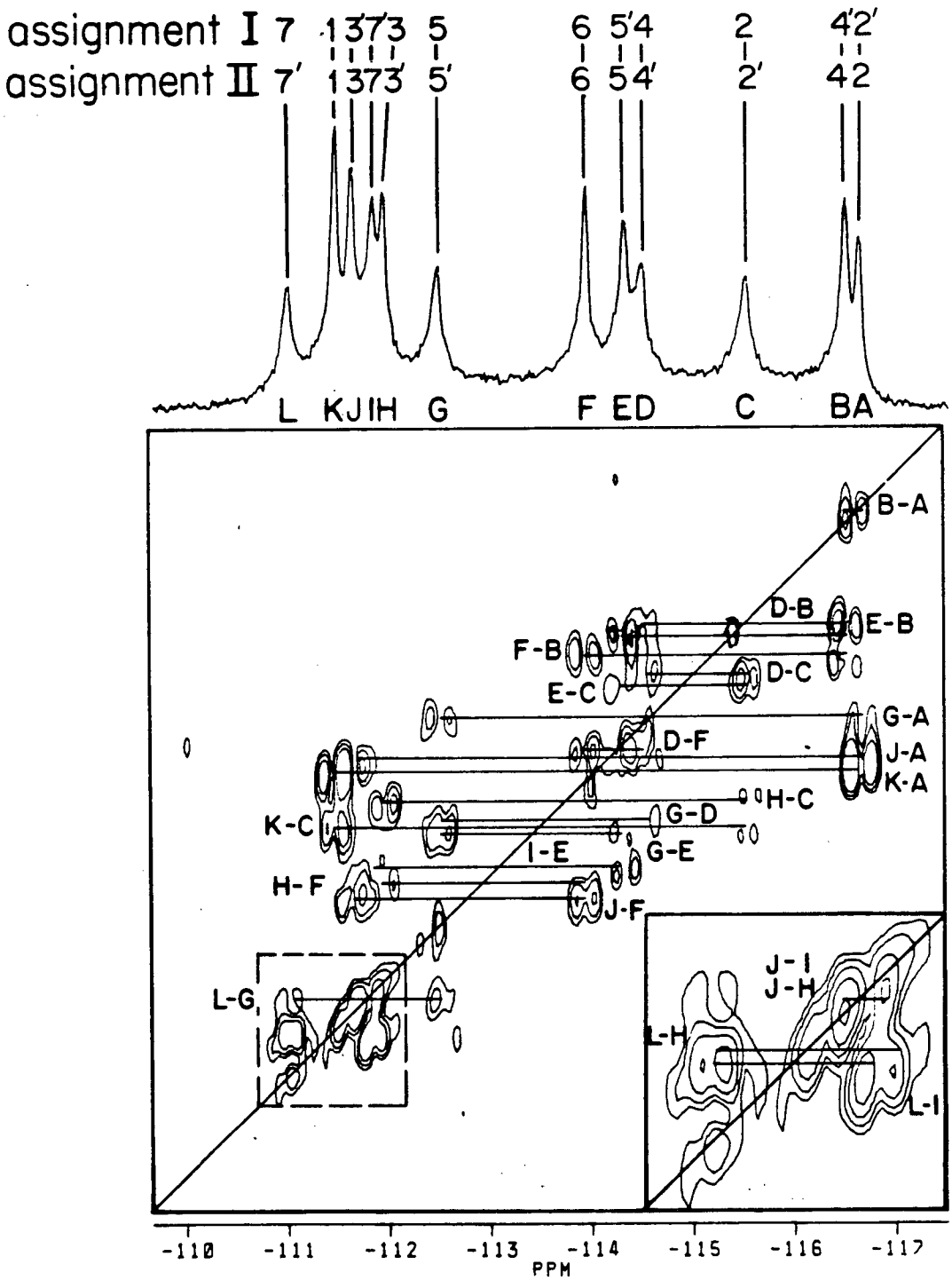
assignment I 7 1 3 7 3 5 6 5 4 2 4 2
assignment II 7' 1 3 7 3' 5' 6 5 4' 2' 4 2
L KJIH G F ED C BA
B-A
D-B
E-B
F-B
D-C
E-C
G-A
D-F
J-A
K-A
H-C
K-C
G-D
I-E
G-E
H-F
J-F
L-G
J-I
J-H
L-H
L-I
-110 -111 -112 -113 -114 -115 -116 -117
PPM

Table 26 Connectivity Scheme of the Resonances of ZSM-11 in the Low Temperature Form from the 2D NMR Data of Figure 95

Resonance	Connectivities					
A	B	K	G	J		
B	A	D	E	F		
C	D	E	H	K		
D	B	C	G	F		
E	B	C	G	I		
F	B	D	H	J		
G	A	E	D	L		
H	C	F	L		J*	
I	E	L			J*	
J	A	F			H*	i*
K	A	C				
L	G	H	I			

Table 27 Connectivities of the T-sites within the Asymmetric Unit of the Low Temperature Form of ZSM-11

T-site	Connectivities			
1	2			
2	1	3	4	
3	2	6	7	
4	2	4′	5	
5	4			
6	3	4′		
7	3	7′		
2′	3′	4′		
3′	2′	7′		
4′	2′	4	5′	6
5′	4′			
7′	3′	7		

of the results of the variable-temperature experiments (Figure 88 and 89). Below the transition, increasing the temperature induces gradual shifts of individual resonances (Figure 96A). Although there are ill-defined changes in the 10-15 K temperature range during the phase transition, it is possible to trace the variation in the chemical shifts of the various resonances and to correlate them in groups between the two phases, as shown in Figure 96B. Finally, the assignment of the

individual resonance to T-sites of the low-temperature form can be made using the information presented in Tables 26, 27, and Figure 96B. The assignment is started at K → 1, then resonances A and C are assigned to be 2 and 2′, since four T_1 silicons form a four-membered ring. At this stage either A or C can be selected to be 2, leading to two possible assignments which are equally valid. To proceed, one is arbitrarily chosen: i.e., A → 2 and C → 2′. From A → 2, the other two assignments of B → 4 and J → 3 can be made, In a similar manner, the assignments of H → 3′ and D → 4′ can be obtained from the assignment of C → 2′. In this way a complete assignment is obtained. The alternate assignment corresponding to the exchange of X ↔ X′ is equally valid. The two possible assignments are shown above the 1D spectrum of Figure 95.

Step 2. Connectivities of the structure of ZSM-11 in the low-temperature form.

The bonding connection between T-sites 5 and 5′ indicates that the mirror plane, which is perpendicular to the a axis (Figure 92-A) is missing. Then T-site 3′ must be connected to 3 and 7′ respectively. Thus the connections marked with '*' in Table 26 are confirmed. The connectivity table of the low-temperature structure can now be completed as shown in Table 28.

If all T-sites X′ and X are changed to X, exactly the same connectivity pattern as for the high-temperature form shown in Table 24 is obtained. This is true for both of the possible assignments and it is proof of self-consistency since it means that the lower symmetry induced by the phase transition only removes the twofold degeneracy of the doubly occupied sites in the asymmetric unit.

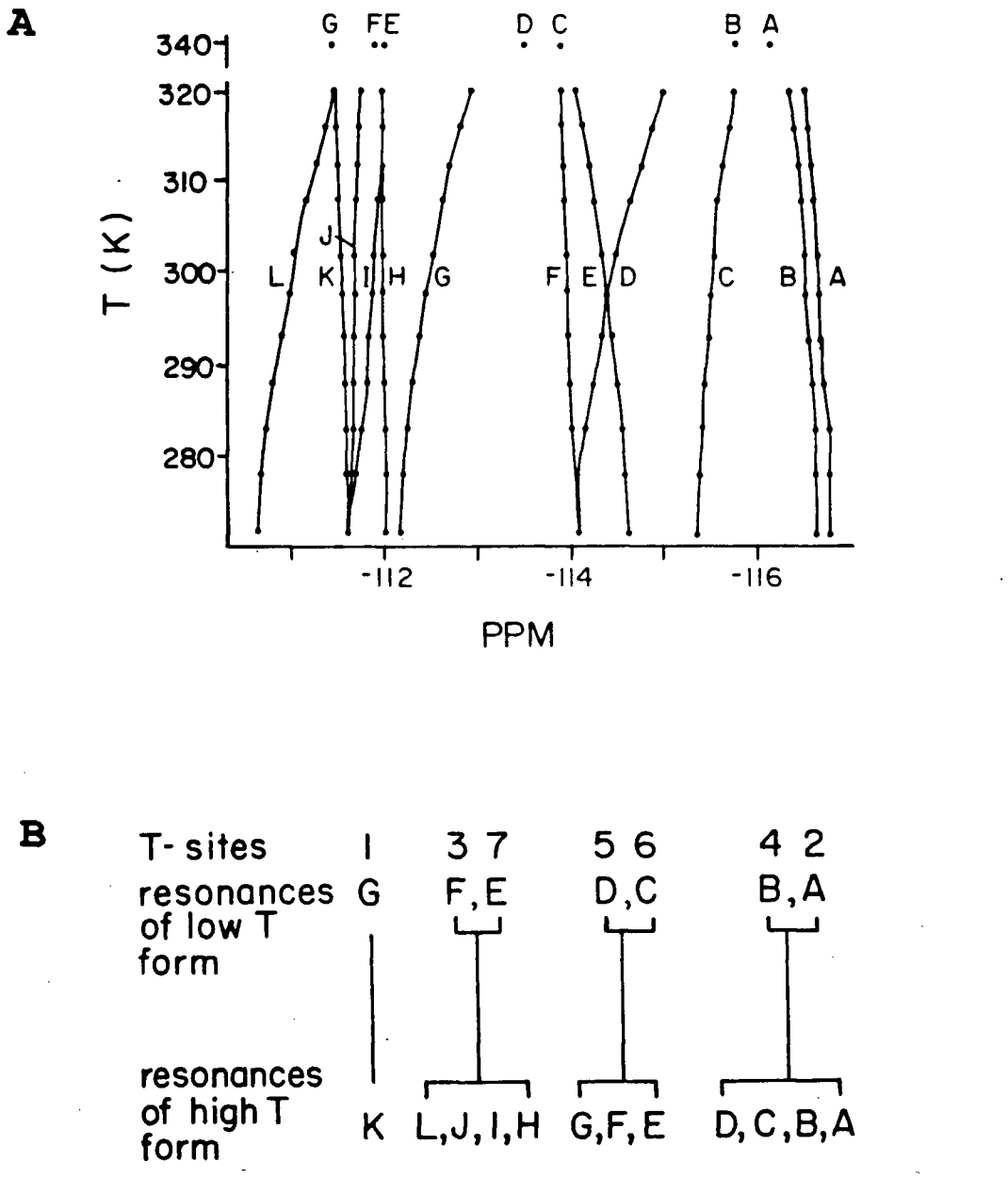

Figure 96 (A) Graphical representation of the variation of chemical shift with temperature for the individual resonances in the ^{29}Si MAS NMR spectra of ZSM-11.
(B) Proposed correlations of individual resonances between the low and high temperature forms.

Table 28 Complete Connectivities of T-sites in the Low Temperature Form of ZSM-11

T-site	Connectivities			
1	1	1	2	2′
2	1	3	4	5′
3	2	3′	6	7
4	2	4′	5	6
5	2′	4	5′	7
6	3	3′	4	4′
7	3	5	7′	7′
2′	1	3′	4′	5
3′	2′	3	6	7′
4′	2′	4	5′	6
5′	2	4′	5	7′
7′	3′	5′	7	7

Step 3. Consideration of some possible space groups.

Careful examination of the asymmetric unit and the symmetry elements of space group $I\bar{4}m2$ suggests that the symmetric element of a twofold axis parallel to the diagonal of the ab plane is lost when the phase transition occurs from the high- to low-temperature forms. From a subgroup-supergroup relationship, the subgroups of $I\bar{4}m2$ could be $I\bar{4}$ (tetragonal) if the mirror plane is missing, and be Pmm2 (orthorhombic) when the 4 fold screw axes are lost. From the general coordinates of equivalent positions of $I\bar{4}m2$, values of the coordinates of the additional five T-sites, X', are estimated, which are good enough to run the ORFFE computer program to obtain the theoretical connectivities resulting from lattice symmetries. All space groups that are subgroups of $I\bar{4}m2$ were considered, and of these, only $I\bar{4}$ leads to connectivities that match those in Table 28. This space group is thus considered to be the correct one for the low-temperature form of ZSM-11.

In the 2D work described earlier in this thesis, the structures of the zeolites investigated were well-determined by X-ray diffraction experiments, especially in the case of single crystal diffraction. The interpretation of these NMR data is based on the XRD data. The successful assignments of the 2D NMR data are in good support of the proposed structures, and in some cases give more detailed information about the structures, for example the case of DD3R (see Chapter Three). Diffraction experiments are primarily sensitive to long- range orderings and periodicities and give information on the average crystal structure. However, the quantitative interpretation of powder diffraction data, which one is often forced to use due to the lack of single crystals, is always hampered by loss

of information through signal overlap. NMR spectroscopy probes the local environments of the T-sites in the unit cell, and is more sensitive than XRD to moderate deviations from a regular structure such as those induced by changes in temperature, or the presence of organic molecules. By applying 2D NMR techniques a more complete picture of the zeolite structure can be obtained, as illustrated in previous chapters. NMR has helped to solve the space group ambiguities in ZSM-12 (see Chapter One). In the case of ZSM-11, the room temperature synchrotron diffraction data set showed almost no extra peaks which would indicate the lowering of symmetry and the refinement did not smoothly proceed to match NMR results with 12 T-sites in the asymmetric unit[155]. In contrast, the NMR is very sensitive to the subtle changes in the local geometry of the T-atoms due to the phase transition. As seen above, the connectivities of the low-temperature form of ZSM-11 have been deduced from NMR experiments alone and the knowledge of the structure of the high-temperature form, and the structure of the low temperature form is proposed to be $I\bar{4}$. A low temperature synchrotron data set is currently being refined by the research group of Dr. H. Gies, U. Bochum, based on the structure derived from 2D NMR results. Thus NMR can provide important complementary information for the refinement of diffraction data.

B. NATURAL ABUNDANCE TWO-DIMENSIONAL ^{29}SI MAS NMR INVESTIGATION OF THE THREE-DIMENSIONAL BONDING CONNECTIVITIES AND STRUCTURE OF ZEOLITE ZSM-23

I. INTRODUCTION

ZSM-23 is a medium- pore size and high silica zeolite first synthesized by Plank, Rosinsk and Rubin [158]. Its framework topology has been proposed to have either orthorhombic symmetry, Pmmn with 7 crystallographically inequivalent T-sites and 24 T atoms per unit cell [159,160], or orthorhombic symmetry, $P2_1mn$ also with 7 independent T-sites [160]. The pore structure consists of a one-dimensional channel along the a axis with teardrop- shaped openings of ca. 4.5 X 5.6 Å. The projection (bc- face) of the framework structure is presented in Figure 97.

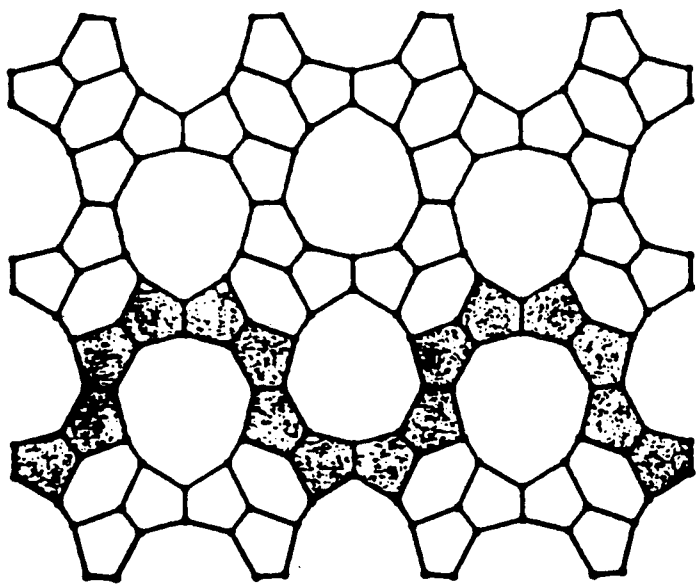

Figure 97 The projection (bc- face) of zeolite ZSM-23 lattice framework.

II. EXPERIMENTAL

The as-synthesized ZSM-23 sample was kindly provided by Dr. S. Ernst, and was synthesized according to the literature [161] using hydrothermal techniques with N, N, N, N', N', N'- hexamethylheptamethylenediammonium dibromide as template. Powder XRD data were in excellent agreement with those previously reported[159,160]. A highly siliceous and crystalline sample was obtained by calcination and ammonium exchange followed by steaming twice at 750 C for three days. Further steamings gave no improvement in the quality of this material.

High-resolution ^{29}Si MAS NMR spectra were obtained at 79.5 MHz on a Bruker MSL 400 spectrometer using the techniques previously discussed.

III. RESULTS AND DISCUSSION

a) 1D experiments

The ^{29}Si MAS NMR spectrum (Figure 98A) of the highly siliceous sample used in these experiments shows a series of sharp resonances at room temperature. These lines can be deconvoluted in terms of nine signals of relative intensities 1:1:2:1:1:2:1:2:1, as indicated in Figure 98C, reflecting an asymmetric unit with at least nine independent T-sites. This is in clear disagreement with both of the proposed structures, in which the asymmetric unit has seven T-sites of relative occupancies 1: 1: 2: 2: 2: 2: 2. Clearly, if the proposed framework is correct, the symmetry must be lower than postulated. Raising the temperature to 100°C does not induce large changes in the spectrum which would indicate a transition to a higher symmetry form although there are small and gradual changes consistent with lattice expansion. As the temperature is lowered, small

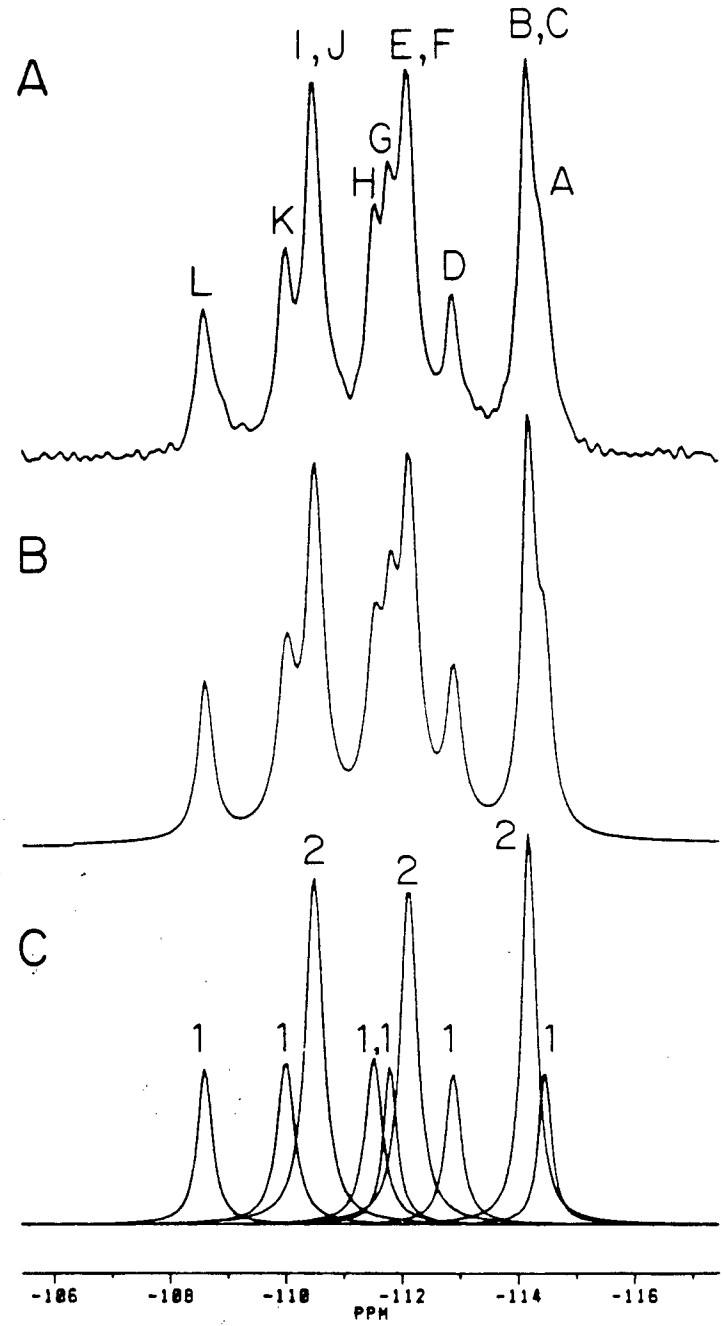

Figure 98 ^{29}Si MAS NMR spectra of zeolite ZSM-23 and its deconvolution:
(A) Experimental spectrum;
(B) A computer simulation of A;
(C) The individual Lorentzian curves used in the simulation.

shifts again occur and the double intensity line marked as E/F is split into two lines of equal intensity giving a total of ten lines in the spectrum. This behavior suggests that the intensities of all three double intensity lines in the room temperature spectrum (B/C, E/F, I/J) might be due to the degeneracy of two resonances with unit intensity and that the asymmetric unit contains twelve T-sites of equal occupancy.

b) 2D INADEQUATE experiments

The results of a 2D INADEQUATE experiment at ambient temperature are shown in Figure 99. There are a considerable number of connectivities clearly observable, as indicated in the figure. Taking the relative intensities of the signals into account and using the constraint that the maximum number of connectivities is four for a given silicon atom, there are clear indications that the signals J/K and B/C in the 1D spectrum are also degenerate as previously indicated. Therefore, it is assumed that there are 12 independent T-sites in the structure. If two resonances are very close in frequency, the connectivity between them may be anticipated to be of much lower intensity or perhaps not observable at all due to the coupling being second-order so it is possible that some connectivities might not have been detected. Those connectivities which are clear and reproducible are indicated in Figure 99.

Thus, the results of present 2D NMR experiments can not be in agreement with XRD data, suggesting at least that the proposed space group, Pmmn, based on powder X-ray diffraction data for zeolite ZSM-23 is in error. It is hoped that the combination of synchrotron powder diffraction and high resolution solid state NMR experiments can solve the structure of zeolite ZSM-23.

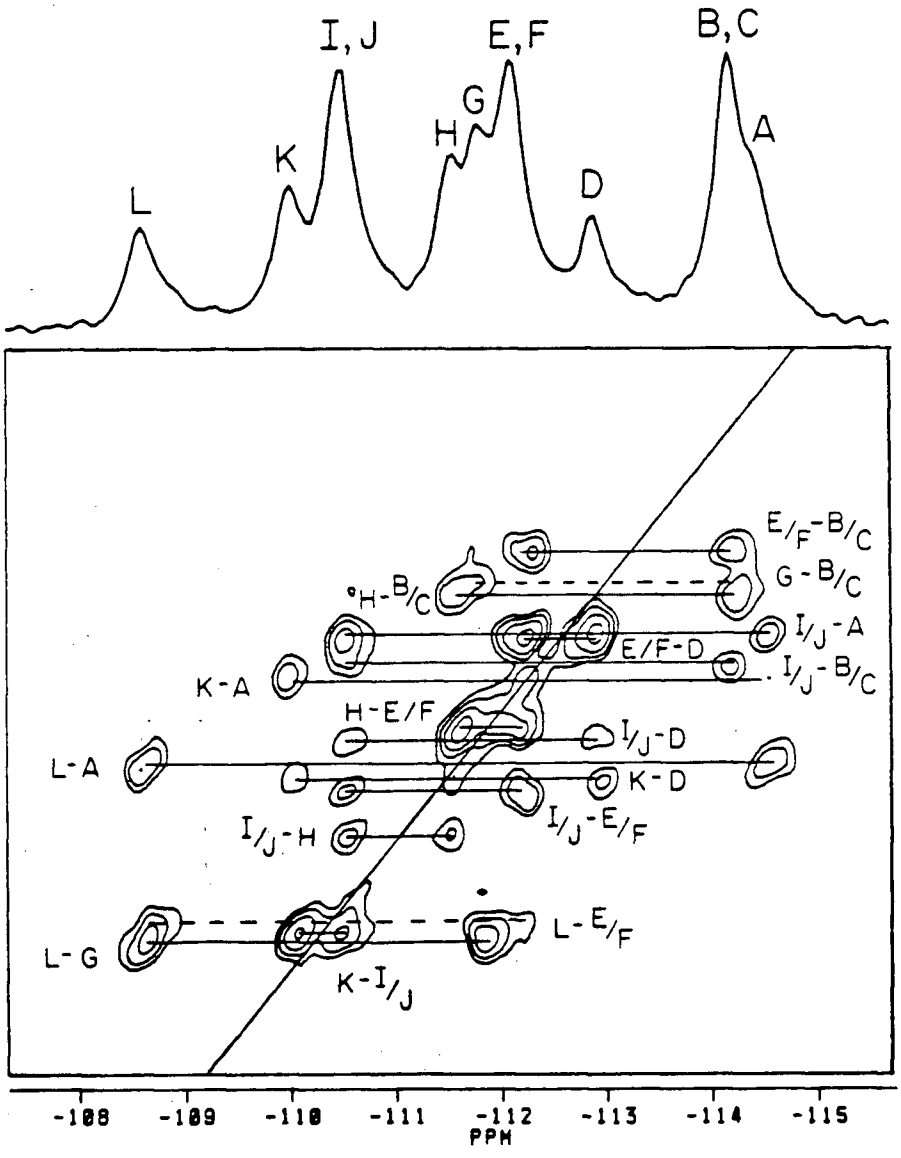

Figure 99 Contour plot of an INADEQUATE experiment of ZSM-23 at 300 K with a 1D MAS NMR spectrum on top. 54 experiments with 864 scans in each experiment were performed with a recycle time of 12 s. and the total time for the experiment was approximately 156 h. A sweepwidth of 740 Hz, fixed delay of 16 ms and 200 data points were used. Sine-bell apodizations in both dimensions and a power calculation were used for the data processing. The dashed lines indicate connections which are not as well defined but which appear reproducible over a series of experiments.

CHAPTER SEVEN

CONCLUSIONS AND SUGGESTIONS FOR FUTURE WORK

A. CONCLUSIONS

The present work has demonstrated for the first time that two-dimensional homonuclear correlation ^{29}Si MAS NMR, mainly INADEQUATE and COSY types of experiments, can be successfully used to investigate the three-dimensional silicon bonding networks in zeolites. The structural information obtained from this study includes:

1) Confirming the structure determined by XRD techniques, when the 2D data can be successfully interpreted in terms of the known crystal structures, e. g. ZSM- 39, ZSM- 12, ZSM- 22 etc.

2) Providing additional details on lattice structures. For example, in the case of zeolite DD3R, careful analysis of the 2D data indicates that the symmetry is lower than that proposed.

3) Indicating that some proposed structures may be in error if the number of resonances and the connectivity pattern of the 2D map are not in agreement with the number of independent T-sites and the 'theoretical' connectivity scheme based on the XRD data. Zeolite ZSM-23 is an example of this case.

4) Investigating the structures for some poorly- defined zeolites in terms of determining an appropriate space group. For example, the structure of ZSM-11 in the room temperature form is suggested to be I4 and that of ZSM-5 loaded with 8 molecules of *p*- dichlorobenzene is proposed to have space group $P2_12_12_1$.

Thus it is felt that the 2D experiments developed and described in this thesis can be used in the future with confidence in the investigation of unknown zeolite structures and may be extended to other three- dimensional lattice structures.

B. SUGGESTIONS FOR FUTURE WORK

I. APPLICATION OF DYNAMIC- ANGLE SPINNING (DAS) AND DOUBLE- ROTATION (DOR) NMR TO THE STUDY OF ZEOLITE STRUCTURES

As mentioned in Chapter One, all of the atoms making up the zeolite lattice have NMR active isotopes and thus can be investigated by solid-state NMR, which are ^{29}Si (4.6 %), ^{27}Al (100 %) and ^{17}O (0.04%). The work in this thesis is concentrated on the investigation of their ^{29}Si spectra which give the most direct information on the lattice itself. ^{29}Si is a spin 1/2 nucleus and MAS averages the orientation-dependent interactions to zero or to their average 'isotropic' values, giving NMR spectra with narrow resonances. ^{27}Al and ^{17}O, however, are quadrupolar nuclei with I = 5/2 and their solid- state spectra are more complex. The line shape due to the central transition (+ 1/2 $\leftrightarrow$ - 1/2) is distorted and shifted by the second-order quadrupolar interaction and other transitions are usually too broad to be observed directly.

Magic-Angle Spinning technique can average only the first order quadrupolar interaction but dynamic- angle spinning (DAS) and double rotation (DOR) [161,162] techniques can average the second-order as well as first-order broadening. In double rotation experiments, the axis of the rotor is moved continuously in a cone by spinning the sample in a spinner within another spinner, each with its own spinning axis, and in the case of dynamic angle spinning, the sample is contained within a single spinner but the orientation axis of the spinner is switched between two discrete angles with respect to the external magnetic field. The success of the DOR and DAS techniques has been

recently demonstrated for ^{17}O in a variety of silicates[164], where it is possible to resolve crystallographically inequivalent oxygens. However, ^{17}O results of DOR or DAS on zeolites have not been reported to date and would be very informative. It is predictable that they will be successful if applied to the highly siliceous zeolite systems described in this thesis. Furthermore ^{17}O- ^{29}Si heteronuclear correlation experiments will provide additional useful information on zeolite structures. Since the assignments of ^{29}Si spectra can be obtained from ^{29}Si 2D experiments as described in this thesis, the interpretation of the ^{17}O spectra will be possible through heteronuclear correlation experiments. Consequently, the correlation of ^{17}O chemical shifts and T- O- T angles could be studied, and it is particularly important that the ^{17}O shifts will correlate with discrete angles and not averages as in the case of ^{29}Si. Thus it will give more significance to the ^{17}O chemical shifts and a closer linking the two major techniques, XRD and NMR, in zeolite structure studies.

II. ROTATIONAL-ECHO DOUBLE-RESONANCE (REDOR) NMR STUDIES OF ZEOLITES

Magic- angle spinning has been widely used to reduce the broadening effects of chemical shift anisotropy and dipole- dipole coupling in order to obtain high-resolution solid state spectra, as discussed in Chapter One. Therefore the direct detection of weak dipolar couplings in MAS NMR experiments is often difficult. In order to solve this problem, Schaefer[165] has proposed the rotational-echo double-resonance (REDOR) pulse sequence, which was derived from spin-echo double resonance[166,167], to obtain molecular geometric information. This kind of experiment has been extended to rotational-echo

triple-resonance NMR[168] and DANTE-selected REDOR NMR[169]. The application of these techniques has concentrated on ^{13}C- ^{15}N labeled spin pairs. Fyfe and Grondey have recently applied these types of experiment to the interactions involving quadrupolar nuclei[170], and investigated the dipolar interactions between ^{31}P and ^{27}Al pairs in a sample of VPI- 5. The preliminary results are promising and suggest that it should be possible to carry out these kinds of experiments on the ^{29}Si- ^{27}Al pairs in zeolites, although there are some difficulties due to the 4.7% natural abundance of ^{29}Si. These may yield a better understanding of zeolite structures and it may be possible to extend them to other related three-dimensional structures.

LIST OF REFERENCES

1. A. F. Cronstedt, Kongl. Svenska Vetenskaps Academiens Handlingar Stockholm, **17**, 120 (1756).

2. D. W. Breck, *"Zeolite Molecular Sieves: Structure, Chemistry and Use"* Wiley, New York (1974).

3. R. M. Barrer, *"Zeolites and Clay Mineral as Sorbents and Molecular Sieves"*, Academic Press, London and New York (1978)

4. R. M. Barrer, *"Hydrothermal Chemistry of Zeolites"* Academic Press, London and New York (1982).

5. W. M. Meier and D. H. Olson, *"Atlas of Zeolite Structure Types"* International Zeolite Assoc., 2nd version, Butterworths (1987).

6. G. T. Kokotailo, Zeolite Crystallography, in *"Zeolites: Science and Technology"*, Eds. F. R. Riebeiro, A. E. Rodriques, L. D. Rollmann and C. Naccache, NATO ASI Series E, No. **80** (1984).

7. W. M. Meier, in *"SCI Monograph on Molecular Sieves"*, Eds. R. M. Barrer, Soc. Chem. Ind., London (1978).

8. A. Dyer, *"An Introduction to Zeolite Molecular Sieves"* John Wiley & Sons. Chichester, (1988).

9. E. M. Flanigen, in *"Zeolites: Science and Technology"*, Eds. F. R. Reiberiro, A. E. Rodriques, L. D. Rollmann and C. Naccache, NATO ASI Series E, No. **80** (1984).

10. W. Hölderich, M. Hesse and F. Näumann, *Angew. Chem. Int. Ed. Engl.*, **27**, 226 (1988).

11. A. K. Cheetham, in *"High Resolution Powder Diffraction"*, Materials Science Forum, Eds. C. R. A. Catlow, Trans. Tech. Publication Andermannsdorf, Switzerland, Vol. 9 (1986).

12. J. E. Post and D. L. Bish, in *"Modern Powder Diffraction"*, Reviews in Mineralogy, Eds. D. L. Bish and J. E. Post, The Mineralogical Society of America, Washington, D. C., Vol. 20 (1989).

13. H. M. Rietveld, *J. Appl. Crystallogr.*, **2**, 65 (1969).

14. L. W. Finger, in *"Modern Powder Diffraction"*, Reviews in Mineralogy, Eds. D. L. Bish and J. E. Post, The Mineralogical Society of America, Washington, D. C., Vol. 20 (1989).

15. P. Eisenberger, J. M. Newsam, D. E. W. Vaughan and M. Leonowiz, *Nature*, **45**, 309 (1984).

16. B. Marler, *Zeolites*, **7**, 393 (1987).

17. G. Engelhardt and D. Michel, *"High-Resolution Solid State NMR of Silicates and Zeolites"*, John Wiley and Sons, New York, (1987).

18. J. M. Thomas, G. R. Millward, S. Ramdas and M. Audier, in *"Intrazeolite Chemistry"*, Eds. G. D. Stucky and F. G. Dwyer, ACS Symp. Ser., **218** 181 (1983).

19. J. M. Thomas, G. R. Millward, S. Ramdas and M. G. Barlow, *"proceedings of the 6th International Conference on Zeolites"* , Reno, NV, Paper S-53, (1983).

20. R. A. Jackson and C. R. A. Catlow, *Molecular Simulation*, **1**, 207 (1988).

21. S. M. Tomlinson, R. A. Jackson and C. R. A. Catlow, *J. Chem. Soc., Chem. Commun.*, 813 (1990).

22. P. A. Wright, J. M. Thomas, A. K. Cheetham and A. K. Nowak, *Nature (London)*, **318**, 611 (1985).

23. J. O. Titiloye, S. C. Parker, D. C. Sayle, F. S. Stone and C. R. A. Catlow, in *"Recent Advances in Zeolite Science"*, Eds. J. Klinowski and P. J. Barrie, Elsevier, Oxford, (1989).

24. U. Haeberlen, *"High Resolution NMR in Solids: Selective Averaging"*, Adv. Magn. Reson., Suppl. 1, (1976).

25. M. Mehring, *"High Resolution NMR in Solids"* 2nd ed., Springer-Verlag, Berlin and New york, (1983).

26. C. A. Fyfe, *"Solid State NMR for Chemists"*, C. F. C. Press, Guelph, Ontario, Canada, (1984).

27. G. E. Pake, *J. Chem. Phys.* **16**, 327 (1948)

28. R. K. Harris, *"Nuclear Magnetic Resonance Spectroscopy"*, Pitman, Lonton, (1983).

29. E. R. Andrew, A. Bradbury and R. G. Eades, *Nature (London)*, **183**, 1802 (1959).

30. I. J. Lowe, *Phys. Rev. Lett.*, **2**, 285 (1959).

31. A) A. Pines, M. G. Gibby and J. S. Waugh, *Chem. Phys. Lett.*, **15**, 273 (1972).

B) M. G. Gibby, A. Pines and J. S. Waugh, *Chem. Phys. Lett.*, **16**, 296 (1972).

32. A. Pines, M. G. Gibby and J. S. Waugh, *J. Chem. Phys.*, **59**, 569 (1973).

33. L. W. Jelinski and M. T. Melchior, in "*NMR Spectroscopy Techniques*", Eds. C. Dybowski and R. L. Lichter, Marcel Dekker, inc., New York and Basel, (1987).

34. S. R. Hartmann and E. L. Hahn, *Phys. Rev.*, **128**, 2042 (1962).

35. J. Schaefer and E. O. Stejskal, *J. Am. Chem. Soc.* **98**, 1031 (1976).

36. F. A. Bovey, *"Nuclear Magnetic Resonance Spectroscopy"* Academic Press (1987)

37. C. A. Fyfe, Y. Feng, H. Grodey and G. T. Kokotailo, *J. Chem. Soc., Chem. Commun.*, 1224 (1990).

38. G. Engelhardt, D. Kunath, A. Samoson, M. Tarmak, M. Mägi and E. Lippmaa, "*Workshop on Adsorption of Hydrocarbons in Zeolites*", Berlin-Adlershof, November 19-22, (1979).

39. A) E. lippmaa, M. Mägi, A. Samoson, G. Engelhardt and A. R. Grimmer, *J. Am. Chem. Soc.* **102**, 4889 (1980).

B) G. Engelhardt, M. MÄgi, and E. Lippmaa, *"Second Workshop on the Adsorption of Hydrocarbons in Microporous Sorbents"*, Eberswalde, G. D. R. Vol. 2, (1982).

40. J. Klinowski, S. Ramdas, J. M. Thomas, C. A. Fyfe and J. S. Hartman, *J. Chem. Soc., Faraday Trans.* 2, **78**, 1025 (1982).

41. W. Loewenstein, *Amer. Mineralog.*, **39**, 92 (1954).

42. C. A. Fyfe, J. M. Thomas, J. Klinowski and G. C. Gobbi, *Angew. Chem. Int. Ed. Engl.*, **22**, 259 (1983).

43. G. T. Kokotailo, C. A. Fyfe, Y. Feng and H. Grondey, in "*Fluid Catalytic Cracking II*", *ACS Symp. Ser.*, **452**, Eds. M. L. Occelli, (1991).

44. C. A. Fyfe, H. Gies, G. T. Kokotailo, Y. Feng, H. J. Strobl, B. Marler and D. E. Cox, in *"Zeolites: Facts, Figures, Future"*, Eds. P. A. Jacobs, R. A. Van Santen, 545, Elsevier Science Publisher, B. V., Amsterdam (1989)

45. H. Strobl, C. A. Fyfe, G. T. Kokotailo and C. T. Pasztor, *J. Am. Chem. Soc.* **109**, 4733 (1987).

46. R. B. LaPierre, A. C. Rohrman, Jr., J. L. Schlenker, J. D. Wood. M. K. Rubin and W. J. Rohrbough, *Zeolites* **5**, 346 (1985).

47. C. A. Fyfe, H. Gies, G. T. Kokotailo, B. Marler and D. E. Cox, *J. Phys. Chem.*, **94**, 3718 (1989)

48. C. A . Fyfe, G. J. Kennedy, C. T. De Schutter and G. T. Kokotailo, *J. Chem. Soc., Chem. Commun.*, 541 (1984).

49. C. A. Fyfe, H. J. Strobl, G. T. Kokotailo, G. J. Kennedy and G. E. Barlow, *J. Am. Chem. Soc.*, **110**, 3373 (1988)

50. C. A. Fyfe, G. T. Kokotailo, H. Strobl, C. S. Pasztor and S.Bradley, *Zeolites*, **9**, 531 (1989).

51. C. A. Fyfe, H. Strobl, H. Gies and G. T. Kokotailo, *Can. J. Chem.* **66**, 1942 (1988).

52. A. Bax, *"Two Dimensional Nuclear Magnetic Resonance in Liquids"*, Delft University Press and D. Reidel Publishing Co., Dordrecht, Holland, (1982).

53. R. Benn and H. Guenther, *Angew. Chem., Int. Ed. Engl.* **22**, 350 (1983).

54. R. R. Ernst, G. Bodenhausen and A. Wokaun, *"Principles of Nuclear Magnetic Resonance in One and Two Dimensions"*, Claredon, Oxford, (1987).

55. A. E. Derome, *"Modern NMR Techniques for Chemistry Research"*, Pergamon Press, New York, (1987).

56. J. Sanders and B. Hunter, *"Modern NMR Spectroscopy, A Guide for Chemists"*. Oxford University Press, (1987).

57. J. Jeener, Ampere International Summer School, Basko Polje, Yugoslavia, (1971).

58. A. Kumar, D. D. Welti and R. R. Ernst, *J. Magn. Reson.*, **18**, 69 (1975).

59. R. R. Ernst, *Chimia*, **29**, 179 (1975).

60. W. P. Aue, E. Bartholdi and R. R. Ernst, *J. Chem. Phys.*, **64**, 2229 (1976).

61. R. L. Vold and J. S. Waugh, *J. Chem. Phys.*, **48**, 3831 (1968).

62. C. P. Slichter, *"Principles of Magnetic Resonance"*, 2nd ed., Spring, Berlin, 1978.

63. K. Blum, *"Density Matrix Theory and Applications"*, Plenum Press, New York, 1981.

64. O. W. Sorensen, G. W. Eich, M. H. Levitt, G. Bodenhausen, R. R. Ernst, *Prog. Nucl. Magn. Reson. Spectrosc.*, **16**, 163 (1983).

65. H. Kessler, M. Gehrke and C. Griesinger., *Angew. Chem. Int. Ed. Engl.* **27** 490 (1988)

66. A. Bax, R. Freeman and S. P. Kempsell, *J. Am. Chem. Soc.*, **102**, 4851 (1980).

67. N. M. Szeverenyi, M. J. Sullivan and G.E. Maciel, *J. Magn. Reson.*, **47**, 462, (1982).

68. A. J. Vega, *J. Am. Chem. Soc.*, **110**, 1049 (1980).

69. R. Benn, H. Grondey, C. Brevard and A. Pagelot, *J. Chem. Soc., Chem. Commun.*, 102 (1988).

70. A. Bax, N. M. Szeverenyi and G. E. Maciel, *J. Magn. Reson.*, **51**, 400 (1983).

71. S. J. Opella and J. S. Waugh, *J. Chem. Phys.*, **66**, 4919 (1977).

72 G. Bodenhausen, R. E. Stark, D. J. Ruben and R. G. Griffin, *Chem. Phys. Lett.*, **67**, 424 (1979).

73. P. Caravatti, J. A. Deli, G. Bodenhausen and R. R. Ernst, *J. Am. Chem. Soc.*, **104**, 5506 (1982).

74. J. B. Higgins, D. E. Woesner, J. C. Trewella and J. L. Schlenker, *U.S. Patent*, **3,832,449.**

75. R. K. Harris and C. T. G. Knight, *J. Chem. Soc. Faraday Trans.* 2, 1539 (1983), and references therein.

76. R. K. Harris, M. J. O'Connor, E. H. Curzon and O. W. Howarth, *J. Magn Reson.*, **57**, 115 (1984).

77. C. T. G. Knight, R. J. Kirkpatrick and E. Oldfield, *J. Am. Chem. Soc.*, **108**, 30 (1986).

78. D. E. Woessner and J. C. Trewella, *J. Magn. Reson.*, **59**, 352 (1984).

79. P. A. Jacobs, "*Synthesis of High-Silica Aluminosilicate Zeolites*", Elsevier, Amsterdam (1987).

80. J. Scherzer, *ASC Symp. Ser.*, No. **248**, 157 (1984).

81. A) C. V. McDaniel and P. K. Maher, in *"Molecular Sieves"*, Eds. R. M. Barrer, Soc. Chem Ind., London (1968).

B) C. V. McDaniel and P. K. Maher, *Adv. Chem. Ser.*, **171**, 285 (1976).

82. R. von Ballmoos, "The ^{18}O Exchange Method in Zeolite Chemistry", Otto Salle Verlag, Frankfurt/Main (1981).

83. J. S. Frye and G. E. Maciel, *J. Magn. Reson.*, **48**, 125 (1982).

84. W. E. Hull, in *"Two-Dimensional NMR Spectroscopy, Applications for Chemists and Biochemists"* Eds W. R. Croasmum and R. M. K. Carlson. VCH (1987).

85. A) H. Y. Carr and E. M. Purcell, *Phys. Rev.*, **94**, 630 (1954).
S. Meiboom and D. Gill, *Rev. Sci. Instr.*, **29**, 688 (1958).

B) D. J. Cookson and B. E. Smith, *J. Magn. Reson.*, **63**, 217 (1985).

86. J. Klinowski, T. A. Carpenter and J. M. Thomas, *J. Chem. Soc., Chem. Commun.*, 956 (1986).

87. F. G. Dwyer and E. E. Jenkins, *U.S. Patent* **4287166** (1981).

88. J. L. Schlenker, F. D. Dwyer, E. E. Jenkins, W. J. Rohrbuagh, G. T. Kokotailo and W. M. Meier, *Nature (London)*, **294**, 340 (1981).

89. H. Gies, F. Liebau and H. Gerke, *Angew. Chem.*, **94**, 214 (1982).

90. G. T. Kokotailo, C.A. Fyfe, G. C. Gobbi, G. J. Kennedy and C. T. De Schutter, *J. Chem. Soc., Chem. Commun.*, 1208 (1984).

91. P. Bodart, J. B. Nagy. G. Debras, Z. Gabelica, E. G. Derouane and P. A. Jacobs, *Bull. Soc. Chim. Belg.*, **92**, 711 (1983).

92. E. J. J. Groenen, N. C. M. Alma, A. G. T. M. Bastein, G. R. Hays, R. Huis and A. G. T. G. Kortbeek, *J. Chem. Soc., Chem. Commun.*, 1360 (1983).

93. H. Strobl, C. A. Fyfe, G. T. Kokotailo and C. T. Pasztor, *J. Am. Chem. Soc.*, **109**, 4733 (1987).

94. J. A. Ripmeester, M. A. Desando, Y.P. Handa and J. S. Tse, *J. Chem. Soc., Chem. Commun.*, 608 (1988).

95. C. A. Fyfe, H. Gies and Y. Feng, *J. Am. Chem. Soc.*, **111**, 7702 (1989).

96. N. M. Szeverenyi, M. J. Sullivan and G. E. Maciel, *J. Magn. Reson.* **47**, 462 (1982).

97. D. L. VanderHart, *J. Magn. Reson.* **72**, 12 (1987).

98. P. Caravatti, G. Bodenhausen and R. R. Ernst, *J. Magn. Reson.*, **55**, 88 (1983).

99. D. Suter and R.R. Ernst, *Phys. Rev. B* **25**, 6038 (1982), **32**, 5608 (1985).

100. A. Kubo and C. A. McDowell, *J. Chem. Phys.*, **89**, 63 (1988).

101. H. Gies, *Zeitschrift fur Krist.*, **175**, 93 (1986).

102. H. Gies, F. Liebau and H.Gerke, *Angew. Chem.*, **94**, 214 (1982).

103. T. H. Mareci and R. Freeman, *J. Magn. Reson.*, **48**, 158 (1982).

104. H. van Koningsveld, J. C. Jansen and H. van Bekkum , *Zeolites*, **10**, 235 (1990).

105. H. Gies, unpublished work.

106. E. J. Rosinski and M. K. Rubin, US Patent **3, 832, 449** (1974).

107. R. B. Lapierre, A. C Rohrman, J. L. Schlenker, J. D. Wood, M. K. Rubin and W. J. Rohrbaugh, *Zeolites*, **5**, 346 (1985).

108. C. A. Fyfe, Y. Feng, H. Gies, H. Grondey and G. T. Kokotailo, *J. Am. Chem. Soc.*, **112**, 3264 (1990).

109. D. L. Turner, *J. Magn. Res.*, **49**, 175 (1982).

110. S. A. I. Barri, P. Howard and C. D. Telford, *Eur. Pat.* **0057049** (1982).

111. D. H. Olson, E. W. Valyocsik and R. B. Calvert, *Eur. Pat. Appl.*, **EP A 0102716** (1984).

112. L. M. Parker and D. M. Bibby, *Zeolites*, **3**, 8 (1983).

113. Idemitsu Kosan Co.,Ltd., *Jap. Pat. Appl.* No., **154037**, Pub. No. **59-44331** (1982).

114. P. J. Hogan, A. Stewat and T. V. Whittam, *Eur. Pat.* **0065400** (1982).

115. S. A. I. Barri, G. W. Smith, D. White and D. Young, *Nature*, **312**, 533 (1984).

116. G. T. Kokotailo, J. L. Schlenker, F. G. Dwyer and E. W. Valyocsik, *Zeolites*, **5**, 349 (1985)

117. C. A. Fyfe, H. Strobl, G. T. Kokotailo, C. T. Pasztor, G. E. Barlow and S. Bradley, *Zeolites*, **8**, 132(1988).

118. M. Tielen, M. Geelen and P. A. Jacobs, *Proc. Int. Sym. Zeolite Catalysis*, Siofok, Hungary (1985).

119. F. G. Dwyer in *"Catalysis of Organic Reactions"*, Eds. W. R. Moser, Dekker, New York, (1981).

120. G. T. Kokolailo, S. L. Lawton, D. H. Olson and W. M. Meier, *Nature*, **272**, 437 (1978).

121. D. H. Olson, G. T. Kokotailo and S. L. Lawton, *J. Phys. Chem.*, **85**, 2238 (1981).

122. H. van Koningsveld, H. van Bekkum and J. C. Jansen, *Acta Cryst.*, **B43**, 127 (1987).

123. H. van Koningsveld et al., *Acta Cryst. B*, in press.

124 H. van Koningsveld, F. Tuinstra, H. van Bekkum and J. C. Jansen, *Acta Cryst.*, **B45**, 423 (1989).

125. C. Baerlocher, *Proceedings of the 6th International Conference on Zeolites*, Reno 1983 , Butterworths, London, (1984).

126. H. Gies and co-workers, to be published.

127 C. A. Fyfe, G. T. Kokotailo, G. J. Kenndy and C. T. De Schutter, *J. Chem. Soc., Chem. Commun.*, 306 (1985).

128 C. A. Fyfe, G. J. Kenney, C. T. De Schutter, and G. T. Kokotailo, *J. Chem. Soc., Chem. Commun.*, 541 (1984).

129. G. W. West, *Aust. J. Chem.*, **37**, 455 (1984).

130. D. G. Hay, H. Jaeger and G. W. West, *J. Phys. Chem.*, **89**, 1070 (1985).

131. G. Engelhardt, R. Radeglia, U. Lohse, A. Samoson and E. Lippmaa, *Z. Chem.*, **25**, 252 (1985).

132. H. Tham, *J. Phys. Chem.*, **91**, 8 (1987).

133. R. E. Richards and L. V. C. Rees, *Zeolites*, **8**, 35 (1988).

134. B. F. Mentzen, F. Bosselet and J.Bouix, *C. R. Acad. Sci.*, **305**, 581 (1987).

135. C. A. Fyfe and G. L. Kennedy, unpublished work.

136. J. B. Nagy, E. G. Derouane, H. A. Resing and G. R. Miller, *J. Phys. Chem.*, **87**, 833 (1983).

137. C. A. Fyfe and B. Fahie, in preparation.

138. H. J. Strobl, *Ph.D Thesis*, University of Guelph, (1989).

139. J. B. Higgins and D. E. Woessner, *EOS*, **63**, 1139 (1982).

140. A. R. Grimmer and R. Radeglia, *Chem. Phys. Lett.*, **106**, 262 (1984).

141. J. V. Smith and C. S. Blackwell, *Nature*, **303**, 223 (1983).

142. J. M. Thomas, J. Klinowski, S. Ramdas, B. K. Hunter and D. T. B. Teenakoon, *Chem. Phys. Lett.*, **102**, 158 (1983).

143. M. Magi, E. Lippmaa, A. Samoson, G. Engelhardt and A. R. Grimmer, *J. Phys. Chem.*, **88**, 1518 (1984).

144. S. Ramdas and J. Klinowski, *Nature*, **308**, 521 (1984).

145. N. Janes and E. Oldfield, *J. Am. Chem. Soc.* **107**, 6769 (1985).

146. G. Engelhardt and R. Radeglia, *Chem. Phys. Lett.*, **108**, 271 (1984).

147. E. G. Derouane and R. A. Hubert, *Chem. Phys. Lett.*, **132**, 315 (1986).

148. G. Engelhardt, S. Luger, J. Ch. Buhl and J. Felsche, *Zeolites*, **9**, 182 (1989).

149. L. B. Young, *U.S. Patent*, **4,181,811** (1978).

150. W. W. Kaeding, M. M. Wu, L. B. Young and G. T. Burgess, *U.S. Patent* **4,197,413** (1987).

151. G. Giannetto, G. Perot and M. Guisnet, in *"Zeolites Synthesis, Structure, Technology and Application"* Eds. B. Drzaj, S. Hocevar and S. Pejovnik, (1985).

152. G. T. Kokotailo, P. Chu, S. L. Lawton and W. M. Meier, *Nature*, 275, 119 (1978).

153. J. P. Nagy, Z. Gabelica, E. G. Deruane and P.A. Jacobs, *Chem, Lett.*, 2003 (1982).

154. B. H. Toby, M. H. Eddy, C. A. Fyfe, G. T. Kokotailo, H. Strobl and D. E. Cox, *J. Mater. Res.*, **3**, 563 (1988).

155. C. A. Fyfe, H. Gies, G. T. Kokotailo, C. Pasztor, H. Strobl and D. E. Cox, *J. Amer. Chem. Soc.*, **111**, 2470 (1989).

156. P. Chu, *U.S. Patent*, **3,709,979** (1973).

157. G. T. Kokotailo, A. C. Rohrman, Jr., *U.S. Patent*, **4,703,025** (1987).

158. C. J. Plank, E. J. Rosinski and M. K. Rubin, *U.S. Patent*, **4,076,842** (1978).

159. A. C. Rohrman Jr., R. B. La Pierre, J. L. Schlenker, J. D. Wood, E. W. Valyocsik, M. K. Rubin, J. B. Higgins and W.J. Rohrbaugh, *Zeolites*, **5**, 352 (1985).

160. P. A. Wright, J. M. Thomas, G. R. Millward, S. Ramdas and S. A. I. Barri, *J. Chem. Soc., Chem. Commun.*, 1117 (1985).

161. E. W. Valyocsik, *U.S. Patent*, **4,490,342** (1984).

162. B. F. Chmelka, K. T. Mueller, A. Pines, J. Stebbins, Y. Wu and J. W. Zwanziger, *Nature* (London) **339**, 42 (1989).

163. K. T. Mueller, B. Q. Sun, G. C. Chingas, J. W. Zwanziger, T. Terao and A. Pines, *J. Magn. Res.*, **86**, 470 (1990).

164. K. T. Mueller, Y. Wu, B. F. Chmelka, J. Stebbins and A. Pines, *J. Amer. Chem. Soc.*, **113**, 32 (1991).

165. T. Gullion and J. Schaefer, *J. Magn. Res.*, **81**, 196 (1989).

166. S. E. Shore, J. P. Ansermet, C. P. Slichter and J. H. Sinfelt, *Phys. Rev. Lett.*, **58**, 953 (1987).

167. P. K. Wang, C. P. Slichter and J. H. Sinfelt, *Phys. Rev. Lett.*, **53**, 82 (1984).

168. S. M. Holl, R. A. McKay, T. Gullion and J. Schaefer, *J. Magn. Res.*, **89**, 620 (1990).

169. Y. Pan and J. Schaefer, *J. Magn. Res.*, **90**, 341 (1990).

170. C. A. Fyfe and H. Grondey, in preparation.